UNCLASSIFIED

AD NUMBER

AD815292

NEW LIMITATION CHANGE

TO

Approved for public release, distribution unlimited

FROM

Distribution authorized to U.S. Gov't. agencies and their contractors; Administrative/Operational Use; FEB 1967. Other requests shall be referred to Air Force Materials Lab., AFSC, Wright-Patterson AFB, OH 45433.

AUTHORITY

AFML ltr, 7 Dec 1977

THIS PAGE IS UNCLASSIFIED

AFML-TR-66-270

AD815292

RESEARCH AND DEVELOPMENT OF NONDESTRUCTIVE TESTING TECHNIQUES FOR COMPOSITES

GEORGE MARTIN and J. F. MOORE

TECHNICAL REPORT AFML-TR-66-270

DDC
RECEIVED
JUN 15 1967
B

FEBRUARY 1967

This document is subject to special export controls and each transmittal to foreign governments or foreign nationals may be made only with prior approval of the Metals and Ceramics Division, MAM, Air Force Materials Laboratory, Wright-Patterson Air Force Base, Ohio 45433.

AIR FORCE MATERIALS LABORATORY
RESEARCH AND TECHNOLOGY DIVISION
AIR FORCE SYSTEMS COMMAND
WRIGHT-PATTERSON AIR FORCE BASE, OHIO



Best
Available
Copy

AFML-TR-66-270

RESEARCH AND DEVELOPMENT OF NONDESTRUCTIVE TESTING TECHNIQUES FOR COMPOSITES

GEORGE MARTIN and J. F. MOORE

This document is subject to special export controls and each transmittal to foreign governments or foreign nationals may be made only with prior approval of the Metals and Ceramics Division, MAM, Air Force Materials Laboratory, Wright-Patterson Air Force Base, Ohio 45433.

FOREWORD

This is a summary technical report prepared by North American Aviation, Inc./Los Angeles Division under Air Force Contract No. AF 33(615)-2865, per line Item 1b, Exhibit B, Paragraph IC. The contract was initiated under Project 7360, (the Chemistry and Physics of Materials,) Task No. 736002, (Nondestructive Methods). The work was administered under the direction of the Metals and Ceramics Division of the Air Force Materials Laboratory, MAMN, with Mr. H. Kamm, MAMN, Project Engineer. This report covers the period 1 July 1965 to 30 April 1966.

The report manuscript was released by the authors in May 1966 under North American Aviation report number NA-66-466, for review and publication approval as an RTD Technical Report.

The program was conducted by Materials and Producibility, Mr. N. Klimmek, Manager, under the direction of Dr. George Martin, Program Manager, and the supervision of Mr. J.F. Moore, Project Engineer. The research described in this report was conducted by Dr. George Martin, Mr. J.F. Moore, Mr. H.S. Varney, Mr. W.E. Nagel, and Mr. N.M. Ewbank.

The authors express their appreciation to Mr. C.W. Russell and Mr. D.G. Atteridge for assistance in preparation of the composite specimens, to Mr. R.A. Brose for the metallographic work, and Miss J.A. Brown of the Space and Information Systems Division for microradiography. Boron fibers used for specimen preparation were supplied by the Air Force Materials Laboratory.

This technical report has been reviewed and is approved.

THOMAS B. COOPER
Chief, Processing &
Nondestructive Testing Br
Metals & Ceramics Division

ABSTRACT

Results of a research and development program relating to evaluation of nondestructive testing techniques for fiber-reinforced metallic matrix composites are reported. A bibliography, based on an extensive literature search, was compiled. Methods for continuous cleaning and inspection of boron fibers were investigated and an experimental system developed. Boron-aluminum, boron-titanium, and tungsten-copper composite specimens were fabricated with fiber volume ratios ranging from 10 to 25 percent and containing specific anomalies. Nondestructive test methods used were radiography, ultrasonics, and magnetic testing. In addition, experiments proved the feasibility of an optical method for continuous fiber surface inspection. Radiographic methods were found to be adequate to determine single fiber breaks as well as major fiber gaps and general fiber alignment. The feasibility of microradiographic inspection was demonstrated for small single layer boron composites. Ultrasonic pulse echo methods are capable of determining matrix disbonds as small as 1/4 inch square. Ultrasonic velocity measurements show a relation between velocity and fiber ratio. In addition to the experimental work, a literature survey of the problem areas was carried out and recommendations for future extensions of the work are detailed.

"This document is subject to special export controls and each transmittal to Foreign Governments or Foreign Nationals may be made only with prior approval of the Metals and Ceramics Division (MAM), Air Force Materials Laboratory, Wright-Patterson Air Force Base, Ohio 45433."

PAGES NOT FILMED ARE BLANK

TABLE OF CONTENTS

Section		Page
I	INTRODUCTION	1
II	SUMMARY	3
III	LITERATURE SURVEY	5
IV	COMPOSITE SPECIMENS	7
	Defect Characterization	7
	Specimen Design	10
	Defect Simulation	10
	Specimen Fabrication	15
	Material Selection and Preparation	15
	Filament Winding	19
	Diffusion Bonding	22
	Composite Fabrication Summary	24
	Metallography	27
V	RADIOGRAPHIC INSPECTION	31
	Technical Approach	31
	Penetrameters	35
	Radiography of Tungsten-Copper Composite	35
	Radiography of Boron-Titanium Composite	45
	Radiography of Boron-Aluminum Composite	49
	Radiograph Densitometry	51
	Dynamic Radiography	51
	Microradiography	55
	Photographic Enlargement of Radiographs	59
VI	ULTRASONIC INSPECTION	63
	Ultrasonic Property Measurement	63
	Velocity Measurement for Tungsten-Copper Composites	64
	Velocity Measurement for Boron-Titanium Composites	64

Section		Page
	Velocity Measurement for Boron-Aluminum Composites	64
	Ultrasonic Attenuation Tests	68
	Ultrasonic C-scan Inspection	70
	Technical Approach	70
	Preliminary Ultrasonic Inspection	72
	Ultrasonic Inspection of Tungsten-Copper Composites	73
	Ultrasonic Inspection of Boron-Titanium Composites	75
	Ultrasonic Inspection of Boron-Aluminum Composites	77
	Summary	
VII	ELECTROMAGNETIC INSPECTION	79
VIII	FIBER OPTICAL INSPECTION	85
IX	CONCLUSIONS AND RECOMMENDATIONS	93
	Radiographic Inspection	93
	Ultrasonic Inspection	99
	Electromagnetic Inspection	103
	Fiber Inspection	103
	Residual Stresses	103
	General Conclusions	103
X	REFERENCES	105
	APPENDICES	
	Appendix I Metallographic Inspection of Fiber-Matrix Specimens	107
	Appendix II Radiographic Inspection	131
	Appendix III Ultrasonic C-scan Records	169
	Appendix IV Literature Survey	195

LIST OF ILLUSTRATIONS

Figure No.	Title	Page
1	Automated Hand Loom for Weaving Defect Mats.	15
2	Defect Guide and Mats Using Boron and Silver for Boron-Aluminum Composite	14
3	Basic Specimen Fabrication Operations	16
4	Experimental "In-line" Fiber Cleaning System	18
5	Photographs of Boron Fiber Showing Effectiveness of Cleaning (750X)	20
6	Mandrel Winding Setup	21
7	Retort and Layup for Diffusion Bonding	23
8	Diffusion Bonding Press	25
9	Boron-Aluminum Specimen - Metallographic Inspection of Section Parallel to Fibers	29
10	"In-motion" Narrow-beam Radiograph Assembly.	32
11	Collimator Assembly	33
12	Radiographic Fan-form Penetrameter	36
13	Radiographic Penetrameter at 90-, 110-, and 130 KV	37
14	Penetrameter - Copper Foil	38
15	Penetrameter - Titanium Foil	39
16	Penetrameter - Aluminum Foil	40
17	Tungsten-Copper 15BF Narrow Beam Radiograph at 10X Enlargement, Type M Film	43
18	Tungsten-Copper 15BF Broad Beam Radiograph at 10X Enlargement, Type R Film	44
19	Tungsten-Copper 15BF Stereo-Radiograph, Left View.	46
20	Tungsten-Copper 15BF Stereo-Radiograph, Right View	47
21	Norelco "Searchray" System	52
22	Fixture Used for Specimen Location	53
23	Microradiograph Showing Boron-Aluminum Specimen End With Foil Tabs	56
24	Microradiograph of Boron-Titanium 25BF at 40KV, 25 ma, 3-hour Exposure, Showing Two Photographic Sensitivity Levels	57
25	Microradiograph of Boron-Titanium Single Layer Composite, - Etched (25KV, 23 ma, 2 Hour Exposure)	58
26	Tungsten-Copper Specimen 25BF Radiograph Showing Deliberate Defect Areas	60
27	Tungsten-Copper 25BF Radiograph, 5X Photographic Enlargement of Square Defect Sections and Area Containing a Broken Fiber (Lower Right)	61
28	Tungsten-Copper 25BF Radiograph, 5X Photographic Enlargement of Deliberate Fiber Breaks	62

Figure No.	Title	Page
29	Ultrasonic Through-transmission Test System Inspection of Composite Specimens	67
30	Ultrasonic Inspection System for Composite Inspection by the Immersion Method	71
31	Ultrasonic C-Scan Record of Tungsten-Copper Evaluation Specimen; Test Sensitivity 1.0	73
32	Magnetic Inspection System	80
33	Magnetic Inspection, Boron-Titanium 25BF, Record of Calibration at 3-, 10-, 50-Gauss	81
34	Magnetic Inspection, Boron-Titanium 25BF, Sensitivity Range 0.5 Gauss/Inch, 1-inch and 1/4-inch Defect Location Noted	82
35	Magnetic Inspection, Tungsten-Copper 25BF, Sensitivity Range 0.5 Gauss/Inch, 1-inch Defect Location Noted	83
36	Block Diagram of Experimental Boron Fiber Inspection System	86
37	Continuous Fiber Inspection System	87
38	Inspection System Fiber-Feed Alignment Fixture	88
39	Film Excerpts Showing Movement of Boron Fiber Past Viewing Field During Continuous Inspection Process	89
40	Photographs of Broken Boron Fiber	90
41	Relationship of Composite Specimen Thickness Versus Radiographic Inspection Voltage	95
42	Relationship of Composite Specimen Volume Ratio Versus Radiographic Inspection Voltage	96
43	Optimum Radiographic Voltage Versus Normalized Attenuation for Composite Specimens	98
44	Calculated Acoustic Velocity ($\sqrt{E/\rho}$) Versus Measured Velocity for Composites and Materials	102
45	Tungsten-Copper - 10 BF	109
46	Tungsten-Copper - 15 BF	110
47	Tungsten-Copper - 20 BF	111
48	Tungsten-Copper - 25 BF	112
49	Tungsten-Copper - 15 A	113
50	Tungsten-Copper - 15 FM	114
51	Tungsten-Copper - 15 M	115
52	Boron-Titanium - 10 BF	116
53	Boron-Titanium - 15 BF	117
54	Boron-Titanium - 20 BF	118
55	Boron-Titanium - 25 BF	119
56	Boron-Titanium - 15 FM	120
57	Boron-Titanium - 15 M	121

Figure No.	Title	Page
58	Boron-Aluminum - 10 BF Specimen Edge After Polishing. . .	122
59	Boron-Aluminum - 15 BF.	123
60	Boron-Aluminum - 20 BF.	124
61	Boron-Aluminum - 25 BF.	125
62	Boron-Aluminum - 15 FM	126
63	Boron-Aluminum - 15 M	127
64	Section of Tungsten-Copper and Boron-Titanium Specimen at 5600X Magnification	128
65	Section of Boron-Aluminum Specimen at 5600X and 32,000X Magnification	129
66	Section of Boron-Aluminum Specimen Sliced Parallel to Fibers, 150X and 250X Magnification.	130
67	Tungsten-Copper 10-25 BF Evaluation Specimen at 75 KV, 10 MA, 4 MM Dia, 2 Min	132
68	Tungsten-Copper 10-25 BF Evaluation Specimen at 80 KV, 10 MA, 4 MM Dia, 2 Min.	133
69	Tungsten-Copper 10-25 BF Evaluation Specimen at 80 KV, 3.5 MA, 2 MM Dia, 6 Min	134
70	Tungsten-Copper 10-25 BF Evaluation Specimen at 90 KV, 3 MA, 2 MM Dia, 4.5 Min	135
71	Tungsten-Copper 10-25 BF Evaluation Specimen at 100 KV, 3.5 MA, 2 MM Dia, 4 Min	136
72	Tungsten-Copper 10-25 BF Evaluation Specimen at 170 KV, 4 MA, 2 MM Dia, 2.5 Min, With Lead Screen	137
73	Tungsten-Copper 10-25 BF Evaluation Specimen at 150 KV, 3.75 MA, 2 MM Dia, 6 Min, With Lead Screen, R Film. . .	138
74	Tungsten-Copper 10-25 BF Evaluation Specimen at 150 KV, 3.5 MA, 2 MM Dia, 3 Min, With Lead Screen	139
75	Tungsten-Copper 10-25 BF Evaluation Specimen at 90 KV, 3.75 MA, 2 MM Dia, 10 Min	140
76	Tungsten-Copper 10-25 BF Evaluation Specimen at 90 KV, 3.75 MA, 2 MM Dia, 6 Min, With Lead Screen Both Sides .	141
77	Tungsten-Copper 10-25 BF Evaluation Specimen at 90 KV, 3.75 MA, 2 MM Dia, 6 Min, With Lead Screen Below Film .	142
78	Tungsten-Copper 10-25 BF Evaluation Specimen at 150 KV, 3.75 MA, 2 MM Dia, 1.75 Min	143
79	Tungsten-Copper 10 BF Specimen at 150 KV, 1.2 MM Dia, 1.25 Min.	144
80	Tungsten-Copper 15 BF Specimen at 150 KV, 1.2 MM Dia, 6 Min	145
81	Tungsten-Copper 20 BF Specimen at 170 KV, 1.2 MM Dia, 2 Min	146
82	Tungsten-Copper 25 BF Specimen at 190 KV, 1.2 MM Dia, 2.25 Min.	147

Figure No.	Title	Page
83	Tungsten-Copper 15 FM Specimen at 170 KV, 1.2 MM Dia, 2.25 Min.	148
84	Tungsten-Copper 15 A Specimen at 150 KV, 1.2 MM Dia, 4 Min	149
85	Tungsten-Copper 15 M Specimen at 250 KV, 1.2 MM Dia, 10 Min.	150
86	Boron-Titanium 10 BF Specimen (Front) at 90 KV, 3.5 MA, 1.2 MM Dia, 4.5 Min	151
87	Boron-Titanium 10 BF Specimen (Back) at 90 KV, 3.5 MA, 1.2 MM Dia, 4.5 Min	152
88	Boron-Titanium 15 BF Specimen (Front)at 90 KV, 3.5 MA, 1.2 MM Dia, 4.75 Min.	153
89	Boron-Titanium 15 BF Specimen (Back) at 90 KV, 3.5 MA, 1.2 MM Dia, 4.75 Min.	154
90	Boron-Titanium 20 BF Specimen (Front) at 90 KV, 4 MA, 1.2 MM Dia, 5 Min	155
91	Boron-Titanium 20 BF Specimen (Back) at 90 KV, 4 MA. 1.2 MM Dia. 5 Min	156
92	Boron-Titanium 25 BF Specimen (Front) at 90 KV, 4 MA, 1.2 MM Dia, 5 Min	157
93	Boron-Titanium 25 BF Specimen (Back) at 90 KV, 4 MA, 1.2 MM Dia, 5 Min	158
94	Boron-Titanium 15 M Specimen (Front) at 130 KV, 4 MA, 1.2 MM Dia, 5 Min	159
95	Boron-Titanium 15 M Specimen (Back) at 130 KV, 4 MA, 1.2 MM Dia, 5 Min	160
96	Boron-Titanium 15 F Specimen (Front) at 110 KV, 4 MA, 1.2 MM Dia, 5 Min	161
97	Boron-Titanium 15 F Specimen (Back) at 110 KV, 4 MA, 1.2 MM Dia, 5 Min	162
98	Boron-Aluminum 10 BF Specimen at 90 KV, 4 MA, 1.2 MM Dia, 3.75 Min	163
99	Boron-Aluminum 15 BF Specimen at 100 KV, 3 MA, 1.2 MM Dia, 4 Min.	164
100	Boron-Aluminum 20 BF Specimen at 100 KV, 4 MA, 1.2 MM Dia, 3.5 Min.	165
101	Boron-Aluminum 25 BF Specimen at 110 KV, 4 MA, 1.2 MM Dia, 3.5 Min.	166
102	Boron-Aluminum 15 M Specimen at 120 KV, 4 MA, 1.2 MM Dia, 4 Min.	167
103	Boron-Aluminum 15 F Specimen at 110 KV, 4 MA, 1.2 MM Dia, 4 Min.	168

Figure No.	Title	Page
104	Tungsten-Copper - 10 BF-3: 33 Percent Saturated Indication From Flat Bottom Hole in a No. 8 Aloca D Block.	170
105	Tungsten-Copper - 15 BF-3: 95 Percent Saturated Indicating From Flat Bottom Hole in a No. 5 Aloca D Block.	171
106	Tungsten-Copper - 20 BF-3: 33 Percent Saturated Indication From Flat Bottom Hole in a No. 8 Aloca D Block.	172
107	Tungsten-Copper - 25 BF-3: 70 Percent Saturated Indication From Flat Bottom Hole in a No. 8 Alcoa D Block.	173
108	Tungsten-Copper - 15 A-3: 48 Percent Saturated Indication From Flat Bottom Hole in a No. 4 Alcoa D Block.	174
109	Tungsten-Copper - 15 FM-2: 82 Percent Saturated Indication From Flat Bottom Hole in a No. 8 Alcoa D Block.	175
110	Tungsten-Copper - 15 M-3: 60 Percent Saturated Indication From Flat Bottom Hole in a No. 5 Alcoa D Block.	176
111	Boron-Titanium - 10 BF-3: 85 Percent Saturated Indication From Flat Bottom Hole in a No. 8 Alcoa D Block.	177
112	Boron-Titanium - 15 BF-3: 38 Percent Saturated Indication From Flat Bottom Hole in a No. 8 Alcoa D Block.	178
113	Boron-Titanium - 20 BF-3: 68 Percent Saturated Indication From Flat Bottom Hole in a No. 8 Alcoa D Block.	179
114	Boron-Titanium - 25 BF-3: 68 Percent Saturated Indication From Flat Bottom Hole in a No. 8 Alcoa D Block.	180
115	Boron-Titanium - 15 FM-3: 15 Percent Saturated Indication From Flat Bottom Hole in a No. 8 Alcoa D Block.	181
116	Boron-Titanium - 15 M-2: 15 Percent Saturated Indication From Flat Bottom Hole in a No. 8 Alcoa D Block.	182
117	Boron-Aluminum - 10 BF-3: 8 Percent Saturated Indication From Flat Bottom Hole in a No. 8 Aloca D Block.	183
118	Boron-Aluminum - 15 BF-3: 15 Percent Saturated Indication From Flat Bottom Hole in a No. 6 Alcoa D Block.	184

Figure No.	Title	Page
119	Boron-Aluminum - 20 BF-3: 40 Percent Saturated Indication From Flat Bottom Hole in a No. 8 Alcoa D Block.	185
120	Boron-Aluminum - 25 BF-8-1: 5 Percent Saturated Indication From Flat Bottom Hole in a No. 8 Alcoa D Block; Sensitivity Control Set at 1 x 6.	186
121	Boron-Aluminum - 25 BF-802: 5 Percent Saturated Indication From Flat Bottom Hole in a No. 8 Alcoa D Block; Sensitivity Control Set at 1 x 4.	187
122	Boron-Aluminum - 25 BF-8-3: 5 Percent Saturated Indication From Flat Bottom Hole in a No. 8 Alcoa D Block; Sensitivity Control Set at 1 x 3.	188
123	Boron-Aluminum - 25 BF-8-R-1: 5 Percent Saturated Indication From Flat Bottom Hole in a No. 8 Alcoa D Block; Sensitivity Control Set at 1 x 6.	189
124	Boron-Aluminum - 25 BF-8-R-2: 5 Percent Saturated Indication From Flat Bottom Hole in a No. 8 Alcoa D Block; Sensitivity Control Set at 1 x 4.	190
125	Boron-Aluminum - 25 BF-8-R-3: 5 Percent Saturated Indication From Flat Bottom Hole in a No. 8 Alcoa D Block: Sensitivity Control Set at 1 x 3.	191
126	Boron-Aluminum - 15 F-3: 8 Percent Saturated Indication From Flat Bottom Hole in a No. 7 Alcoa D Block.	192
127	Boron-Aluminum - 15 M-3: 40 Percent Saturated Indication From Flat Bottom Hole in a No. 7 Alcoa D Block.	193

LIST OF TABLES

Table No.	Title	Page
I	Composite Specimens - Nominal Dimensions and Design. . .	11
II	Composite Specimen Thickness and Volume Ratio Measurements	26
III	Radiographic Inspection of Tungsten-Copper 10/25BF Evaluation Specimens	34
IV	Radiographic Data for Tungsten-Copper Specimen Inspection	41
V	Radiographic Data for Boron-Titanium Specimen Inspection	48
VI	Radiographic Data for Boron-Aluminum Specimen Inspection	50
VII	Summary of Ultrasonic Velocity Measurements and Data . .	65
VIII	Summary of Radiographic Detection Results for Fiber-Matrix Composites.	94
IX	Summary of Ultrasonic Detection for Fiber-Matrix Composites	100
X	Composite Specimen Thickness and Volume Ratio Measurements	108
XI	Sensitivity Responses for Conventional Ultrasonic Transducers - Aluminum	197
XII	Beam Characteristics for Conventional Focused Lithium-Sulfate and Ferroelectric Transducers.	198
XIII	Ultrasonic Attenuation and Velocity in Metals.	203
XIV	Commercial Eddy Current Equipment.	216
XV	Narrow Beam Linear Attenuation-Coefficients (CM^{-1}) . . .	219
XVI	Maximum Material Thicknesses and Half Value Layers . . .	220
XVII	Minimum Detectable Depth Dimensions.	221

Section I

INTRODUCTION

The recent availability of high modulus high strength material fibers has led to the development of new families of materials which very significantly upgrade the properties of conventional monolithic aerospace materials. These new groups of materials depend on the interaction of fibers or laminae set in a matrix to produce properties in the composite which are equal to or better than the proportionate sum of the properties of both matrix and fiber of laminae. Such composite materials are particularly promising because they allow the utilization of very high strength, high modulus and low density materials such as boron fibers, which could otherwise not be utilized in airframe or engine structures.

In order to allow commercial utilization of composite materials, reliable methods of assuring integrity and reliability of the materials must be available. Furthermore, since these materials are still in the development stage, now is the time to learn as much as possible about their properties in order that effective quality control and improvement is assured during manufacture and maintained in service. Such methods must be appropriate to the specific problems encountered in composite materials and relatable to composite material properties as determined by destructive tests. The knowledge of this relationship implies a good understanding of the fundamental mechanisms of the nondestructive tests involved, so that data obtained may be extrapolated or interpolated with some degree of assurance.

The present program is concerned solely with composites consisting of continuous reinforcing fibers embedded in metallic matrices. Being an initial study, the work is directed towards the evaluation of conventional nondestructive test methods. The objective of the program is an evaluation of general applicability of such conventional methods for the evaluation of defects such as fiber breaks, matrix disbonds, fiber alignment and fiber volume ratio. The evaluation includes the determination of factors required for optimization of such conventional methods as well as an estimate of the limits of resolution in various types of composites. The objective requires the manufacture of special test specimens incorporating deliberate defects.

Further objectives were a review of the pertinent literature and studies directed toward the development of methods for the inspection of the fibers themselves.

PAGES NOT FILMED ARE BLANK

Section II

SUMMARY

The report describes the evaluation of conventional nondestructive techniques as applied to filament reinforced metal matrix composites. The evaluation included ultrasonic, radiographic, metallographic, and electromagnetic techniques for inspection of tungsten-copper, boron-aluminum, and boron-titanium composites. A literature survey was conducted into all aspects of the nondestructive testing of composites. The literature indicated that although negligible effort had been conducted in terms of inspecting such composites, both ultrasonic and radiographic techniques appeared highly feasible.

Composite specimens were fabricated with deliberately introduced defects, including broken and misaligned fibers, and disbonds at the fiber-matrix and matrices junctures. Metallographic inspection confirmed the general specimen integrity and fiber-matrix volume ratios which ranged from 9.8 to 20.1 percent.

Radiographic inspection of the composites included an evaluation of broad and narrow beam techniques. Single broken fibers, fiber gaps, and fiber misalignment were detected in all composite specimens; however, the intentional disbonds were not detected. Dynamic radiographic and stereoradiographic techniques were evaluated and were proved feasible for these materials. Photographic enlargement of the radiographic negative was successfully employed up to approximately 10X with excellent detail sensitivity. Experimental microradiographic tests also demonstrated the feasibility of enlarging the fiber-matrix detail as high as 50 to 100 times.

Ultrasonic inspection using pulse-echo, reflector plate techniques were successful in detecting deliberate disbonds as small as 1/4-inch square. Ultrasonic velocity measurements of all materials showed a possible relationship between velocity and fiber ratio. Ultrasonic attenuation studies of the composites were not successful at the frequencies tested.

Electromagnetic inspection, although not capable of detecting the introduced defects, showed evidence of eddy current effects associated with the composite mechanical properties.

An optical fiber inspection system was developed which demonstrated the feasibility of continuously inspecting on entire fiber surface at magnifications up to 100X.

Conclusions are presented including an evaluation of conventional equipment for nondestructive inspection. The conclusions are presented in terms of

defect sensitivity, relationships between the inspection equipment parameters and the composite material responses. Recommendations are presented for future radiographic development in terms of material and defect variables, and the further development of microradiography and stereoradiography techniques.

Ultrasonic studies should consider the determination of attenuation information, the acoustic properties of the diffusion products, and correlation of velocity data with volume ratio to define the exact relationship. It is generally concluded that the proper combination of conventional ultrasonic and radiographic techniques are adequate for the detection of defects presently known to be significant. The applicability of these techniques to production inspection requires further defect analysis in terms of the required composite properties.

Section III

LITERATURE SURVEY

A comprehensive literature survey was conducted during the first month of program effort. The purpose of the survey was to determine the extent of defect detectability for similar and/or allied materials, by various nondestructive testing methods. Results of this survey are presented in Appendix IV.

From the survey of the limitations of commercial equipment for nondestructive testing, it can be concluded that the resolution limits of such equipment are at best at the border line of limits required for the inspection of defects in metallic matrix filamentary composite materials. Throughout the survey, only the simplest shape of metallic matrix-filamentary composite material, sheets with parallel fibers, has been considered. However, it can be assumed that such materials will also find application in many more complex combinations and configurations such as turbine blades reinforced along principal stress directions. A number of methods and approaches are suggested which can improve the sensitivity of commercial test equipment, but these methods generally require nonstandard modifications to the test equipment. Considerable experimental work is therefore required to assess whether relatively minor modification of standard commercial test equipment will result in usable information as to composite material defects or whether major alterations or new equipment design and approaches will be required.

The initial phase of the contract effort was concentrated on specimen design and material preparation. A literature survey was conducted to determine a suitable means of inspecting the 0.004-inch diameter filamentary material. The survey (Appendix IV) revealed the successful use of microscopic, ultrasonic and eddy current inspection techniques for fine diameter wire. The ultrasonic and eddy current systems were not commercially available as required for this application, however, a microscopic system was developed (Section VIII) for continuous filament inspection.

The literature survey of nondestructive test method for fiber-matrix composites and their constituents was continued throughout the contract period. A partially annotated bibliography covering a wide range of nondestructive testing literature was compiled and published as an NAA/LAD report (Reference 1).

Section IV

COMPOSITE SPECIMENS

DEFECT CHARACTERIZATION

A defect is defined as a material, or structural or stress inhomogeneity which significantly affects the performance of the material, part or structure. Upon initiation of the program, one of the major problems was the decision as to what inhomogenities in a fiber-matrix composite can be considered a defect according to this definition. Assuming that the performance of the material is given by its tensile strength (Ref 2), the simplest approach is that given by the law of mixtures which states that

$$s_c = s_f V_f + s_m V_m \tag{1}$$

where s is the strength, V the volume ratio, and the subscripts c, f, and m refer to the composite, the fiber and the stress born by the matrix if the composite is strained to the fracture strain of the fibers, respectively. Based upon this assumption, the only quantities to be determined by an inspection method are the volume ratio and whether there has been any degradation of the strength properties of the filament and the matrix. However, it has been shown experimentally by a number of studies that this simple equation (Equation 1) only applies if the volume ratio of the fibers exceeds a critical value. This critical volume, V_{crit}, is given by

$$V_{crit} = (s_u - s_m)/(s_f + s_u - s_m) \tag{2}$$

where s_u is the ultimate strength of the matrix. For the materials considered here, the critical volume fraction of fibers is of the order of 10 to 30 per cent. For volume fractions lower than this critical limit, the strength of the composite is then determined by

$$s_c' = s_u V_m \tag{3}$$

Equation 3 indicates that for low fiber volume fractions, the ultimate strength of the matrix is the strength determining factor; thus, determination of matrix deterioration becomes more important than strength loss of the fibers.

It must be noted that the above equations make a number of simplifying assumptions. For example, the constraint exercised on the matrix by the closeness of the fibers has been ignored. This constraint leads to a tri-axial stress field with a matrix strengthening, therefore, the determination of fiber spacing becomes important in these low volume ratio fiber composites.

Another assumption made is that all fibers are parallel. For a composite with a volume fraction greater than the critical fraction, failure due to misalignment is most likely to occur through shear in the matrix parallel to the fibers. The stress to produce failure under these conditions s_s is given by

$$s_s = \tau_v / \sin \beta \cos \beta \qquad (4)$$

where β is the angle of misalignment and τ_v the ultimate shear strength. If τ_v is of the order of 0.01 s_c, then this angle is only 30 minutes. If τ_v = 0.1 s_c, then β is 6° and if β is 11°, the strength of the composite is halved. Misalignment of fibers to even quite a small degree thus has an appreciable effect on composite strength, even without considering the variations caused by the varying degree of constraint effect on the matrix. The above analysis applies to composites with volume fractions larger than the critical fraction. If the volume ratio of the fibers is less than the critical fraction, it can be assumed that the misalignment effect due to shear failure will be reduced, but the misalignment effect due to constraint variations on the matrix strength will be increased. In either case therefore, alignment control is an important variable.

The effect of broken fibers can be assessed from two considerations. First, a broken fiber constitutes a notch in the continuum of the composite, which can be associated with a stress concentration factor. This analysis has been carried out by Hedgepeth (Ref 3) who gives the stress concentration factor K_n due to a number of broken fibers 'r' as

$$K_r = [4 \times 6 \times 8 \times \ldots(2r+2)] \; / \; [3 \times 5 \times 7 \ldots\ldots(2r+1)] \qquad (5)$$

which, for various values of r gives:

r :	1	2	3	4	5
K_r:	1.33	1.6	1.83	2.04	2.28

The factor K_r reduces the effective strength of the matrix. For low fiber volume ratios this strength is the decisive factor in the strength of the composite. It is thus apparent that even small numbers of broken fibers may have an appreciable affect on the strength of the composite.

The second consideration in the study of the affect of fiber breaks is the assumption made in equations (1) to (3) that the fibers are continuous. This condition applies if the length of the fibers exceeds a critical length l_c as given by (Ref 2),

$$l_c = d \, s_f \; / \; 2\tau_B \qquad (6)$$

where d is the fiber diameter and τ_B the shear strength of the fiber/matrix bond. For d = 0.005 inches and s_f = 300,000 psi:

$$l_c = 750\ \tau_B \tag{7}$$

Thus it appears that even very low bond strength will give critical length of macroscopic size. Therefore, unless there is very extensive fragmentation of fibers, matrix to fiber disbonds will play a minor role in the strength determination of a composite.

In summary, the defects which are likely to be of importance are, in decreasing order of relative importance, as follows:

1. Composites with fiber volume fraction greater than the critical:

   a. volume ratios
   b. fiber degradation
   c. changes in modulus of matrix
   d. matrix degradation (disbonds, voids, diffusion zones etc.)
   e. fiber misalignment
   f. fiber breaks
   g. fiber matrix disbonds

2. Composites with fiber volume fraction less than the critical:

   a. matrix degradation
   b. fiber breaks
   c. fiber misalignment
   d. volume ratios
   e. fiber degradation
   f. changes in modulus of matrix
   g. fiber matrix disbonds.

In the foregoing analysis, tensile strength has been made the criterion of composite performance. However, there are many other criteria which could affect the performance of a composite structure. Compressive strength and modulus considerations will generally parallel those made for tensile strength. As far as fracture toughness and fatigue are concerned, our present understanding of the correlation of the various factors involved do not allow even an approximate analysis for the characterization of defects. Other factors, such as airtightness, electric insulation or resistance, etc., which may be important for special applications, can be covered by existing tests for non-composite materials.

SPECIMEN DESIGN

The selection of test specimens depends on a number of factors, among which the following were considered to be the most important:

1. Limitations of manufacturing technology: This limited the size of specimens to sheets about 3 x 10 inches and 1/4 inch thick.

2. Limitations of available raw materials: Boron fiber was available only in a 0.004 inch diameter fiber. Titanium sheets were available in thickness down to 0.008 inch only. Other materials were available in a wider range of sizes but, for the sake of uniformity, similar dimensions were chosen for all materials. This limited the fiber volume ratio to about 25 percent maximum.

3. Use of composite combinations considered for actual service or composite combinations with properties significant from a NDT point of view: At the beginning of the program, a boron fiber - titanium alloy composite was the prime contender for actual applications; while a boron fiber - aluminum composite gave the conditions of minimal diffusion reactions, possible applicability in practice and minimal density variations between fiber and matrix. A tungsten fiber-copper composite had the advantages of ease of manufacture, low cost and good density variations and was therefore selected for initial experiments in spite of its unlikelihood of ever becoming industrially important.

4. Defect selection: Defects selected for deliberate incorporation into the specimens had to encompass the range covered in the defect characterization discussed above. Matrix degeneration could only be simulated by deliberate matrix-matrix disbonds. No method could be developed to deliberately change the modulus of the matrix material, for any given selected material.

Specimen requirements for the subject program are listed in Table I. This called for fabrication of three different types of fiber-matrix composite specimens. The specimen identification code, based on volume ratio and defect type, was assigned to provide ready identification of the specimens. This code, in combination with the particular fiber-matrix composite, is used throughout this report.

DEFECT SIMULATION

The study of fiber-matrix composites and the factors that affect their properties indicated four basic types of defects, namely broken fibers, misaligned fibers, fiber disbonds, and matrix disbonds. The evaluation of nondestructive testing techniques was established as the capability of defect detection.

Table I

COMPOSITE SPECIMENS - NOMINAL DIMENSIONS AND DESIGN

Filament	Matrix	Thickness (In.)	Volume Ratio Percent	No. of Specimens	Defect	Specimen Identification
Tungsten	Copper	.040	10	1	Broken Fibers	W-Cu 10BF
Tungsten	Copper	.040	15	1	Broken Fibers	W-Cu 15BF
Tungsten	Copper	.040	20	1	Broken Fibers	W-Cu 20BF
Tungsten	Copper	.040	25	1	Broken Fibers	W-Cu 25BF
Tungsten	Copper	.090	15	1	Lack of Fiber-Matrix Bond	W-Cu 15FM
Tungsten	Copper	.125	15	1	Matrix Voids	W-Cu 15M
Tungsten	Copper	.250	15	1	Fiber Misalignment	W-Cu 15A
Boron	Titanium	.040	10	1	Broken Fibers	B-Ti 10BF
Boron	Titanium	.040	15	1	Broken Fibers	B-Ti 15BF
Boron	Titanium	.040	20	1	Broken Fibers	B-Ti 20BF
Boron	Titanium	.040	25	1	Broken Fibers	B-Ti 25BF
Boron	Titanium	.090	15	1	Lack of Fiber-Matrix Bond	B-Ti 15FM
Boron	Titanium	.125	15	1	Matrix Voids	B-Ti 15M
Boron	Aluminum	.040	10	1	Broken Fibers	B-Al 10BF
Boron	Aluminum	.040	15	1	Broken Fibers	B-Al 15BF
Boron	Aluminum	.040	20	1	Broken Fibers	B-Al 20BF
Boron	Aluminum	.040	25	1	Broken Fibers	B-Al 25BF
Boron	Aluminum	.090	15	1	Lack of Fiber-Matrix Bond	B-Al 15FM
Boron	Aluminum	.125	15	1	Matrix Voids	B-Al 15M

Further, it was planned to simulate defects in a range of sizes to establish detection sensitivity levels for the various inspection methods. Initially, two tungsten-copper composite specimens were fabricated for use as reference specimens, each containing both volume ratios of 10 and 25 percent and three fiber layers. After winding the initial filament layer, the mandrel was removed from the lathe and set into supports on a workbench. Experiments were conducted to develop methods capable of producing repeatable defects. The broken fibers were simulated by cutting one or more tungsten fibers and attempting to tack weld the fiber ends to the matrix with specific spacings between the fiber ends. The tack welding was irregular and frequently exploded the fiber, leaving a deposit. A visit to the Weldamatic Division of the Unitek Corporation for tests and advice yielded negative results. Successful welds were subsequently accomplished by the use of 30-gage tinned solid copper wire as the weld electrode. The weld cycle was approximately 20 watt-seconds. A second problem encountered during spot welding the ends of deliberately broken fibers occurs due to the extremely close spacing for the higher volume ratios (0.0007 inches for 25 percent ratio). Adjacent fibers are frequently displaced causing gross fiber misalignment. Because of these problems, and the unsuitability of the boron fiber for welding, an alternate method was considered for simulating broken fiber defects.

Concurrent composite development had demonstrated the successful bonding of fiber mats, woven with thin foil of the matrix material. The mat is placed between the matrix sheets and diffusion bonded. The minimal amount of added foil material is negligible. This technique provides fiber control and support at the regular intervals necessary to prevent fiber movement when fibers are broken or removed. A trial fiber mat was evaluated and proved satisfactory for broken fibers and fiber misalignment defect simulation. The weaving process is illustrated in Figure 1 showing the hand loom and mat materials. The loom is a 14-inch Nilec two-harness hand loom. Commercially pure copper, silver or titanium foil strips measuring 0.005 by 0.1875 inch and approximately 36 inches long are used as the warp material. The foil strips are stored at the rear of the loom and fed to the front, approximately 1/2 inch apart, through the heddles and the comb and attached to the front take-up cylinder. The fiber is cut to the weave length and placed in a pneumatically actuated filament shuttle tube. A single filament is removed from the shuttle tube each time the tube is fed through the warp/shed. The warp is closed and the filament combed forward. The comb has a fixed stop to assure the same filament placement. The filament spacing is controlled by the takeup cylinder which is automatically rotated a preset angle after each filament is combed into place. The woven fiber mat is wound on this cylinder until the desired length is achieved. Weaving for each type of composite was performed in a continuous mat (Figure 2) which was later cut apart into six mats measuring approximately 5 x 10 inches each.

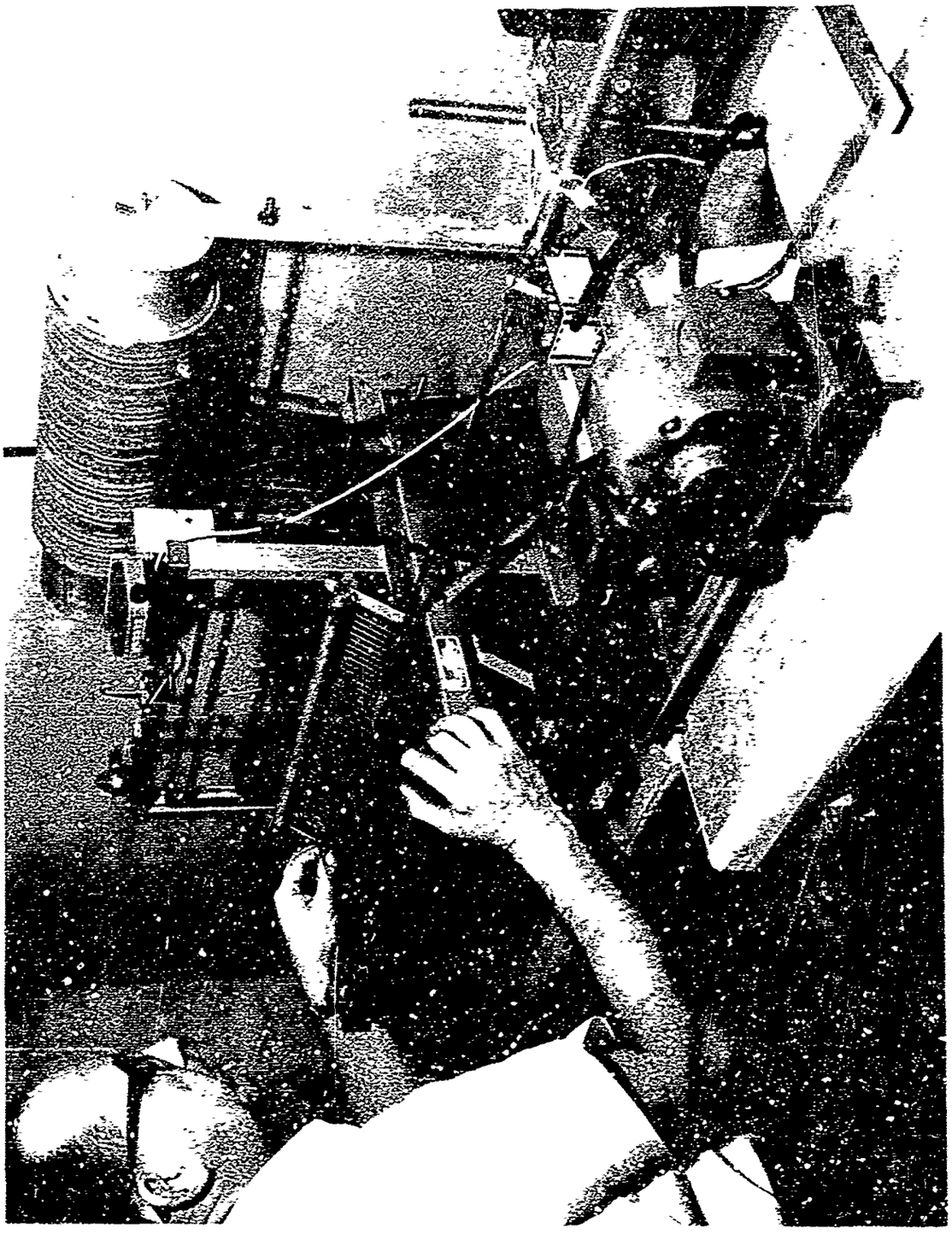
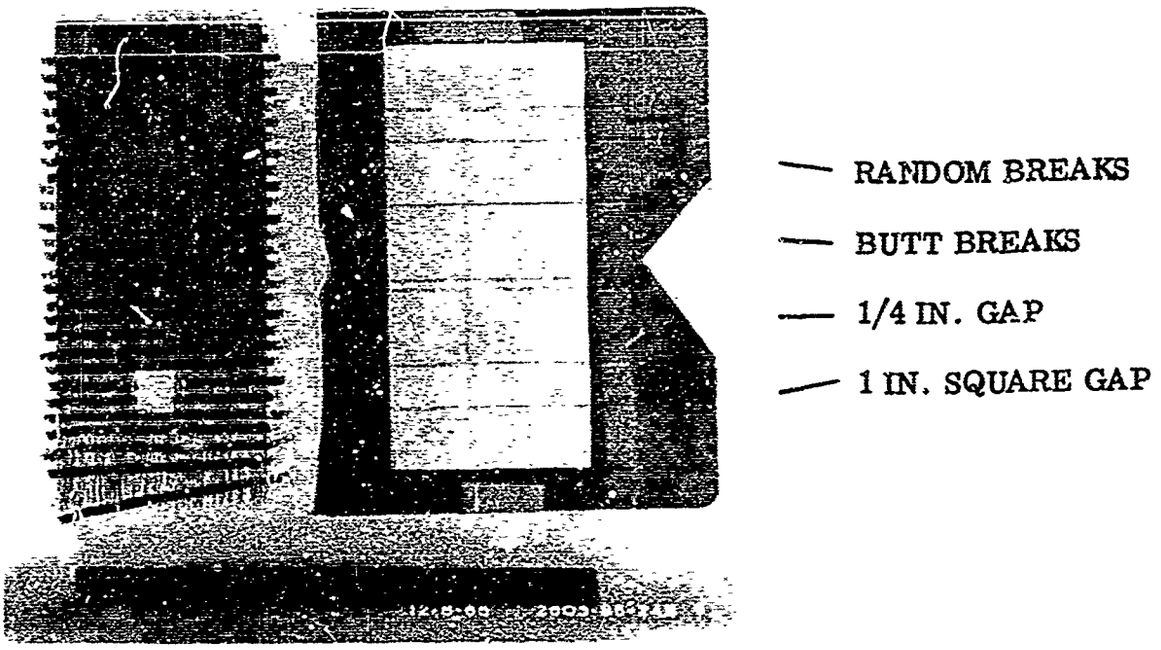


Figure 1. Automated Hand Loom for Weaving Defect Mats



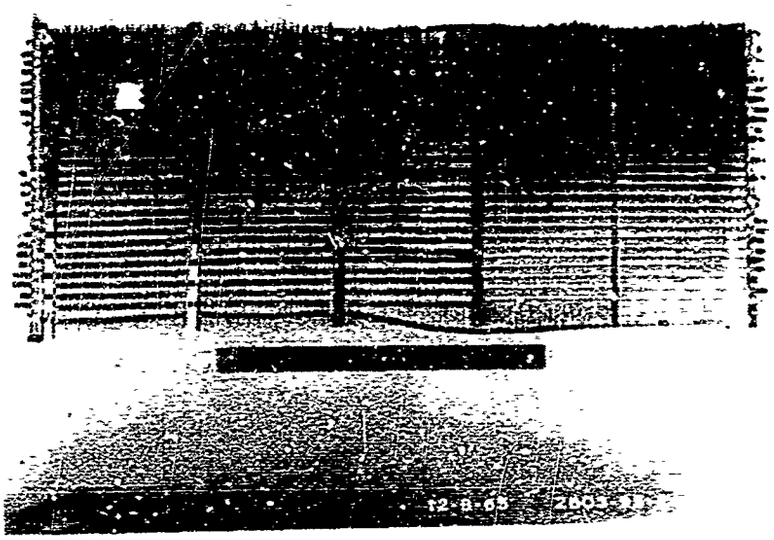


Figure 2. Defect Guide and Mats Using Boron and Silver for Boron-Aluminum Composite

The broken fiber defects in one layer of each composite were designed for four conditions as follows: the removal of fiber in a one-inch and quarter-inch square area; 10 to 12 fibers broken in line with the fibers in contact; and 1, 2, and 3 random fiber breaks in a two-inch area.

A defect layout template was prepared (Figure 2) with cross wires to permit exact positioning of the fiber breaks. The fiber mat was positioned on a strip of stainless steel sheet. The defect template was overlayed, and the fibers were cut with a carbide cutting tool shaped as a small chisel. The broken fiber pieces were carefully removed and the mat was cleaned and stored for use in the winding process.

The fiber disbonds and matrix-matrix disbonds were simulated by painting alumina, in a phosphoric acid solution, on the surfaces to be bonded. This process was evaluated on the trial specimen and proved to be an efficient disbond mechanism. The alumina solution was applied with a small artist paint brush. Since the fibers were very closely spaced, there was a tendency for the fluid to draw or wick away from the desired area. A similar experience was encountered on the clean matrix sheets. There was a tendency for an excessive alumina buildup. After painting, the disbond areas were completely dried with an electric heat gun. The disbond location and size was determined by the use of a template. The disbonds ranged in size from one square inch, one-quarter square inch, one-quarter by one inch rectangle and a one-inch isosceles triangle.

SPECIMEN FABRICATION

The basic fabrication process for the composite specimens is illustrated in the flow diagram shown in Figure 3. The process begins with the cleaning of the composite materials and preparation of mandrel. This is followed by the filament wrapping of multiple layers of fibers separated by matrix sheets or the insertion of a defect fiber mat. After the desired number of layers are wound, the mandrel with specimens is welded into a retort and solid state diffusion bonded under selected pressure and temperature conditions. Specimen materials and the operations involved in specimen fabrication are described in the following paragraphs.

MATERIAL SELECTION AND PREPARATION

Copper Sheets

Commercially pure copper sheet was used in 0.008 and 0.0108 inch thicknesses. The copper was sheared to 5 x 10 inch specimen size, solvent vapor degreased, and water rinsed. A waviness was noted in the 0.008 inch sheet, however, it was considered useable.

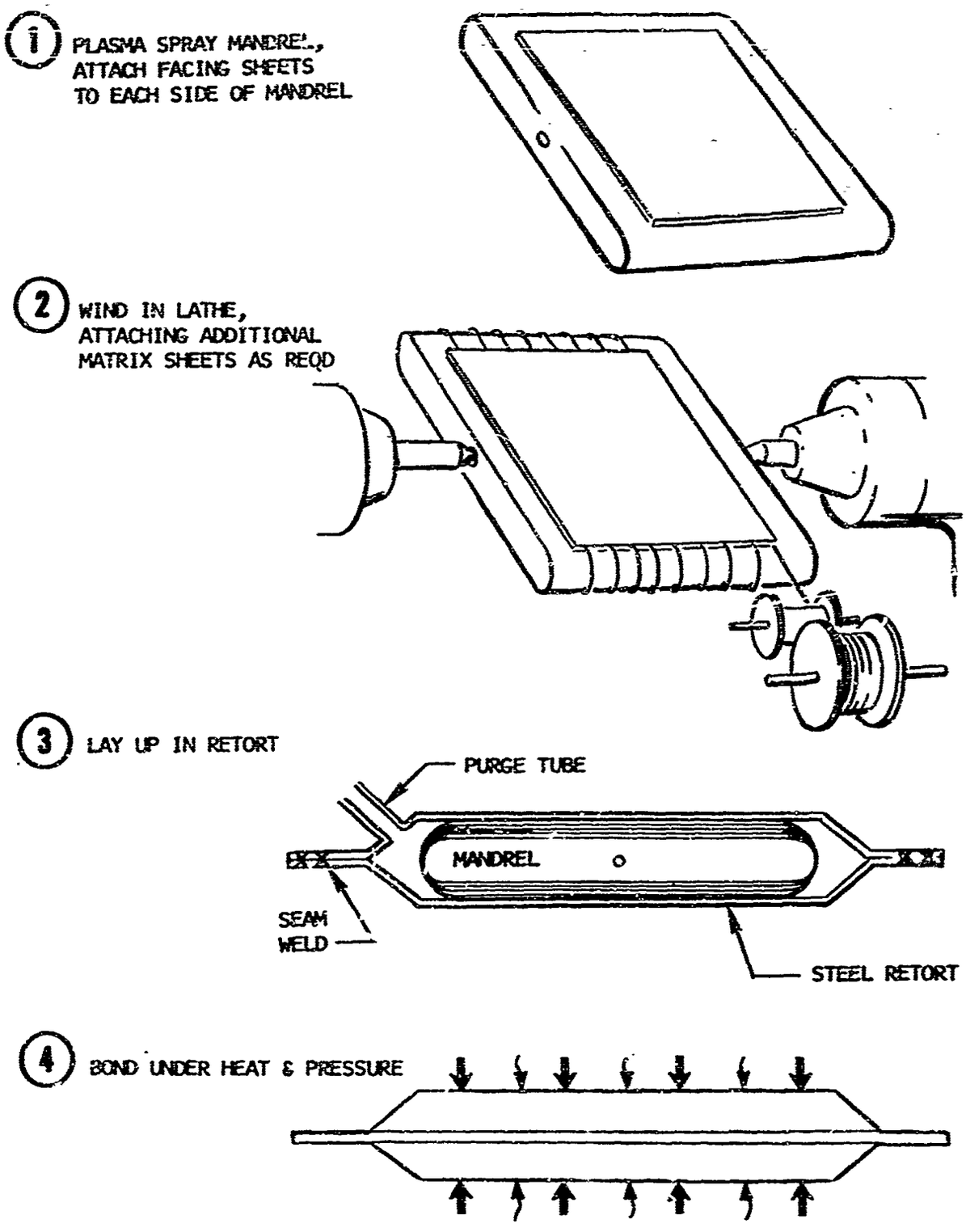


Figure 3. Basic Specimen Fabrication Operations

Titanium Sheets

Titanium alloy Ti-6Al-4V sheet was used in 0.008 and 0.012 inch thicknesses. The titanium was sheared to 5 x 10 inch specimen size. Within 24 hours of use, the titanium was immersion cleaned in alkaline and mild acid solutions, and air dried.

Aluminum Sheets

Aluminum alloy 5052 sheet was used in 0.008 and 0.011 inch thicknesses. It has been shown (Reference 4) that subsequent to cleaning, a thin aluminum oxide layer forms on aluminum and contributes to weak diffusion bonds. Upon exposure of the aluminum to air, the oxide layer forms within a period of a few microseconds. It was therefore decided to use a thin silver plating on the aluminum sheets to reduce oxidation effects until the specimen could be prepared and bonded. NAA Process Specification "Diffusion Bonding of 5052 or 6061 Aluminum Alloy to 5052 With Silver Intermediary Material" was followed. The process included solvent vapor degreasing and silver plating of both sides of the sheet. Subsequent to plating, the plating thickness was measured at 50 $\pm$15 millionths of an inch at six places on each sheet. The sheets were stored in a container with an argon atmosphere until use.

Boron Fiber

Boron fibers wound on spools in approximately 6000 ft lengths were supplied by the Air Force Materials Laboratory. The mechanical properties of these filaments varied considerably with each spool. The presence of numerous splices required breaking the fiber to remove the apparently plastic splicing material which would have contaminated the diffusion process. A fiber diameter variation of 0.0032 to 0.0041 inches from a nominal 0.004 inch, was noted within a given spool.

The boron fibers were cleaned by immersion in a toluene solution, followed by a nitric acid bath and a subsequent distilled water rinse. This cleaning process was considered time consuming and did not ensure removal of all potential contaminants. In addition, nitric acid may degrade the boron fiber and cause a reduction in fiber strength. An experimental cleaning process was developed, utilizing dimethyl sulfoxide (DMSO) with nitric (HNO_3), followed by a distilled water rinse. While DMSO proves to be an exceptionally good solvent for both organics and inorganics when combined with nitric acid, it causes the nitric acid to react with the boron fiber at a higher attack rate as compared to nitric acid with water. However, the rate is dependent upon the solution concentration and temperature. Basic elements of an experimental cleaning system developed for "in-line" processing are illustrated in Figure 4.

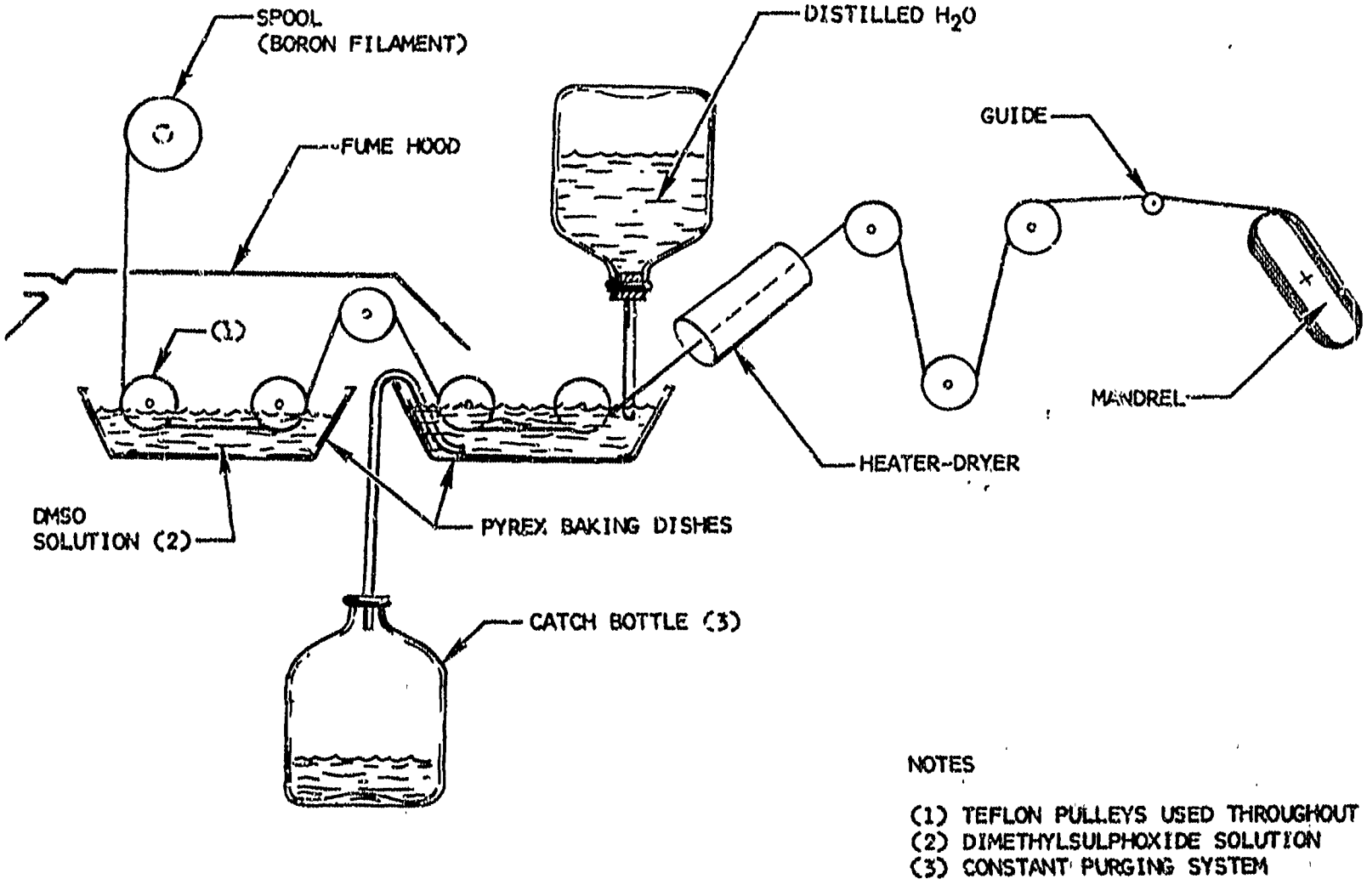


Figure 4. Experimental "In-line" Fiber Cleaning System

The effects of various cleaning agents and methods were investigated. Severe etching of the boron fiber occurred when the fiber was exposed to the DMSO cleaning solution for extended periods. Improved cleaning action was obtained when solution temperature was increased to 270°F and immersion time reduced to 30 seconds. Photos of results obtained from different time-temperature combinations are shown in Figure 5. Proper control of both the time and temperature parameters provides a potential solution for continuous, rapid and effective cleaning of boron fibers. The final distilled water rinse effectively removes all traces of the DMSO solution. Optical inspection, subsequent to the cleaning operation, was performed to determine: (1) cleanliness of the fiber, and (2) the presence of cracks or fractures which would weaken the fiber.

Tungsten Fiber

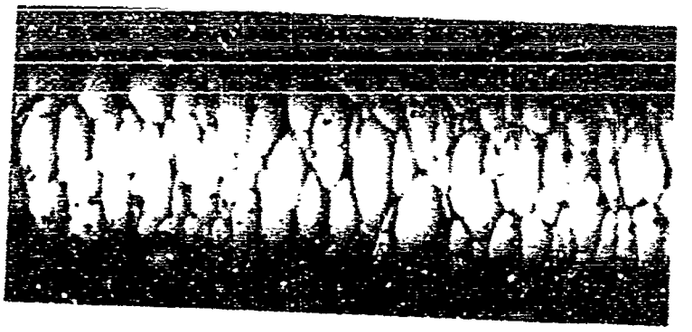
Tungsten fiber, G.E. type 218 Wire CS, 0.004-inch diameter, was used in continuous lengths. The fiber as applied to filament winding operation was quite satisfactory due to the high tensile strength and good uniformity in size. The fiber was factory cleaned with a caustic solution to remove the graphite drawing lubricant and in hydrogen atmosphere to remove oxides. The fiber was handled with cotton gloves subsequent to cleaning and was approved for use following inspection for contaminants prior to beginning specimen fabrication.

FILAMENT WINDING

Filament winding of the three types of composite specimens followed the same pattern in each case. The desired specimen size was approximately 5 x 10 inches. Mandrels measuring approximately 6 x 12-1/2 x 1-1/2 inches were prepared from 321 stainless steel. The mandrel ends were ground to a 1-1/2 inch radius. Mandrel surfaces were ground smooth and center-bored on the sides to fit the lathe chucks. Each mandrel was flame-sprayed prior to being mounted in the lathe in preparation for winding. All specimen materials had been previously cleaned and every effort was made to maintain cleanliness throughout the winding process. White cotton gloves were worn by the operators to protect the materials from contamination. The matrix sheets were affixed to both sides of the mandrel with elastic bands. A piece of 0.002-inch stainless steel foil was placed over each mandrel end, overlapping the matrix sheets by 1/2 inch. The foil covered the sharp edge of the matrix sheet and provided a smooth transition surface for the fiber.

The fiber spool was installed on a support fixture mounted on the motor driven lathe bed as shown in Figure 6. The lathe drive was adjusted for the appropriate number of fiber turns per inch depending on the desired fiber-matrix ratio. The fiber was then pulled over a rotating brake drum, through

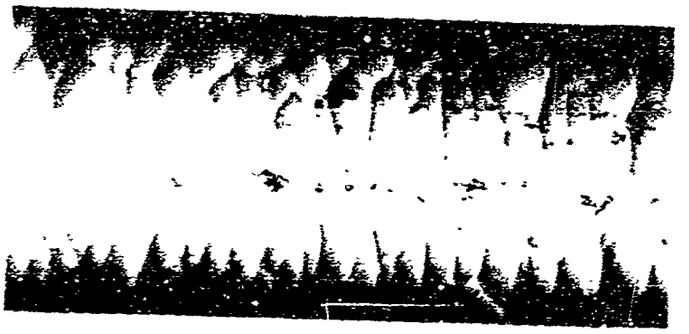
A. FIBER AS RECEIVED



B. FIBER CLEANED -
ROOM TEMP,
5 SEC DMSO,
5 SEC RINSE



C. FIBER CLEANED -
ROOM TEMP,
30 MIN DMSO,
5 SEC RINSE



D FIBER CLEANED
270° F 30 SEC DMSO,
5 SEC RINSE

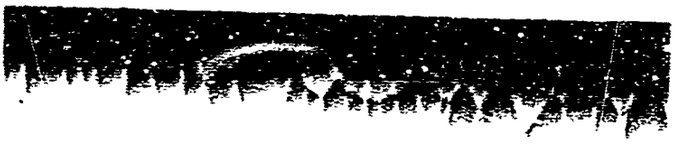


Figure 5. Photographs of Boron Fiber Showing Effectiveness of Cleaning, (750X)

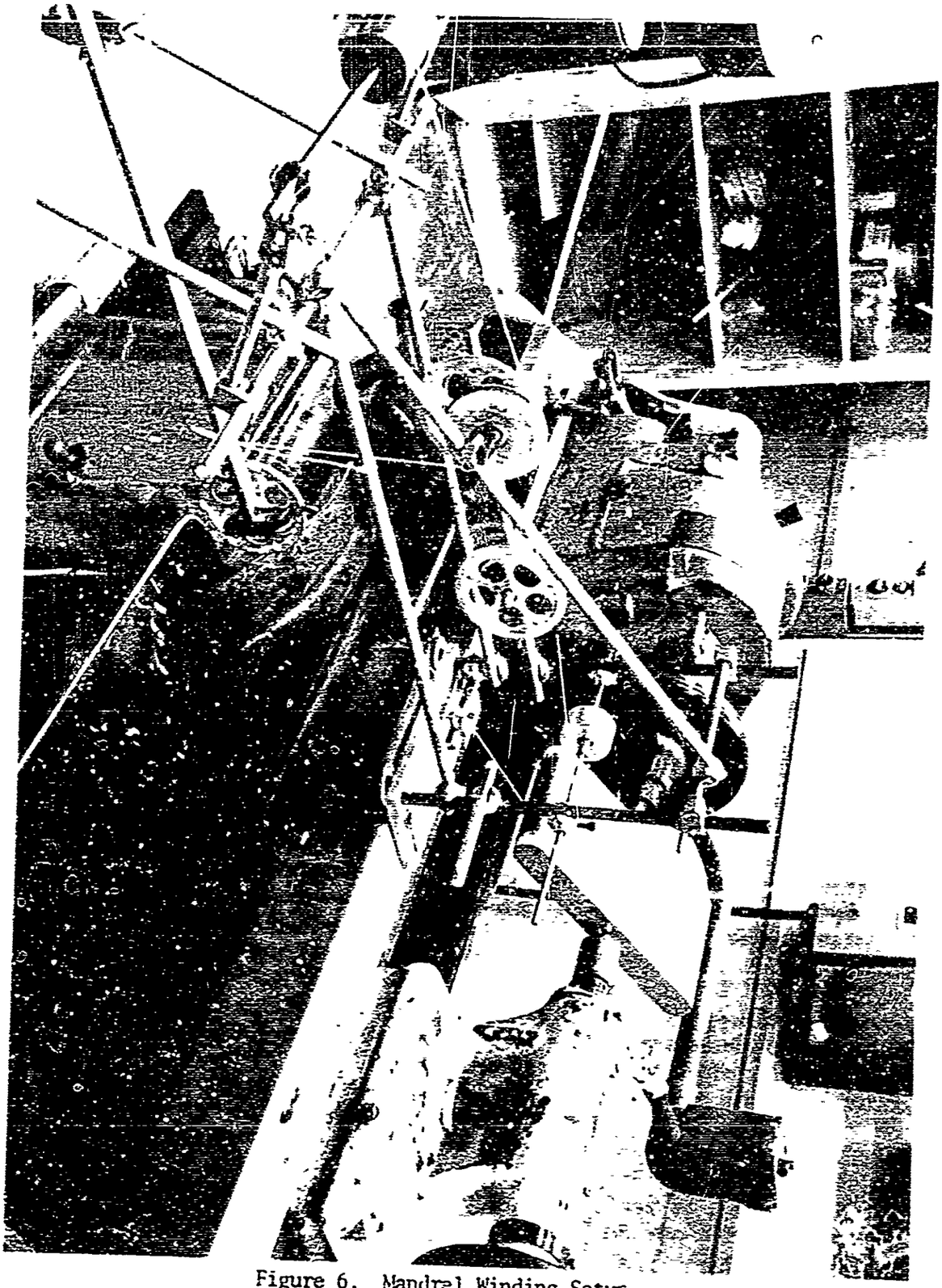


Figure 6. Mandrel Winding Setup

the guide pulleys and attached to the mandrel. Fiber attachment was made by tack welding a tab of foil over the wire to restrain it. Several turns of the mandrel were made manually to ensure fiber alignment and attachment. The lathe was then power driven at a preselected speed and runout to achieve the required fiber spacing. In the event of a fiber break or manufacturing splice, the lathe was stopped and the fiber end was secured with a foil tab tack welded to the mandrel end. Numerous boron fiber breaks were encountered with approximately one-third of the total fiber used. Breaks were generally attributable to a reduced diameter section in the boron fiber. This winding process exerts more strain on the fiber as compared to use of a round mandrel because the fiber feed speed is constantly changing from zero to a maximum. A form of dynamic braking was employed by supporting the fiber spool with a wax string passed over a fixed drum covered with teflon tape.

At the completion of the first filament wrap layer, additional matrix sheets and transition foil were added to the mandrel. The lathe was reversed and the next layer was wound. The filament wrapping was continued until the desired number of layers were completed except for the final layer. At this stage, the defect layer was introduced. The pre-prepared woven fiber mat with broken fiber defects was placed on the mandrel with a top matrix sheet. In the case of disbonds, the prepared alumina suspension was applied to the fiber on the mandrel. The matrix disbonds were prepared on matrix sheets and the sheets were installed in sequence.

DIFFUSION BONDING

After completion of the winding operation, the mandrel and the multiple layer composite were placed within a bonding retort. The retort was hydroformed to shape and fitted with a purge tube. The retort assembly is shown in Figure 7. The retort layup consists of two retort skins, glide sheets adjacent to the skins, with the filamentary composite in the center between glide sheets. The retort and tooling is 321 stainless steel. The glide sheets are either flame-sprayed with alumina and honed, or coated with hard anodized aluminum. The latter proved superior in terms of releasing the specimens subsequent to bonding, and was used during the winding process to separate specimens on a single side.

Layup of the retort materials and specimens on the mandrel was accomplished immediately after the winding. The retort was then evacuated to reduce contamination and stored for brief periods prior to bonding.

The retort, evacuated and sealed, was placed between the ceramic platens of a 500-ton hydraulic press. Two copper pressure plates were placed on either side of the retort to equalize the platen pressure. Thermocouples attached to the copper plates measure bond cycle temperatures. A steel glide sheet was

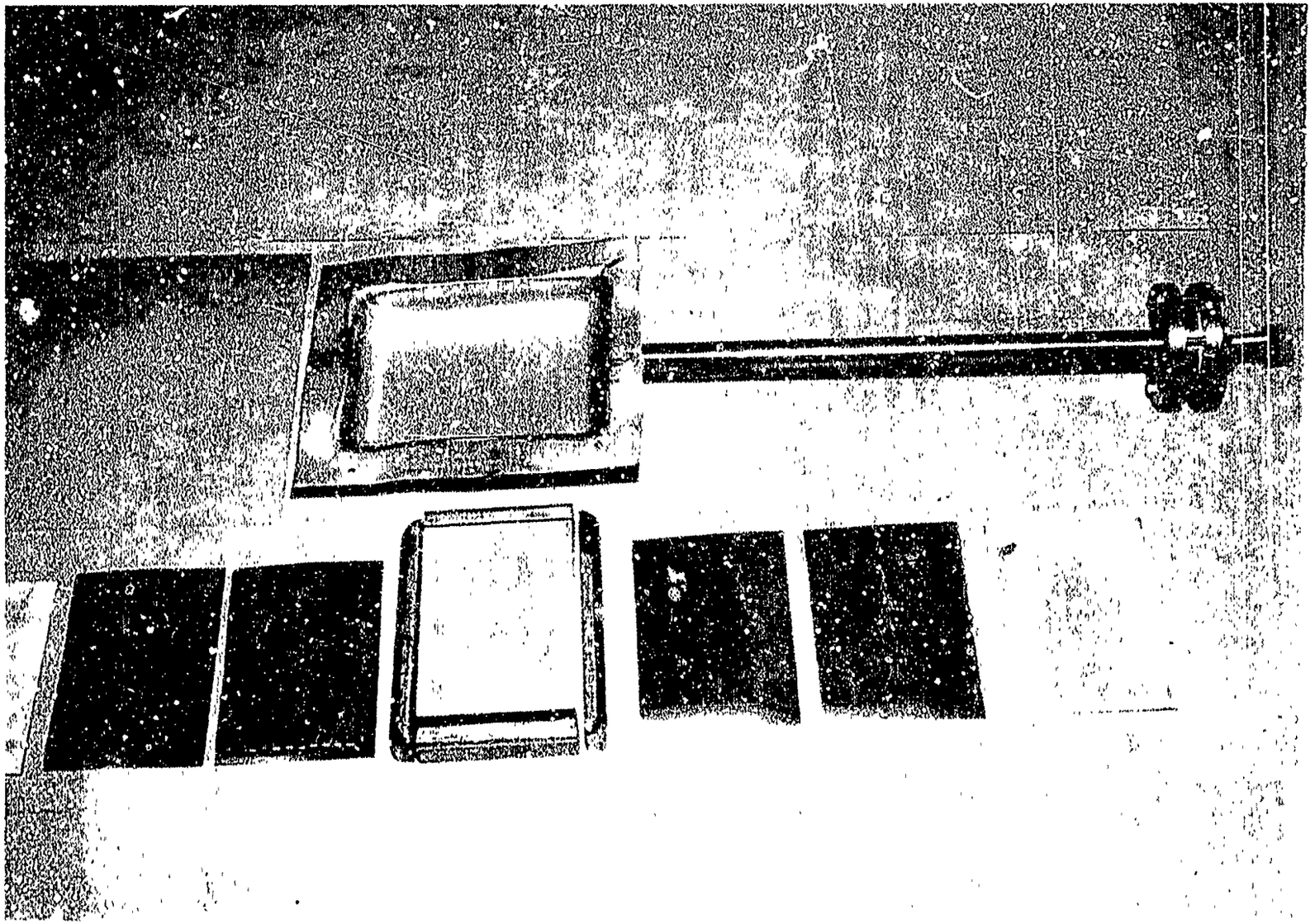


Figure 7. Retort and Layup for Diffusion Bonding

placed between the copper sheets and the platens. The retort was connected to a vacuum system. The two-inch line includes a Pirani gauge next to the retort, a discharge vacuum gauge and an inlet valve for the dry argon purge system. The vacuum system includes a liquid nitrogen cold trap, four-inch oil diffusion pump, and mechanical vacuum pump.

Kaowool ceramic fiber was placed around the retort and the platens for thermal insulation. The diffusion bond cycle is initiated by energizing the electrical resistive heated platens. At a selected temperature, the pressure is also applied. Figure 8 shows the hydraulic press platens and the ceramic fiber packed around the retort.

The diffusion-bonding parameters for the composites were selected from previous tests and analytical predictions of the matrix creep characteristics in relation to the fibers. After the bond cycle was completed, the heaters were turned off, and the composite allowed to cool slowly under bond pressure to room temperature, to minimize distortion and help relieve thermal stresses developed between the fiber and matrix materials.

The metal edges of the retort were cut with a mechanical shear. The mandrel was removed and the exposed fiber at the ends were cut, releasing the specimens. The mandrels were suitable for reuse, but the retorts were not salvageable.

During the composite fabrication, three of the boron-aluminum specimens were apparently incompletely bonded. These three specimens were separated by flame-sprayed alumina stop-off sheets and returned for a second diffusion bond cycle. Upon removal from the vacuum retort, two specimens were found bonded to the stop-off sheet. The specimens were badly damaged during removal and additional specimens were fabricated. In analyzing the inadvertent bonding to the stop-off sheet, it was determined that silver plating (approximately 40 microns thick) on the external surface of the aluminum face sheet had reacted with the alumina and bonded to the stainless steel stop-off sheet. For future bonding, it was planned that the external surfaces of the top and bottom aluminum matrix sheets would not be silver plated.

An alternative stop-off sheet design developed under a concurrent composite program (Reference 5) uses hard anodized aluminum sheets. This sheet was evaluated; the specimens were readily removed and were not encrusted with the transfer alumina present on earlier specimens.

COMPOSITE FABRICATION SUMMARY

The foregoing discussion has described the design and fabrication of the composite specimens. The completed specimens varied slightly from the original design requirements but were considered satisfactory for nondestructive evaluation. The actual composite specimen thicknesses and volume ratios are shown in Table II.

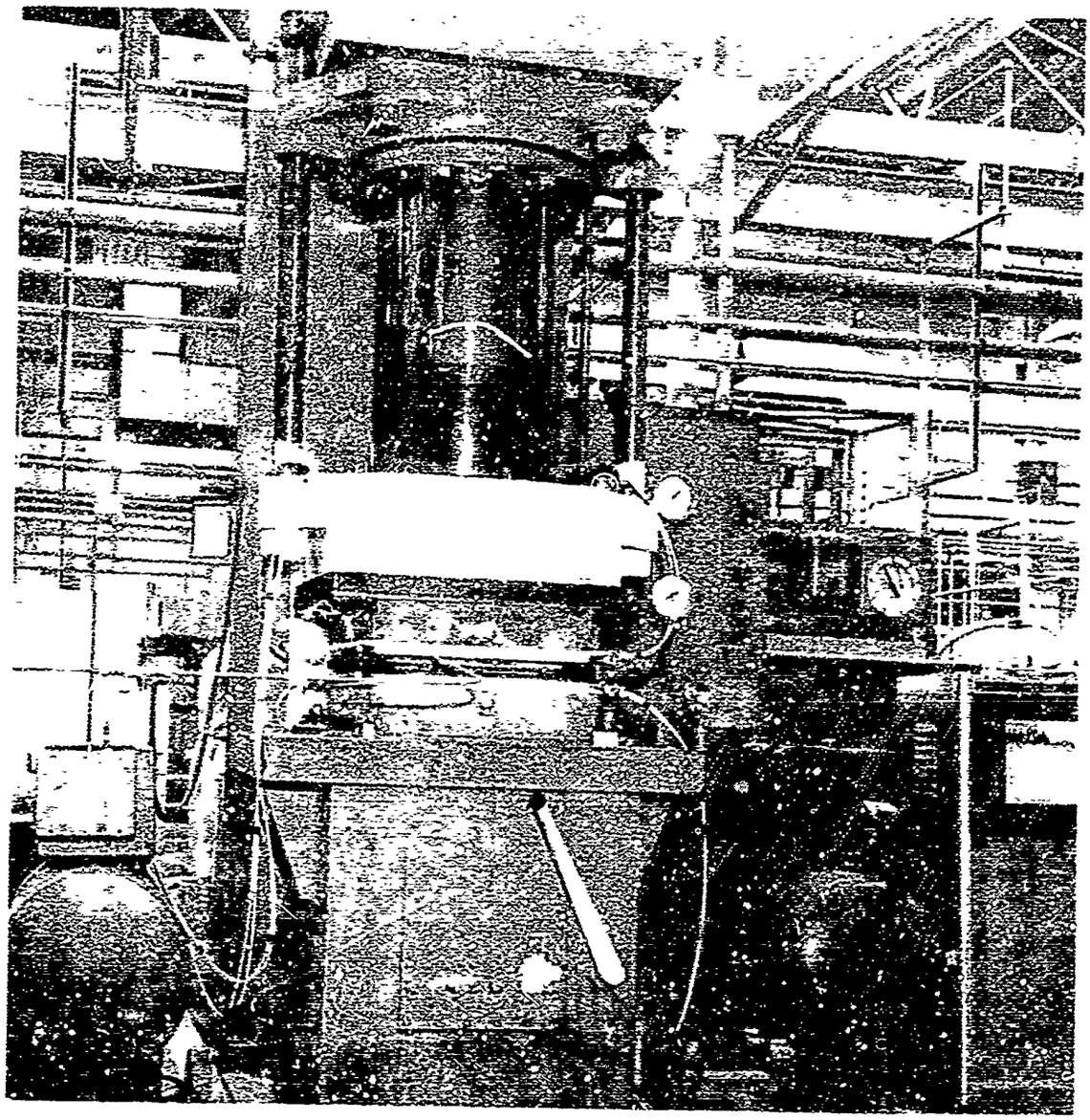


Figure 9. Diffusion Bonding Press

Table II

COMPOSITE SPECIMEN THICKNESS & VOLUME RATIO MEASUREMENTS

Specimen	Thickness (in.)		Volume Ratio	No. of Fiber Layers
	Measured	Required	Calculated %	
Tungsten-Copper				
10 BF	0.039	0.040	8.4	3
15 BF	0.043	0.040	13.4	4
20 BF	0.050	0.040	16.5	3
25 BF	0.051	0.040	23.1	4
15 PM	0.086	0.090	13.2	9
15 M	0.135	0.125	14.1	15
15 A	0.265	0.250	14.3	28
Boron-Titanium				
10 BF	0.056	0.040	8.1	3
15 BF	0.045	0.040	12.2	4
20 BF	0.061	0.040	13.0	3
25 BF	0.041	0.040	21.0	4
15 PM	0.087	0.090	13.4	9
15 M	0.133	0.125	13.7	14
Boron-Aluminum				
10 BF	0.056	0.040	9.8	3
15 BF	0.037	0.040	10.0	3
20 BF	0.040	0.040	12.5	4
25 BF	0.052	0.040	20.1	4
15 PM	0.082	0.090	13.1	8
15 M	0.145	0.125	11.4	14

Specimen Code: 10, 15, 20, 25 - Volume Ratio Percentage; BF - Includes Broken Fibers; PM - Lack of Fiber-Matrix Bond; M - Includes Matrix Voids; A - Fiber Misalignment.

METALLOGRAPHY

Metallographic inspection was performed on all composite specimens to determine the following characteristics: fiber distribution, fiber/matrix ratio, evidence of diffusion bond between fiber and matrix, and between matrices. Metallographic specimens were prepared by shearing one-half inch strips from the end of each composite specimen normal to the fiber length. These strips also contained portions of the foil used during filament wrapping to provide smooth transitional area; however, the foil did not interfere with the inspection.

The specimen strips were polished, etched and viewed on plane normal to the fiber length. Photographs were taken of each specimen at 10X, 150X and 500X magnification and are presented in Appendix I. The boron-aluminum 25 BF specimen was also cut in a plane parallel to the fiber length and viewed at 150X and 250X magnification.

The tungsten-copper specimens were polished with 600 grit silicon carbide paper and macro-etched with a hydrofloric-nitric acid solution. The fiber alignment and volume ratio were determined by optical inspection using a Bausch and Lomb Metallograph. The specimens were again polished with 600 grit paper and given a microfinish with a Syntron Vibratory Polisher and then etched with an ammonium persulfate solution. Upon subsequent inspection at increased magnification, it was concluded that satisfactory bonding, fiber alignment and fiber/matrix volume ratio were achieved for nondestructive testing evaluation.

The boron-titanium composite specimens were cross-sectioned in a Radiac with a water cooled carborundum wheel and rough ground on a 150 grit silicon carbide sanding belt. Further grinding was done using water cooled silicon carbide papers of 320, 400, and 600 grit. Because the hardness of titanium differs greatly from boron, a special polishing technique was employed. The specimen was polished on a nylon fabric covered vibrating table using 0.3 micron alumina powder and distilled water. The specimen was weighted and polished for three hours, etched with a 10 percent nitric acid solution, flushed with ethanol, and air dried.

The boron-aluminum specimens proved extremely difficult to prepare for metallographic inspection due to the extreme difference in hardness of the boron and softness of the aluminum. The polishing process finally adopted was as follows: Initial rough grinding of specimens was accomplished on a water cooled, 150 grit silicon carbide sanding belt. Subsequently, the specimens were ground progressively on 320, 400, and 600 grit silicon carbide paper. After completion of the grinding operations, the specimens were polished on a Syntron vibratory polisher using a slurry of Linde A alumina polishing powder with a nylon polishing cloth for a period of three hours. This produced a minimum of relief between the boron and aluminum. The specimens were then polished

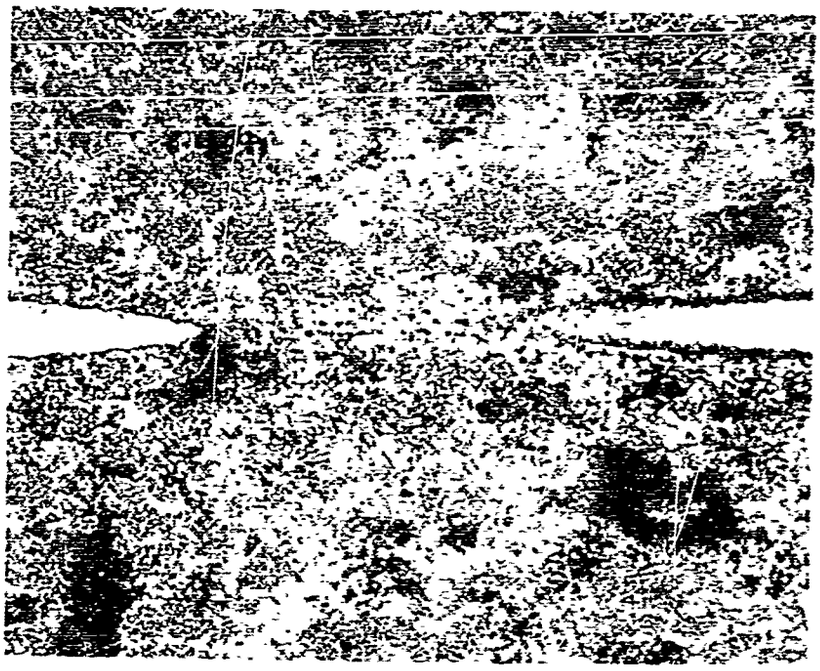
on a stationary lap covered with a Gamal cloth, which was impregnated with 14 micron diamond paste, to remove any pitting. Relief between the boron and aluminum was produced at this point and specimens had to be polished for an additional eight hours on the vibratory polisher. Final polishing was accomplished on a stationary lap covered with a Gamal cloth impregnated with one micron diamond paste. Etching was done with Kellers etch. The microphotographs shown in Appendix I represent results obtained after using this process.

Preparation of the micro specimen cut in the plane of the fibers was done by a further improvement in the polishing method. After grinding on the 150 grit silicon carbide belt, the specimens were polished on a lead lap with extremely fine boron carbide powder. This was followed with Syntron vibration polishing for eight hours, and final hand lapping on a one micron diamond cloth. The specimens were etched, rinsed and photographed at 150X and 250X magnification (Figure 9). A distinct improvement was noted in specimens prepared by this method although some evidence of aluminum gouging and relief still occurs. Although additional work on the polishing process would be beneficial, the method is satisfactory for the intended purpose. Better metallurgical resolution might be achieved by electropolishing or ion etching techniques.

Representative specimens of the W-Cu, B-Ti, and B-Al composites were examined by means of a Hitachi HU-11 Electron Microscope. Replicas of the micropolished specimens were studied in detail and representative photographs (included in Appendix I) were taken at 5600X and 32,000X magnification. The two-stage replica method employed in specimen preparation is described below.

A cellulose-acetate sheet was softened on one side with an acetone-cellulose acetate solution. The soft side was pressed by hand onto the micro specimen and held until the cellulose-acetate partially hardened. After the replica was thoroughly dry, it was carefully stripped from the specimen and mounted face up in a vacuum evaporator. At a vacuum of 10^{-5} torr, platinum-carbon was evaporated at a shadowing angle of 30 degrees. Carbon was then deposited normal to the replica surface while the replica was revolved for complete film formation over its rough surface. The composited replica was then removed from the vacuum chamber and the plastic dissolved by submersion in acetone. The remaining carbon-platinum shadowed carbon replica was collected on a microscope grid for examination in the electron microscope.

The photographs of the W-Cu specimen showed evidence of polishing marks and minor dirt spots. The fiber-matrix juncture is clearly seen. The B-Al photographs show the boron-aluminum juncture and the aluminum matrices juncture. An amount of carbon socking is seen in the cracks due to specimen surface roughness. The B-Ti photograph showed the fiber matrix juncture, particles of boron displaced in the matrix, and carbon socking. Direct replicating could improve the appearance of the specimen.



250X



150X

Figure 9. Boron-Aluminum Specimen - Metallographic Inspection of Section Parallel to Fibers

Section V

RADIOGRAPHIC INSPECTION

TECHNICAL APPROACH

Both broad and narrow beam x-ray inspections were performed on the three types of composite specimens. The Seifert Industrial X-Ray Unit, "Isovolt 300" was used for the source of the x-ray beam. The x-ray unit has a twin focus capability, two-pole operation, and both broad beam and narrow beam radiographic performance. The target to film distance was maintained at 44 inches for all broad beam testing, to obtain maximum resolution. For the same reason, the smaller available diameter target focal spots were used although the maximum current was limited and longer exposure times were required. Exposures were made with the standard Eastman Kodak Company Type M double emulsion film and the high resolution but slower Type R single emulsion x-ray film. The films were all developed by manual methods in a standard Eastman Kodak developer in accordance with the manufacturer's recommended process.

Narrow beam radiography was conducted with a lead collimator over the outlet port of the x-ray head. The 2-1/4 inch thick collimator had a bore 1/2 inch by 1/4 inch. The plate and film were placed on a traversing-indexing mechanism (normally used for ultrasonic inspection). Specimen to focal spot distance was 9-1/2 inches and the 4 mm focal spot was used. Preliminary studies were made to investigate the scanning rate requirements. The slowest rate of travel is 7.5 cycles per minute with an approximate 0.05 inch index travel per cycle. At this rate, the 5 x 10 inch specimens were scanned in approximately 20 minutes. The test system and collimator are shown in figures 10 and 11.

Preliminary tests designed to study the techniques of defect simulation were carried out on two tungsten-copper specimens, each 0.050 inches thick and both of which contained 10 percent and 25 percent volume ratio (nominal) sections. This specimen was radiographed under various voltage, current and exposure time conditions. The results were evaluated for possible improvement of defect detectability. Table III shows the test conditions and the radiographic results. Photographic prints of the radiographs are shown on Appendix II, Figures 67 to 78. Optimum results were obtained at 90 KV, 3.5 ma, 2 mm target and 4.5 minute exposure for the simultaneous detection of broken or misaligned fibers in the two sections. The 150 KV exposures were best for photographic prints and resolution details within the specimen.

For subsequent composite specimens, the optimum exposure conditions were determined by making exposures for 5 to 8 voltages varying in steps of not more than 10 KV and for at least three exposure conditions. In the discussion of results, only the optimum conditions are considered, which have been selected from 100 to 150 trial radiographs for each composite specimen type.

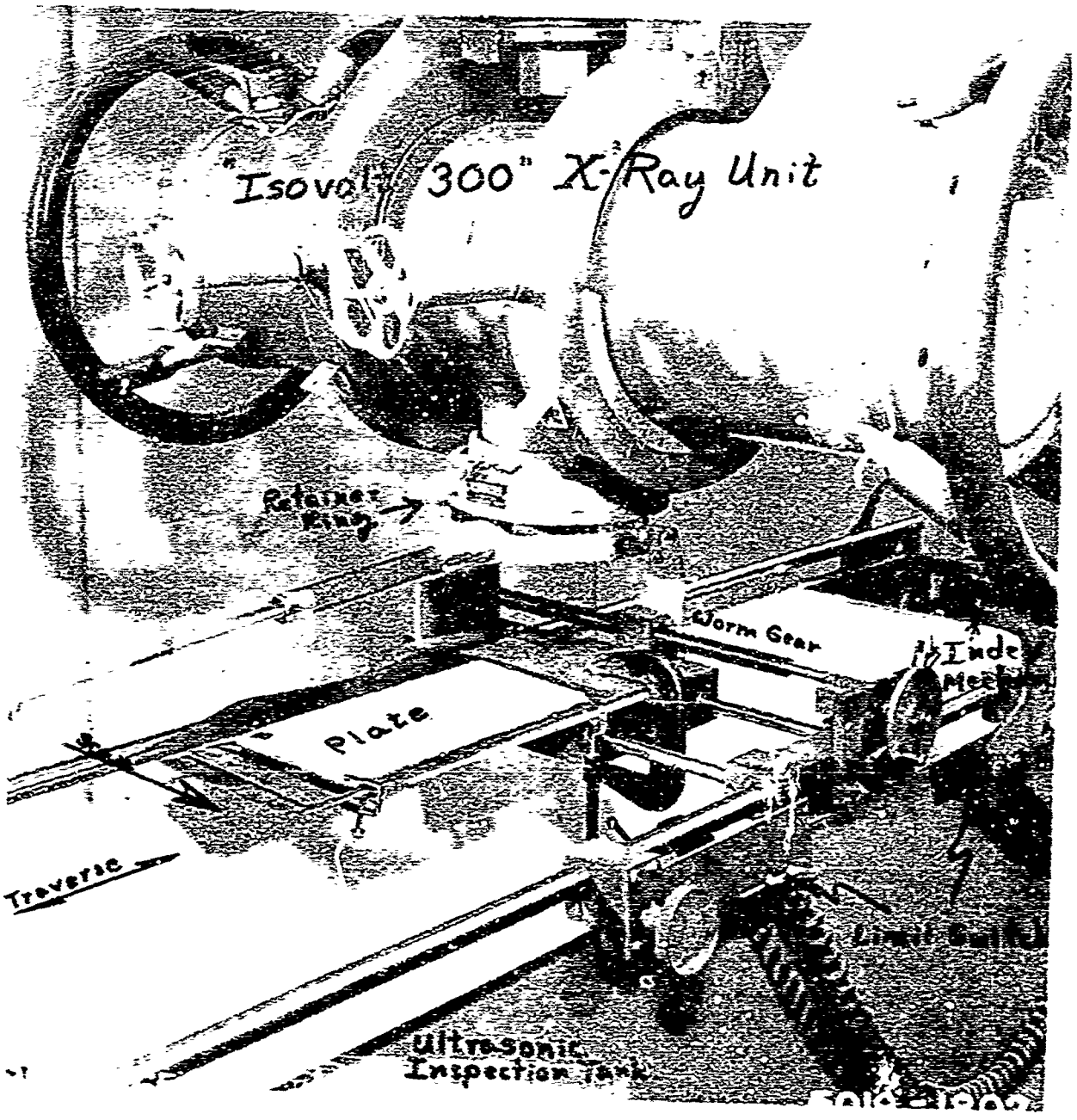


Figure 10. "In-motion" Narrow-beam Radiograph Assembly

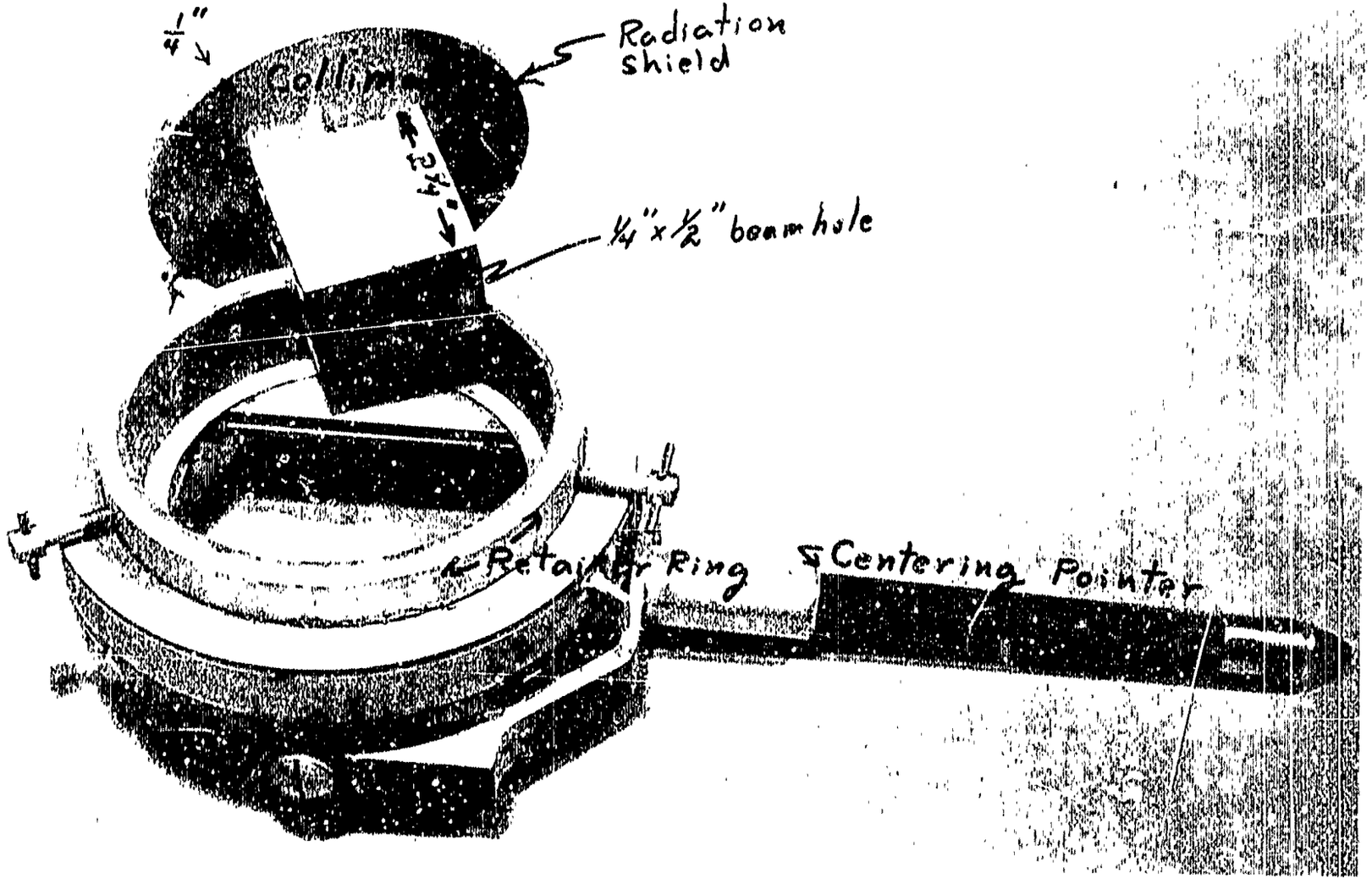


Figure 11. Collimator Assembly

Table III

RADIOGRAPHIC INSPECTION OF TUNGSTEN-COPPER 10/25BF
EVALUATION SPECIMENS

Figure No.*	Voltage (KV)	Current (ma)	Focal Diameter (mm)	Exposure Time (min)	REMARKS
B-1	75	10	4	2	Fiber detail obscurred; specimen edges without fiber layers clearly defined.
B-2	80	10	4	2	10 percent fiber area resolution improved.
B-3	80	3.5	2	6	Longer exposure and smaller target greatly improves 10 percent area resolution.
B-4	90	3	2	4.5	Radiograph slightly under exposed; best resolution of 10 and 25 percent areas.
B-5	100	3.5	2	4	Same as above, with slight loss of 10 percent area detail.
B-6	170	4	2	2.5	Used 0.005 inch thick lead screen under film; major loss of detail.
B-7	150	3.75	2	6	Type R film and lead screen used; good resolution in 25 percent area only.
B-8	150	3.5	2	3	Exposure optimized for 25 percent area; single fiber breaks evident on negative.
B-9	90	3.75	2	10	Specimen turned over; results similar to B-4, above.
B-10	90	3.75	2	6	Lead screens, both sides, with significant overall loss of resolution.
B-11	90	3.75	2	6	Lead screen below film; no apparent improvement.
B-12	150	3.75	2	1.75	No screens used; results similar to B-4, above.

*Photographs, Appendix II

PENETRAMETERS

Three basic types of penetrameters were developed for establishing radiographic sensitivity levels for fiber matrix composites. The penetrameter design considered the detection sensitivity of the two types of fiber materials as related to the respective matrix material.

Two forms of fiber penetrameters were constructed by casting the fibers in a plastic form. The first form contained 0.002, 0.003, and 0.005 inch diameter fibers positioned to form right angles. The second form of fiber penetrameter used six 0.004 inch diameter boron or tungsten fibers positioned in a fan form spaced five degrees apart and convergent at the center. Figure 12 is a photograph of one of the fan penetrameters approximately 1/4 inch thick by 5-1/2 inch diameter. The fibers all pass through a common point and fan out at five degrees increments. Figure 13 shows a radiograph taken of the penetrameter positioned over the matrix material. Radiographs were taken at 90, 110, and 130KV tube voltages. Good detail is shown at the higher voltages.

Since little was known about the effect of boron in radiography, a number of elemental chunks of pure boron were procured for penetrameter application. The chunks were first rough polished to tapered forms, cast in plastic and finish polished. These tapered sections were subsequently inspected radiographically. However, little information could be obtained due to the comparative gross thickness of the boron.

A form of step penetrameter was prepared using the matrix material. A 0.005 x 1/4 x 6 inch foil strip was obtained of pure copper, titanium and aluminum. The foil was drilled with four holes ranging from 0.0037 to 0.010 inch diameter. The strips were adhesive bonded to 1/4 inch thick sheet stock of the same material. Figures 14, 15 and 16 show these strips and related microphotographs at 250X magnification of the holes. The holes were remarkably well formed considering the use of mechanical drilling. The foil penetrameters were checked radiographically at up to 100 KV without detecting the presence of the holes. Some data was obtained at 150 KV; the fiber fan penetrameter was centered over the largest hole to determine the capability of simultaneous detection. The result was negative.

The foil strip penetrameters were subsequently used in the composite specimen inspection. The copper penetrameter was placed beside the tungsten-copper specimen during broad beam radiographic inspection. Inconclusive data were obtained to relate the penetrameter information to the specimen defect detection sensitivity.

RADIOGRAPHY OF TUNGSTEN-COPPER COMPOSITE

Radiographic test conditions are shown in table IV. Both Eastman Kodak Type M and R film were evaluated. Photographs of the radiographic negatives

PENETRAMETERS

Three basic types of penetrameters were developed for establishing radiographic sensitivity levels for fiber matrix composites. The penetrameter design considered the detection sensitivity of the two types of fiber materials as related to the respective matrix material.

Two forms of fiber penetrameters were constructed by casting the fibers in a plastic form. The first form contained 0.002, 0.003, and 0.005 inch diameter fibers positioned to form right angles. The second form of fiber penetrameter used six 0.004 inch diameter boron or tungsten fibers positioned in a fan form spaced five degrees apart and convergent at the center. Figure 12 is a photograph of one of the fan penetrameters approximately 1/4 inch thick by 5-1/2 inch diameter. The fibers all pass through a common point and fan out at five degrees increments. Figure 13 shows a radiograph taken of the penetrameter positioned over the matrix material. Radiographs were taken at 90, 110, and 130KV tube voltages. Good detail is shown at the higher voltages.

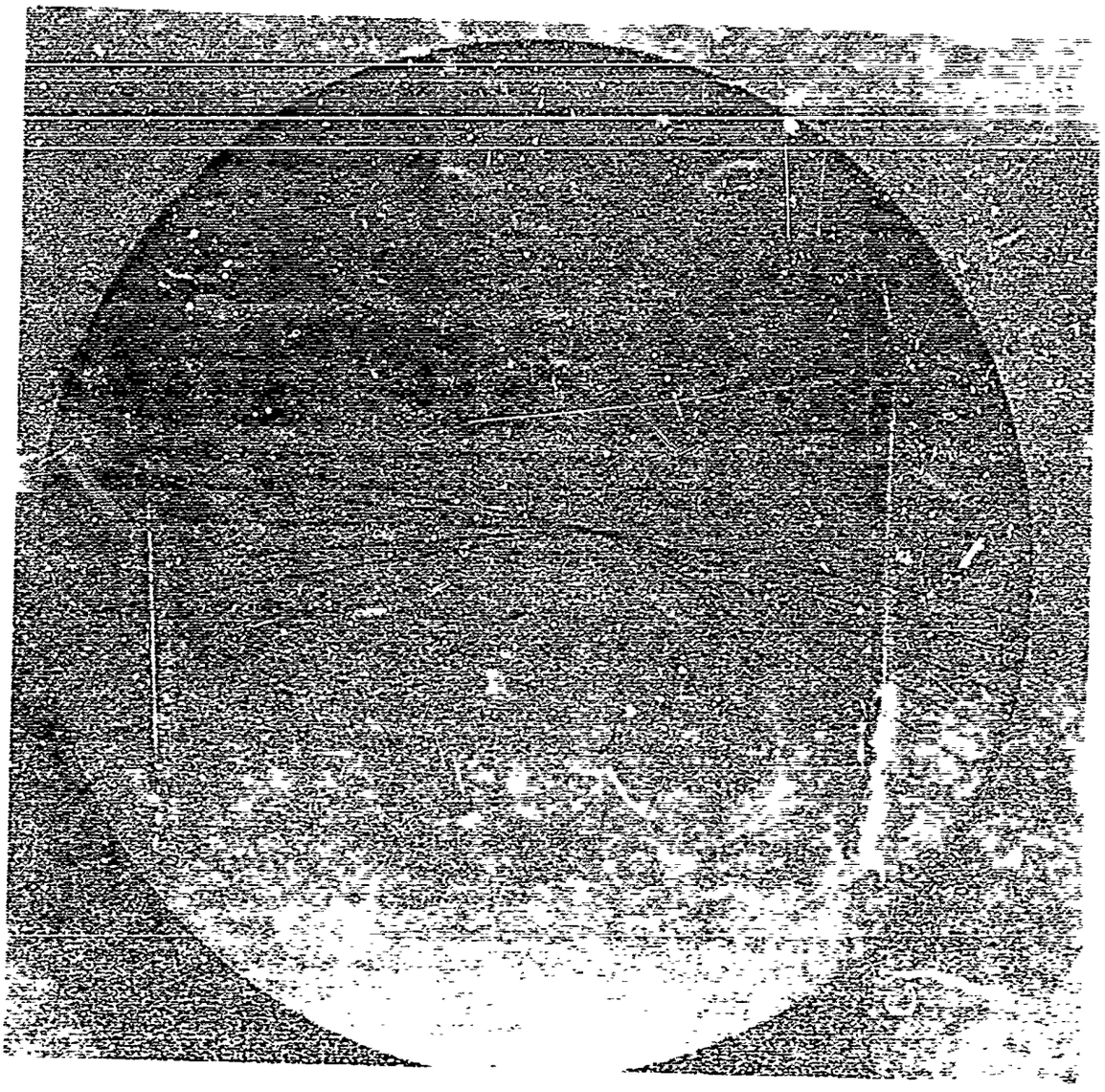
Since little was known about the effect of boron in radiography, a number of elemental chunks of pure boron were procured for penetrameter application. The chunks were first rough polished to tapered forms, cast in plastic and finish polished. These tapered sections were subsequently inspected radiographically. However, little information could be obtained due to the comparative gross thickness of the boron.

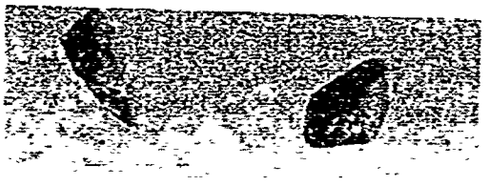
A form of step penetrameter was prepared using the matrix material. A 0.005 x 1/4 x 6 inch foil strip was obtained of pure copper, titanium and aluminum. The foil was drilled with four holes ranging from 0.0037 to 0.010 inch diameter. The strips were adhesive bonded to 1/4 inch thick sheet stock of the same material. Figures 14, 15 and 16 show these strips and related microphotographs at 250X magnification of the holes. The holes were remarkably well formed considering the use of mechanical drilling. The foil penetrameters were checked radiographically at up to 100 KV without detecting the presence of the holes. Some data was obtained at 150 KV; the fiber fan penetrameter was centered over the largest hole to determine the capability of simultaneous detection. The result was negative.

The foil strip penetrameters were subsequently used in the composite specimen inspection. The copper penetrameter was placed beside the tungsten-copper specimen during broad beam radiographic inspection. Inconclusive data were obtained to relate the penetrameter information to the specimen defect detection sensitivity.

RADIOGRAPHY OF TUNGSTEN-COPPER COMPOSITE

Radiographic test conditions are shown in table IV. Both Eastman Kodak Type M and R film were evaluated. Photographs of the radiographic negatives





Boron Specimen

Figure 12. Radiographic Fan-form Penetrameter

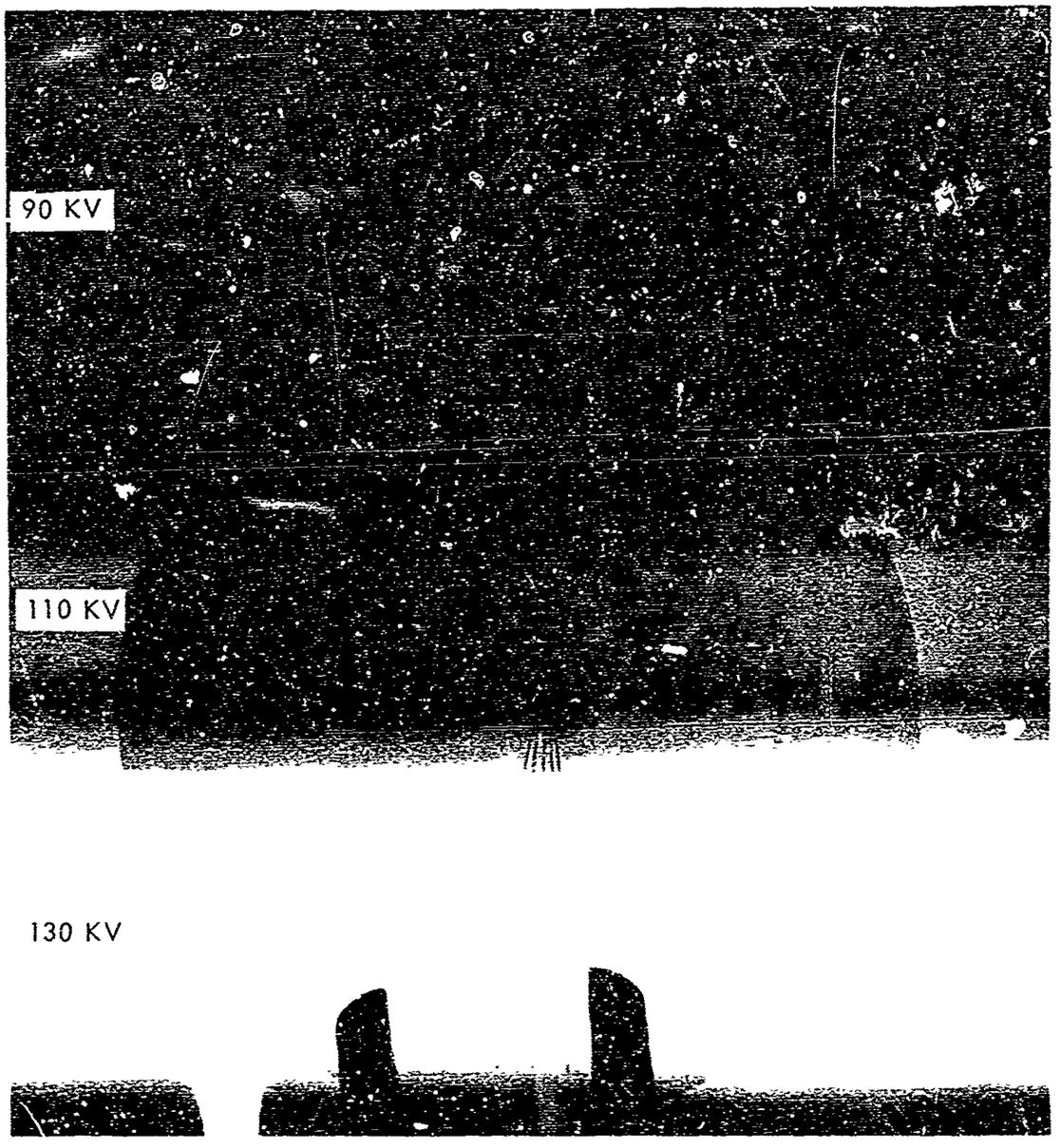
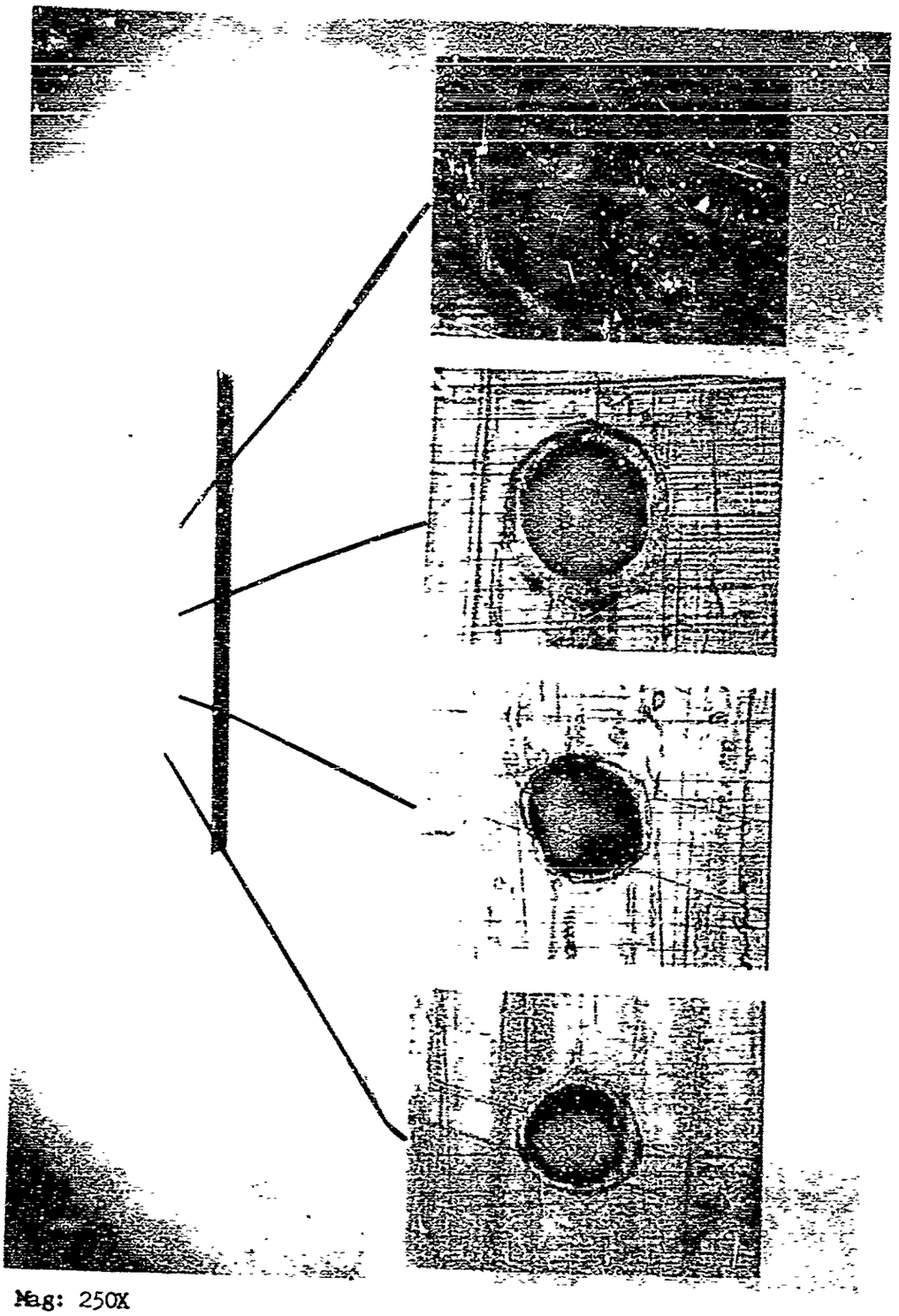
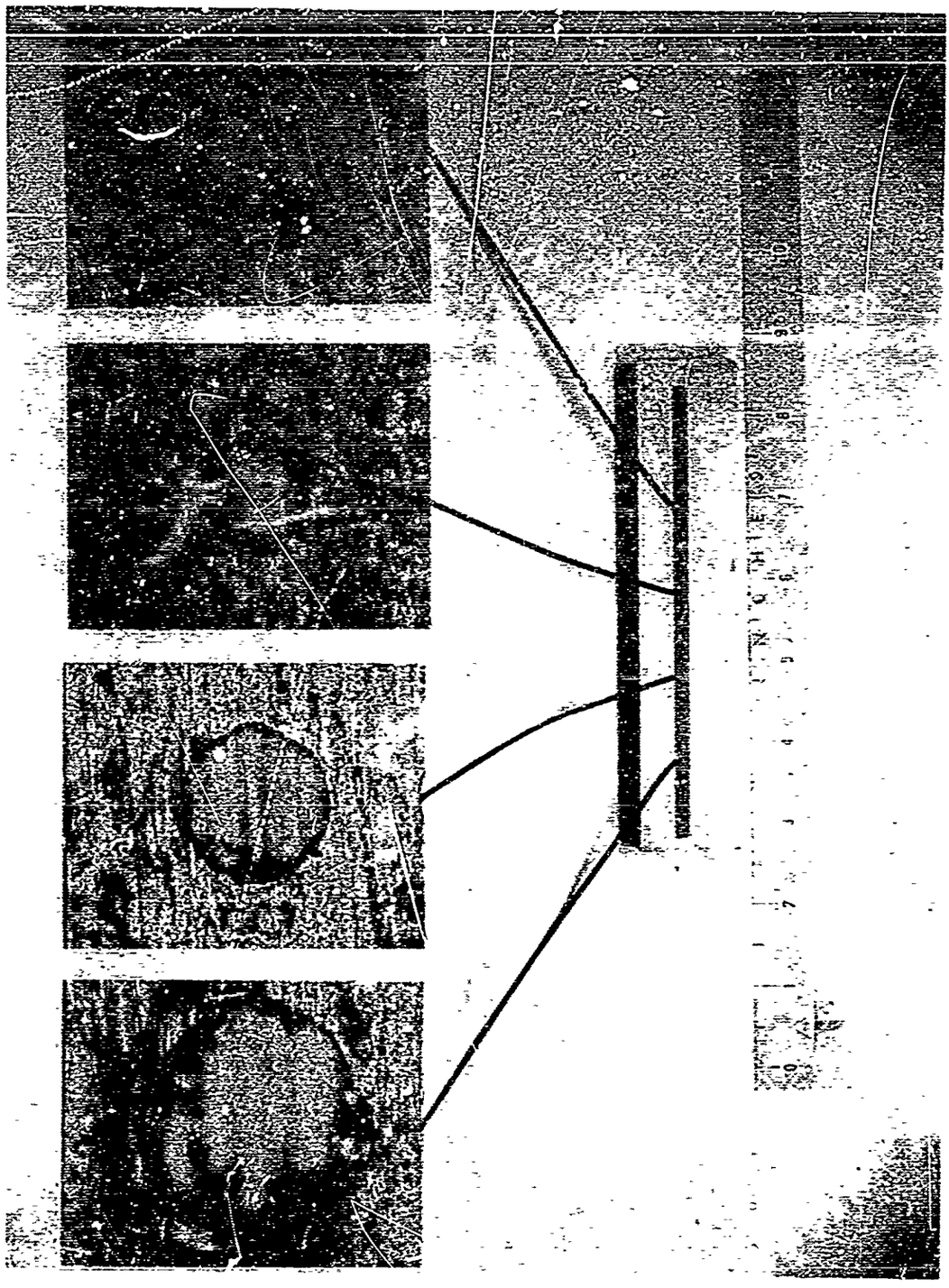


Figure 13. Radiographic Penetrameter at 90-, 110-, and 130 KV



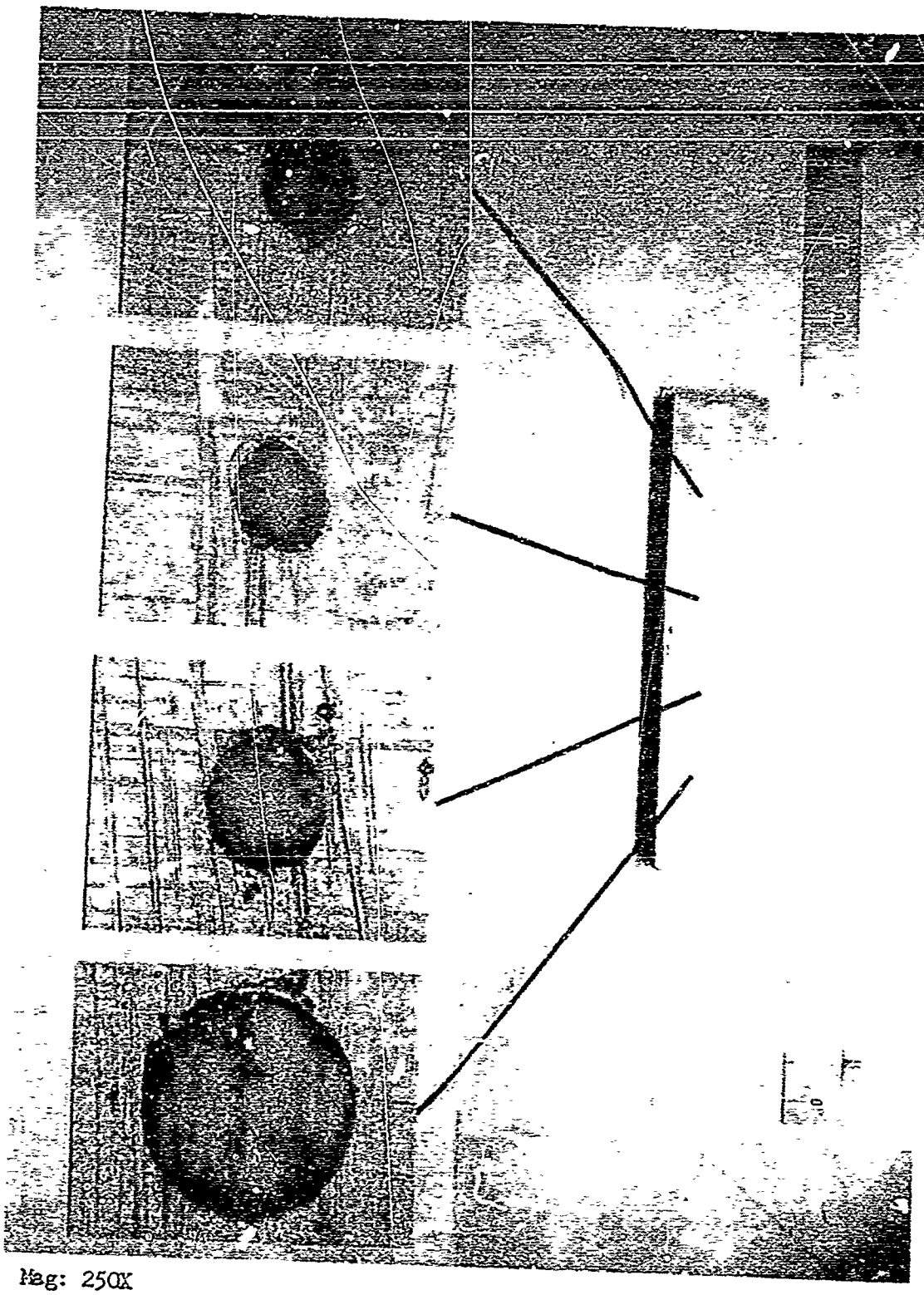
Mag: 250X

Figure 14. Penetrameter - Copper Foil



Mag: 250X

Figure 15. Penetrameter - Titanium Foil



Mag: 250X

Figure 16. Penetrameter - Aluminum Foil

are presented in Appendix II. The following discussion describes the radiographic inspection of the tungsten-copper, boron-titanium, and boron-aluminum composite specimens.

Table IV

RADIOGRAPHIC DATA FOR TUNGSTEN-COPPER SPECIMEN INSPECTION

Specimen Identification	Method	Film Type*	Tube Potential	Exposure Time-Min	Focal Spot Diameter	Focal Spot Film Distance
10BF	Broad Beam	M	150 KV	1.25	1.2 mm	45 in.
15BF	Broad Beam	M	150 KV	1.75	1.2 mm	45 in.
15BF	Broad Beam	R	150 KV	6	1.2 mm	45 in.
15BF	Broad Beam	R	150 KV	10 sec	4.0 mm	9 1/2 in.
20BF	Broad Beam	M	170 KV	2	1.2 mm	45 in.
25BF	Broad Beam	M	190 KV	2.25	1.2 mm	45 in.
15FM	Broad Beam	M	170 KV	2.25	1.2 mm	45 in.
15M	Broad Beam	M	190 KV	4	1.2 mm	45 in.
15A	Broad Beam	M	250 KV	10	1.2 mm	45 in.

*All M film was double emulsion, while all R film was single emulsion.

Broken Fiber Defect Detection

Examination of the x-rays for the four W-Cu specimens 10, 15, 20, and 25 BF clearly shows all deliberately introduced fiber breaks. A number of misaligned fiber ends and short pieces of loose fiber are also visible in the x-rays; these are outlined in black on the radiograph positive prints. There is also evidence of striation in the specimen, i.e., a dense strip approximately 1/4 x 5 alternating with a less dense strip across the length of the specimen. This striation is the result of bunching of the fibers and is shown by the

pattern changes from a slat form to a herringbone form with increasing tungsten content; the striations do not appear in the RM, M, and A specimen x-ray prints. In the prints of the 10 BF and 25 RF specimens, it appears that the fibers following the series of five breaks have pushed together creating a dense overlap. All x-rays show individual fibers in broken or misaligned conditions. The radiographs also indicate that the narrow beam radiography provides a better image than broad beam, and Type R film is better than Type M film; however, the quality of the Type M film is sufficient for this examination, with significant time savings.

The radiograph of the W-Cu Specimen 15 A shows only a slight fiber misalignment. This misalignment appears as unusual density variation in the specimen.

Film exposures were made by the broad beam method on both Type M double emulsion film and Type R single emulsion film. Stationary method narrow beam exposures were made of the defect areas on Type R single emulsion film. The defect areas for all three radiographic techniques were enlarged to 10X magnification, and printed as positives for further evaluation of test techniques. Examination of the film demonstrated the superior image sharpness or clarity of the broad and narrow beam techniques on Type R film as compared to the broad beam technique on Type M film. The difference between image sharpness for the broad and narrow beam techniques was at best slight, with the narrow beam technique exhibiting the sharper film images. However, it must be noted that all three methods were equally effective in disclosing the actual defect conditions.

Disbond Defect Detection

Three areas of the radiograph of W-Cu Specimen 15 RM showing lack of fiber-matrix bond are visible on the x-ray film. The disbond areas appear as a slightly more dense area than the surrounding view. This density difference results from the alumina used to create the deliberate disbonds.

The areas of matrix disbond on W-Cu Specimen 15 M are visible on the radiographic film and the film positive prints. The fiber misalignment is evidently the result of manufacture of the disbonds and shows the relief apparent on the x-ray film.

Film exposure on W-Cu Specimen 15 BF was made by the broad beam method on both Type M double emulsion film and Type R single emulsion film. Stationary method narrow beam exposures were made of the defect areas in this specimen on Type R single emulsion film. The defect areas for all three radiographic techniques were enlarged to 10X magnification, and printed as positives for further evaluation (Figures 17 and 18). Examination of the figures demonstrated the superior image sharpness or clarity of the broad and narrow beam techniques on

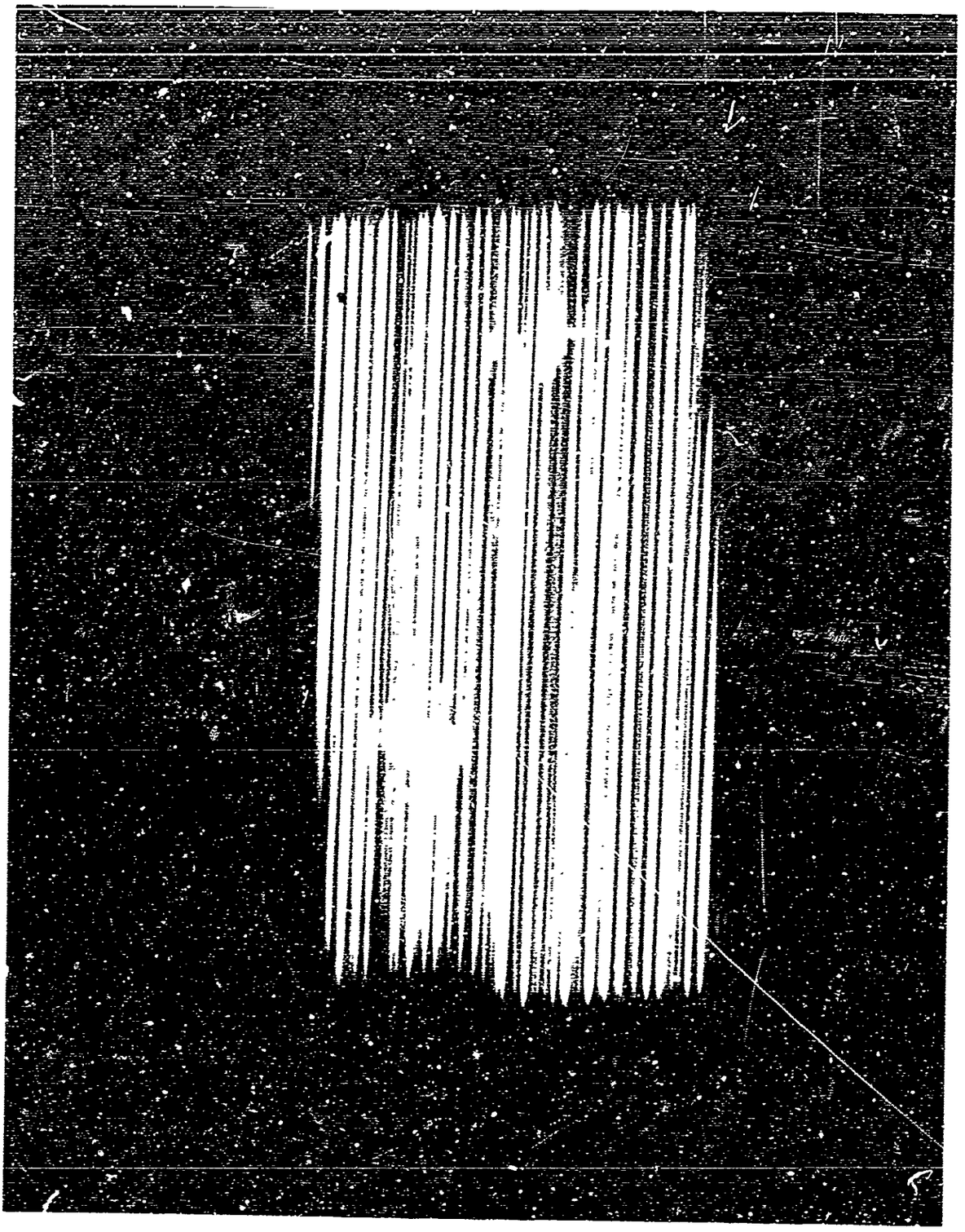


Figure 17. Tungsten-Copper 15BF Narrow Beam Radiograph at 10X Enlargement, Type M Film

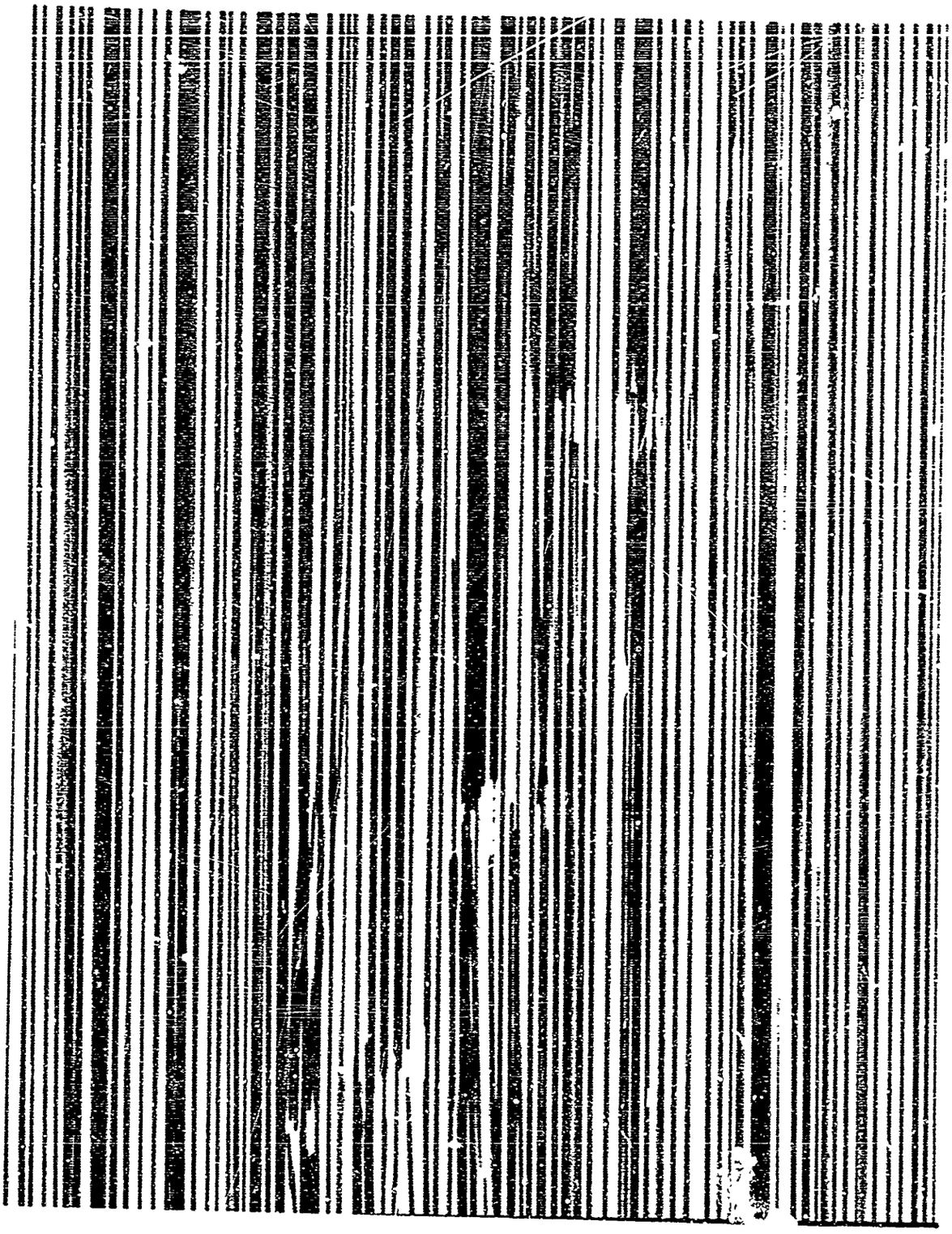


Figure 18. Tungsten-Copper 15EF Broad Beam Radiograph at 10X Enlargement, Type R Film

Type R film as compared to the broad beam technique on Type M film. The difference between image sharpness for the broad and narrow beam techniques was at best slight with the narrow beam technique exhibiting the sharper film images. However, all three methods were equally effective in disclosing the actual defect conditions.

Stereo Radiography

A stereo radiograph was made of W-Cu Specimen 15 BF using Type R double emulsion film (developed manually in Kodak Rapid X-Ray Developer at 68.F for five minutes). Lead screens, 0.005 inch thick, were used both in front and back of the films. The films were exposed for a period of six minutes with the x-ray tube operating at 150 KV with the small target and maximum current. Initially, the x-ray tube was centered approximately 47 inches above the specimen; the tube was then moved 12 inches to the left, and tilted to an angle of 10° toward the specimen. The right-hand photo was made in a similar manner. The x-ray films and photographic prints of the films were both viewed in three dimensions with a GE Medical Stereoscope. The pictures were mounted with 14 inches center displacement and viewed with the eyes about 13 inches from the plane of the prints. An unsuccessful attempt was made to enlarge a section of the stereo x-ray film by 10X and to view a section in stereo. Figures 19 and 20 show left and right stereo views of the W-Cu 25 BF specimen. They can be viewed stereographically by placing them side by side about 14 inches apart and using a simple stereo device or cardboard sheet between the eyes. Such observation indicates that the fiber breaks are located in the bottom layer of the specimen.

RADIOGRAPHY OF BORON-TITANIUM COMPOSITE

The boron-titanium specimens were inspected by broad beam radiographic techniques. Initial tests were made using both Eastman Kodak Company Type M double emulsion x-ray film and Type R double emulsion x-ray film. The x-ray mass absorption coefficients of boron and titanium are much closer than for the tungsten-copper specimens; therefore, the superior resolution of the Type R film relative to the more standard Type M became significant. The electron density of the boron-titanium specimens is considerably lower than the tungsten-copper specimens. Therefore, lower beam energies and much shorter exposure times could be employed. For these reasons, Type R double emulsion x-ray film was selected for inspecting the boron-titanium specimens. Lead screens, 0.005 inches thick, were used at the back of all films. Lead screens this size cannot be used in front of the films for tube energies less than 150 kilovolts.

The preliminary inspection of these specimens paralleled that of the tungsten-copper where a series of trial exposures were made to determine

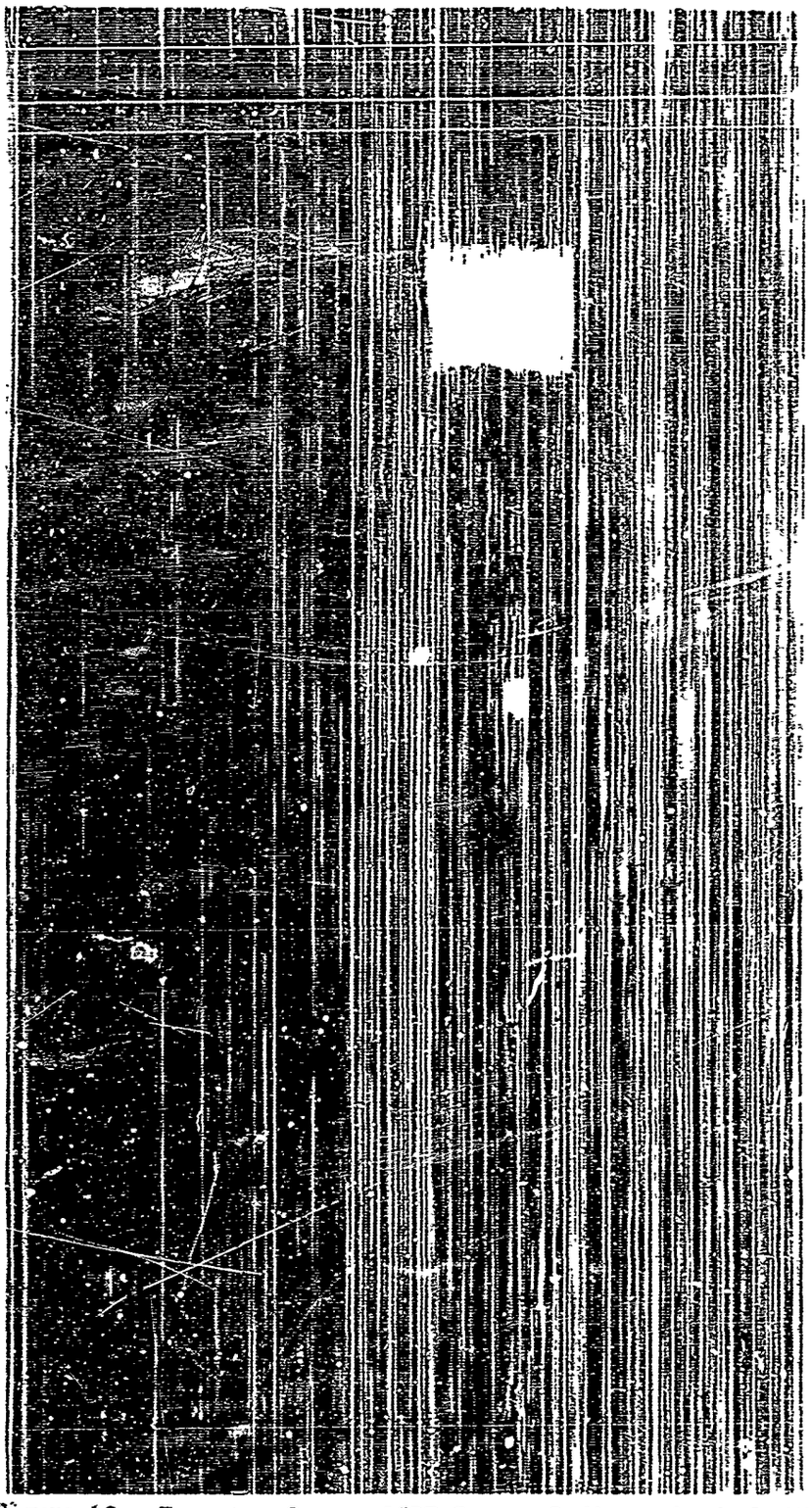


Figure 19. Tungsten-Copper 15BF Stereo-Radiograph, Left View

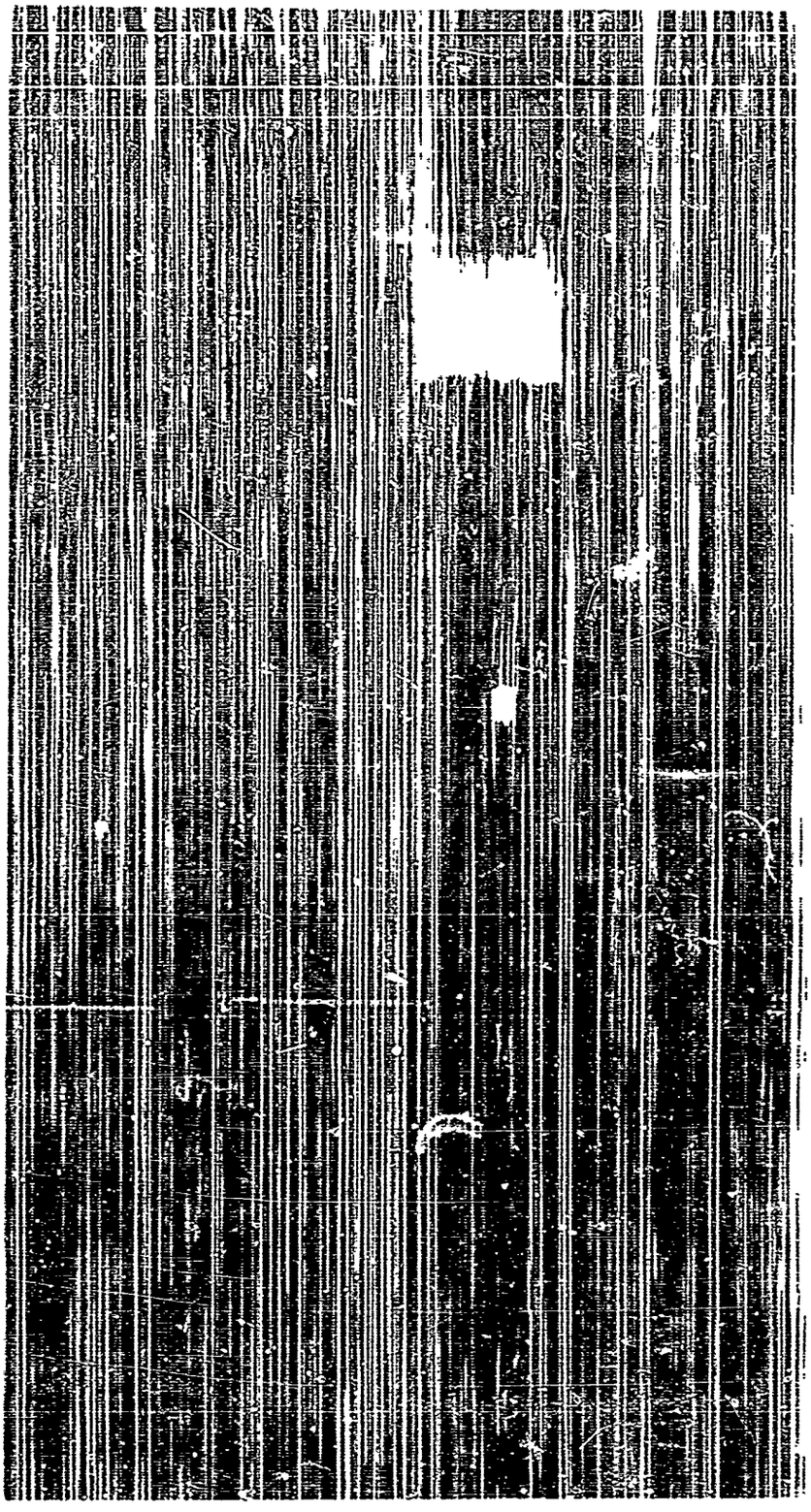


Figure 20. Tungsten-Copper 15BF Stereo-Radiograph, Right View

optimum radiographic conditions. The optimum radiographic conditions are summarized in Table V. Photographs of the x-ray negative for each specimen are shown in Appendix II, Figures 86 to 97. Radiographs were taken from both sides of all specimens to determine the effect of depth on defect detection.

Table V

RADIOGRAPHIC DATA FOR BORON-TITANIUM SPECIMEN INSPECTION

Specimen Identification	Tube Potential	Current (ma)	Focal Spot Diameter (mm)	Exposure Time (minutes)
10BF	90KV	3.5	1.2	4.5
15BF	90KV	3.5	1.2	4.75
20BF	90KV	4	1.2	5
25BF	90KV	4	1.2	5
15PM	110KV	4	1.2	5
1?M	130KV	4	1.2	5

Focal spot distance 45 inches
Type M double emulsion film

Broken Fiber Defect Detection

B-Ti Specimen 10 BF - The four broken fiber areas are readily identified; however, close examination is required to identify the actual fiber breaks. A series of unexplained defects is also evident. The dark spots that appear as ink spots were caused by pin holes in the x-ray film emulsion.

B-Ti Specimen 15 BF - The four broken fiber areas are apparent; however, detail fiber characteristics cannot be identified. It appears that tension was lost on a series of filaments and several fibers appear to cross over each other.

B-Ti Specimen 20 BF - A large number of defects were apparent in this specimen. The deliberate defects were identified as well as crossed-over fibers, and other unaccountable indications.

B-Ti Specimen 25 BF - The best defect resolution was obtained with this specimen. A break in the outer titanium matrix sheet is quite light. Deliberate defects as well as crossed fibers were apparent.

Disbond Defect Detection

B-Ti-Specimen 15 F - The appearance of fiber disbond areas is similar to that of fiber gaps. The disbond areas were clearly evident. A break in the matrix sheet is also seen.

B-Ti Specimen 15 M - The matrix-to-matrix disbonds were not detected. Several crossed fibers were evident.

RADIOGRAPHY OF BORON-ALUMINUM COMPOSITE

The boron-aluminum specimens were inspected by normal broad-beam radiographic techniques. All tests were made using Eastman Kodak Company Type R single-emulsion x-ray film. The single emulsion film was considered to give better resolution for the boron-aluminum specimens than the double-emulsion type The x-ray mass absorption coefficients of boron and aluminum are very close and delineation becomes difficult.

The silver foil used in fabrication of the defect mat created a problem in the determination of optimum exposure. The silver foil gives the radiographs a venetian blind appearance. The foil appeared to have many small cracks perpendicular to the width of the foil and followed the fibers. Areas where the foil was folded were also readily visible. Lead screens, 0.005-inch-thick, were used at the back of all films. All films were developed by manual methods in Kodak Rapid X-Ray Developer at 68 degrees Fahrenheit for five minutes.

All of the specimens were radiographically inspected; photographs are included in Appendix II, Figures 98 to 103. A number of general observations can be made relative to the radiographs. The individual fibers are visible on close examination of the original x-ray negative. The use of a microscope helps in identification of individual wires but is a tedious and fatiguing operation. Definition of the individual wires is lost in some positive prints of the x-ray films, however, the loss of a group of wires is readily visible in a print which has been properly processed. Stress cracks can be seen in all of the silver foils. Specific observations for the individual specimen are discussed in the following paragraphs. The optimum radiographic conditions are summarized in Table VI.

Broken Fiber Defect Detection

B-Al Specimen 10BF - The large and small broken fiber squares were visible in both the print and the radiograph. The large square was visible in the radiograph but not in the print. The section of foil visible below the cutout area does not contain stress cracks, nor does it have superimposed fibers. It

Table VI

RADIOGRAPHIC DATA FOR BORON-ALUMINUM SPECIMEN INSPECTION

Specimen Identification	Tube Potential	Current (ma.)	Focal Spot Diameter (mm)	Exposure Time (minutes)
10BF	90KV	4	1.2	3.75
15BF	100KV	3	1.2	4
20BF	100KV	4	1.2	3.5
25BF	110KV	4	1.2	3.5
15BM	110KV	4	1.2	4
15M	120KV	4	1.2	4

Focal spot distance 45 inches
Type M double emulsion film

can be seen that this section of undamaged foil is over the large square area where the fibers were removed.

B-Al Specimen 15BF - The large and small broken fiber squares were visible in both the print and radiograph upon close examination. Two of the series of fiber breaks were readily visible.

B-Al Specimen 20BF - The large and small broken fiber square, and three of the broken fiber cuts were visible in both the original radiograph and print. The 1/4 inch square was easier to locate on the print than on the radiograph.

B-Al Specimen 25BF - This specimen was radiographed twice, once with each side in the up position. The large and small squares formed by cut fibers are readily visible in the prints. It appears that the series of four cuts near the top of the prints were made through the foil and, during fabrication, the cut wire positions relative to foil have changed. The apparent positions of the cut fibers and strips of apparent fiber separation were visible.

Disbond Defect Detection

B-Al Specimen 15F - The fiber disbonds were not detected. The series of blotches appearing on the photograph were caused by contact with the alumina stop-off sheet during bonding.

B-Al Specimen 15M - The matrix disbonds were not detected.

RADIOGRAPH DENSITOMETRY

Radiographs of the 25 BF boron-aluminum, boron-titanium, and tungsten-copper specimens were examined by a light densitometer. The radiographic negative was placed in a Photovolt Model 52 search head with an approximate 1/8-inch diameter light source. A Photovolt Model 501M readout indicator was used to set the average light intensity value for properly fabricated specimen areas. The radiograph was then repositioned for viewing areas where a gross section of fiber layer had been removed. The average light intensity value was significantly increased. Additional examination was made in local areas where single and multiple fiber breaks were known to exist; here, indicative light changes were not apparent. It was concluded that smaller light sources and/or higher sensitivity light detectors are needed. Presently available photoelectric cells could be adapted for detection improvement. Although manual scanning was employed, the light densitometric system is available in automatic scanning models and would be applicable for this type of inspection. Nominal light sensitivity trigger level could be established based on the radiographic film type and preparation, and actual fiber spacing/stacking density factor.

DYNAMIC RADIOGRAPHY

In order to study failure mechanism characteristics of fiber-matrix composites, direct observation of the fibers during failure is most desirable. Experiments were therefore conducted to determine the feasibility of using dynamic x-ray techniques to monitor the fibers in a composite during fracture. Two-inch tensile test specimens were prepared using a single layer boron-titanium and tungsten-titanium composite materials. The specimens were mounted in a small controlled hydraulic loading tensile fixture. Strain markers were located on each specimen to monitor the elongation. The loading fixture and specimen were mounted beneath a Norelco "Searchray" x-ray system. A Vidicon camera mounted below the specimen provided direct television display for the test and provided a signal for a magnetic tape recorder. The test system (Figures 21 and 22) was checked out statically to determine the system resolution. It was found that the tensile test specimen needed to be in immediate contact with the Vidicon camera shield for optimum sensitivity. Since this could have damaged the camera, some resolution was lost by moving the camera slightly.

A second factor affecting sensitivity was due to the reduced specimen to x-ray tube spacing caused by the specimen holder, which resulted in some parallax error. A slight fuzziness due to these factors could not be avoided, however, good fiber detail was evident in both of the boron and tungsten fibers. For the tungsten fiber, voltages of 75 KV showed the best contrast, but the 0.005 inch diameter tungsten boride center of the boron fibers, which can be seen clearly in the routine x-rays, appeared to be just beyond the limit of

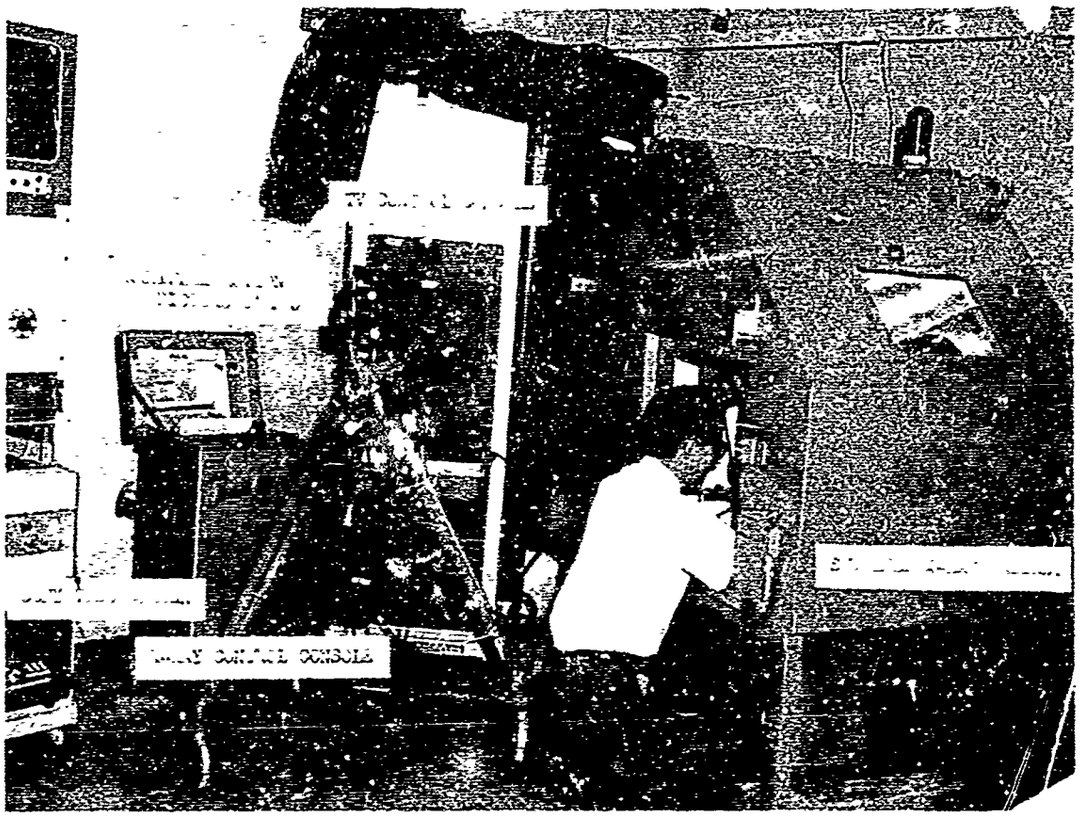


Figure 21. Norelco "Searchray" System

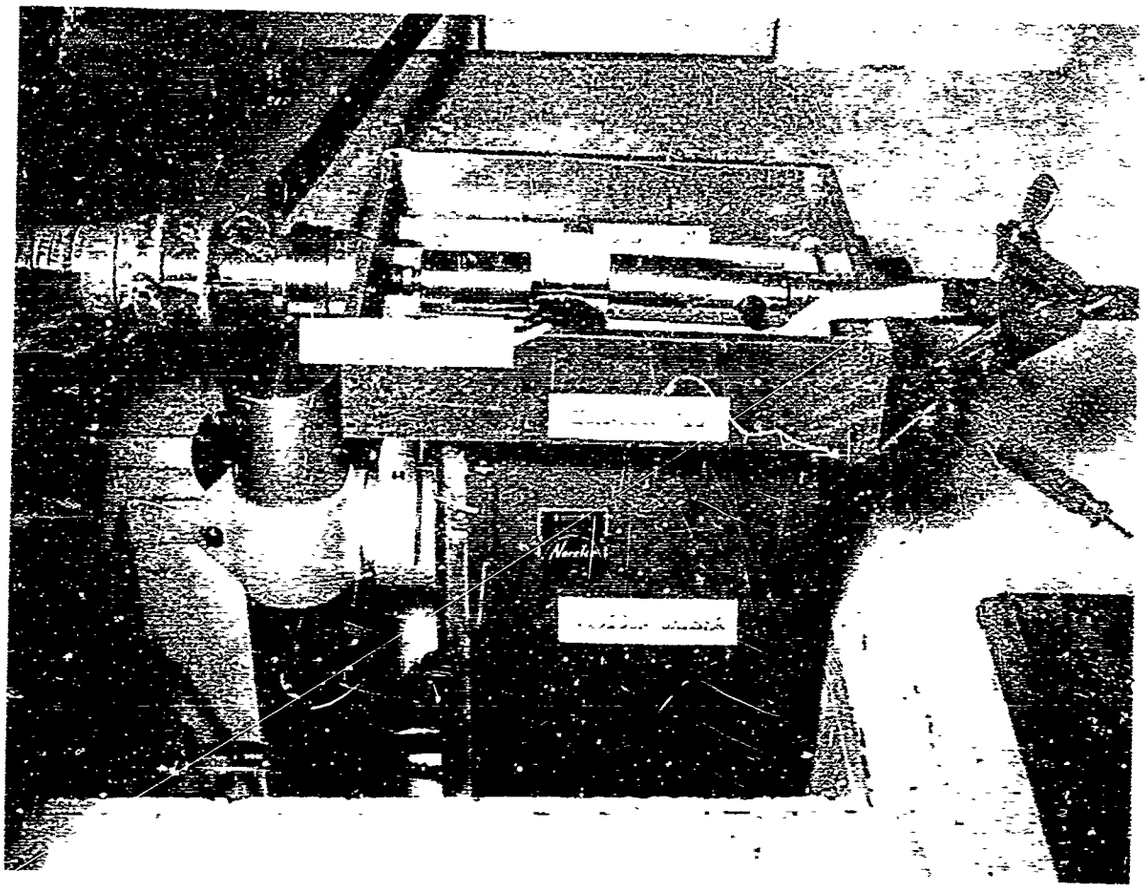


Figure 22. Fixture Use for Specimen Location

resolution. A two inch collimator was evaluated, without apparent improvement. No trouble was experienced in showing up strain markers of tungsten fiber.

The magnetic tape recording was subsequently converted to cinematographic film and printed in the form of a 16 mm film. The edited film shows both the test setup and examples of dynamic shots made during a tensile test. Pictures of tungsten filament indicated clearly that these fibers, in the specimens tested, fracture simultaneously with the entire specimen. However, the fracture of boron fibers, which is known to occur prior to failure of the entire specimen, could not be resolved. Both radiographic test sequences end abruptly with fracture, as the specimen ends fly away from the observation area, which is approximately 3/8 inch square.

Measurement of the strain is possible by measuring the movement of the strain markers placed on the specimen. However, this movement is too small to be observed at standard motion picture speeds and must be measured frame by frame. It must be emphasized that these tests were done on standard equipment not specifically designed for the testing of metal matrix composites. Apart from selecting the optimum voltage, no modifications were carried out. Furthermore, some resolution is lost in making a film from the tapes. Direct observation during the test gives better contrast and definition.

The principal conclusions which could be drawn from these experiments were as follows:

1. The dynamic radiographic observation of composites is entirely feasible.

2. Power output of tubes should be, for tungsten material resolution, in excess of 75 KV and 15 ma. Vidicon tube-specimen distance should not exceed 1/32 inch and the specimen x-ray tube should be as large as possible. Another possible future development would be the use of a collimating system.

3. The Vidicon tube used has a memory of about one minute. During a dynamic test, this memory image interferes with the changing instantaneous image. No memory should be included in dynamic test tubes.

4. The Vidicon tube used had a line resolution of 0.0005 inches per line. Improved resolution would allow demonstration of the tungsten filament in boron fiber, for example.

5. Contrast resolution appears adequate for the materials used.

MICRORADIOGRAPHY

The successful microradiographic inspection of thin materials and coatings (several thousandths of an inch thick) has been reported by a number of investigators (McClung, R.W.; McMaster, R.). They report extension of the radiographic process to inspection detail in the order of one micron. The feasibility of applying microradiography to the metal fiber-matrix composite specimens was evaluated. Microradiography differs from conventional radiography in the energy levels, focal film distances, exposure times and recording media used. It is a sophisticated technique utilizing a vacuum chamber, a vacuum cassette and a photo-sensitized, single emulsion glass slide having a resolving power of 2000 or more lines per millimeter. Exceptional sharpness and contrast are obtained and the resulting image may be magnified many times without loss of definition.

Trial specimens were obtained by using the ends of the 5 x 10 inch specimens that had been cut off for microscopic inspection. The end pieces contained the fiber-matrix materials and pieces of the 0.002 in. stainless steel foil used during fabrication to provide a smooth transition surface for the filament winding. An end piece approximately 1/2 by 1-1/4 inch was selected from each of the 15 percent volume ratio specimens B-Al 15 BF, B-Ti 15BF, and W-Cu 15BF.

Microradiographic techniques were applied on the three specimens using the General Electric Micro Unit which has an energy range of 50 kilovolts and 50 milliamperes. Excellent results were obtained on all except the copper-tungsten which is too dense for the energy range of the micro unit. The B-Al 15BF microradiograph (Figure 23) shows excellent resolution of fiber, and 0.002-inch thick stainless steel foil. The microradiograph was taken with the following inspection conditions: 40 KV; 25 ma; 9-inch focal film distance; 3-hour exposure; Eastman Kodak-type 649-0 micrographic plate. Study of the microradiograph slide with a Bausch & Lomb Trisimplex Projector shows even further fiber detail.

Successful boron-titanium specimen microradiographs were obtained at 40 KV, 25 ma, 9-inch focal distance, 3-hour exposure (figure 24). The tungsten-copper specimen was successively exposed to higher voltages until at 250 KV and 3-hour exposure conditions, successful microradiographs were obtained. The 649-0 Kodak plate negative may be magnified by photographic and microslide projection up to 100X.

Microradiographic inspection was also applied to study the fracture area in a fiber matrix composite. A tensile test specimen with a single layer of boron fiber and titanium matrix was fractured. The portion of the specimen adjacent to the fracture was used for the microradiographic inspection. Figure 25 shows the fracture zone at 10X magnification. The fiber detail clearly shows that numerous cracks occurred within the matrix.

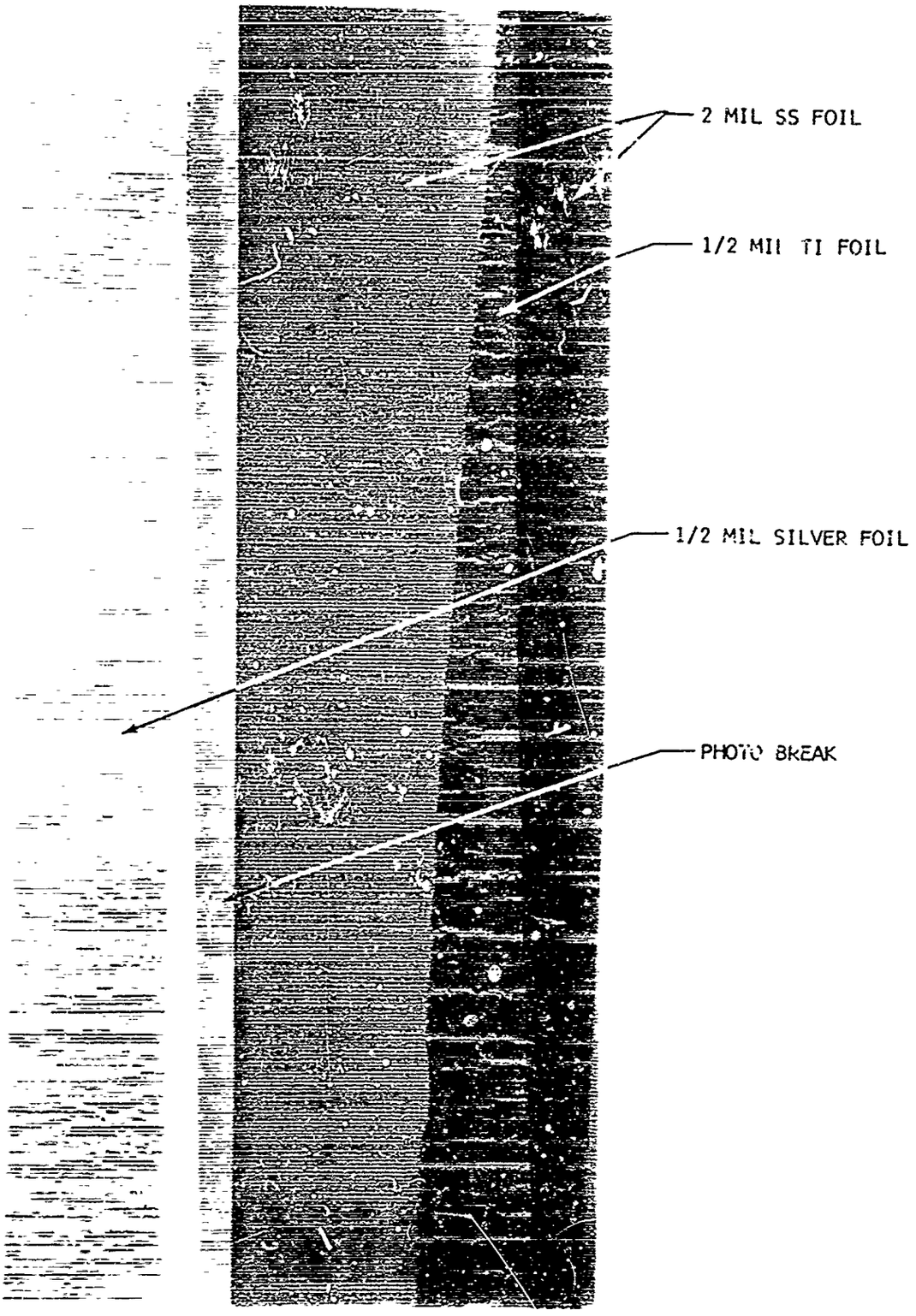


Figure 23. Microradiograph Showing Boron-Aluminum Specimen End With Foil Tabs

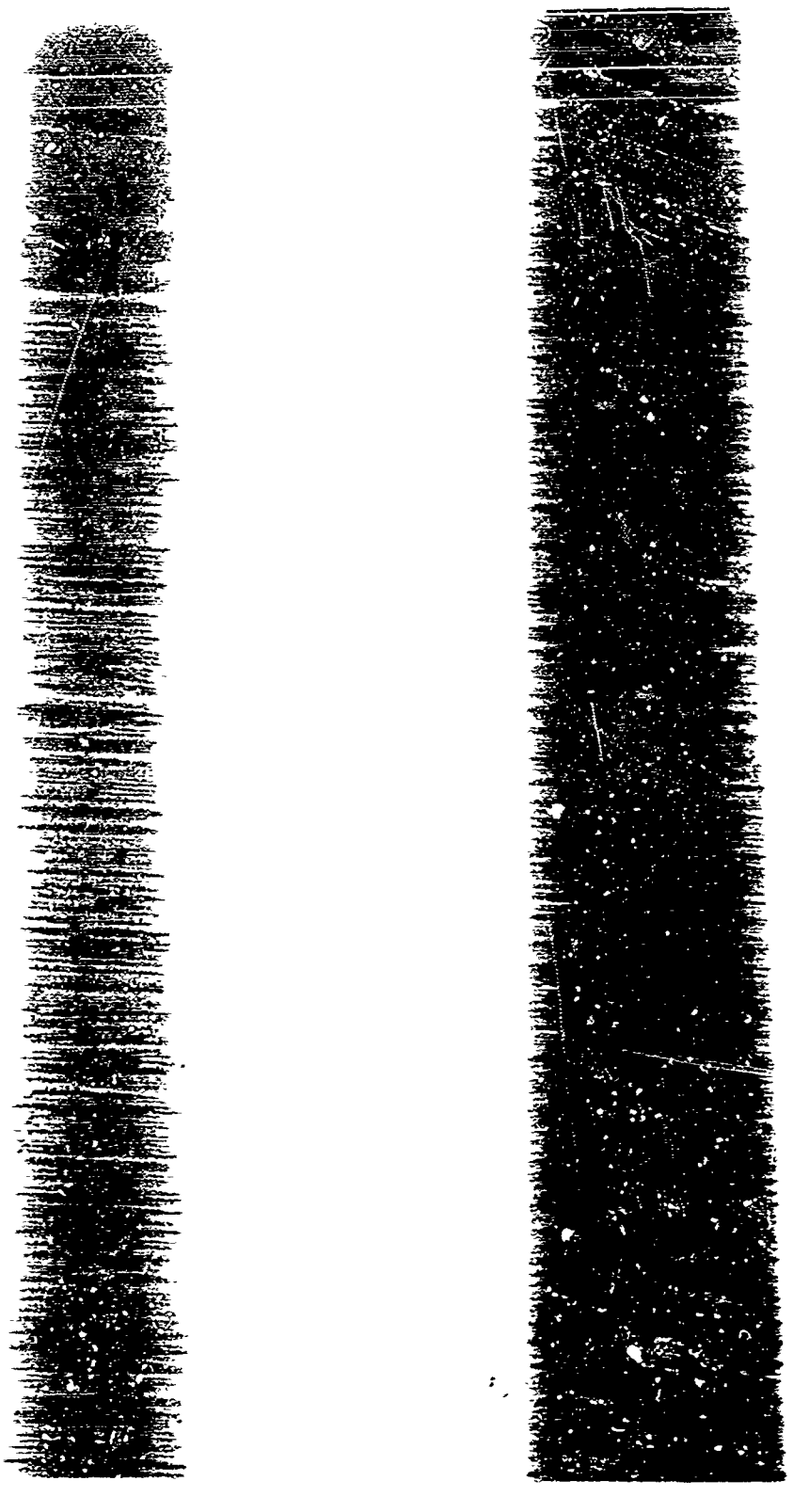


Figure 24. Microradiograph of Boron-Titanium 25BF at 40KV, 25ma, 3 Hour Exposure, Showing Two Photographic Sensitivity Levels

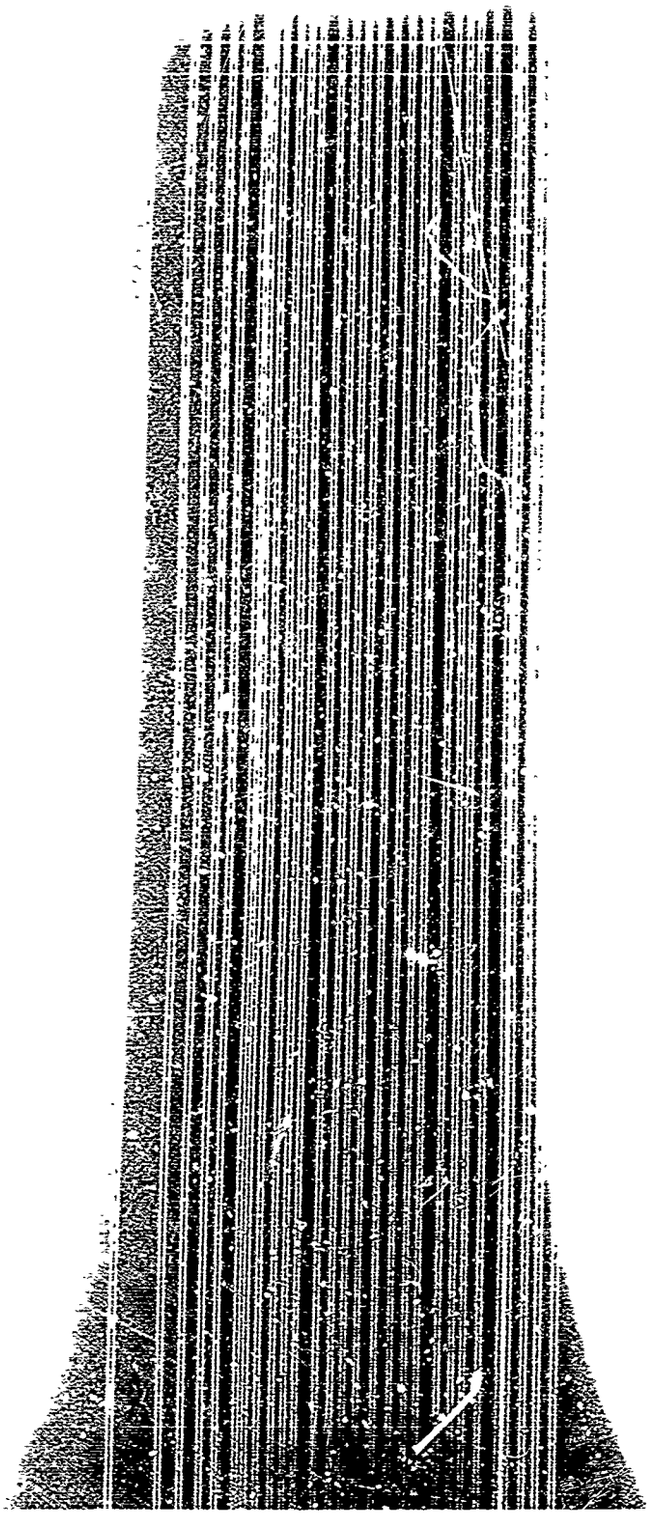


Figure 25. Microradiograph of Boron-Titanium Single Layer Composite, Etched (25KV, 23ma, 2 hour exposure).

PHOTOGRAPHIC ENLARGEMENT OF RADIOGRAPHS

Prints and enlargements were made from the tungsten-copper 25BF specimen radiograph. Radiographic exposure was from the top of the specimen, at 90 KV for 5 minutes. A direct print and related 5X photographic enlargements were made from the negative to determine if photographic enlargement would increase detectability of deliberate broken fiber defects, such as breaks and fiber gaps, introduced during specimen fabrication. Results are shown in Figures 26, 27 and 28. The enlargements significantly increase visibility of defect areas. A single broken fiber which is evident only through microscopic inspection of Figure 26, shows up very plainly in the 5X enlargement (Figure 27). Minute fiber end filaments left after cutting out the square defect section are also visible. Four out of place fibers, barely visible in the original radiograph, are very evident in Figure 28.

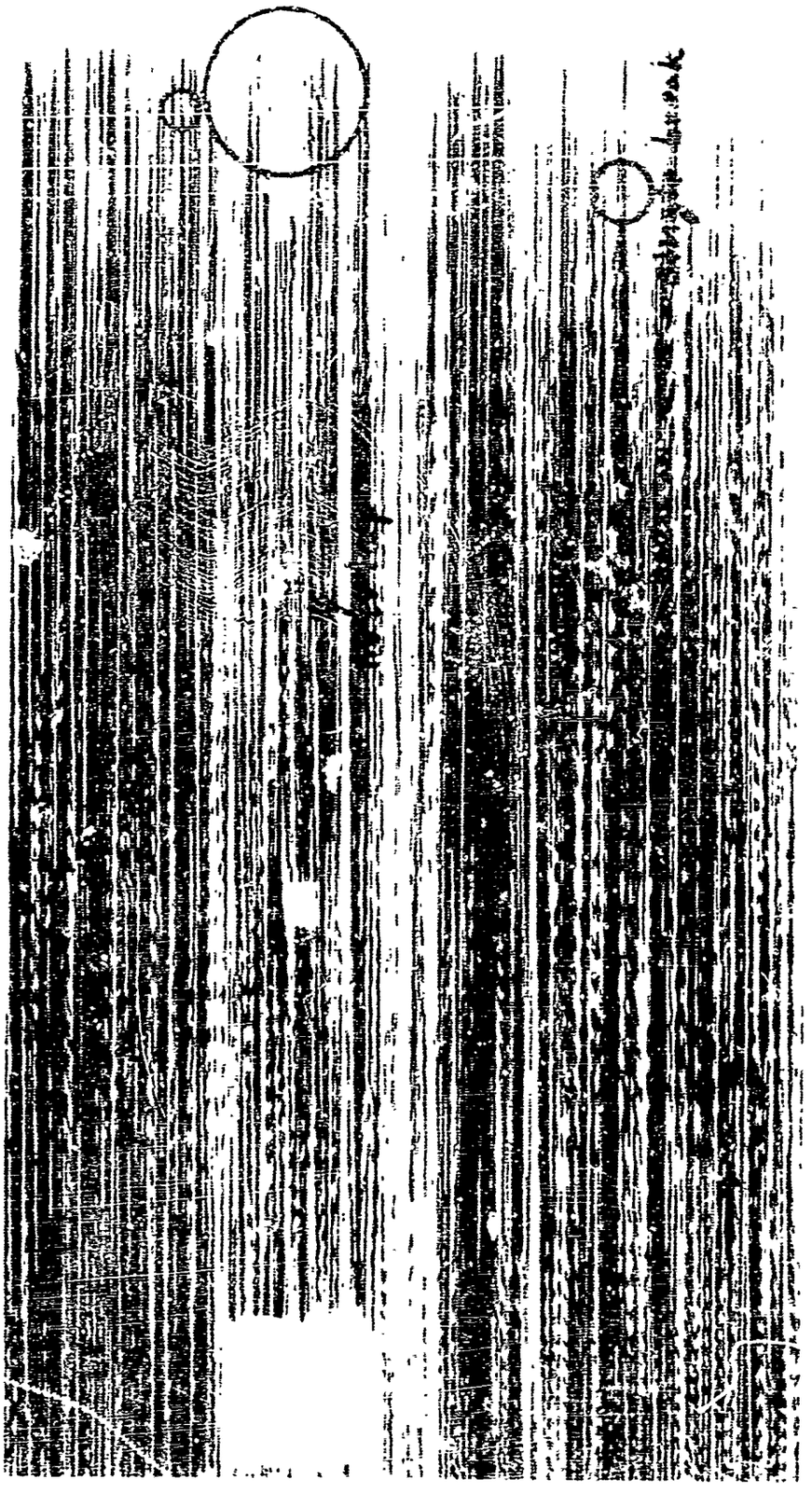


Figure 26. Tungsten-Copper Specimen 25BF Radiograph Showing Deliberate Defect Areas

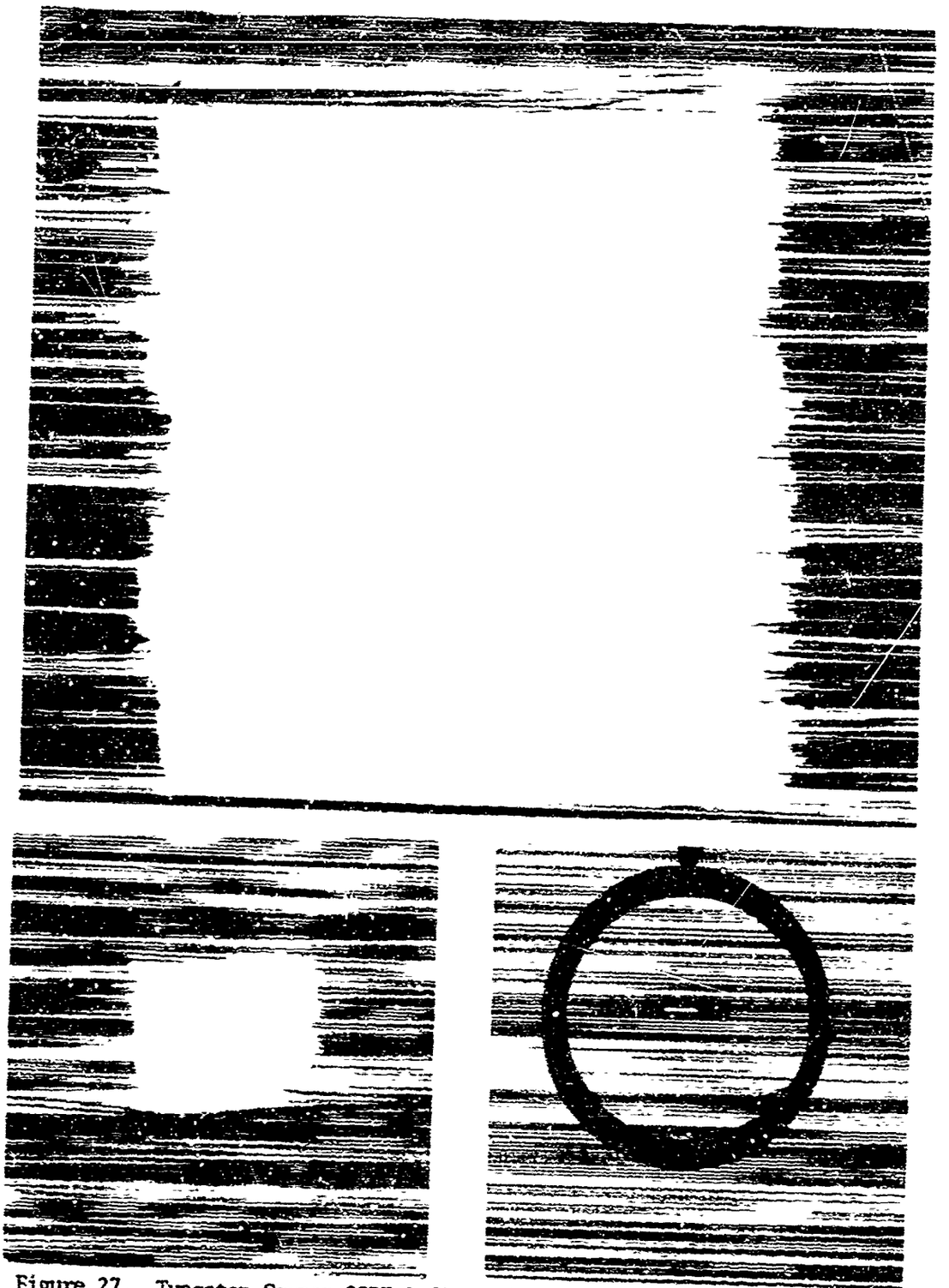


Figure 27. Tungsten-Copper 25BF Radiograph, 5X Photographic Enlargement of Square Defect Sections and Area Containing a Broken Fiber (lower right)

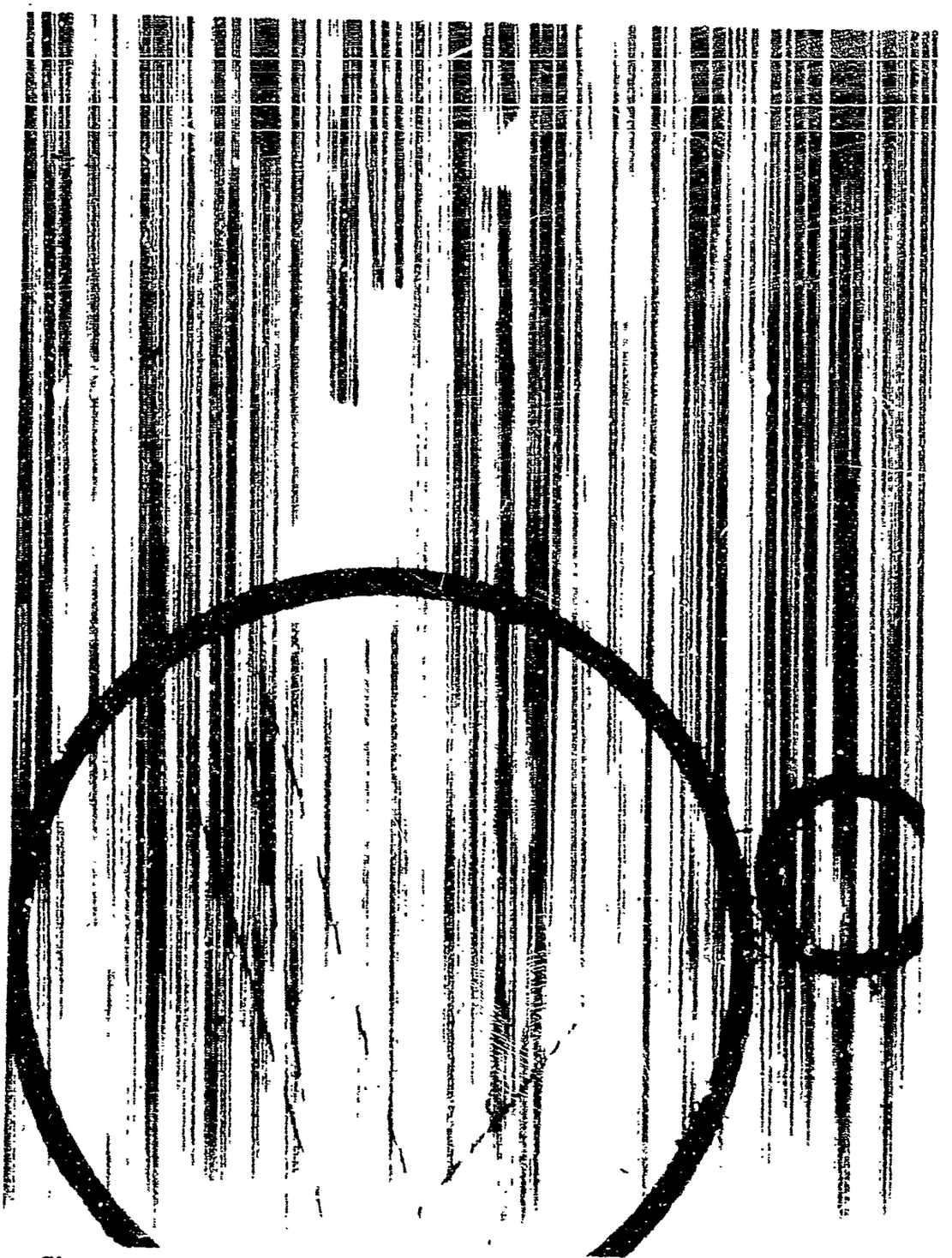


Figure 28. Tungsten-Copper 25BF Radiograph, 5X Photographic Enlargement of Deliberate Fiber Breaks

Section VI

ULTRASONIC INSPECTION

ULTRASONIC PROPERTY MEASUREMENT

Ultrasonic velocity measurements were made on the composite specimens using pulse-echo ultrasonic instrumentation and employing the "multiple back reflection comparison" technique. Distilled water was used as both the coupling and sound velocity comparison medium. This technique for resolving front and back surface reflections limited its use to those samples thick enough for front and back surface reflections which could be obtained and reliably identified and counted. Sound velocity was calculated from the following relationship:

$$V = \frac{vnt}{d} \quad \text{where,}$$

V is the longitudinal (compressional) wave velocity of the material under test,

v is the sound velocity of the comparison medium,

t is the thickness of the specimen being tested,

d is distance between the transducer face and the front surface of the specimen being tested, and

n is the number of back reflections.

The test procedure included positioning the transducer over the specimen and adjusting the Reflectoscope for an A-scan presentation wherein the maximum number of first order, back reflections were clearly distinguishable on the CRT trace. The search tube containing the transducer was then positioned to set the last first order back reflection over the second front reflection trace. The distance "d" was measured for the sound velocity measurement computation using a combination of gage blocks placed between the transducer and test specimen and compared with a dial indicator mounted on the search tube. The sample thickness was measured for the actual test region using a standard vernier micrometer.

A longitudinal wave, sound velocity test was performed with an aluminum alloy standard reference block to establish the validity of the test method. Duplicate test runs were made using an Automation Industries 7075-T6 No. 5-0025 Standard Reference Block. Test results performed in distilled water at 20°C were as follows:

Test No.	Water Distance "d" (inches)	No. of Back Reflections	Calculated Sound Velocity (in/sec)
1	1.176	5	2.494×10^5
2	1.186	5	2.474×10^5
		Average	2.49×10^5

The sound velocity used for water in these computations was 0.587×10^5 in/sec, and was converted from the cgs value given in the 1963 edition of the Non-destructive Testing Handbook. The 2.49×10^5 in/sec value obtained experimentally compares well with the 2.48×10^5 in/sec value in the same reference source for 2017-T4 alloy. A brief literature search and contact with Alcoa Research Laboratories in New Kensington, Pennsylvania failed to disclose an established velocity figure in 7075 aluminum alloy. However, based on a comparison of elastic constants and density values, it appears that longitudinal wave velocity for both alloys are the same to three significant figures. The results of this verification provide support for the accuracy of the results on the composite specimens.

VELOCITY MEASUREMENT FOR TUNGSTEN-COPPER COMPOSITES

Initial ultrasonic velocity measurements were made on specimens W-Cu 15M (0.135 inch thick) and W-Cu 15A (0.265 inch thick). The front and the first back reflection could not be resolved for specimen W-Cu 15PM (0.085 inch thick) at 10 MHz which was the highest test frequency available on the UM-721 Reflectoscope. Three defect-free areas of the tungsten-copper composites were tested for sound velocity, and the arithmetic average of these taken as the plate characteristic. At each location tested, the specimen thickness (t) and water distance (d) were determined in triplicate. The test results are summarized in Table VII.

VELOCITY MEASUREMENT FOR BORON-TITANIUM COMPOSITES

Longitudinal wave ultrasonic velocity measurements were made on boron-titanium composites by the "multiple back reflection comparison" method and a constant water path, "through transmission time" method. The latter method was considered to determine sound velocities in material too thin to employ the multiple back reflection method. However, the through transmission method was found highly inaccurate for thin specimens because of the difficulty in measuring pulse shifts on an oscilloscope screen. With the short time involved (less than one microsecond), the pulses were several centimeters wide on the screen, and the measuring error of the oscilloscope was approximately plus and minus

Table VII.

SUMMARY OF ULTRASONIC VELOCITY MEASUREMENTS AND DATA

Specimen	Method	Longitudinal Wave Sound Velocity
**Tungsten	Pulse-Echo Multiple Back Reflection	2.08×10^5/ In./Sec.
** Copper	Pulse-Echo Multiple Back Reflection	1.84×10^5 In./Sec.
*W-Cu 15M	Pulse-Echo Multiple Back Reflection	1.73×10^5 In./Sec.
*W-Cu 15A	Pulse-Echo Multiple Back Reflection	1.78×10^5 In./Sec.
*Elemental Boron	Continuous Through Transmission	1.95×10^5 In./Sec.
*Elemental Boron	(A.P.) Pulse Echo Multiple Back Reflection	4.80×10^5 In./Sec.
*Ti-6Al-4V Alloy	Continuous Through Transmission	2.41×10^5 In./Sec.
*Ti-6Al-4V Alloy	Pulse-Echo Multiple Back Reflection	2.53×10^5 In./Sec.
*B-Ti 15M	Continuous Through Transmission	2.39×10^5 In./Sec.
*B-Ti 15M	Pulse-Echo Multiple Back Reflection	2.36×10^5 In./Sec.
*Aluminum 7075-T6	Pulse-Echo Multiple Back Reflection	2.49×10^5 In./Sec.
*Aluminum 2017-T4	Pulse Echo Multiple Back Reflection	2.48×10^5 In./Sec.
*B-Al 15M	Pulse-Echo Multiple Back Reflection	2.50×10^5 In./Sec.

*Experimentally Determined
**Nondestructive Testing Handbook, 1963.

one centimeter at the 0.2-1.0 sec/cm sweep speed. At metal thickness approaching one inch, the through transmission method gave comparable accuracy to the back reflection method. Inserting a thick metal block in the sound path with the thin specimen did not improve the test sensitivity, because the thin material badly distorted the pulse waveform.

The through transmission test method used the output of the Model 424A Immerscope fed into an oscilloscope capable of time measurements down to 0.01 microsecond. The instrument was operated in the continuous transmit-receive mode at 10 Mhz. A 3/8 inch diameter flat lithium sulphate transmit transducer and a 3/4 inch diameter flat receiving transducer were used. Testing was performed in water with the test object positioned between the two transducers (Figure 29). When the specimen was in position, the transmit search tube was repositioned to maintain a constant water path. Thus, the time shift of the receive pulse on the oscilloscope screen represented the transmission time of sound in the specimen. This approach was used to simplify calculation and eliminate the need for distilled water. Tap water of unknown sound transmission characteristics was used, and since the water distance was maintained constant (within ±0.001 inch as measured with a dial indicator on the search tube), the velocity of sound in water did not enter the final computations.

Sound velocity measurements were made on the B-Ti 15M specimen (0.130 inch) thick) and a 0.161 inch thick sample of titanium -6Al-4V alloy using both velocity methods (Table VII). The following pertinent test conditions were employed in obtaining the sound velocity data:

Test Frequency	10 Mhz
Transmit Transducer	3/8 inch Dia., Titanium Sulphate, Flat
Receive Transducer	3/4 inch Dia., Titanium Sulphate, Flat
Couplant	Tap Water
Test Temperature	20°C
Instrument	Model 424A Immerscope

Because of the complete lack of data on boron, attempts were made to determine velocity measurements on two available crystalline boron specimens. These specimens had a density of 2.00 gm/cu cm and 2.34 gm/cu cm. The density given in the literature for both amorphous and crystalline boron is 2.30 (Reference 6). The first specimen was ground to a slab 0.1865-inch thick, the second was ground to about 1/4-inch thickness. The sound velocity value for the first was found to be 195,000 ips, for the second specimen 480,000 ips. The second value is probably the more accurate, because of the more representative specimen density. Furthermore, it compares well to that of beryllium, which has approximately similar modulus and density and a sound velocity of 510,000 ips. The data found are applicable to crystalline boron and may or may not apply to the amorphous boron existing in the fibers. Furthermore, no consideration has been taken of the tungsten-boride core of the fibers or of any diffusion layers.

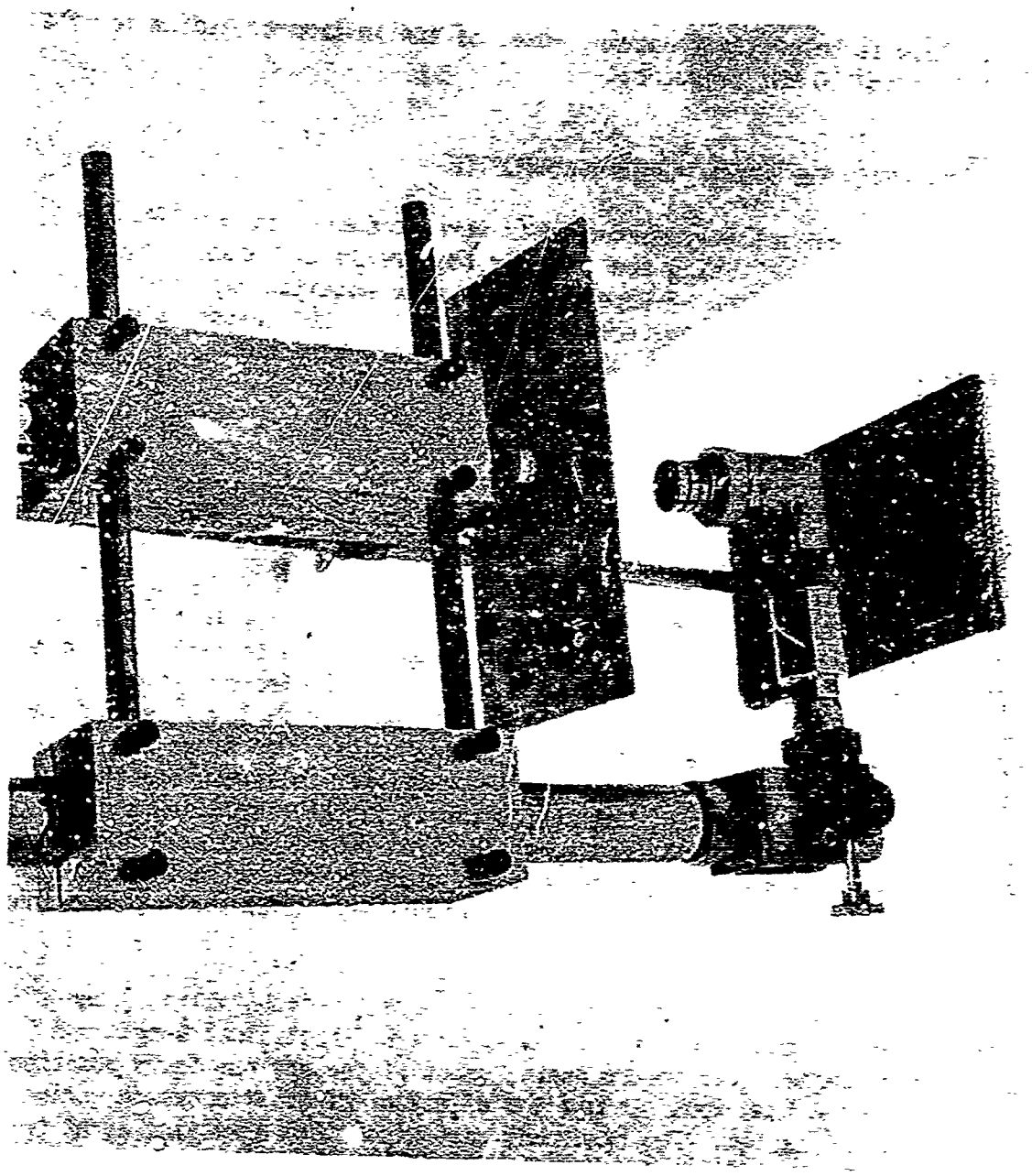


Figure 29. Ultrasonic Through-Transmission Test System for Inspection of Composite Specimens

The high sound velocity in boron explains why the multiple back reflection method could not be used for determining this characteristic in the 0.1865 inch thick first specimen. The transmission time of sound through this specimen is roughly the same as that for metals one half the boron sample thickness or 0.090 inch. This is below the resolving power of the instrument system for the Sperry Reflectoscope 10 MHz frequency.

VELOCITY MEASUREMENT FOR BORON-ALUMINUM COMPOSITES

Longitudinal sound velocity measurements were conducted on the B-Al 15M specimen (0.125 incl. thick) using the multiple back reflection comparison method. The 2.50×10^5 in/sec average velocity value obtained experimentally for this composite is in exact agreement with the 2.50×10^5 in/sec value given in the Nondestructive Testing Handbook for 1100-0 alloy aluminum.

ULTRASONIC ATTENUATION TEST

The pulse echo through-transmission technique was used to measure attenuation in the composite specimens.

The breadboard through-transmission system uses a Shockley four-layer diode used as a free running pulser, driving tuning networks to peak the transmitting transducer at either 1 to 4 MHz. The echo is detected by a receiving transducer tuned to the appropriate frequency. An emitter-follower is used for high impedance input to prevent loading the tuning coils. One stage of amplification follows, feeding a low output impedance-emitter-follower, and the 50 ohm attenuator. The output of the attenuator is further amplified and displayed on a graduated oscilloscope screen. The transducers used well damped 15 MHz lithium sulfate crystals. A pulse mode was used to reduce the interference effects of standing waves. Attenuation measurements were conducted as described in the following paragraphs.

The transmitting and receiving transducers were immersed, aligned, and fixed within a small tank. The transducers have a 1.7-inch focal length and were spaced approximately 2.5 inches apart, short of the optimum focus position so that the broadened beam would reduce the effect of minor attenuation variations within the composites. The specimens were wiped with a wetting agent to ensure good acoustical contact, and positioned between the transducers.

The pulse echo decay pattern was monitored on a high speed oscilloscope. The third echo was adjusted to a reference signal height of four centimeters with a precision attenuator. The specimen was replaced with a sheet of the same matrix material of identical thickness. The third echo amplitude of the

matrix sheet was compared with specimen reference. At one and four MHz, all three types of composite specimens indicated the same amplitude as the respective matrix material within ±1 db, or the measuring accuracy of the system. Similar tests at 22 MHz gave the same results.

Attenuation measurements were considered using the comparison of the exponential of pulse echo train decay within the specimen and an adjustable, calibrated exponential generator. The 25 BF series of composites were tested to determine their decay patterns. In each case the echo pattern was too short (three or four echoes) as the echoes were grossly distorted. Several factors affect the successful use of this technique, i.e., the waveform of the pulse, the transducer characteristics, parallelism of specimen surfaces, etc. The composite specimen surfaces were somewhat rougher than the original cold rolled matrix material, and the parallelism of the surfaces at any one area was questionable.

ULTRASONIC C-SCAN INSPECTION

TECHNICAL APPROACH

Preliminary ultrasonic inspection was performed on the defect evaluation specimen. Based on these tests and studies, an ultrasonic flaw or defect inspection plan was developed. The test equipment, calibration, and test procedures are described in the following paragraphs.

The ultrasonic inspection system included a Sperry UM721 Reflectoscope and an immersion tank with appropriate scanning and recording equipment (Figure 30). Conventional pulse-echo methods could not adequately determine the echoes in the relatively thin specimens. Therefore, the pulse-echo immersion method was employed using the reflector plate technique.

The general test conditions included using both 10 MHz and 5 MHz focused lithium-sulphate transducers. The transducers were focused on the top surface of the part, and the echo from the reflector plate (located 1/4 inch below the test specimen) was gated for 1.1 C-scan recording. The type of recorder used provided a visible trace when the reflector plate echo was being received, and discontinued recording when the signal was lost. For testing, an arbitrary Reflectoscope gain setting was employed to just detect the reflector plate, and a C-scan recording was made at this gain. The gain was then increased a small amount and a recording made at this new level. This procedure was repeated until very little difference was obtained between succeeding runs.

The record test sensitivities were established by (1) performing partial specimen coverage scans at arbitrarily increased instrument gain values, (2) selecting three that provided increasingly meaningful information, and (3) relating the instrument gain values to return signals from convenient standard reference blocks. Alcoa Series "D" Reference Standards were used for the latter purpose. When using these blocks, a few instrument gain settings were too low to give an indication from the largest flat bottom hole (8/64 inch diameter) in the Alco blocks. In these instances, the height of the first back reflection from the No. 8 block was used as a sensitivity measurement.

Where instrument gain setting was too low to give a measurable response from the flat bottom hole in the largest Alcoa reference block (the No. 8 block), the sensitivity was expressed in terms of signal height from the back surface of the reference block. In this case, the transducer was carefully centered over the flat bottom hole to take advantage of shadowing of the sound returning to the test transducer in obtaining a usable sensitivity value.

Certain specimens were tested from both the front and back surfaces. In these cases, the test sensitivity was constant for the front and back surface scans. Actual quantitative sensitivity values are given on the C-scan record. High sensitivity was defined as the lowest Reflectoscope sensitivity control

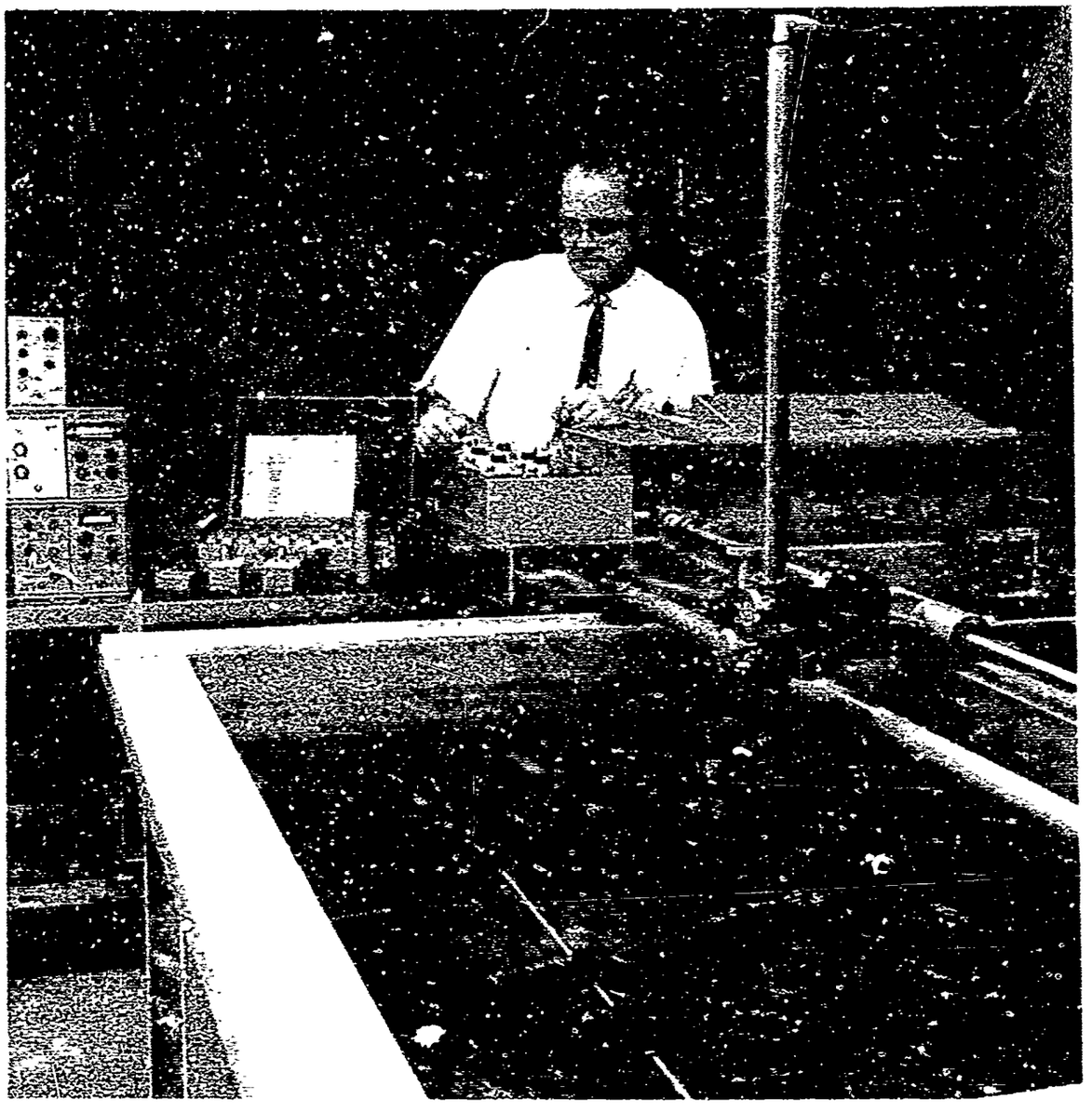


Figure 30. Ultrasonic Inspection System for Composite Inspection by the Immersion Method

setting, at low gain settings, where the test was most sensitive to factors affecting variations in sound transmission. Conversely, low sensitivity was defined as the higher Reflectoscope sensitivity control setting at which point the test is no longer sensitive to the more subtle causes of changes in sound transmission. Increasing the gain beyond this sensitivity value no longer appreciably changed the visual display of information on the C-scan recording, and any nontransmission sound is assumed to result from nonbonds in the material or adverse surface and geometry conditions, e.g., dents, curvature, or excess surface roughness.

The following considerations are to be kept in mind when interpreting the C-scan recordings:

1. The recorder was set to write on the first return signal from the reflector plate. Therefore, a loss of signal appears as a white area on the recordings.

2. The annular loss of a signal at the corners of the plate images were caused by the rubber grommets used to space the specimens over the reflector plate.

3. The record area is slightly larger than the specimens. This was done to prevent loss of information during testing. However, this technique makes exact location of specimen edges on the recordings somewhat difficult to determine.

PRELIMINARY ULTRASONIC INSPECTION

The tungsten-copper 10-25BF evaluation specimens fabricated to determine the effectiveness of the defect mechanisms was tested ultrasonically. Inspection was conducted on the first specimen containing deliberate fiber breaks, and the second specimen containing disbonds. The broken and misaligned fibers were not detected.

Five C-scan recordings were made of the tungsten-copper 10-25 evaluation specimen containing the disbonds. A photographic copy of a typical C-scan recording is shown in Figure 31. The following conclusions were made:

1. At the lower gain settings (0.6 and 0.7), the regions containing the 10 and 25 percent tungsten wire are clearly evident. This differentiation is much less evident at the higher sensitivity settings of 0.8 and 0.9, and has virtually disappeared at a gain setting of 1.0. At a given gain, the region of high fiber content produces more sound scatter, and, therefore, more instances of signal loss.

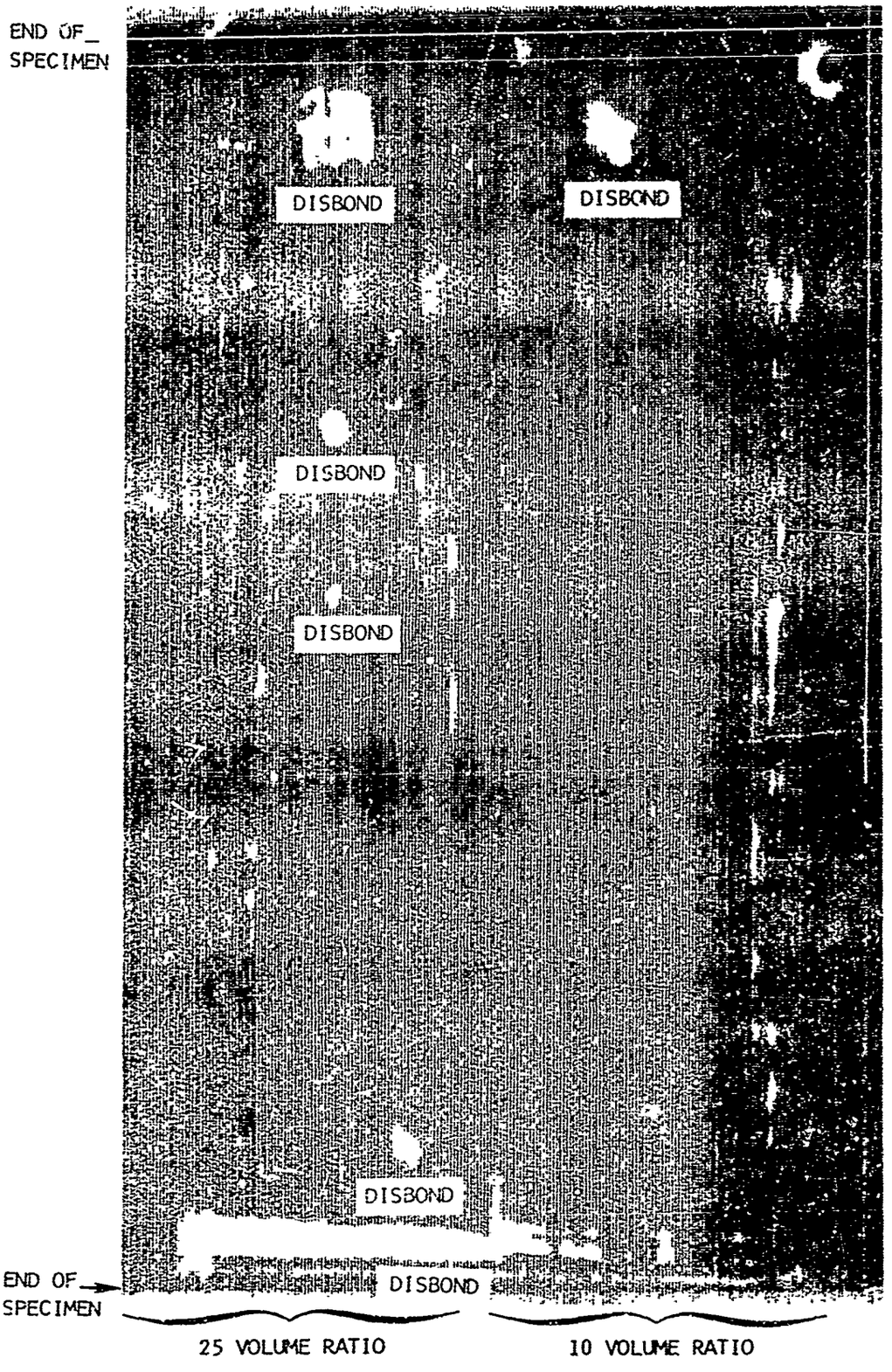


Figure 31. Ultrasonic C-scan Record of Tungsten - Copper Evaluation Specimen; Test Sensitivity 1.0

2. Disbond areas are visible at all gain settings, with the optimum resolution at 1.0, when the interference from scatter had been minimized by virtue of the higher sound intensities at the high gain. The following types of disbond indications were detected:

   a. Disbonds deliberately introduced into the specimen

   b. Inadvertent or natural disbonds resulting from some improper fabrication condition (A large disbond of this type was found along one edge of the sample.)

Inspection was attempted on the evaluation specimen containing broken fiber defects; however, recordings were not made due to the lack of significant detection signal response.

ULTRASONIC INSPECTION OF TUNGSTEN-COPPER COMPOSITES

Detection tests were performed on the seven tungsten-copper composite specimens using the water immersion, pulse-echo ultrasonic method. All testing was performed at 5 MHz, using a 3/4-inch diameter lithium-sulphate transducer. Each specimen was evaluated at three instrument gain or sensitivity values. Records of the C-scan inspection at a 1:1 scan-to-record ratio are shown in Appendix III, Figures 104 to 110. An analysis of the C-scan recordings for each specimen is described in the following:

Broken Fiber Defect Detection

W-Cu Specimen 10 BF

This specimen shows large unintentional or natural disbonds in the center and along the right edge. The intentionally introduced fiber defects were not detected.

W-Cu Specimen 15 BF

A large disbond was found in top center area of the specimen. The deliberately introduced broken fiber defects were not detected.

W-Cu Specimen 20 BF

The three largest deliberately introduced broken fiber defects were detected. The defects were most clearly resolved by the lower sensitivity scans. This fact indicates that detection apparently occurred because of the scattering effects of a poor filament-to-matrix bond rather than because of a matrix nonbond condition. A natural disbond condition, also, was indicated in the center of the sample.

W-Cu Specimen 25 BF

The two largest deliberately introduced broken fiber defects were detected. The defect condition was most pronounced at the edges of the defect zones, and it is believed that sound scatter from the edges of the broken fibers was primarily responsible for the detection of the defect condition.

Fiber Misalignment Detection

W-Cu Specimen 15 A

Loss of signal was detected from both ends of the specimen. This could have resulted from either disbonds or the refraction of the signal away from the transducer by the nonparallel sample ends. Also, there appears to be a disbond condition in the center of the specimen. No evidence was found of the deliberately introduced fiber misalignment.

Disbond Defect Detection

W-Cu Specimen 15 FM

The four deliberately introduced matrix disbonds were detected. In addition, disbonds were located along the right and left edges of the plate.

W-Cu Specimen 15 M

The four deliberately introduced matrix disbonds were detected. In addition, disbonds were located along the right and left edges of the plate.

In the preceding discussion, loss of signal was assumed to have resulted from nonbonds when no obvious surface condition or fiber geometry effects could explain the signal loss. The loss of signal at the specimen edges could be accounted for by the partial absences of fibers and the incomplete bonding in this area.

ULTRASONIC INSPECTION OF BORON-TITANIUM COMPOSITES

Defect detection tests were conducted on the six boron-titanium composite specimens using water immersion, reflector plate pulse-echo technique. Records of the C-scan recordings are presented in Appendix III, Figures 111 through 116. An analysis of the C-scan recordings for each of the six titanium matrix-boron filament composites is described in the following:

Broken Fiber Defect Detection

B-Ti Specimen 10 BF

A minor disbond region was indicated in the center of the specimen. At one end of the specimen is the image of an approximately one-inch square disbond defect which appears related to the deliberately introduced broken fiber defect. Increasing the instrument sensitivity demonstrated poorer sound transmission in the center of the specimen as compared to the edges. This may have resulted from any of the following conditions or a combination thereof: (1) poor titanium alloy matrix bonds, (2) poor bond of the titanium matrix to the boron filaments, and (3) sound scatter from ruptured filaments.

B-Ti Specimen 15 BF

The same observations apply to this specimen as for specimen B-Ti 10 BF. The outline of the large square broken filament region was detected, and an inferior sound transmission region was detected in the center area of the specimen.

B-Ti Specimen 20 BF

The deliberately introduced fiber defects in this specimen were not detected ultrasonically. An unintentional centerline disbond was evident.

B-Ti Specimen 25 BF

The deliberately introduced one-inch square broken fiber defect in this specimen appears as a region of superior sound transmission as shown by the low sensitivity recording. This observation is the opposite of previous observations where the effect showed poor sound transmission in this type of defect area. This specimen contained an area near one surface that had a small segment of the titanium alloy fractured away. The fractured area was sealed with epoxy resin, but the sealed area did not exhibit superior sound transmission characteristics as was the case in specimen B-Ti 15 F where a similar fracture condition occurred. Evidently, the poor sound transmission was not associated with the layer on the broken surface.

Disbond Defect Detection

B-Ti Specimen 15 F

Large deliberate disbond areas were detected in this specimen. A small piece of titanium alloy was broken from one side of the specimen. The damaged area was filled with epoxy resin to prevent any possible water damage to the

filament interface. This area shows on low-sensitivity scan as a dark spot of excellent sound transmission characteristics. This observation suggests that perhaps a low sound transmission condition exists with this particular layer of the composite. Fiber-to-matrix disbonds were intended; however, matrix-to-matrix disbonds are evident. The aluminum oxide painted on the fibers was evidently too thick and did not permit bonding of the matrices.

B-Ti Specimen 15 M

The deliberate matrix disbonds in this specimen were detected without difficulty. The specimen appears unique in one respect. This composite exhibited superior sound transmission characteristics, as compared with the above specimens.

An unsuccessful attempt was made to obtain C-scan recordings of these specimens, using a Sperry Wideband Pulser Receiver, Sperry UM721 Reflectoscope, and a 22 MHz focused transducer. However, poor sound transmission at this frequency appeared to be the cause of the negative results.

ULTRASONIC INSPECTION OF BORON-ALUMINUM COMPOSITES

Ultrasonic inspection was performed on eight boron-aluminum composites specimens using the immersion, reflector plate pulse echo method. Photographic copies of the C-scan records are presented in Appendix III, Figures 117 through 127. An analysis of the C-scan recordings for each of the boron-aluminum composites is described in the following:

Broken Fiber Defect Detection

B-Al Specimen 10 BF

This specimen exhibited an inadvertent lack of bond over the silver foil, predominantly at one side. The higher sensitivity scans show a strong tendency for signal loss over the silver foil. One striking exception to this observation was the uncracked portion of the foil immediately below the one-inch square artificial flaws. The artificial flaws were detected by virtue of their superior sound transmission characteristics at the higher test sensitivities.

B-Al Specimen 15 BF

The ultrasonic results for this specimen were virtually identical to those for specimen B-Al 20 BF. The same large center section disbond was again apparent, which correlated with a characteristic radiographic pattern and specimen surface texture. At the higher sensitivities, the same signal loss

was noted from regions containing the silver foil. Some evidence of the one-inch square broken fiber defect was visible on the highest sensitivity C-scan record.

B-Al Specimen 20 BF

The overall bond integrity of this specimen was quite good as shown by the low sensitivity scan. Some minor disbonds were evident near the centerline and these correlated with a radiographic pattern and a rough surface texture on the reverse side of the plate. Visible cracking of the aluminum facing sheets was not detected. The one-inch square broken fiber defect was detected on the two higher sensitivity scans because improved signal transmission was obtained, due to the missing silver foil. The reverse side surface scans were not significantly different from the front surface scans.

B-Al Specimen 25 BF

The bond integrity of this specimen was generally good with some unintentional disbond conditions located in the center of the specimen as shown on the low sensitivity record. The edge of the surface depression created by the largest deliberate defect was apparent in the low sensitivity scan. Perhaps the most striking feature of the higher sensitivity scans was the large "X" pattern on the C-scan traces. This originated from a varied surface pattern on the reverse side of the specimen and was traced to markings on a copper shim used in fabrication. Again, the reverse side scans were not significantly different than the front surface scans. In the high sensitivity scans, the silver foil pattern was again evident due to differences in signal loss caused by the foil strips.

Disbond Defect Detection

B-Al Specimen 15 F

The bond integrity of this specimen appeared excellent. No evidence of the fiber disbond defects were found ultrasonically. Surface irregularities on the part were more clearly detected giving a good indication of the resolving power of the technique. The reverse side scans were not significantly different than the front surface scans except that the surface irregularities were more clearly visible with the side having the irregularities facing the transducer. Some minor unintentional disbonds were indicated along the edges of the specimen.

Section VII

ELECTROMAGNETIC INSPECTION

A series of magnetic inspection tests were conducted on the contract specimens. These tests were intended to establish the feasibility of detecting gross magnetic effects in the composite specimens. As the specimens contained no ferromagnetic materials, the inspection efforts were directed toward the effects of eddy currents, paramagnetism, and diamagnetism. Diamagnetic material weakens the field; paramagnetic material strengthens the field. These effects, however, are also quite small as seen from the following listing of the elemental magnetic susceptibilities for the composite materials:

Boron - 6.7×10^{-6}
Copper - 5.5×10^{-6}
Tungsten + 59×10^{-6}
Titanium + 153×10^{-6}

The inspection system (Figure 32) used a stationary, permanent magnetic field with a fixed Hall Effect probe for detection. The lower magnet, approximately 200 gauss, was opposed by small magnets mounted circumferentially around the Hall probe. The Hall probe was used with a Dyna Empire Model 900 Gauss meter. The operating principle of this instrument is based on the Hall Effect wherein an alternating current generated by a 2 KHz oscillator is applied across the probe element. When this element is exposed to a magnetic field whose lines of force are perpendicular to the plane of the element, a voltage is developed across the element at right angles to the flaw direction of the excitation current. The developed voltage is proportional to the flux density of the magnetic field. The magnetic field and/or eddy current data was indicated on the gaussmeter. During automatic scanning inspection, the signal was fed to an x-y recorder. Signal amplitude was plotted on the y-axis, scan position on the x-axis.

When a specimen was positioned within the field, a slight change was observed in the magnetic field. When the specimen was scanned between the magnets, additional magnetic field changes were observed which could partially be attributed to irregularities in the spacing due to specimen dimension variations, but may also be due to other effects. A check was made to determine the sensitivity to a 0.001-inch diameter nickel fiber attached to the specimen surface. The fiber was readily detected at signal levels up to 50 to 100 times the background level.

The boron-titanium 25 BF specimen was evaluated first because titanium had an above-average comparative magnetic susceptibility. Scans were made over the on-inch square missing fiber area and apparent differences were noted; however, when the entire specimen area was inspected, the differences were not identifiable (Figures 33, 34, and 35).

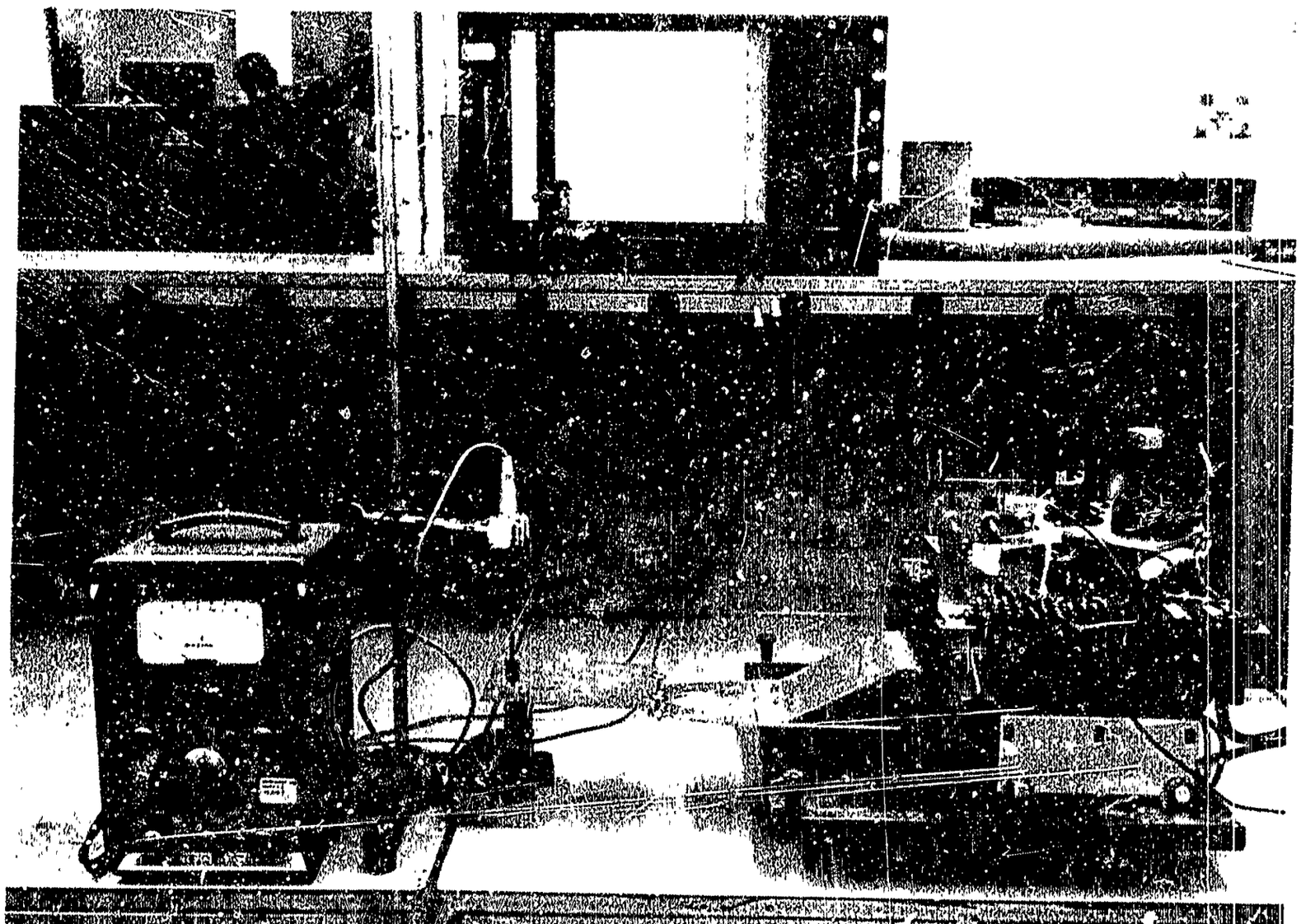


Figure 32 Magnetic inspection system

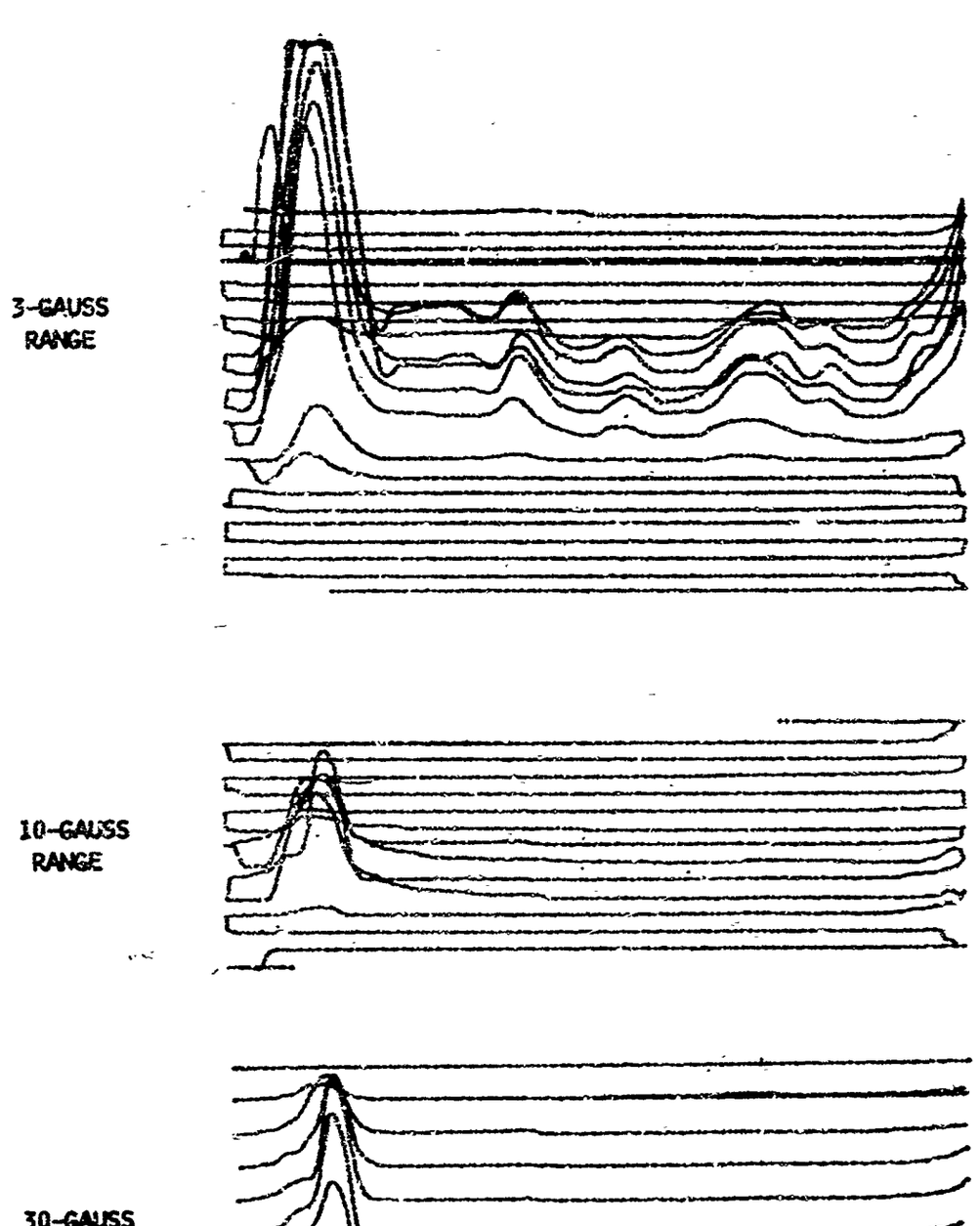


Figure 33. Magnetic Inspection, Boron-Titanium 25BF, Record of Calibration at 3- , 10- , and 30-gauss

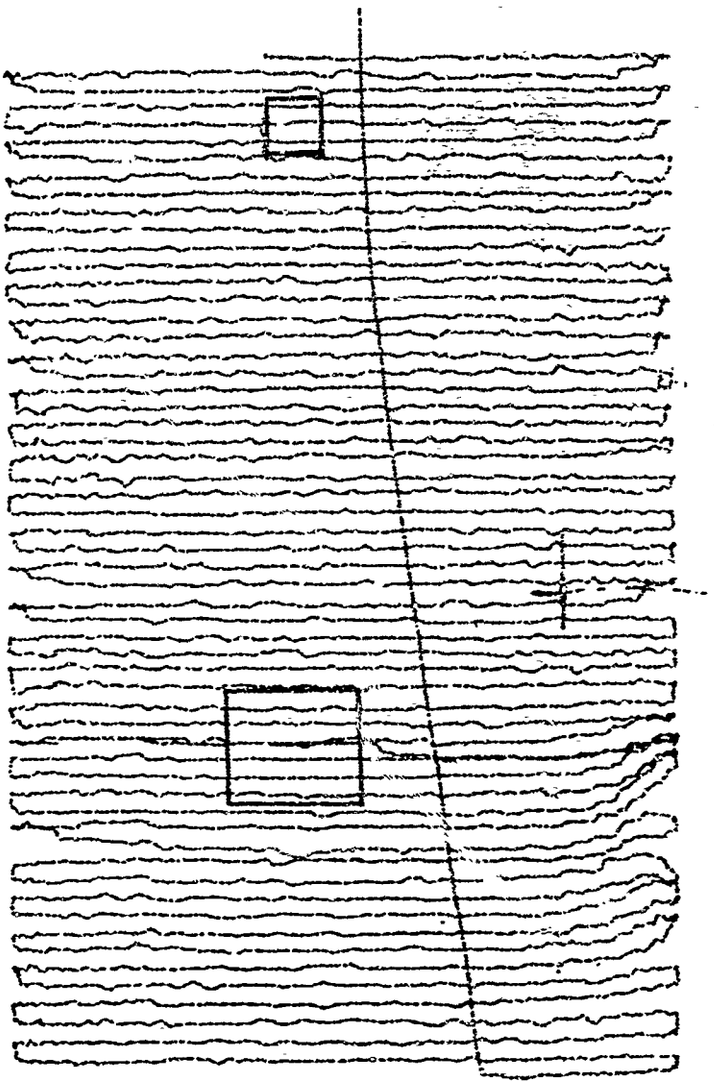


Figure 34. Magnetic Inspection, Boron-Titanium 25DF, Sensitivity Range 0.5 Gauss/Inch; 1-inch and 1/4-inch Defect Location Noted

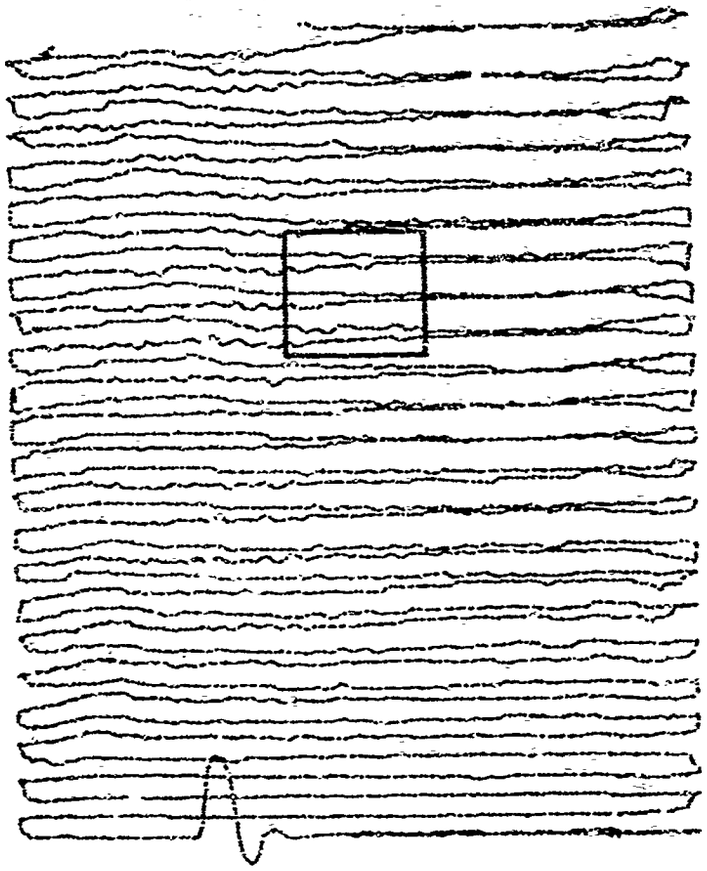


Figure 35. Magnetic Inspection, Tungsten-Copper 25BF, Sensitivity Range 0.5 Gauss/Inch; 1-inch Defect Location Noted

The tungsten-copper 25 BF specimen did not show any magnetic activity but did show evidence of eddy currents. This was identified by a change in polarity in the magnetic field indication with a change in scan direction.

The boron-aluminum 25 BF specimen gave negative results with detected signals barely perceptible, many orders of magnitude below a useful test level.

Section VIII

FIBER OPTICAL INSPECTION

The use of very small diameter fibers in diffusion-bonded composites requires proof of the fiber cleanness and integrity. Further, inspection should be adaptable to continuous, in-line processing to ensure high quality fiber in the final specimen. A number of optical inspection systems were developed using a microscope and various imaging systems. It was desired that the complete circumferential area of the fiber be viewed at one time. Optical imaging systems were evaluated, using front surface mirrors singly and in combinations.

The single mirror system provided two views of the fiber, covering approximately 225 degrees of surface area. The double mirrors providing three views. While photos obtained from the double-mirror arrangement were clear, the method necessitated accurate positioning of the wire in the mirror "V." Some distortion was evident in the image projected from the mirror juncture. The use of a single mirror to achieve two views is preferable because it requires only that the wire pass close to the mirror. 60X magnification proved adequate in revealing small dirt particles and erosion pits in the boron fibers.

The single-mirror imaging system was adapted to a fiber spool system, to determine the feasibility of continuous in-process optical inspection. A pyrex glass guide was made to hold the fiber in focus while the fiber was pulled past the microscope stage. Using a motion picture camera, photographs were taken at the rate of 24 frames per second as the fiber was reeled past the viewing field. A motion picture film was prepared, demonstrating successful detection of anomalies on the wire surface. The in-motion inspection system, and excerpts from the film, are shown in Figures 36 through 39.

The microscope system was calibrated by using a 200-mesh electrolytically prepared electron microscope grid. The grid had a wire diameter of 40 microns and hole size of 80 microns. Discrepancies in the 40-micron wire were noticeable at 60X magnification with the grid at a 60-degree angle. When the focus was adjusted to bring in two horizontal wires, wire imperfections less than 1/20th the hole size were lost. Usable depth of field for this system appeared to be approximately 3.5 mils with a resolution of 0.2 mils.

Attempts to introduce cracks in the boron fiber resulted in fracture. Photographs of a broken fiber are shown in Figure 40. The small longitudinal crack, which was apparent at 500X magnification, could not be discerned at 60X. Fluorescent penetrant was applied to the fiber end, but could not be detected

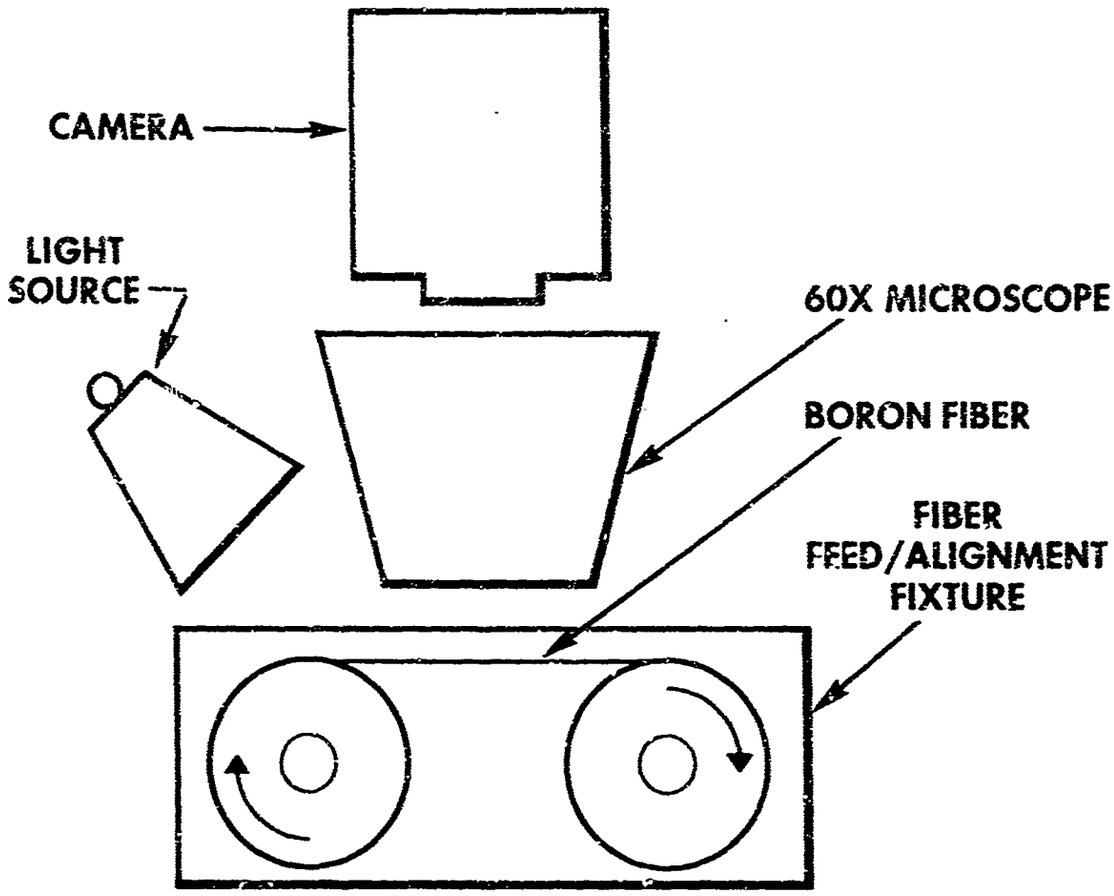


Figure 36. Block Diagram of Experimental Boron Fiber Inspection System

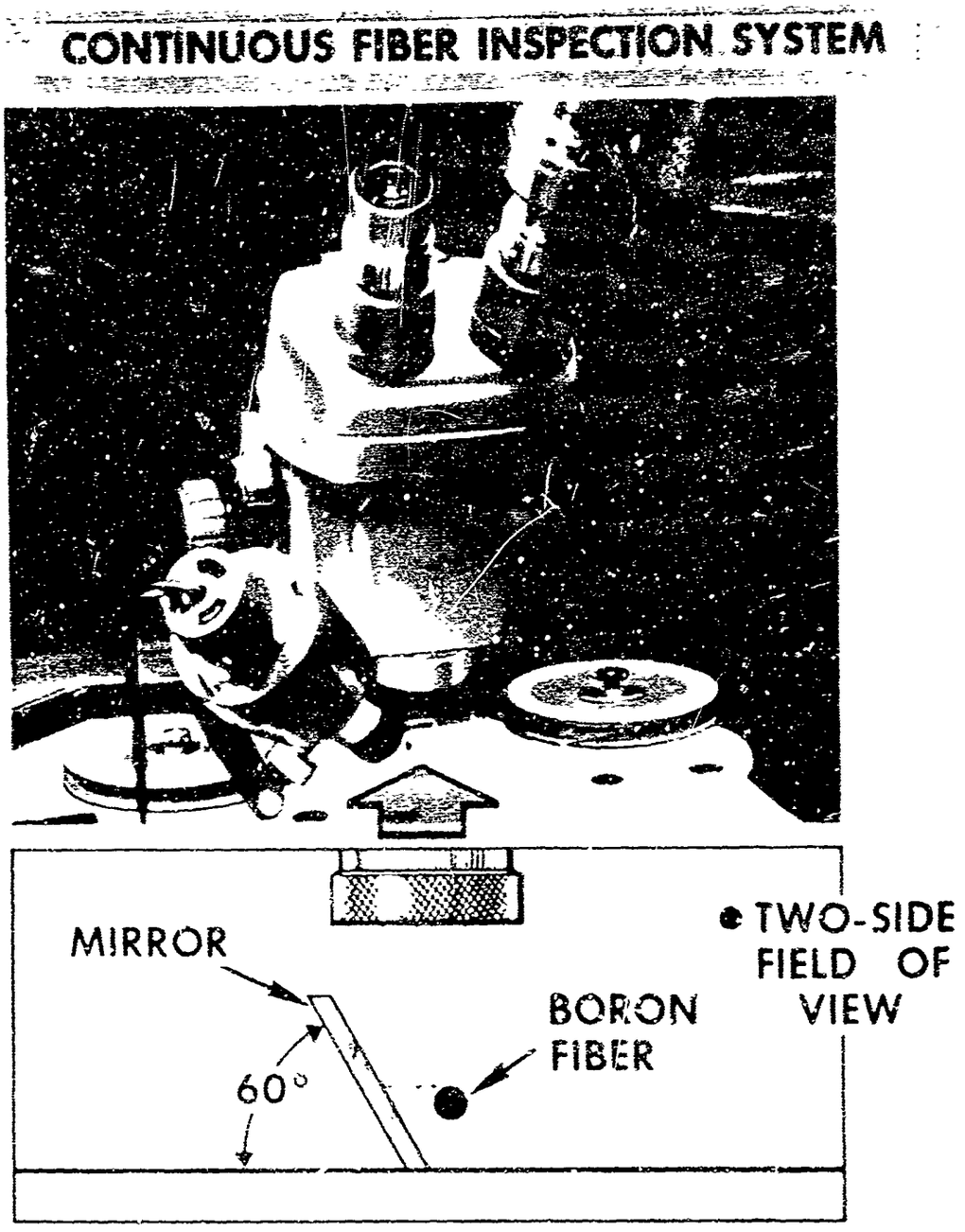


Figure 37. Continuous Fiber Inspection System

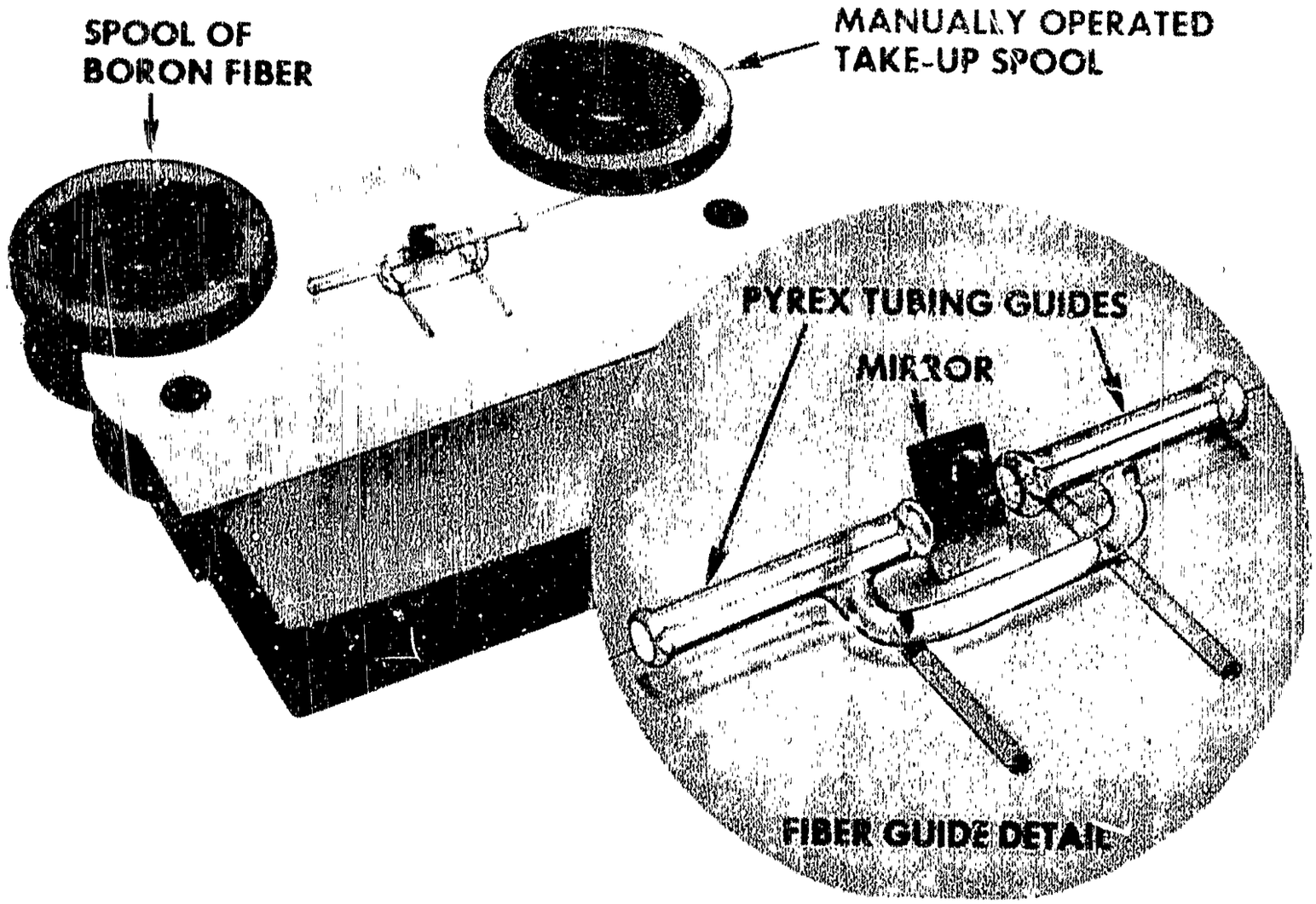


Figure 38. Inspection System Fiber-feed Alignment Fixture

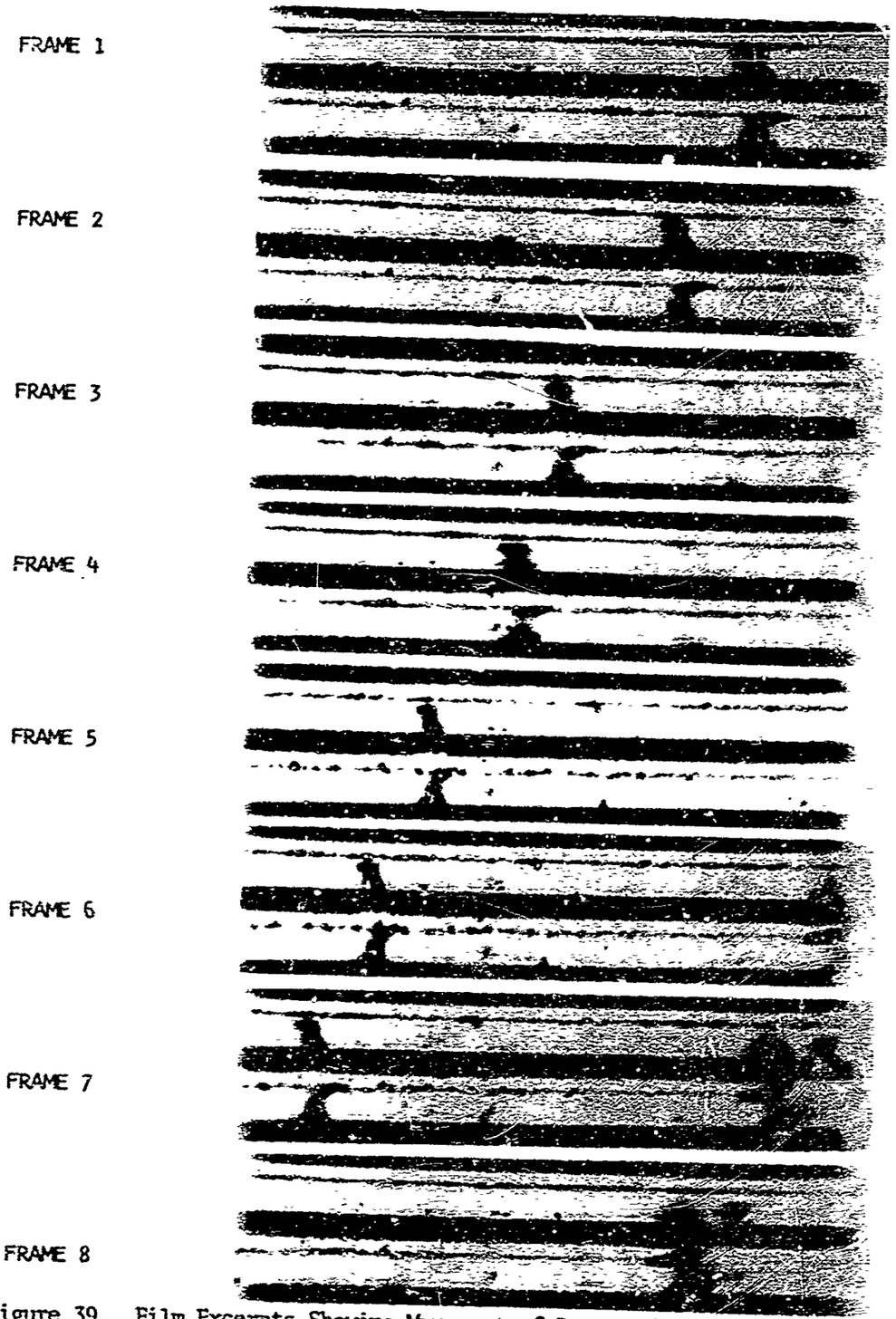
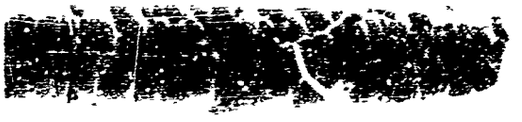
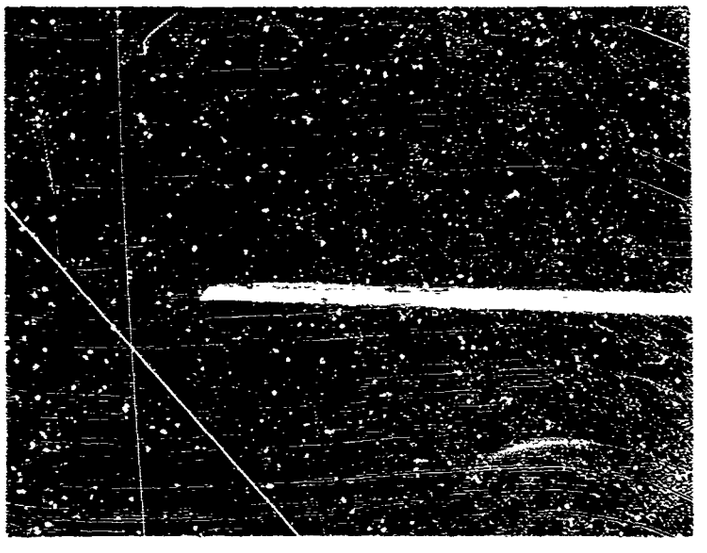


Figure 39. Film Excerpts Showing Movement of Boron Fiber Past Viewing Field During the Continuous Inspection Process



500X



60X

Figure 40. Photographs of Broken Boron Fiber

at up to 100X. However, this test was not conclusive since application of the penetrant to the fiber requires further development in terms of solution concentration and the black light intensity.

An optimized fiber inspection system would include both the cleaning and inspection operations in a two-stage, continuous in-process operation directly prior to the winding and diffusion-bonding process. The cleaning system, depicted in Figure 4, and optical inspection system, shown in Figure 37, provide the basic elements for such an optimized system, having demonstrated the feasibility of in-process systems. Further development of an optimized system involves two significant problems: (1) the present absence of, and need for, definitive fiber inspection criteria; and (2) the need for a scanning and/or analyzing capability for the large volume of data involved in a continuous fiber inspection system. An analysis of the effectiveness of this inspection system must necessarily be deferred until definitive fiber inspection criteria is established. However, certain general conclusions are evident. The feasibility of continuous fiber inspection has been demonstrated. Increasing the inspection area from 225- to 360-degree coverage may be accomplished by using a similar mirror system on the opposite side, or two mirrors "Veed" together, or two microscopes with combined images. The problem of data reduction and analysis is considerable. If each optical display (film, viewer, CRT, etc) presents two or four fiber images approximately 0.020 inches long, one foot of fiber will require 600 displays for complete inspection. A relatively simple composite like the boron-titanium specimen, 0.040 inch thick with a 10 percent volume ratio, required approximately 4000 feet of boron fiber for a 5 x 10 inch specimen. For such a specimen, data reduction must consider a minimum of 2,400,000 displays, plus the several images within a display. This type of data analysis must consider incorporation of a computer. Problems of secondary magnitude involve mechanical considerations in handling and splicing the filamentary fibers, especially boron. A means for splicing the fiber, using a nonorganic joint for diffusion bonding, must be considered in the development of an optimized cleaning-inspection system.

Section IX

CONCLUSIONS AND RECOMMENDATIONS

RADIOGRAPHIC INSPECTION

Three different combinations of composites were studied. In these combinations the ratio of linear attenuation coefficients (for 150KV) of reinforcement fiber to matrix material have the following ratios:

Tungsten-copper	16.5
Boron-titanium	0.4
Boron-aluminum	0.81

Table VIII summarizes the results of radiographic detection capability of the various deliberate defects included in the specimens. As the table indicates, it is possible to detect fiber gaps of 1/4 inch and 1 inch areas in all specimens except in the thinnest boron-aluminum specimen. Fiber breaks of even single fibers could be observed in all radiographs of all material combinations except that of boron-aluminum, where the attenuation coefficient ratio approaches unity. Even here the detection of single fiber breaks was possible in some cases. It should be noted that the boron fiber used is not actually pure boron. A core of tungsten-boride of about 0.0005 inch diameter exists in these fibers; it is likely that the indications found on the radiographs were due, at least in part, to the higher attenuation of x-rays by this core rather than from attenuation by the boron. Resolution, therefore, depends in some measure on the recording medium. For example, in the dynamic radiographic tests, where the specimen was scanned at 625 lines per inch through the vidicon tube and TV scanner, resolution of these thin boron fiber cores was not possible, whereas, the 0.005 inch diameter tungsten fibers were clearly resolved.

Determination of disbonds by radiography was largely unsuccessful. Here again, it is a question of relative absorption coefficients of matrix and fiber material and of the alumina used to produce the disbonds. It is questionable whether a disbond without any intermediate layer could be detected by radiography. However, no attenuation data are available on alumina and the tungsten-boride; an accurate assessment of the relative absorption coefficients of such materials in the composites can therefore not be made at this stage.

Optimization experiments as to voltage are summarized in Figures 41 and 42. As expected for a given composite thickness and combination, the voltages found empirically give the best resolution increase. Optimum voltages for the aluminum and the titanium matrix specimens are very similar, as could be expected. For these, optimization here was carried out for overall contrast rather than for any specific type of defect. The relation of fiber ratio to

Table VIII

SUMMARY OF RADIOGRAPHIC DETECTION RESULTS FOR FIBER-MATRIX COMPOSITES

Specimen	Thickness (In.)	Volume-Ratio (Percent)	Broken Fibers				Disbonds			
			1 In. ■	1/4 In. ■	Approx. 10 Fibers Out in Line	R*	1 In. ■	1/4x1 In. [redacted]	1/4 In. ■	▲
TUNGSTEN-COPPER										
10BF	0.059	8.4	yes	yes	yes	yes	NA	NA	NA	NA
15BF	0.043	13.4	yes	yes	yes	yes	NA	NA	NA	NA
20BF	0.050	16.5	yes	yes	yes	yes	NA	NA	NA	NA
25BF	0.051	21.1	yes	yes	yes	yes	NA	NA	NA	NA
15FM	0.086	13.2	NA	NA	NA	NA	no	no	no	no
15M	0.135	14.1	NA	NA	NA	NA	no	no	no	no
15A	0.265	14.3	yes	NA	NA	NA	NA	NA	NA	NA
BORON-TITANIUM										
10BF	0.056	8.1	yes	yes	yes	yes	NA	NA	NA	NA
15BF	0.045	12.2	yes	yes	yes	yes	NA	NA	NA	NA
20BF	0.061	13.0	yes	yes	yes	yes	NA	NA	NA	NA
25BF	0.051	21.0	yes	yes	yes	yes	NA	NA	NA	NA
15FM	0.087	13.4	NA	NA	NA	NA	yes	yes	yes	yes
15M	0.133	13.7	NA	NA	NA	NA	no	no	no	no
BORON-ALUMINUM										
10BF	0.056	9.8	yes	yes	no	no	NA	NA	NA	NA
15BF	0.037	10.0	yes	no	no	no	NA	NA	NA	NA
20BF	0.040	12.5	yes	yes	no	yes	NA	NA	NA	NA
25BF	0.052	20.1	yes	yes	no	yes	NA	NA	NA	NA
15FM	0.092	13.1	NA	NA	NA	NA	yes	no	no	no
15M	0.145	11.4	NA	NA	NA	NA	yes	no	no	no

R* = Random fiber breaks including 1 to 5 fibers

▲ = 1 x 2 inch triangle disbond

■ = Square-shape defects

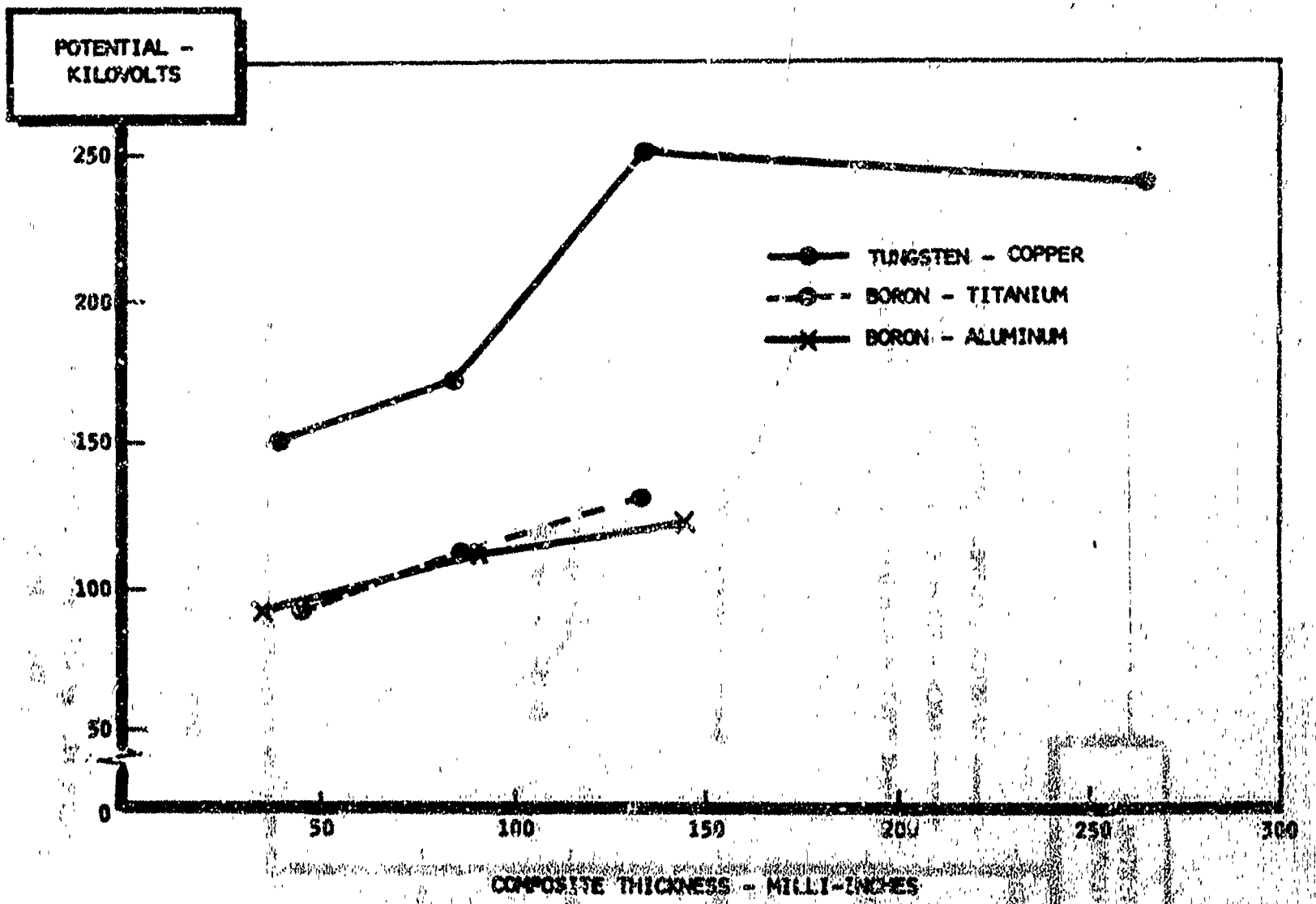


Figure 41. Relationship of Composite Specimen Thickness Versus Radiographic Inspection Voltage

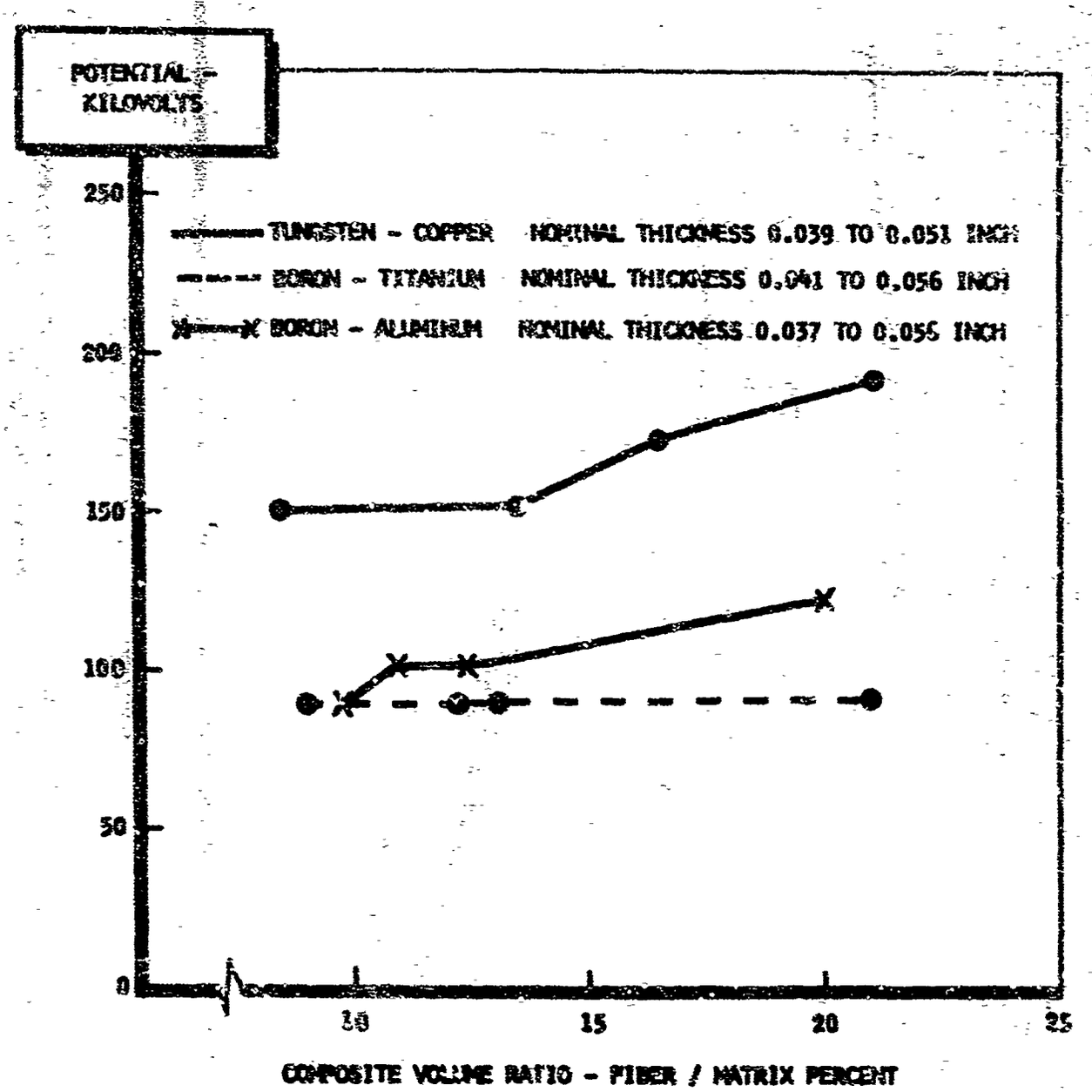


Figure 42. Relationship of Composite Specimen Volume Ratio Versus Radiographic Inspection Voltage

optimum voltage follows a similar relationship, at least as far as the tungsten-copper composite and boron-aluminum composite are concerned. However, optimum voltages appear to be independent of fiber ratio in the boron-aluminum composite. In view of the almost equal absorption coefficients of boron and aluminum, this relationship is also as expected. Part of the scatter of data obtained is due to the fact that, in the case of Figure 42, a uniform volume ratio was assumed and in Figure 41, a uniform thickness for all specimens whose data points are plotted was assumed. There were experimental variations of both volume ratio and thickness from the nominal. In order to test the data, all optimum voltages for the three composite types were plotted in Figure 43 on an attenuation normalized basis. This normalized basis was calculated by means of the relationship

$$\text{basis} = K_m V_m + K_f V_f$$

where K and V are the linear x-ray absorption coefficients and volume ratios, respectively; the suffixes m and f refer to matrix and fiber. As shown in Figure 43, data points show a fairly constant optimum voltage. By means of this relationship, it is thus possible to estimate optimum voltages for any given volume ratio and thickness. As to the optimum x-ray film to be used, the differences found between the various types were rather marginal, with Kodak Type "R" double-emulsion film giving better results, particularly in the case of boron-titanium specimens. In this latter type of material, it was also found that both voltage and exposure time are quite critical and must be rigidly standardized for consistently good results. In the experiments performed, it was found that narrow beam radiography does not have a significant advantage over the standard broad-beam type radiography. However, this result may have been partly due to a somewhat unstable scanning system. In any case, resolution of broad-beam radiography was, in all cases except that of the thin boron-aluminum sections, adequate to resolve single fiber breaks. Figure 17 shows the narrow-beam radiograph taken at 150 KV, 10 ma; fairly good fiber detail is evident. Narrow-beam radiography was also evaluated for the detection of disbonds. Figures 17 and 18 do not show evidence of the deliberate disbonds; however, good fiber detail is evident.

Major fiber break areas and general misalignment of fibers can be readily seen in almost all cases upon a casual inspection of the radiographs. However, in order to determine single fiber breaks, accurate scanning of a magnified radiograph is essential. The microradiography effort was exploratory only and did not yield results which were significantly better than those which could be obtained from a magnified radiograph. Stereoradiography, too, requires more attention. The high resolution obtained with standard methods rather obviates the need for penetrameters. In fact, better details could be observed on the actual specimens than in the case of penetrameters. The inability of radiography to detect disbonds was brought out in the penetrameter tests, using a thin film with holes. However, voltages were optimized for general

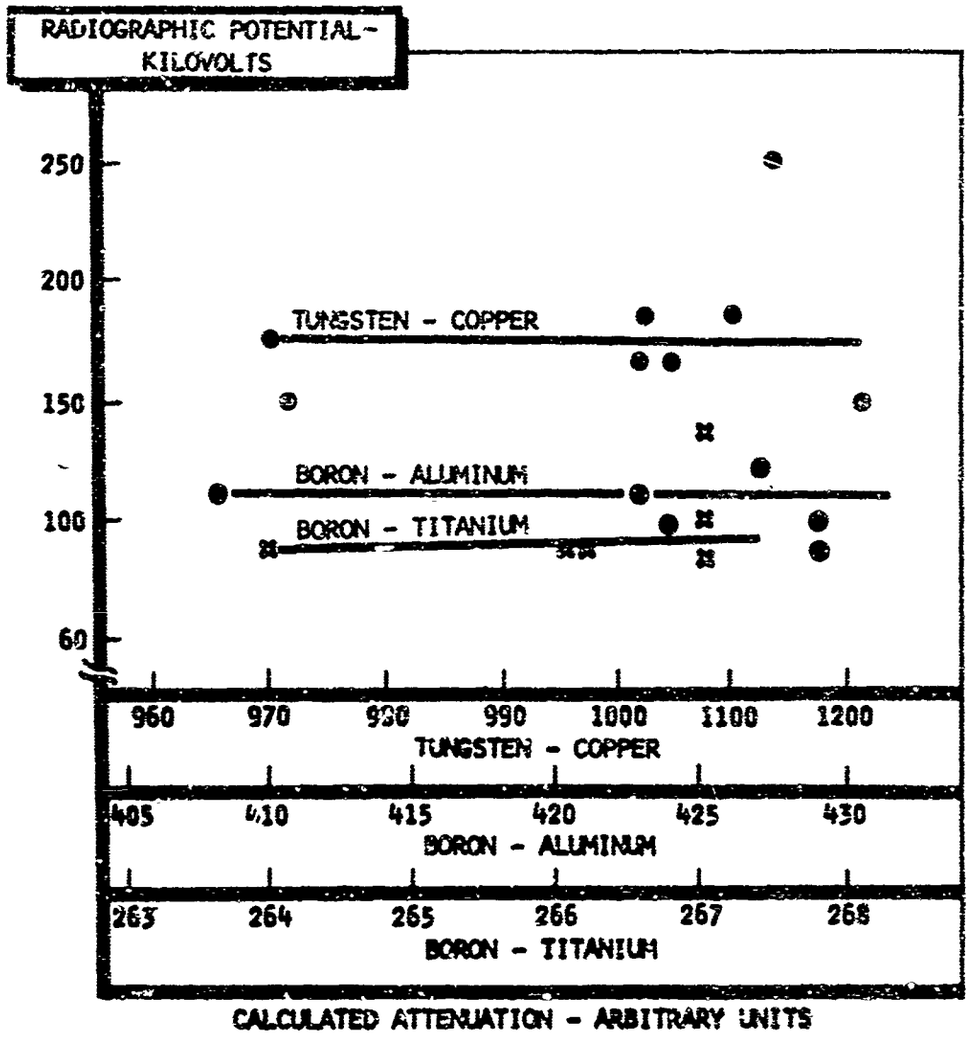


Figure 43. Optimum Radiographic Voltage Versus Normalized Attenuation for Composite Specimens

resolution of the fibers rather than that of minor disbonds; it is possible that differing optimization voltages are required for fiber resolution and for the resolution of disbonds.

Regarding recommendations for future effort relating to fiber-matrix composites, it is suggested that this be concentrated in the following areas:

1. Examination of other composites such as silicon carbide in titanium, or beryllium in titanium, to extend the limits of applicability of the optimization rule.

2. Optimization tests with penetrameters and specimens for disbonds, with and without alumina parting compound.

3. A further analysis of the effects of the tungsten-boride core in boron fiber and the density of inclusions such as the alumina parting compound.

4. Further experiments with improvements in microradiography aimed at revealing the actual shape of the ends of fractured fibers (This would provide valuable information for failure and stress analysis.)

5. Further work on dynamic testing with a better resolution vidicon tube - TV camera arrangement to give higher resolution

6. Further experiments with stereoradiography to investigate the possibility of finding a method allowing determination of the particular layer in which a defect occurs.

ULTRASONIC INSPECTION

Three types of ultrasonic tests were carried on the composite materials. Specimens were inspected by the latest pulse-echo methods. The velocity of sound in the various composites was determined and measurement of the attenuation in the composites was attempted.

The results of the pulse-echo inspection are summarized in Table IX. It is evident that standard pulse-echo methods are satisfactory for the determination of gross disbonds down to 1/4 inch square in all materials except the boron-aluminum composite, where the small area disbonds were not detected. Detection of fiber gaps and fiber breaks is limited to large area gaps. In addition to the deliberate disbonds, a number of other defects were noted, which cannot be identified until the specimens are destructively tested. No identification could be made as to the composite layer in which the disbond occurs.

Table IX

SUMMARY OF ULTRASONIC DETECTION FOR FIBER-MATRIX COMPOSITES

Specimen	Thickness (in.)	Volume-Ratio (percent)	Broken Fibers: 1 In. ■	Broken Fibers: 1/4 In. ■	Broken Fibers: Approx 10 Fibers Cut in Line	Broken Fibers: R*	Disbonds: 1 In. ■	Disbonds: 1/4x1 In. [redacted]	Disbonds: 1/4 In. ■	Disbonds: ▲
TUNGSTEN-COPPER										
10BF	0.039	8.4	no	no	no	no	NA	NA	NA	NA
15BF	0.043	13.4	no	no	no	no	NA	NA	NA	NA
20BF	0.050	16.5	yes	yes	no	no	NA	NA	NA	NA
25BF	0.051	21.1	yes	yes	no	no	NA	NA	NA	NA
15FM	0.086	13.2	NA	NA	NA	NA	yes	yes	yes	yes
15M	0.135	14.1	NA	NA	NA	NA	yes	yes	yes	yes
15A	0.265	14.3	no	NA	NA	NA	NA	NA	NA	NA
BORON-TITANIUM										
10BF	0.056	8.1	yes	no	no	no	NA	NA	NA	NA
15BF	0.045	12.2	yes	yes	no	no	NA	NA	NA	NA
20BF	0.061	13.0	yes	no	no	no	NA	NA	NA	NA
25BF	0.051	21.0	yes	no	no	no	NA	NA	NA	NA
15FM	0.087	13.4	NA	NA	NA	NA	yes	yes	yes	yes
15M	0.133	13.7	NA	NA	NA	NA	yes	yes	yes	yes
BORON-ALUMINUM										
10BF	0.056	9.8	yes	yes	no	no	NA	NA	NA	NA
15BF	0.037	10.0	yes	no	no	no	NA	NA	NA	NA
20BF	0.040	12.5	yes	no	no	no	NA	NA	NA	NA
25BF	0.052	20.1	yes	no	no	no	NA	NA	NA	NA
15FM	0.092	13.1	NA	NA	NA	NA	yes	no	no	no
15M	0.145	11.4	NA	NA	NA	NA	yes	yes	yes	yes

R* = Random Fiber Breaks ▲ = 1 x 2 inch Triangle Disbond ■ = Square Shape Defects

Sound velocity measurements were summarized in Table VII. With regard to the measurements of velocity of sound in boron, the data found are applicable to crystalline boron and may or may not apply to the amorphous boron existing in the fibers. Furthermore, no consideration has been taken of the tungsten-boride core of the fibers or of any diffusion layers. Sound velocity data can be normalized by plotting the estimated velocity of sound against the actual velocity found. The estimated velocity is given by

$$v = \sqrt{E/\rho}$$

where E is the modulus and ρ the density. These data are plotted in Figure 44, together with the data for the raw materials. The value for plotted boron is the best value obtained for crystalline boron. From the plot, it can be seen that the theoretical sound velocity in the tungsten-copper and the boron-aluminum composite should be very similar to that of copper, and aluminum, respectively. In fact, somewhat lower values were obtained experimentally. The boron-titanium alloy, which has a higher theoretical velocity than pure titanium, does show a slightly higher value than anticipated. There is only one significant difference between the tungsten-copper and boron-aluminum composite on the one hand, and the boron-titanium composite on the other hand. In the first two composites, no diffusion reactions take place, whereas, diffusion reactions occur between boron and titanium. Hypothetically, the lowering of the sound velocity could be explained by a multiple diffraction process of the sound waves caused by the fibers. In that case, all three values should be somewhat lower. Whether the slightly larger effective diameter of the boron fibers in the boron-titanium composite would affect this diffraction process is a matter of conjecture at this stage. A very important question which arises is whether this lowering of the sound velocity can be related to the fiber ratio. If it can, then a convenient nondestructive method for the determination of fiber ratio in a specimen of a known combination has been established.

Finally, some work was initiated on the determination of acoustic attenuation in composites. In these tests, the signal-to-noise ratio was too high to obtain any reliable data.

It is recommended that future work on ultrasonic inspection of composites be concentrated on the following problems:

1. A further evaluation of the relation of sound velocity in relation to predicted values and as a function of volume ratio

2. Improvements of the attenuation measurements to obtain reliable data

3. Experimental and theoretical studies to determine acoustic properties of the diffusion products and their likely effect

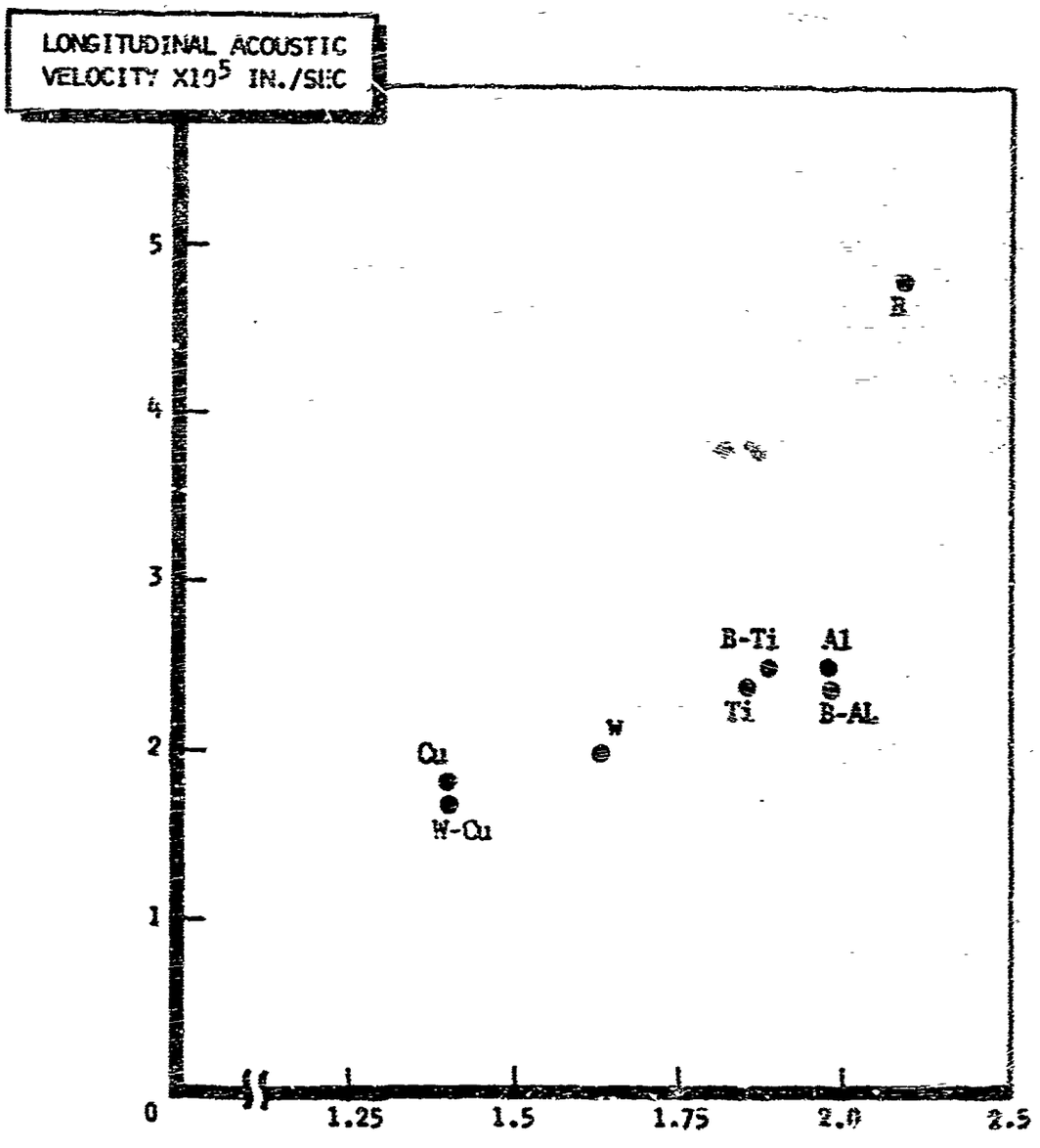


Figure 44. Calculated Acoustic Velocity ($\sqrt{E/\rho}$) Versus Measured Velocity for Composites and Materials

ELECTROMAGNETIC INSPECTION

The tests carried out were of an exploratory nature only, and no reliable conclusions can be drawn. Obviously, more sensitive probes scanning a smaller area than that covered in these exploratory tests must be utilized.

FIBER INSPECTION

The feasibility of an optical fiber inspection system, which is capable of automation and inclusion in a production setup for the manufacture of continuous fiber composites, has been demonstrated. Future work should be directed toward the development of a pilot plant and a survey of methods for the automatic scanning and utilization of data.

RESIDUAL STRESSES

No experimental work on the measurement of residual stresses in either fibers or composites has been carried out. Such work is of importance for the evaluation of composites, both in production and for research and development purposes. Some possible approaches are indicated by the literature survey.

GENERAL CONCLUSIONS

The study has shown that a combination of conventional radiographic and ultrasonic NDT methods are adequate for the routine inspection of sheet-shaped composite materials. By these methods, fiber breaks, fiber gaps, and gross disbonds can be determined. Whether the resolutions obtained on disbond determinations (1/4 inch square) are adequate for predicting composite behavior must be evaluated by a study on the effect of such disbonds on composite behavior and composite properties. The resolution of single fiber breaks and minor alignment differences seen by radiography is as detailed as can be required. Further refinements, such as determining the shape of the end of fractured fibers need to be investigated.

Section X

REFERENCES

1. NAA/LAD, "Bibliography of Nondestructive Testing Theory and Application for Composites," NA-65-813, October 1965

2. A. Kent and C.J. Davies, Met. Rev. Vol 10, n 37, 1965

3. J.W. Hedgepeth, NASA TN D88s, 1961

4. NAA/LAD "Diffusion Bonding of Aluminum to Stainless Steel," NA-64-1211 November 1964

5. NAA/LAD "Development and Evaluation of the Diffusion Bonding Process as a Method for Producing Fibrous Reinforced Metal Matrix Composite Materials," Interim Engineering Progress Report IR-S-355(II) 1965

6. "The Reactor Handbook," Vol III, Sec I, USAEC 1955

Appendix I

METALLOGRAPHIC INSPECTION OF FIBER-MATRIX COMPOSITES

Metallographic inspection was performed on tungsten-copper, boron-titanium, and boron-aluminum composite specimens. The inspection provided information regarding the nature of the diffusion bond and matrix forming characteristics, determination of actual fiber-to-matrix volume ratio, and the regularity of fiber alignment. Metallographic samples were obtained by shearing a 1/2-inch strip from the end of each 5 x 10 inch specimen. A detailed discussion of specimen preparation and inspection techniques is presented in Section IV of this report. Specimen identification and specification data given in table A-1.

The following sequence of photographs show sections of the specimens at 10X, 150X, and 500X magnification. Typical fiber spacing and integrity of the fiber-matrix bond are visible in the photographs.

Table X

COMPOSITE SPECIMEN THICKNESS & VOLUME RATIO MEASUREMENTS

Specimen	Thickness (In.) Design	Measured	Volume Ratio Calculated %	No. of Fiber Layers
Tungsten-Copper				
10 BF	0.040	0.039	8.4	3
15 BF	0.040	0.043	13.4	4
20 BF	0.040	0.050	16.5	3
25 BF	0.040	0.051	21.1	4
15 FM	0.090	0.086	13.2	9
15 M	0.125	0.135	14.1	15
15 A	0.250	0.265	14.3	28
Boron-Titanium				
10 BF	0.040	0.056	8.1	3
15 BF	0.040	0.045	12.2	4
20 BF	0.040	0.061	13.0	3
25 BF	0.040	0.041	21.0	4
15 FM	0.090	0.087	13.4	9
15 M	0.125	0.133	13.7	14
Boron-Aluminum				
10 BF	0.040	0.056	9.8	3
15 BF	0.040	0.037	10.0	3
20 BF	0.040	0.040	12.5	4
25 BF	0.040	0.052	20.1	4
15 FM	0.090	0.092	13.1	8
15 M	0.125	0.145	11.4	14

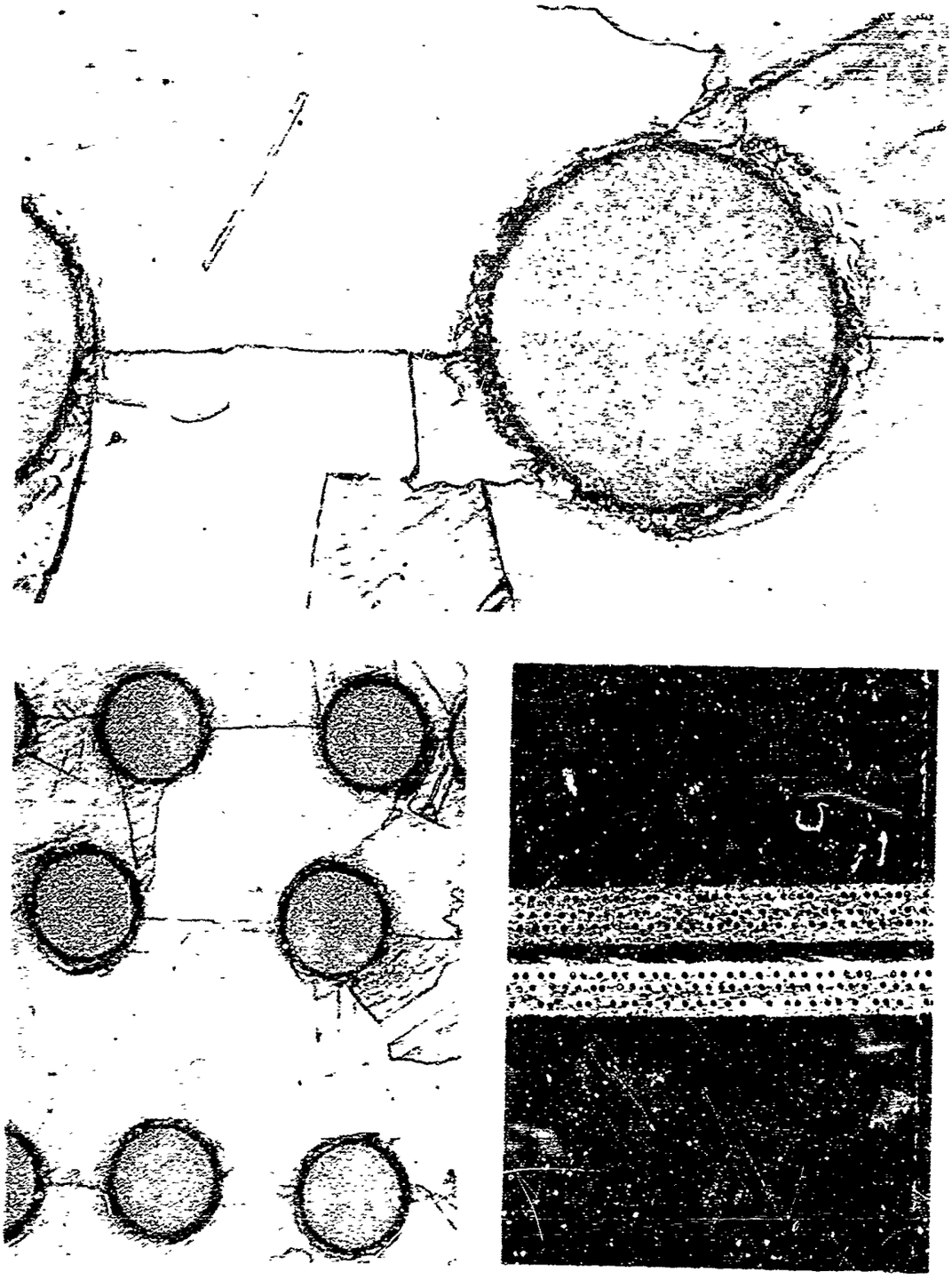


Figure 45 . Tungsten-Copper - 10 BF

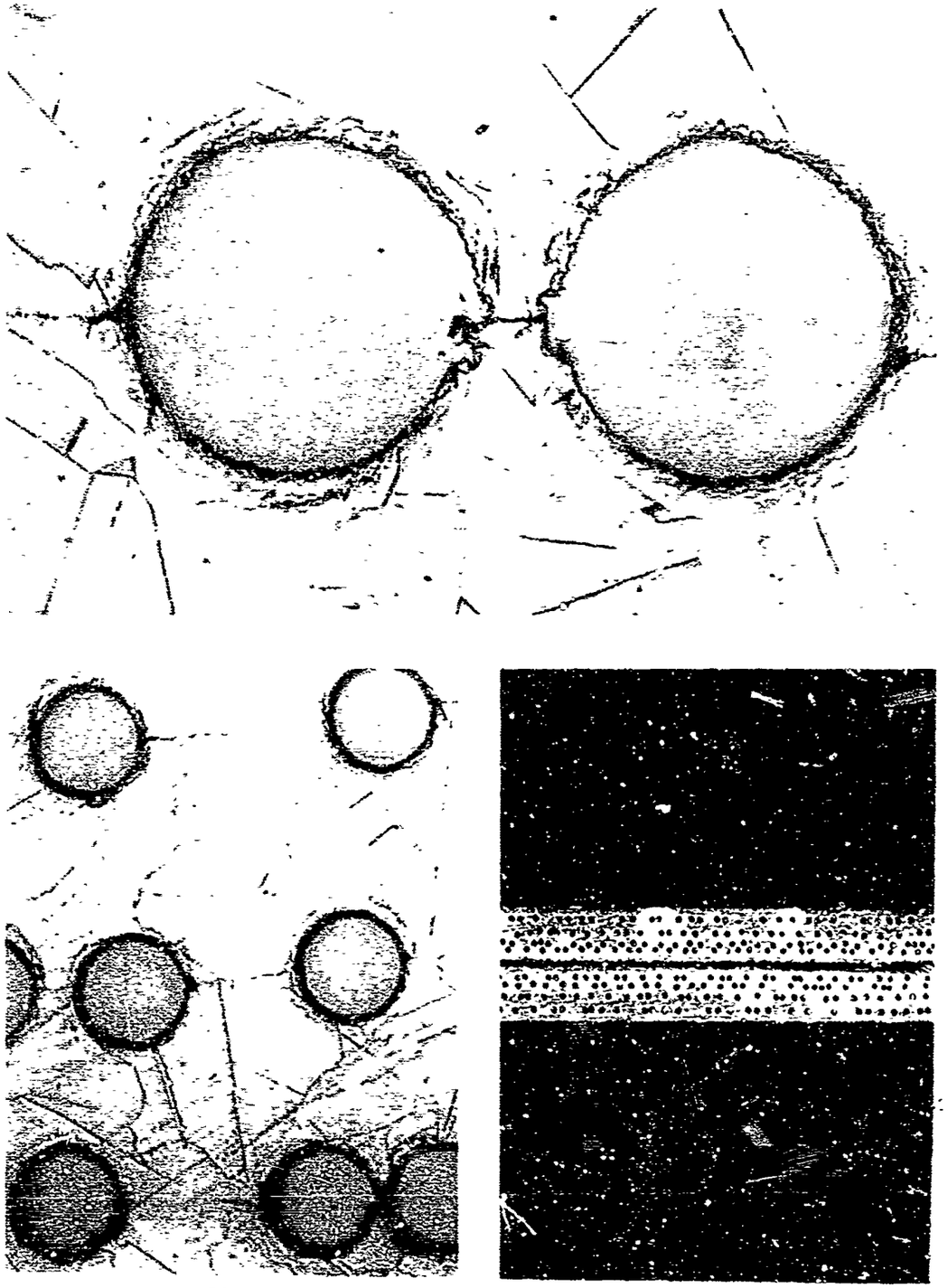


Figure 46. Tungsten-Copper - 15 BF

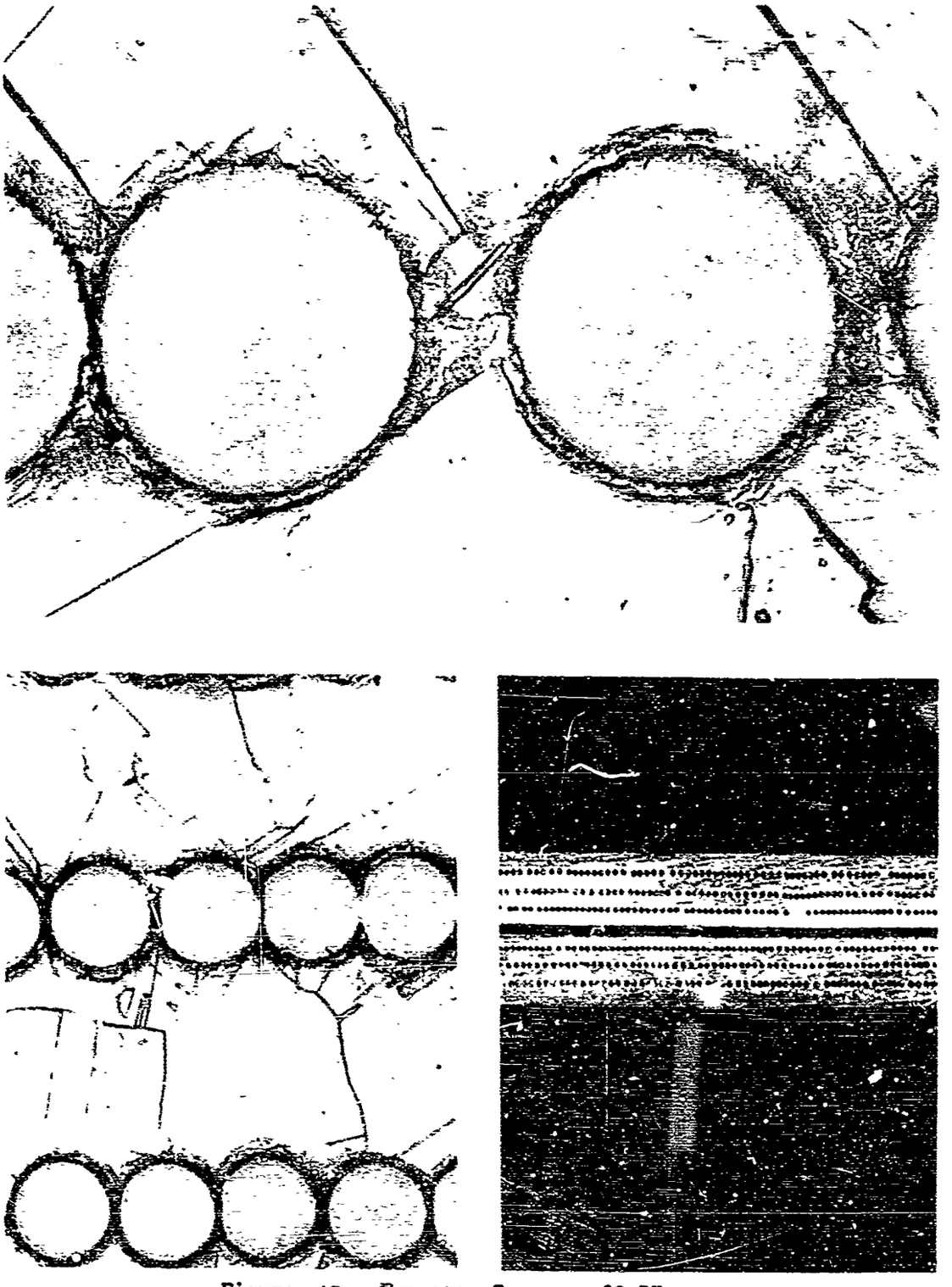


Figure 47, Tungsten-Copper - 20 BF

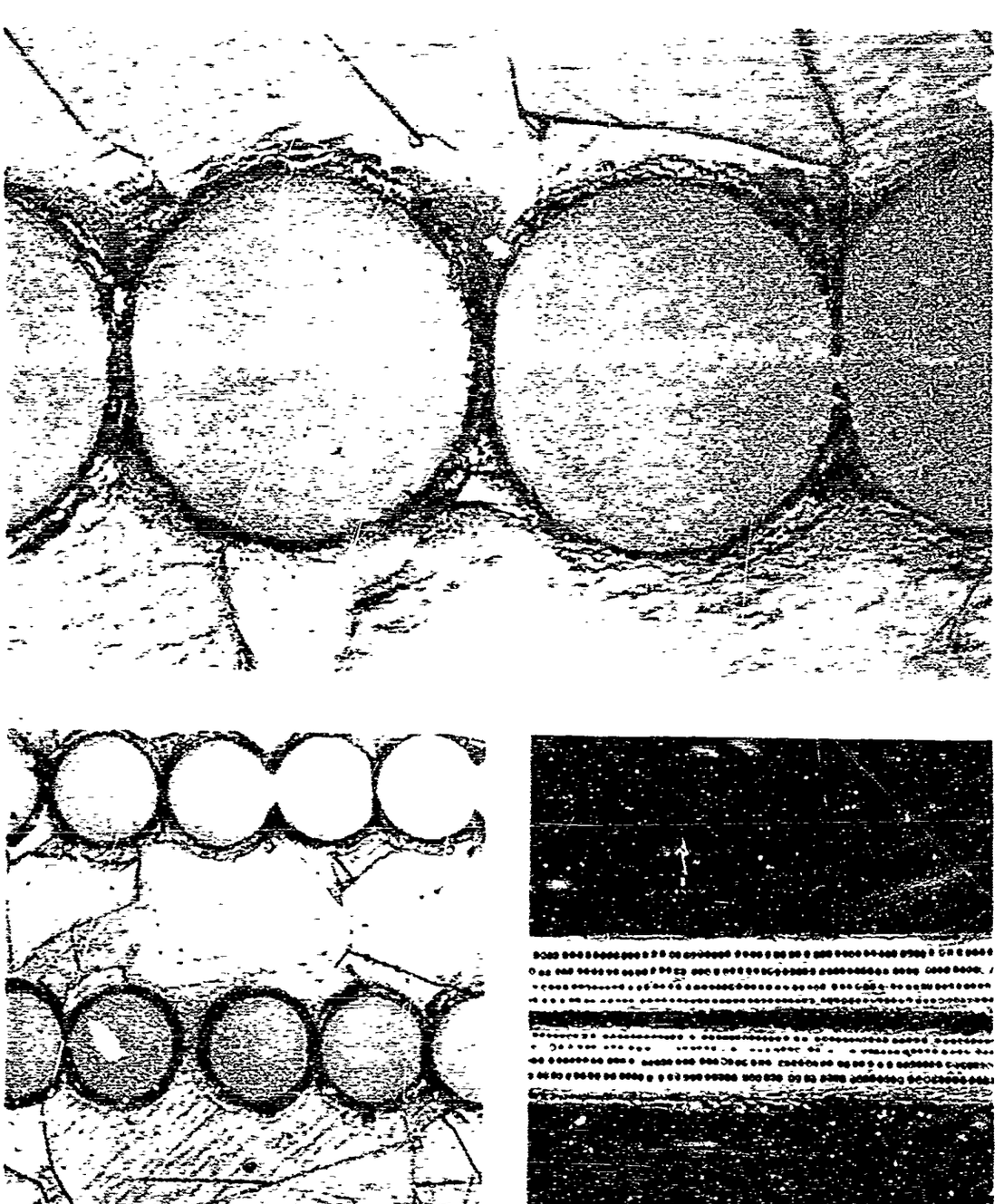


Figure 48. Tungsten-Copper - 25 BF

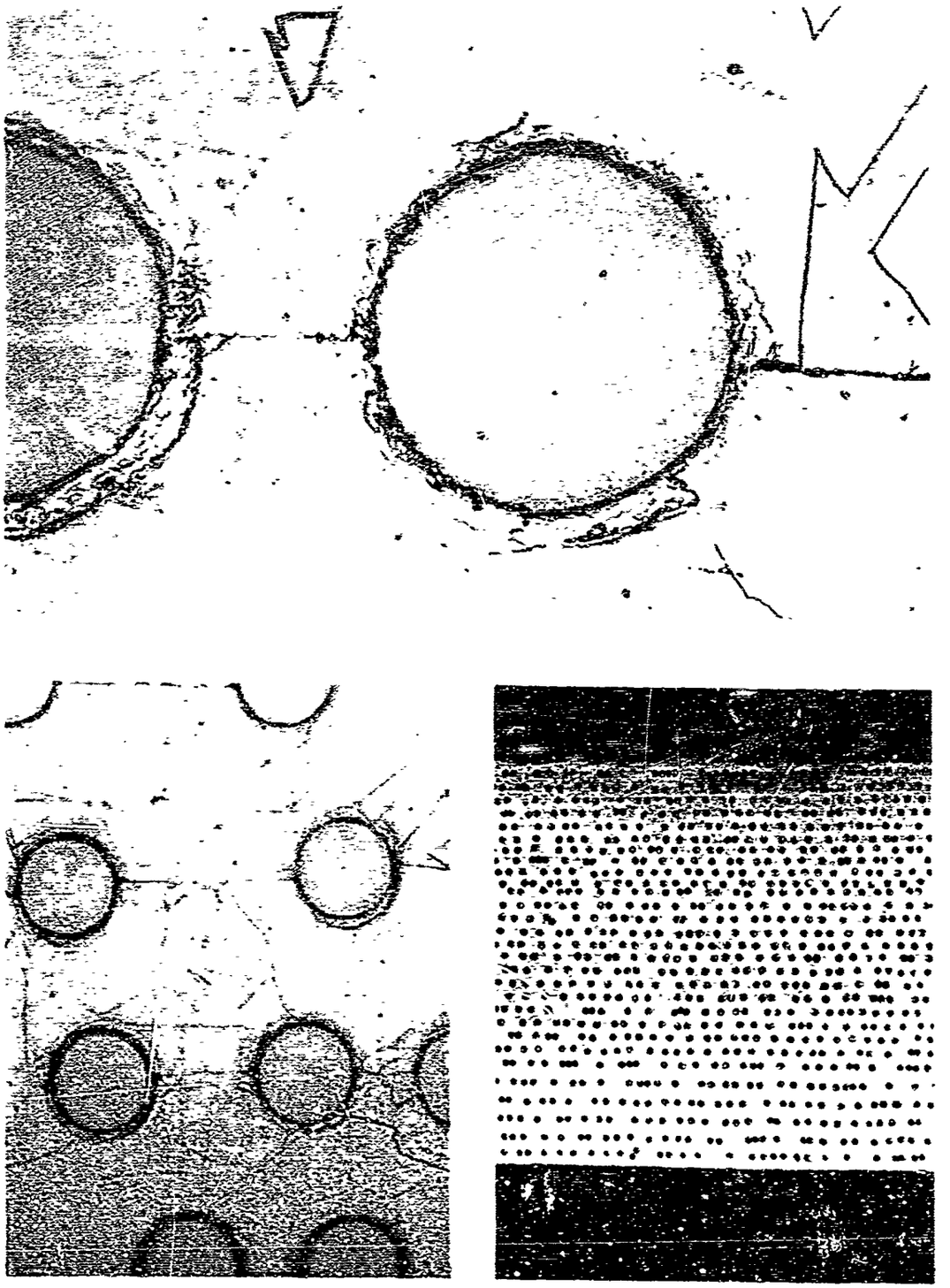
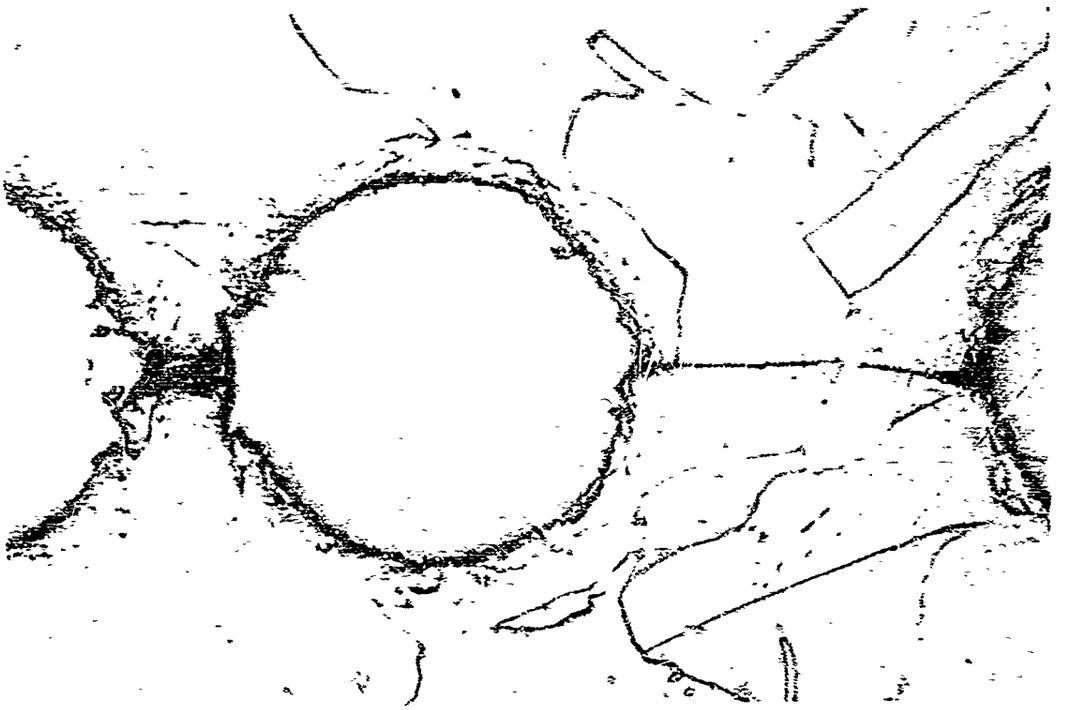
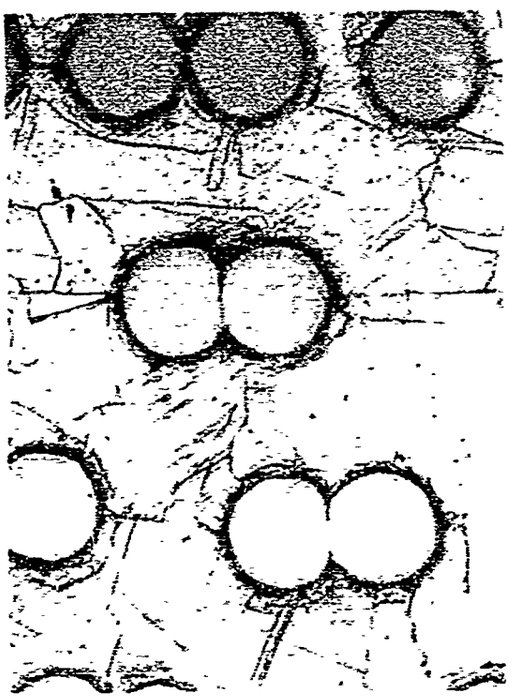


Figure 49. Tungsten-Copper - 15 A





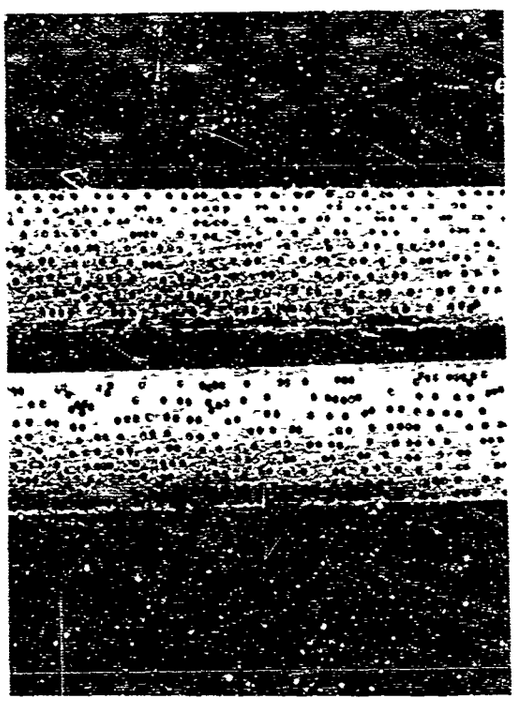


Figure 50. Tungsten-Copper - 15 PM

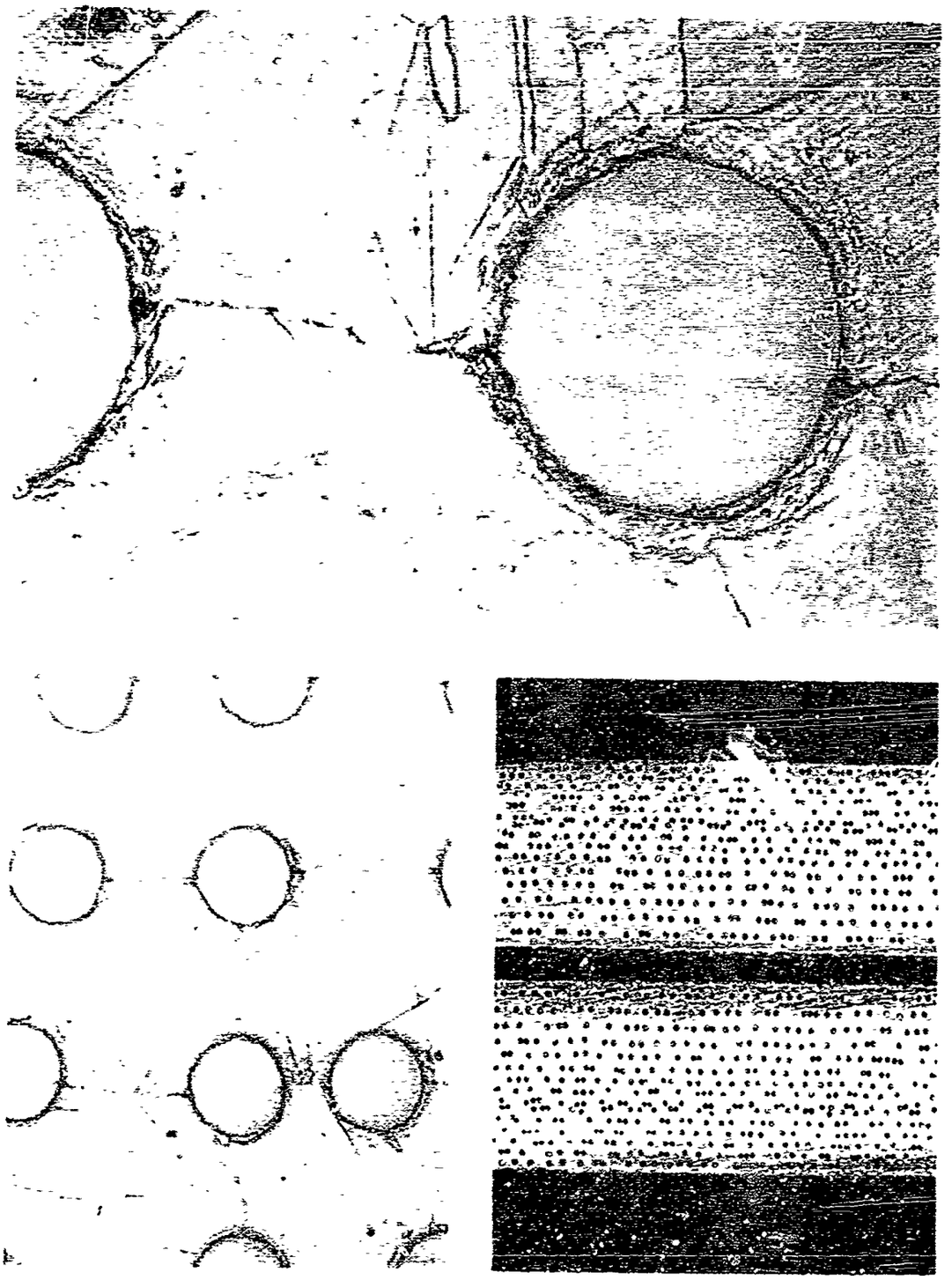


Figure 51. Tungsten-Copper - 15 M

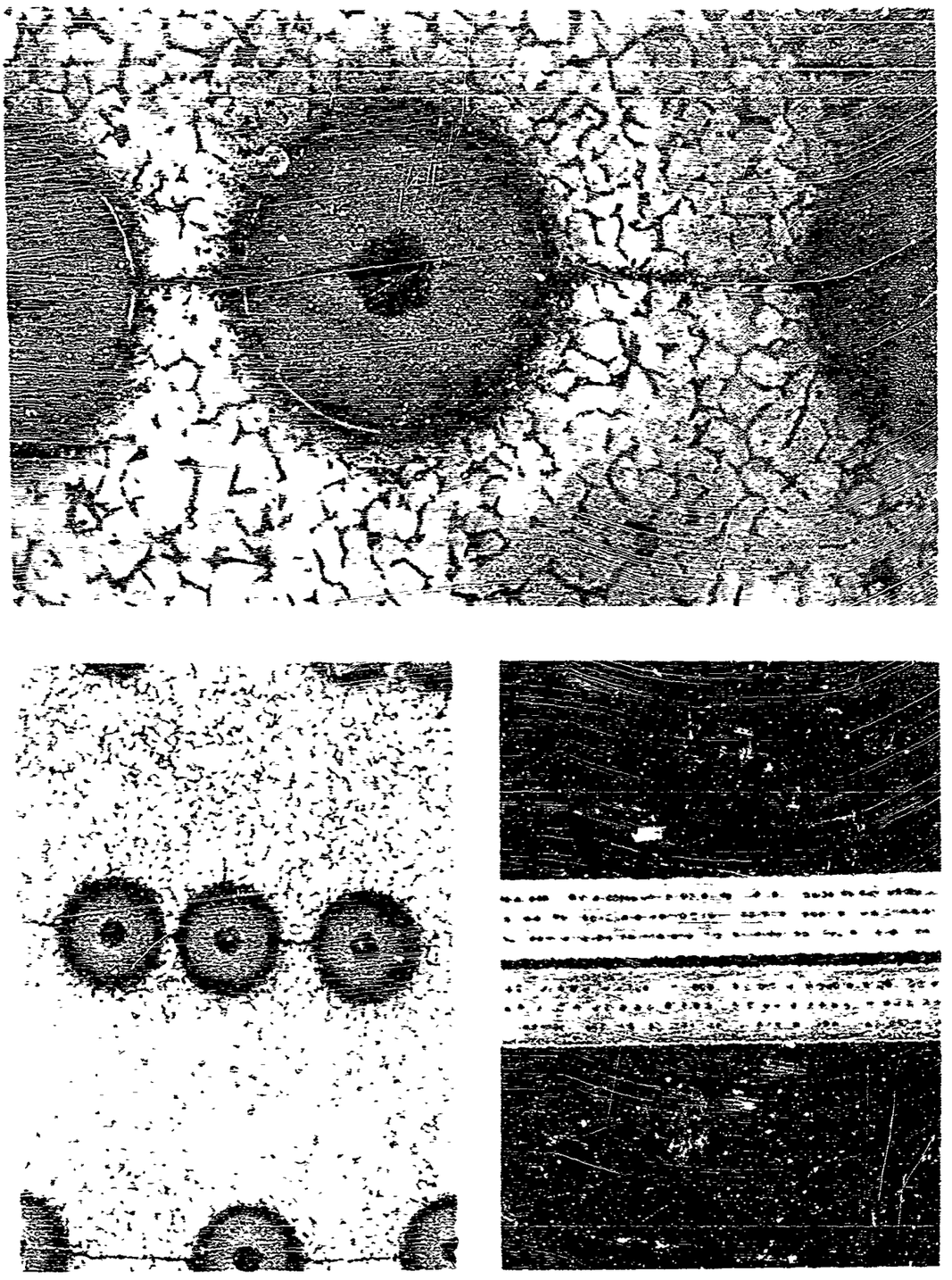


Figure 52. Boron-Titanium - 10 BF

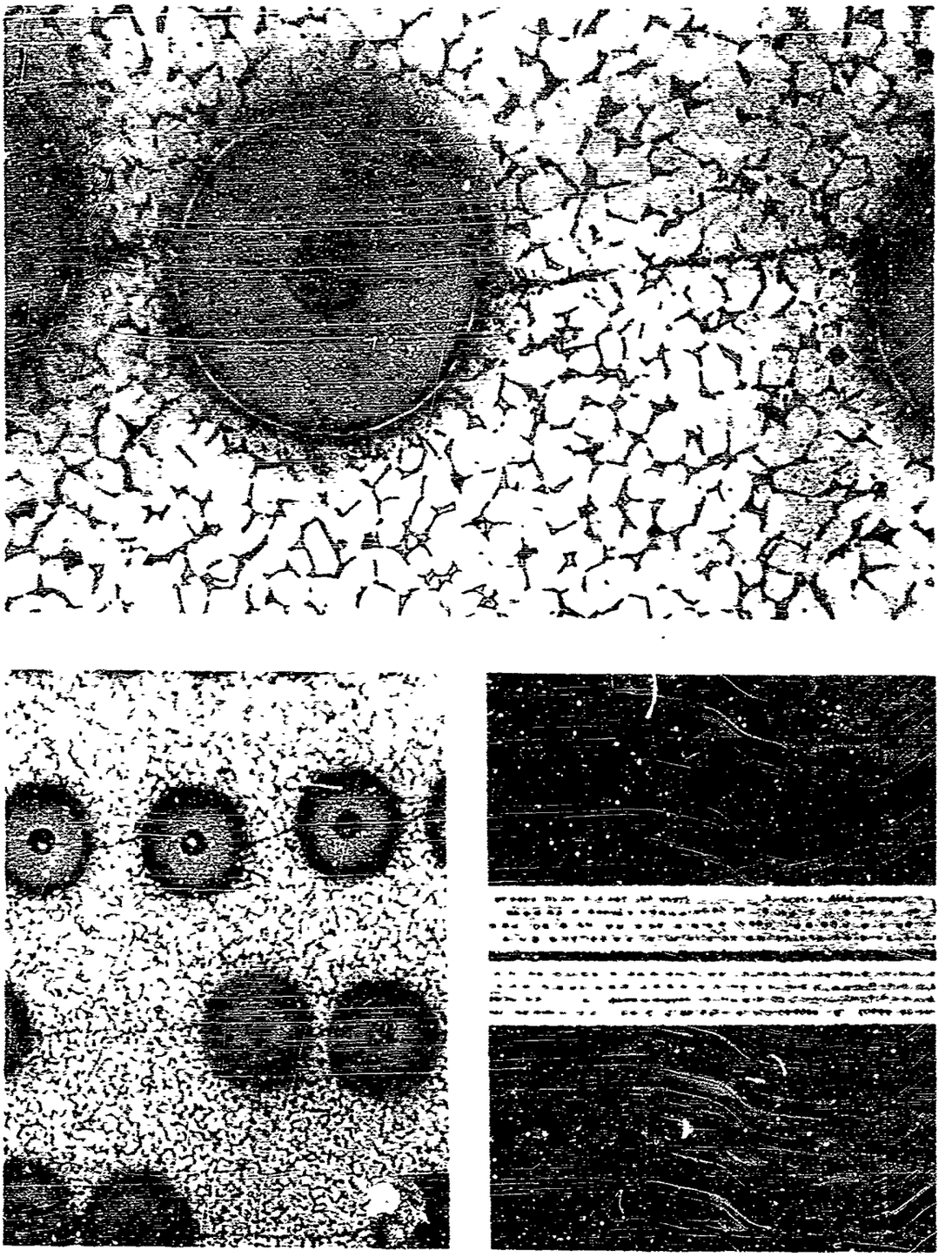


Figure 53. Boron-Titanium - 15 BF

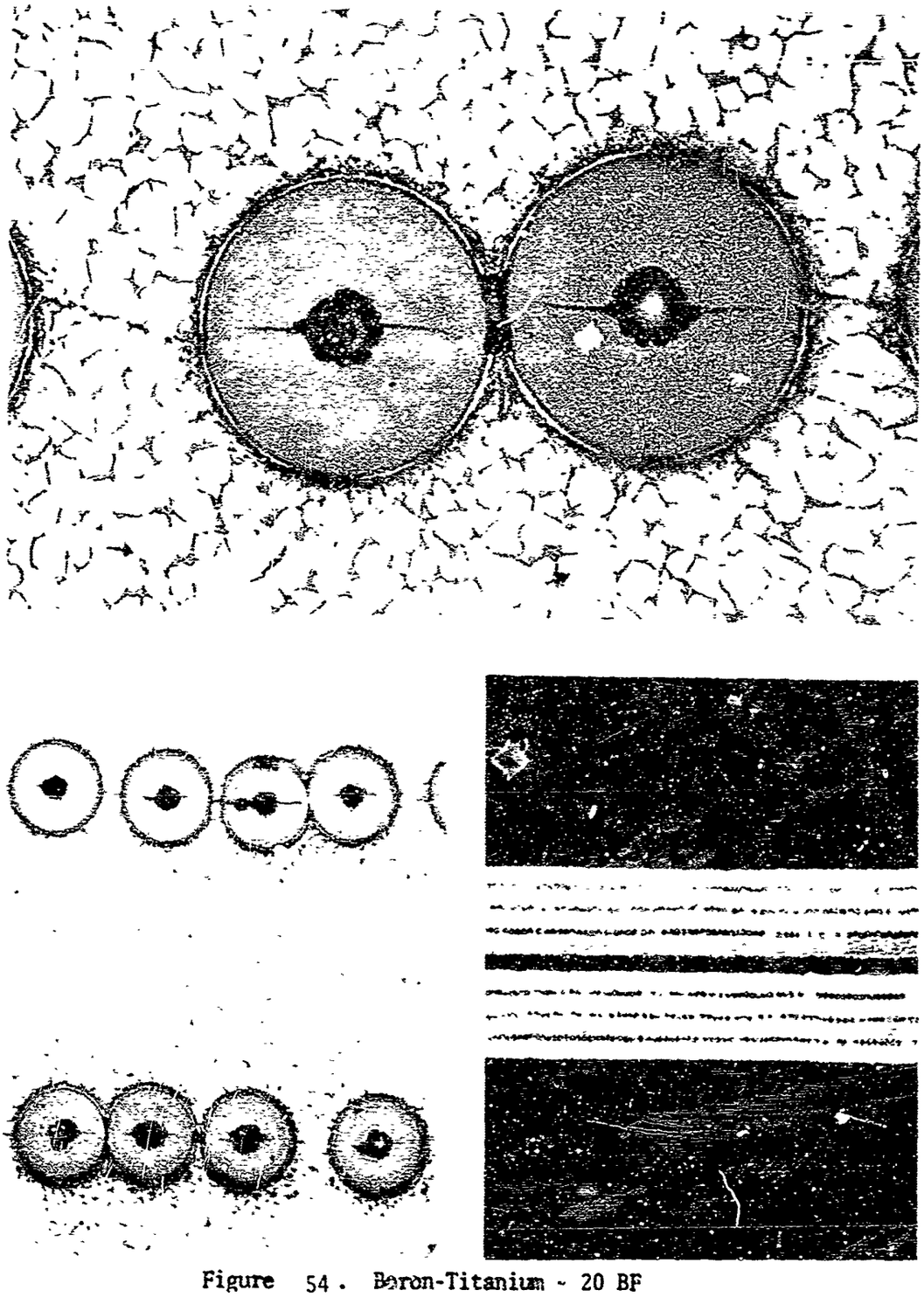


Figure 54. Boron-Titanium - 20 BF

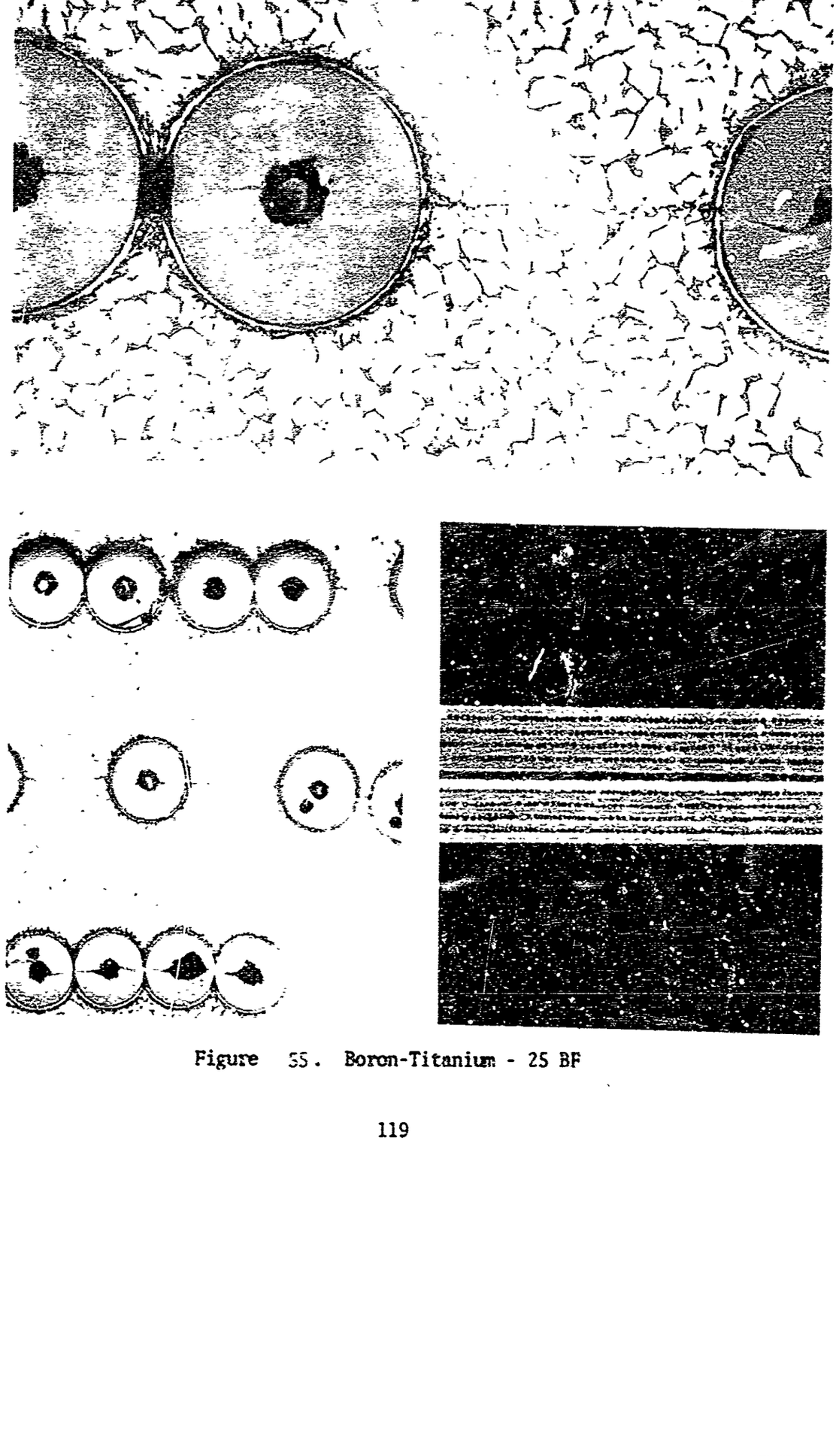
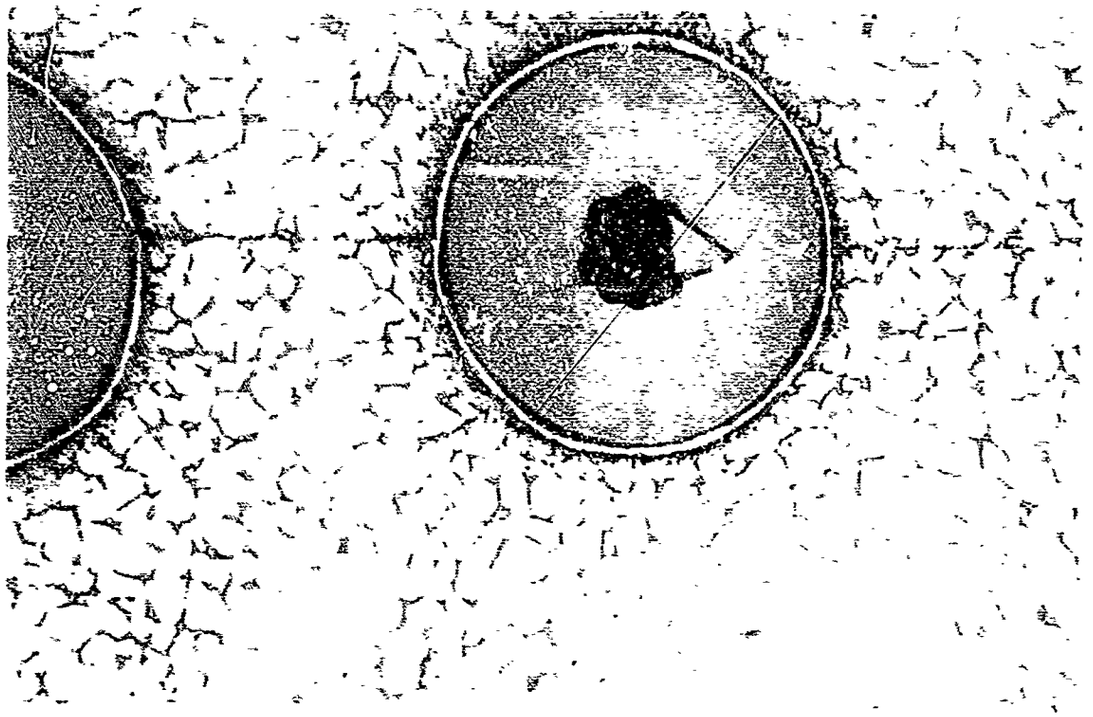


Figure 55. Boron-Titanium - 25 BF



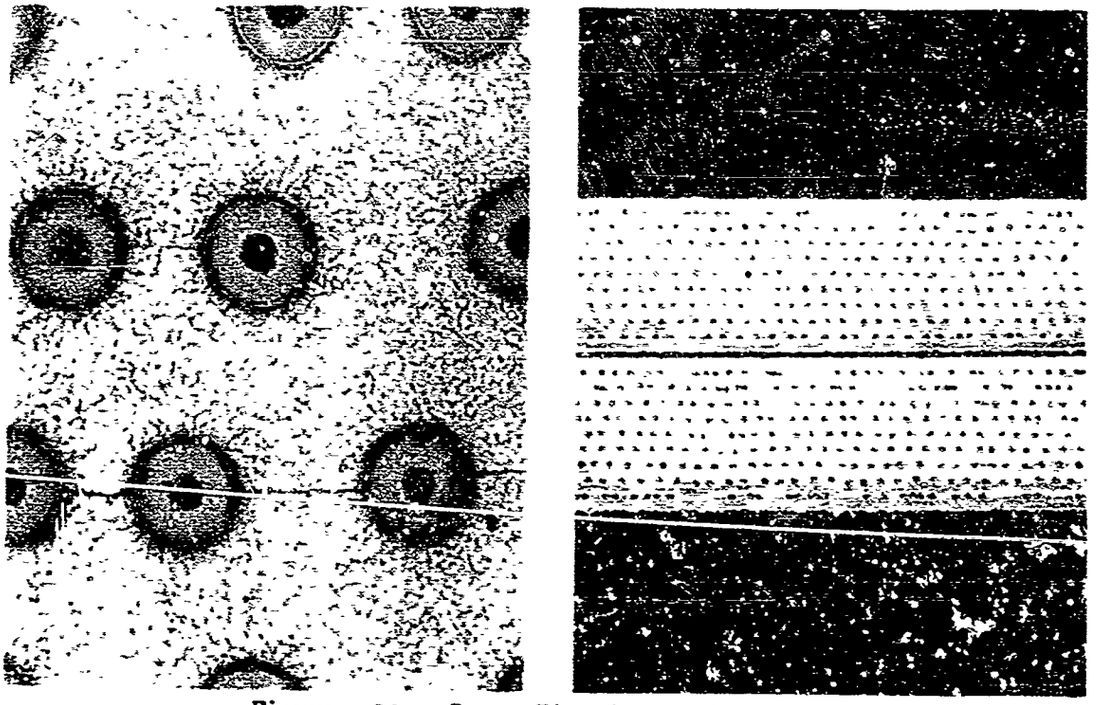


Figure 56. Boron-Titanium - 15 FM

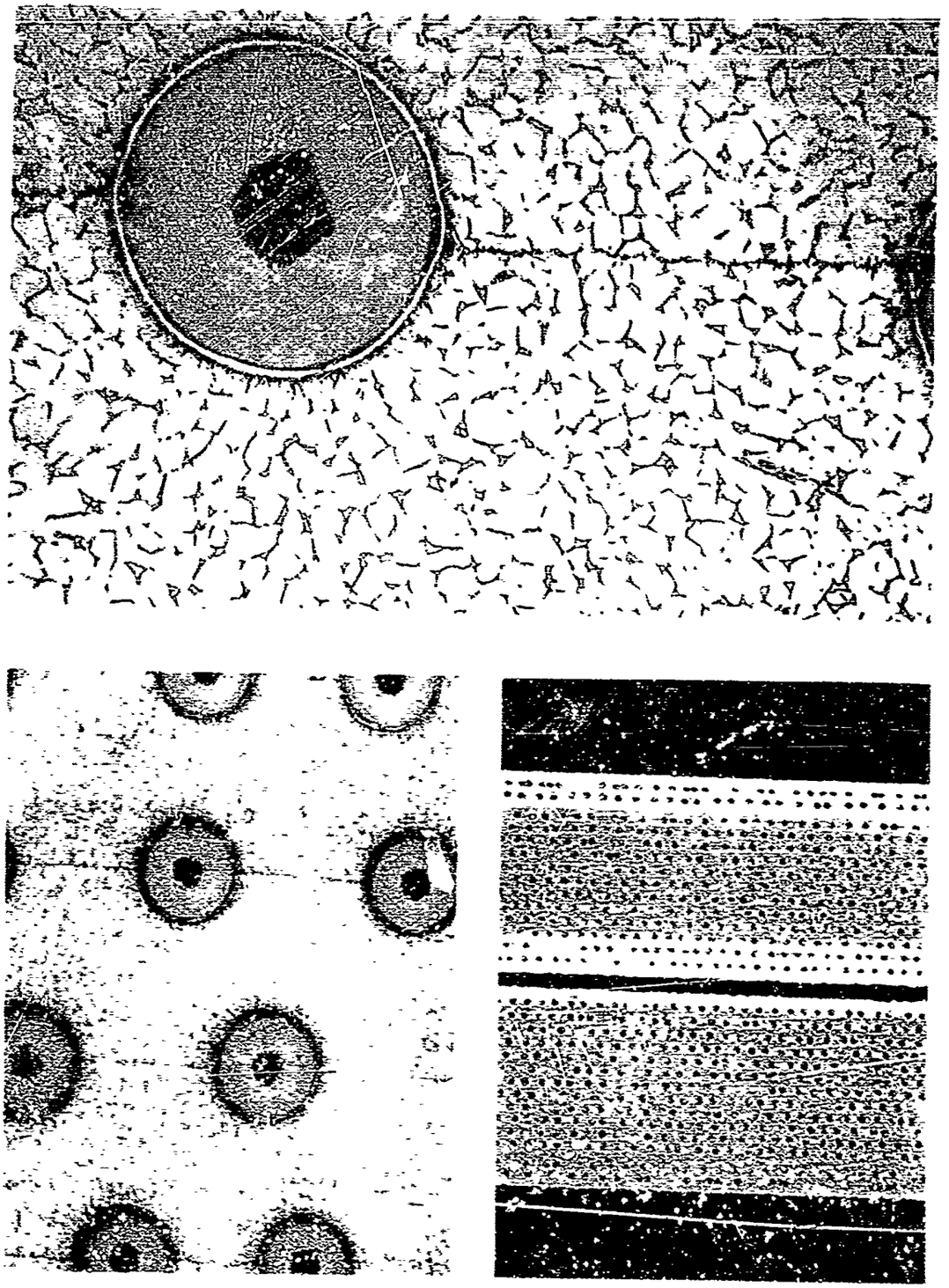


Figure 57. Boron-Titanium - 1SM

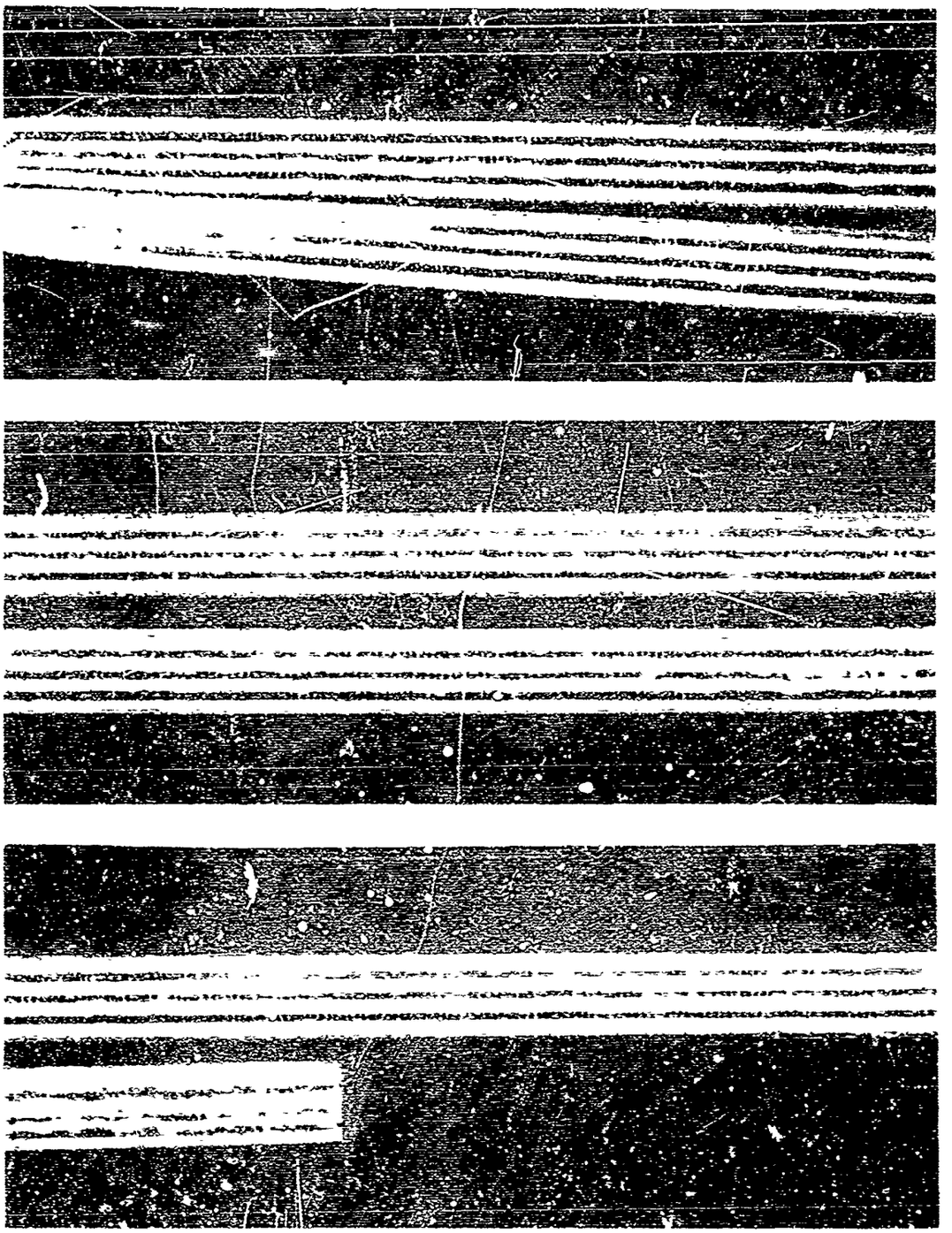


Figure 58. Boron-Aluminum - 10 BF Specimen Edge After Polishing. (Note that polishing method used here failed to produce sharp definition of fiber ends.)

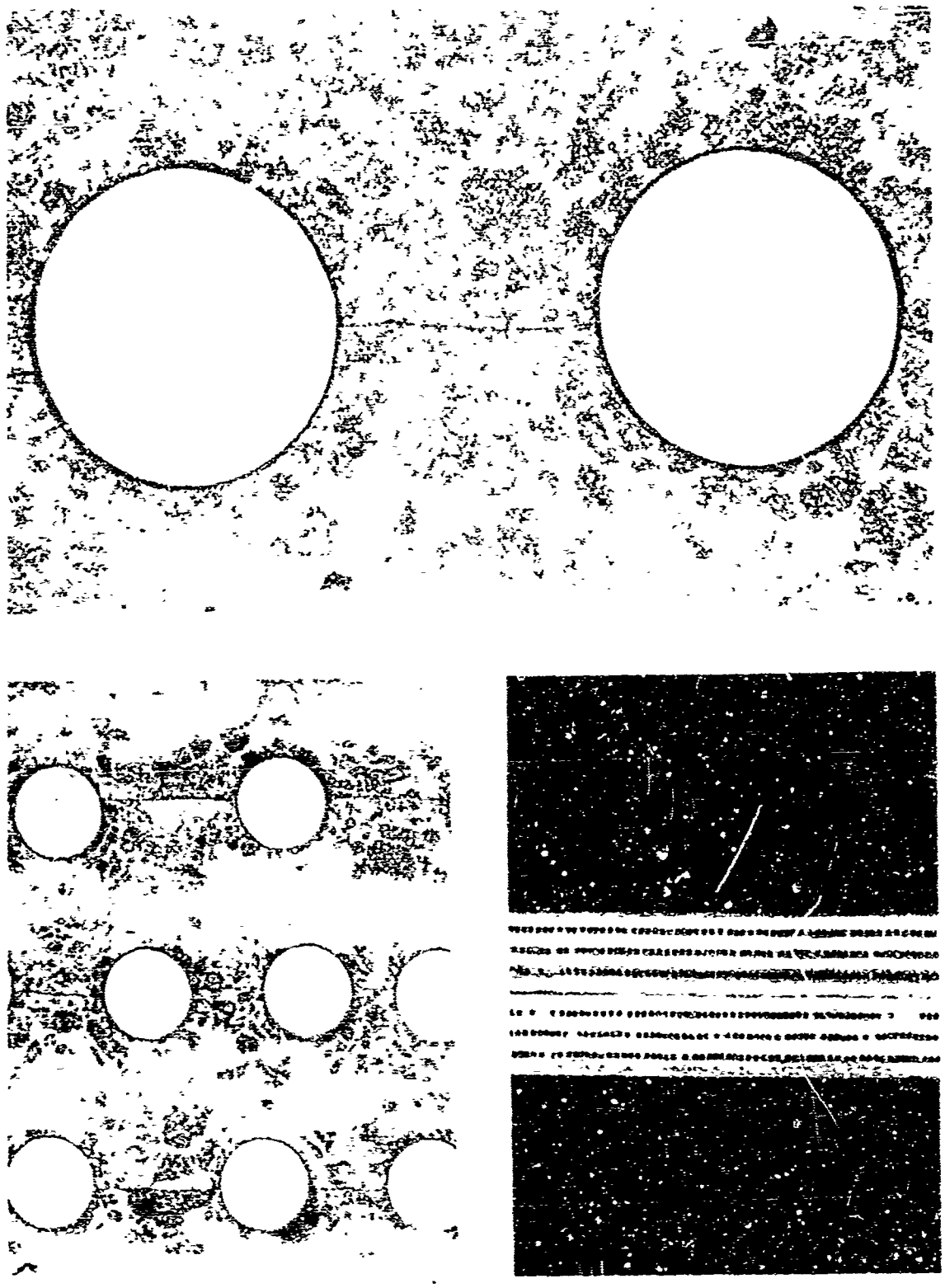


Figure 59. Boron-Aluminum - 15 BF

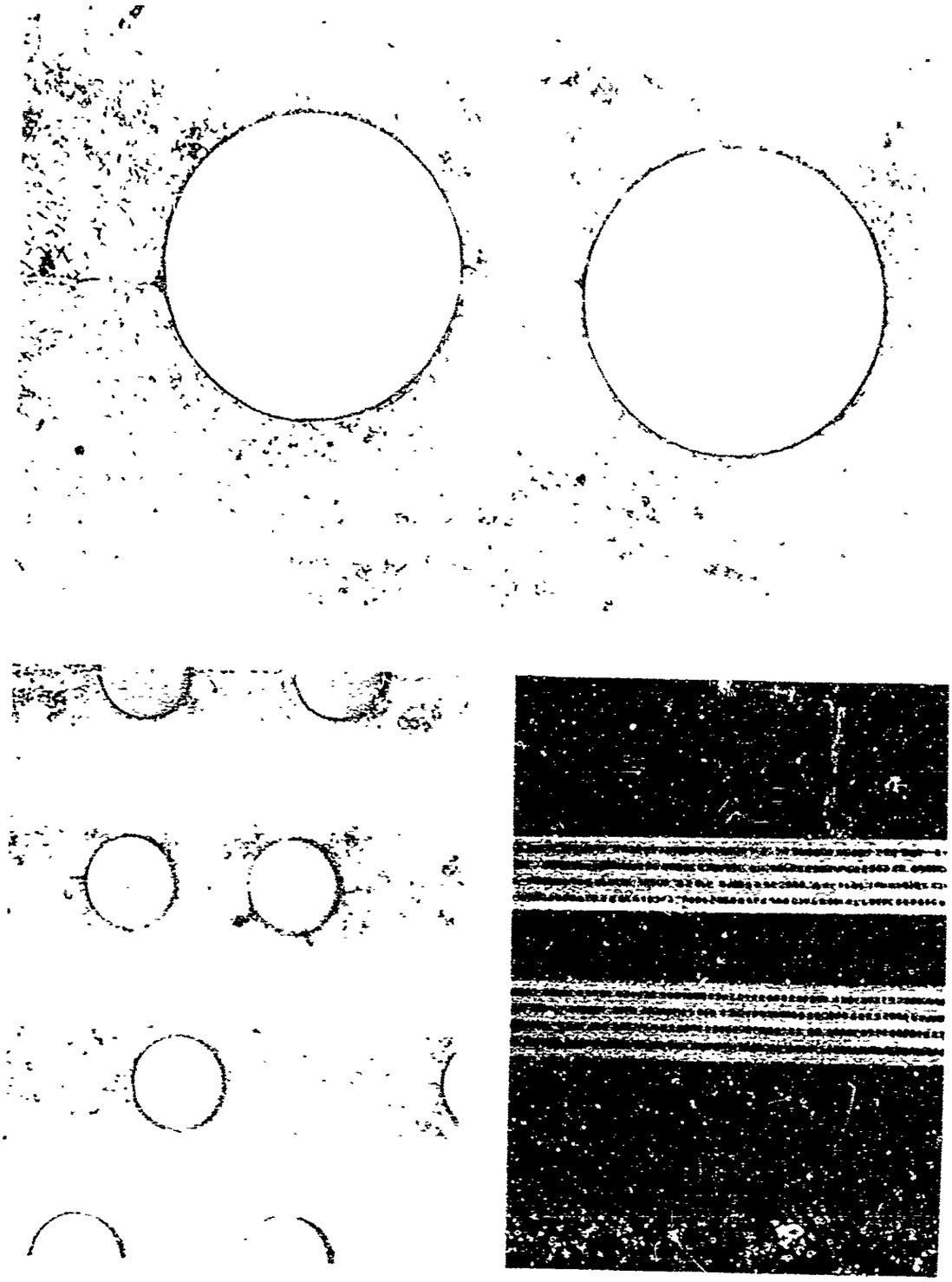


Figure 60. Boron-Aluminum - 20 BF

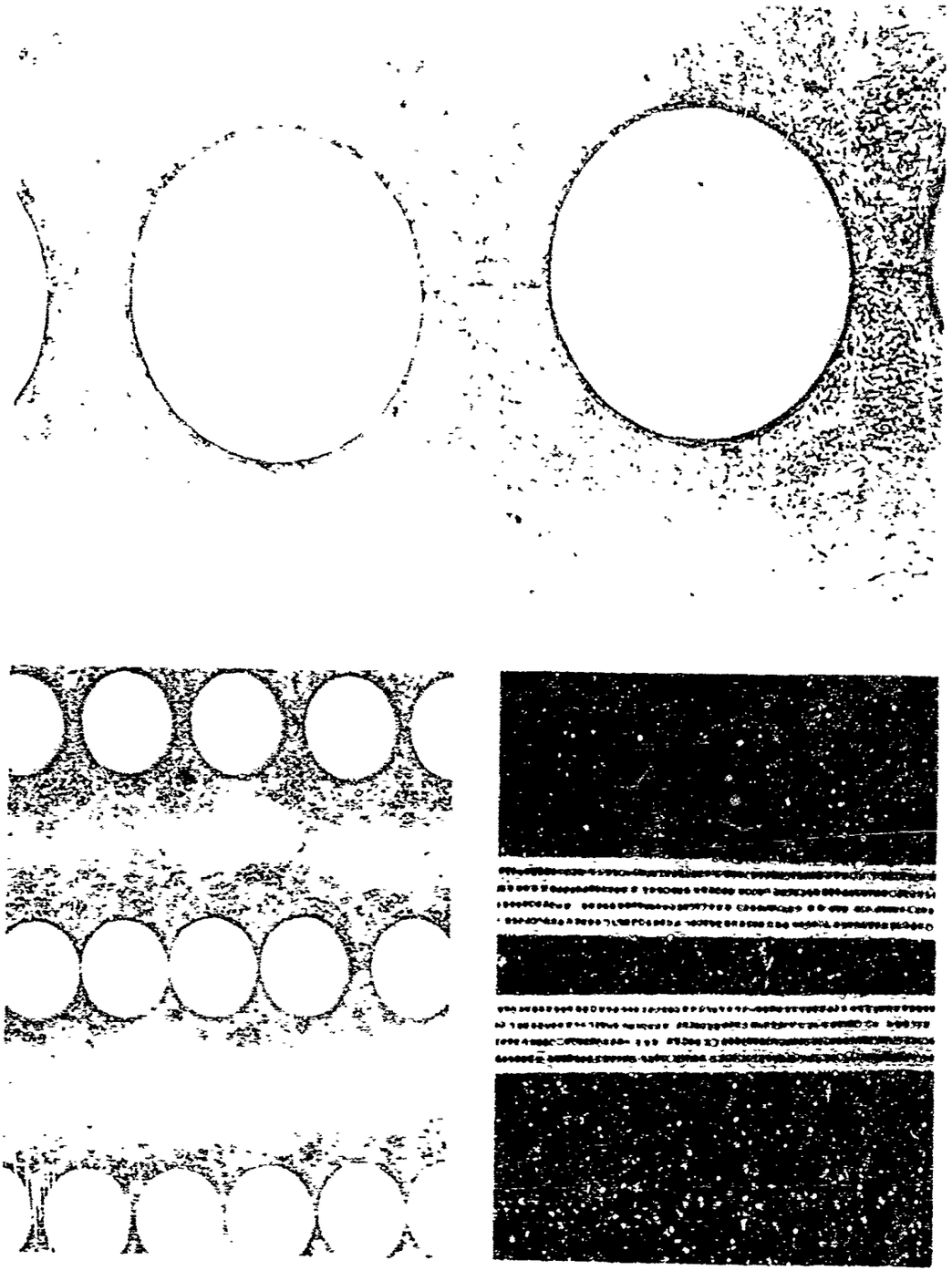


Figure 61. Boron-Aluminum - 25 BF

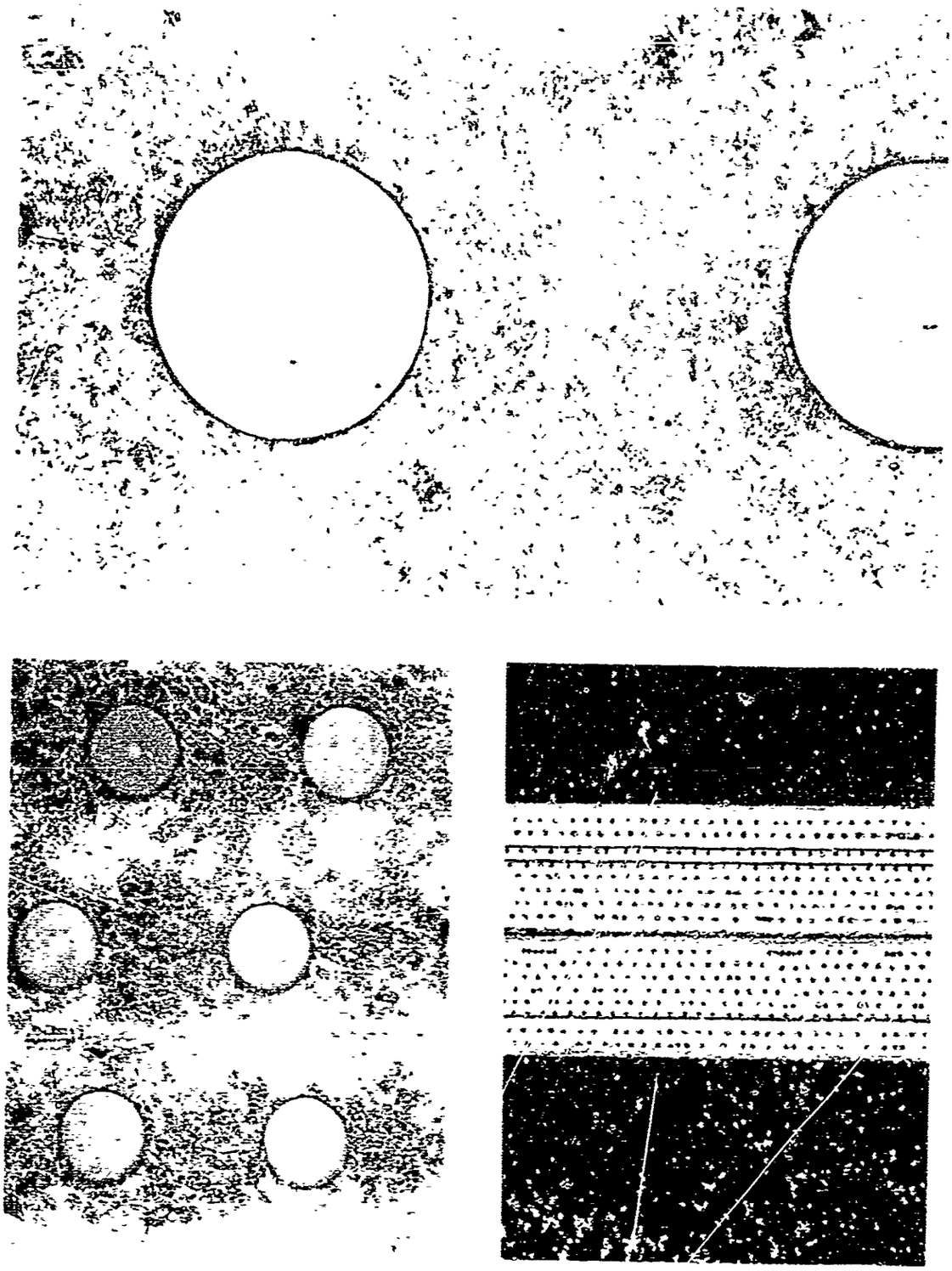


Figure 62. Boron-Aluminum 35 PM

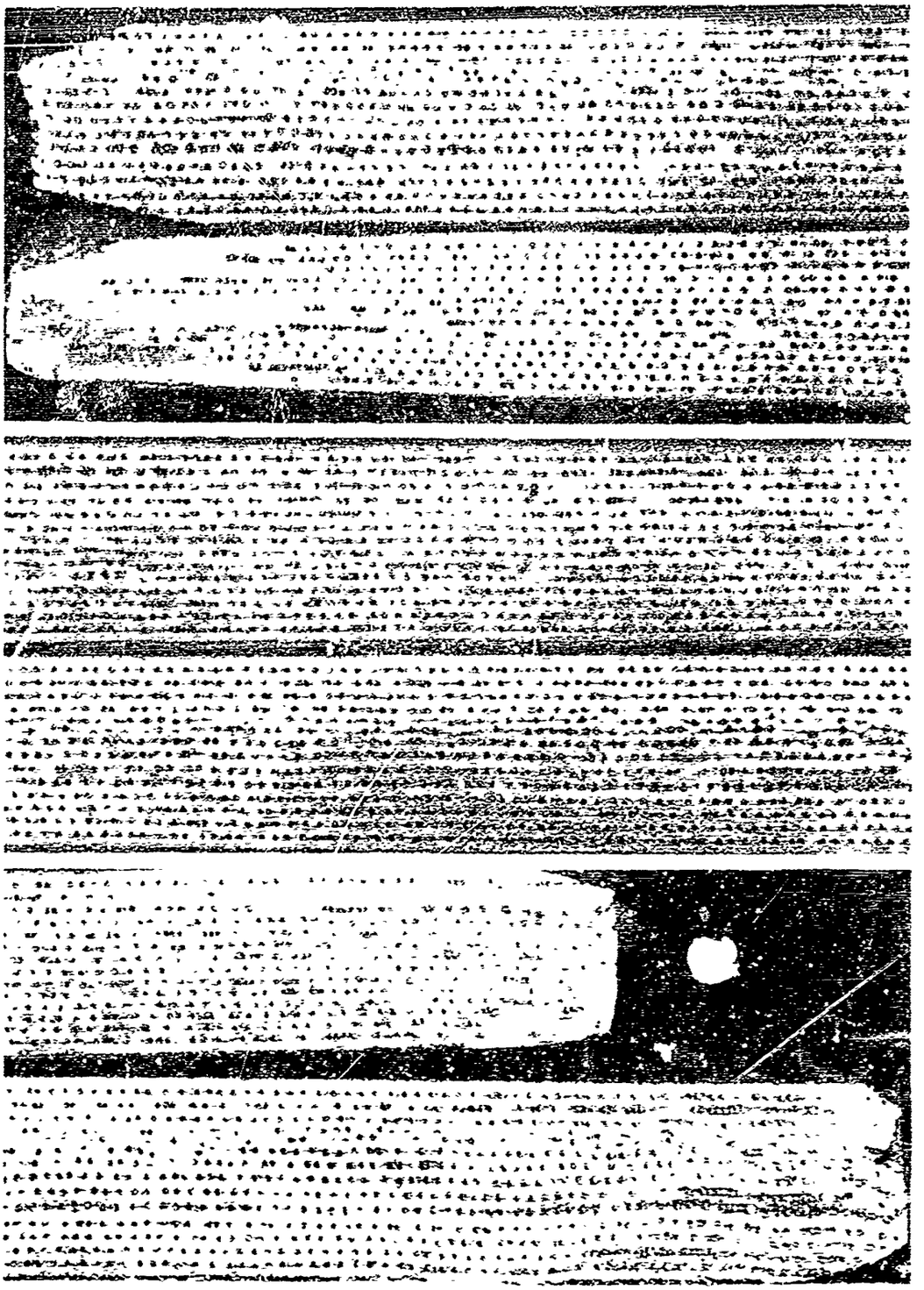


Figure 63. Boron-Aluminum - 15 M

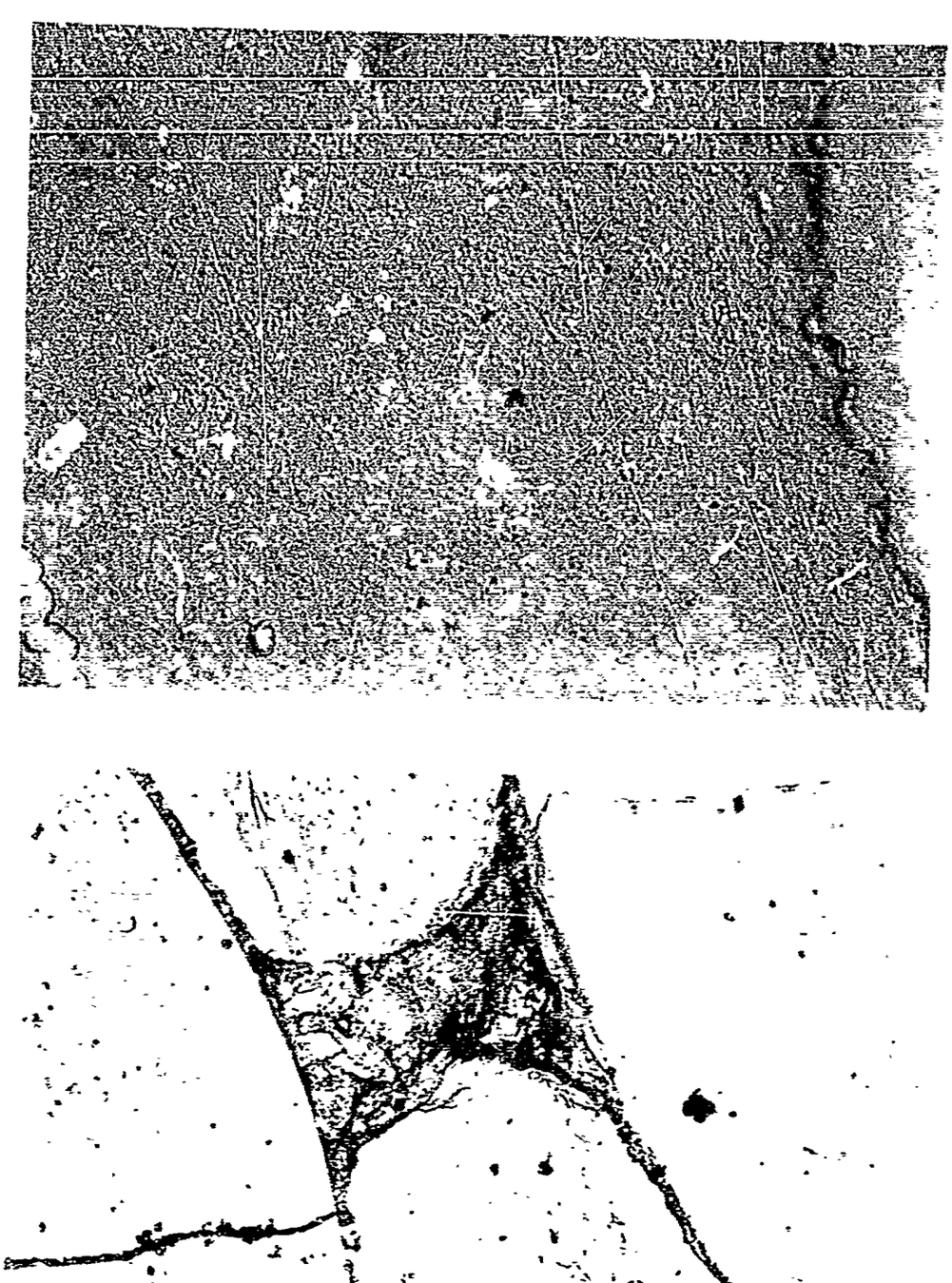


Figure 64. Section of Tungsten-Copper and Boron-Titanium Specimen at 5600X Magnification

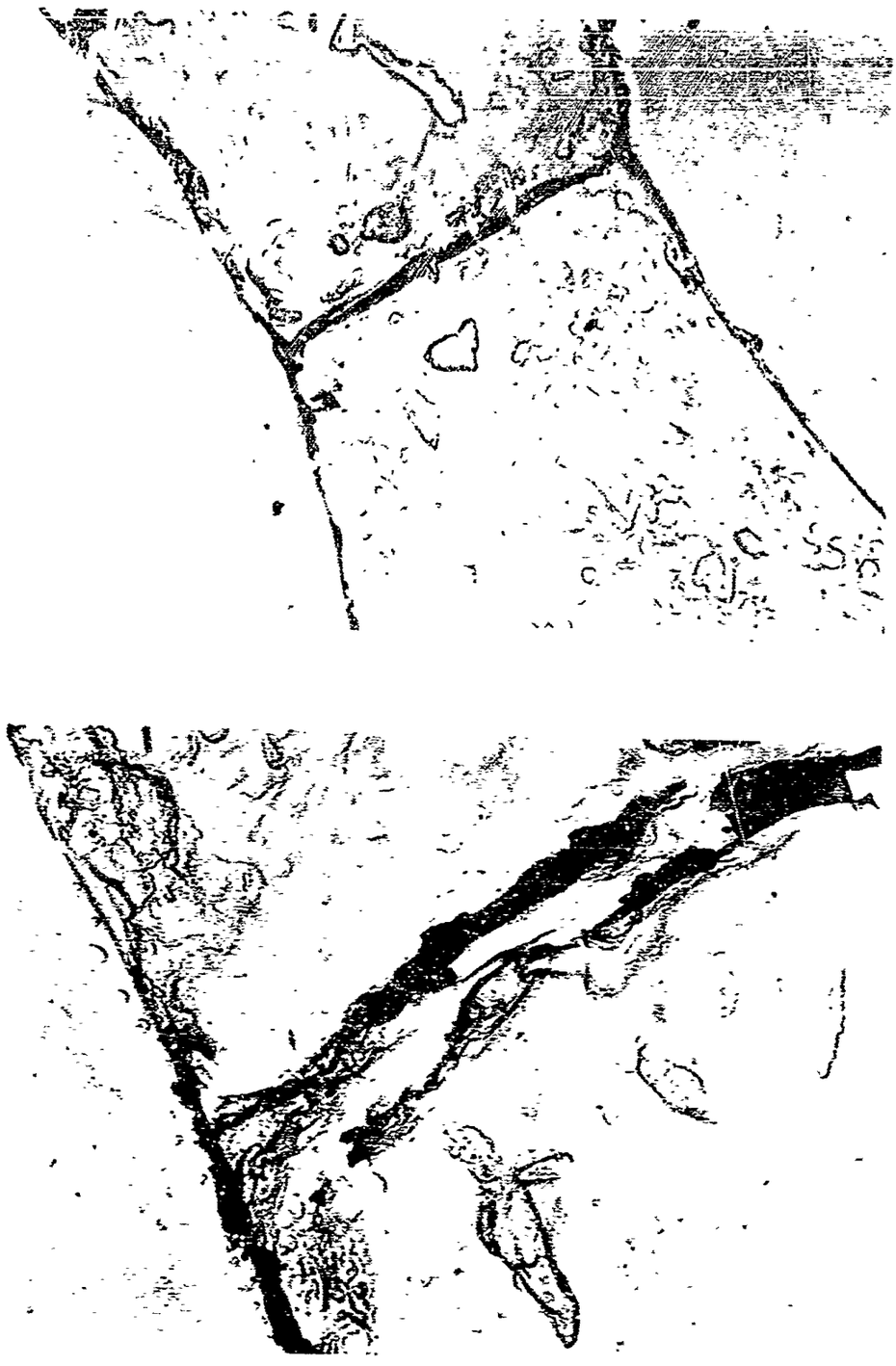
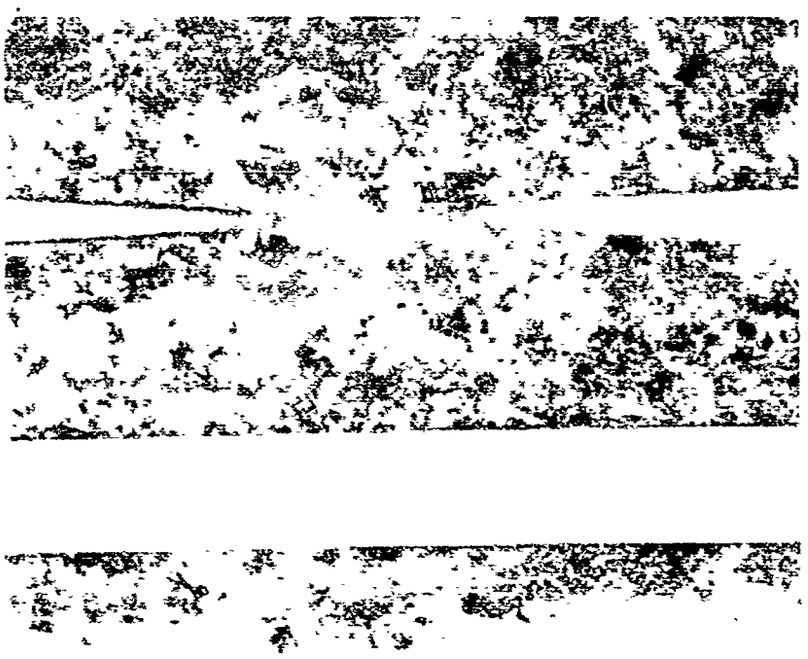


Figure 65. Section of Boron-Aluminum Specimen at 5600X and 32,000X Magnification



250X



150X

Figure 66. Section of Boron Aluminum Specimen Sliced Parallel to Fibers, 150X and 250X Magnification

Appendix II

RADIOGRAPHIC INSPECTION

Radiographic inspection was performed on tungsten-copper, boron-titanium, and boron-aluminum composite specimens. The objective of this effort was to determine the capability of conventional radiographic inspection techniques for the detection of intentionally introduced defects. Photographic prints of the radiographs resulting from the optimization of radiographic techniques are presented in this Appendix. The detailed test conditions are described in Section V of this report. The tungsten-copper evaluation specimens include 10 and 25 percent volume ratio areas and contain broken fiber and disbond defects. One series of photographs is included for each set of tungsten-copper and boron-aluminum specimens. Two sets of boron-titanium specimen photographs are presented to show the minor differences obtained in radiographic inspection from opposite sides of the specimen. The specimen code identifies the fiber-matrix volume ratio of the specimen and the nature of the defect, i.e., 10 BF, where 10 is the volume ratio percent and BF indicates deliberately introduced broken fiber defects.



Figure 67. Tungsten-Copper 10-25 BF Evaluation Specimen at 75 KV, 10 MA, 4 MM Dia, 2 Min

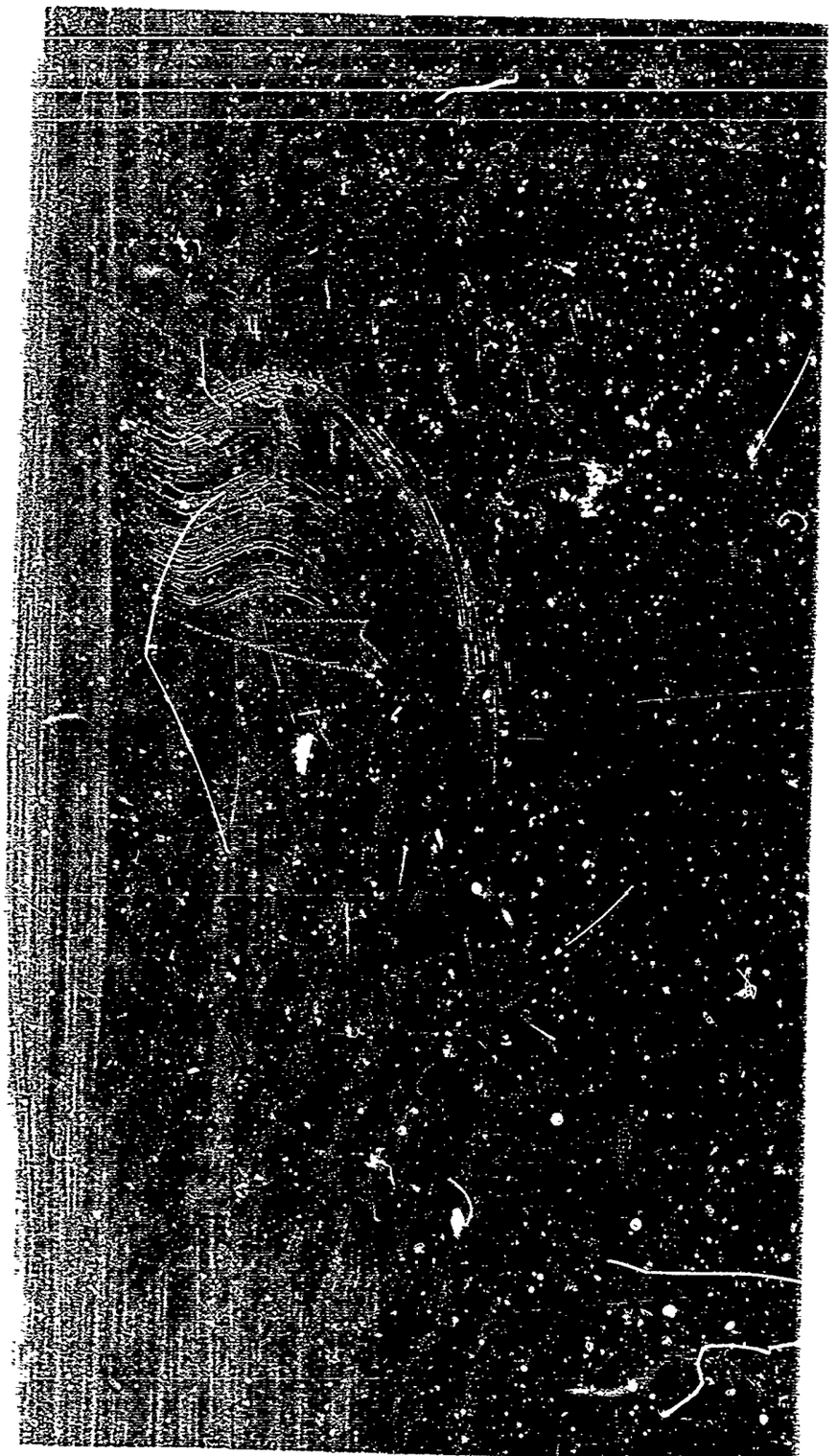


Figure 68. Tungsten-Copper 10-25 BF Evaluation Specimen at 80 KV, 10 MA, 4 MM Dia, 2 Min

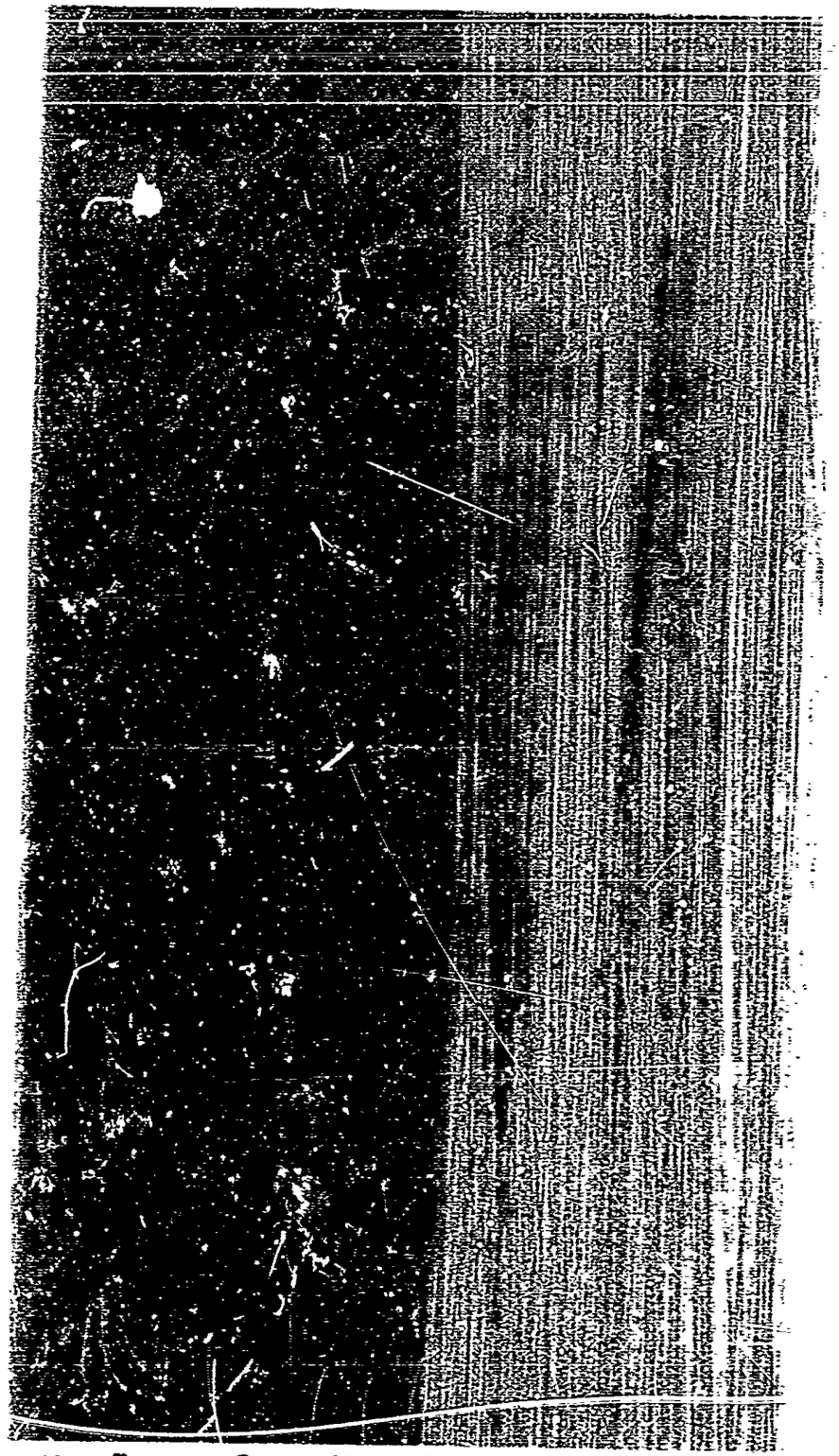


Figure 69 . Tungsten-Copper 10-25 BF Evaluation Specimen at 80 KV, 3.5 MA, 2 MM Dia, 6 Min

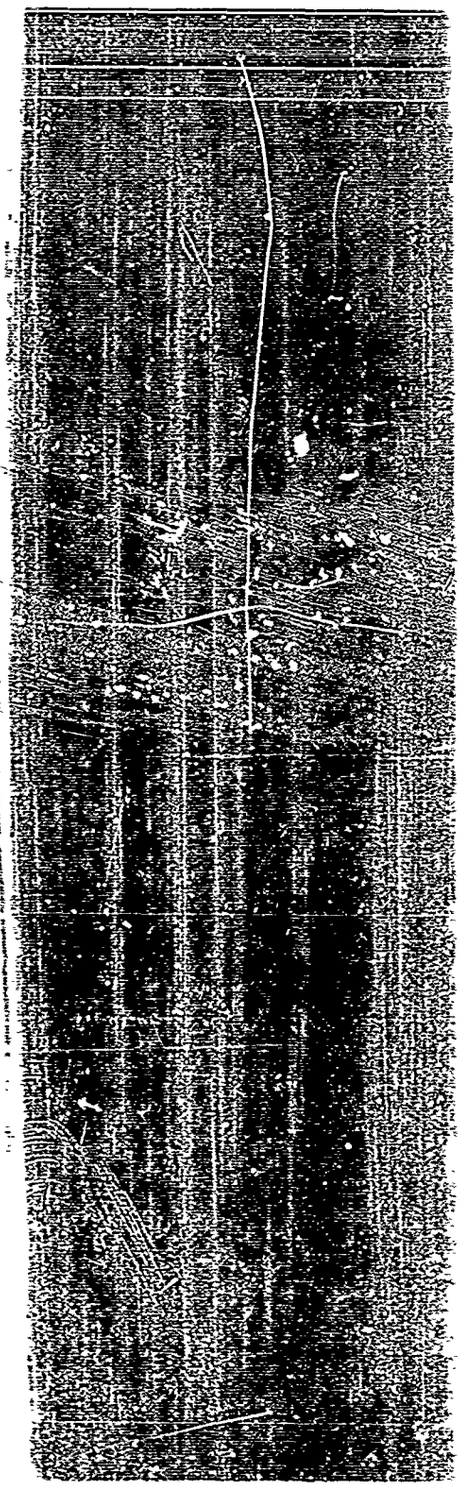


Figure 70. Tungsten-Copper 10-25 BF Evaluation Specimen at 90 KV, 3MA, 2 MM Dia, 4.5 Min

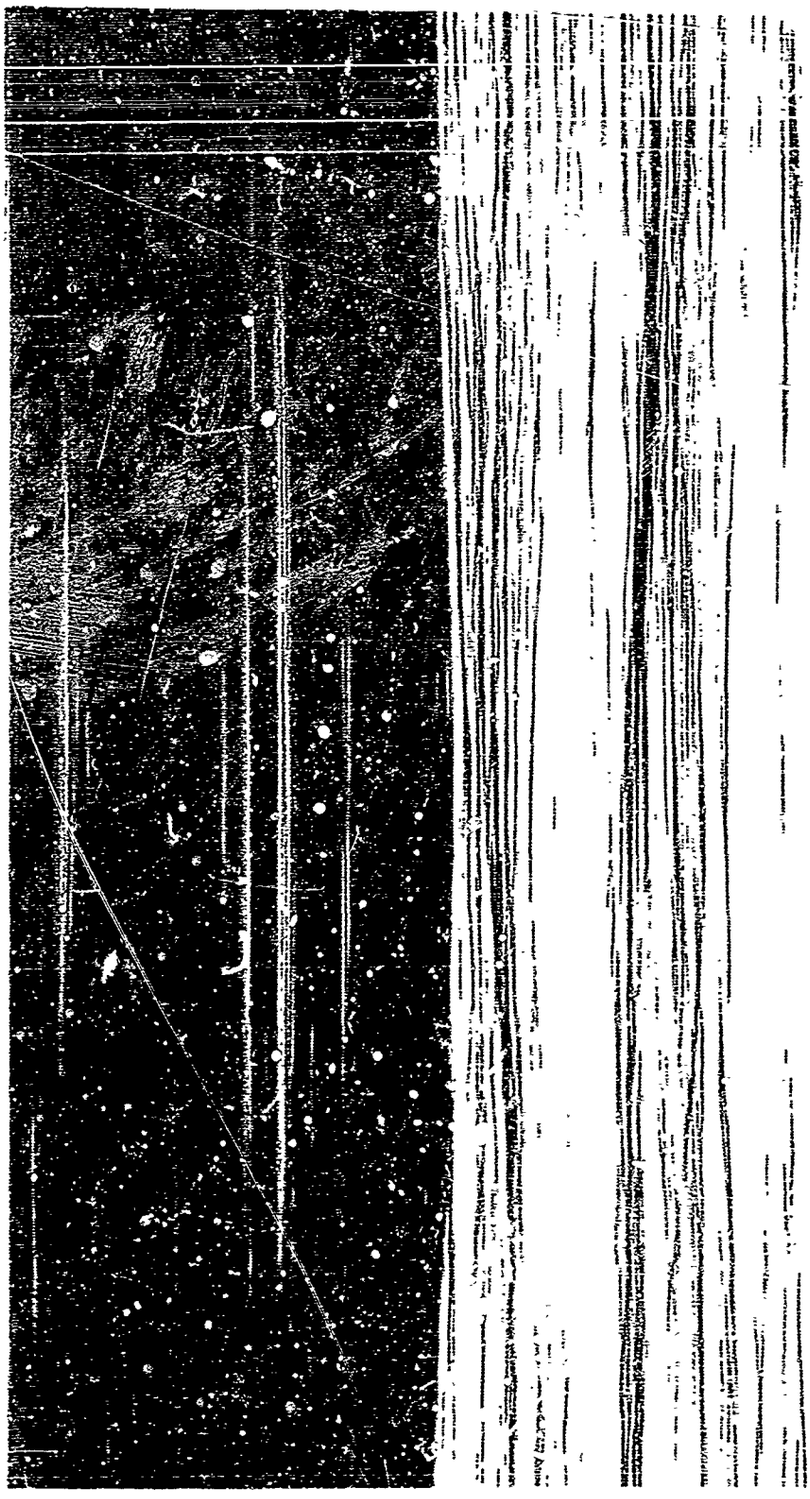


Figure 71. Tungsten-Copper 10-25 BF Evaluation Specimen at 100 KV, 3.5 MA, 2 MM Dia, 4 Min

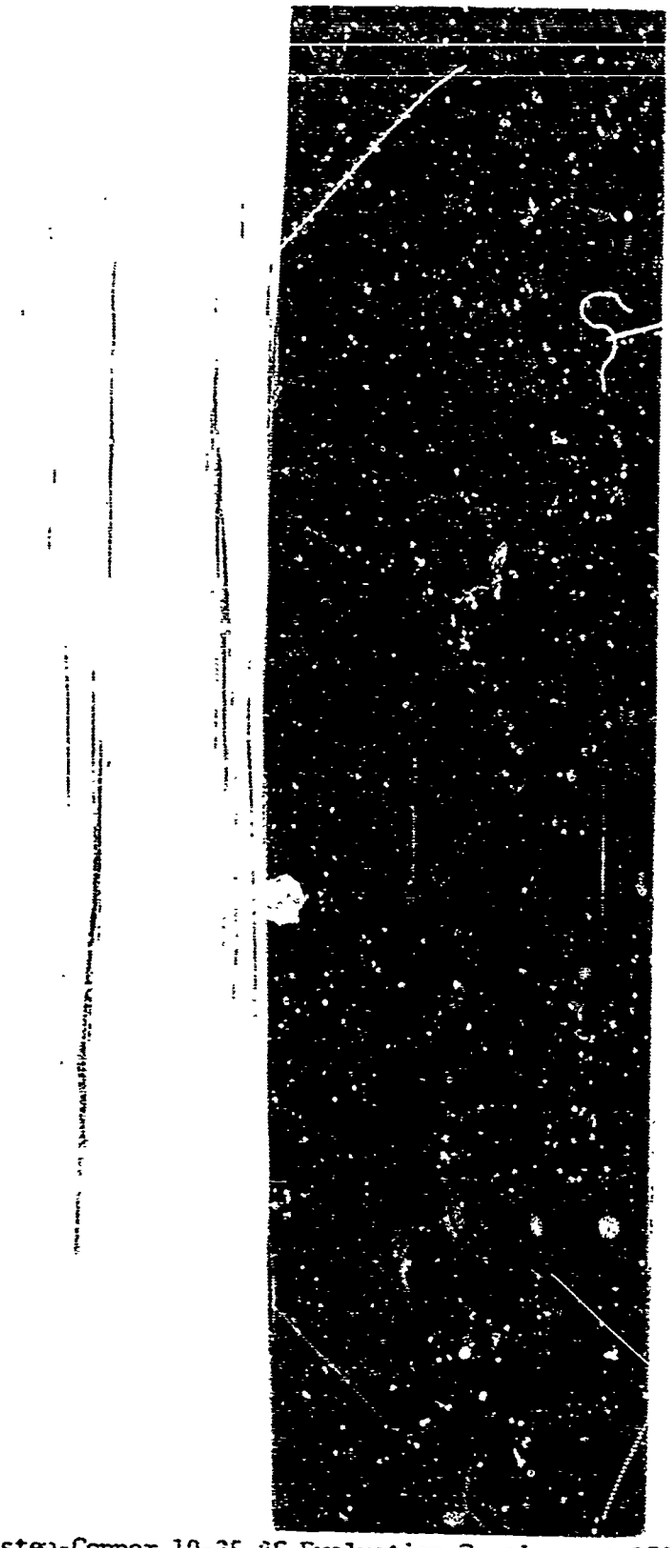


Figure 72. Tungsten-Copper 10-25 BF Evaluation Specimen at 170 KV, 4 MA, 2 MM Dia, 2.5 Min, With Lead Screen

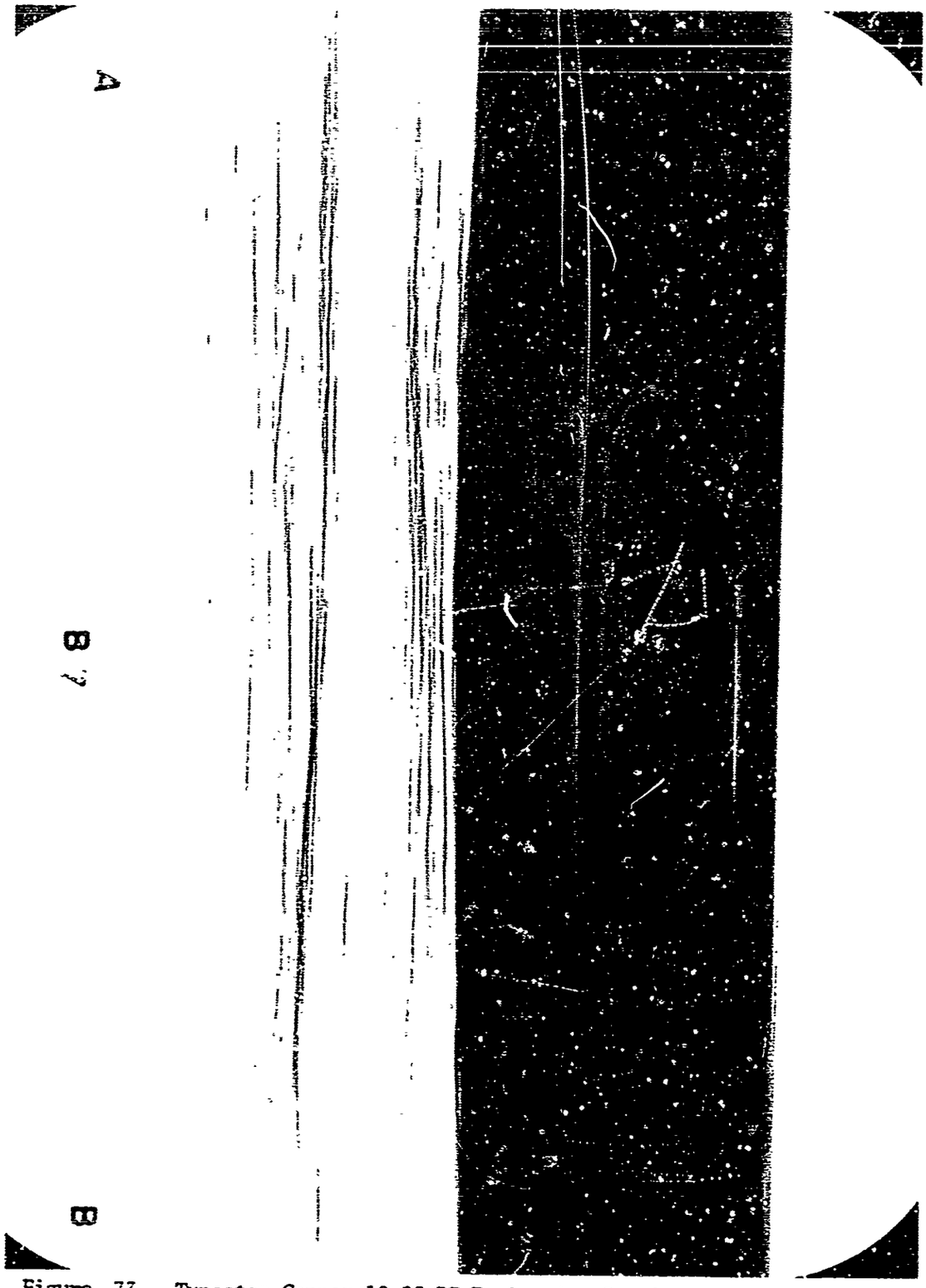


Figure 73. Tungsten-Copper 10-25 BF Evaluation Specimen at 150 KV, 3.75 MA, 2 MM Dia, 6 Min, With Lead Screen, R Film



Figure 74. Tungsten-Copper 10-25 BF Evaluation Specimen at 150 KV, 3.5 MA, 2 MM Dia, 3 Min, With Lead Screen

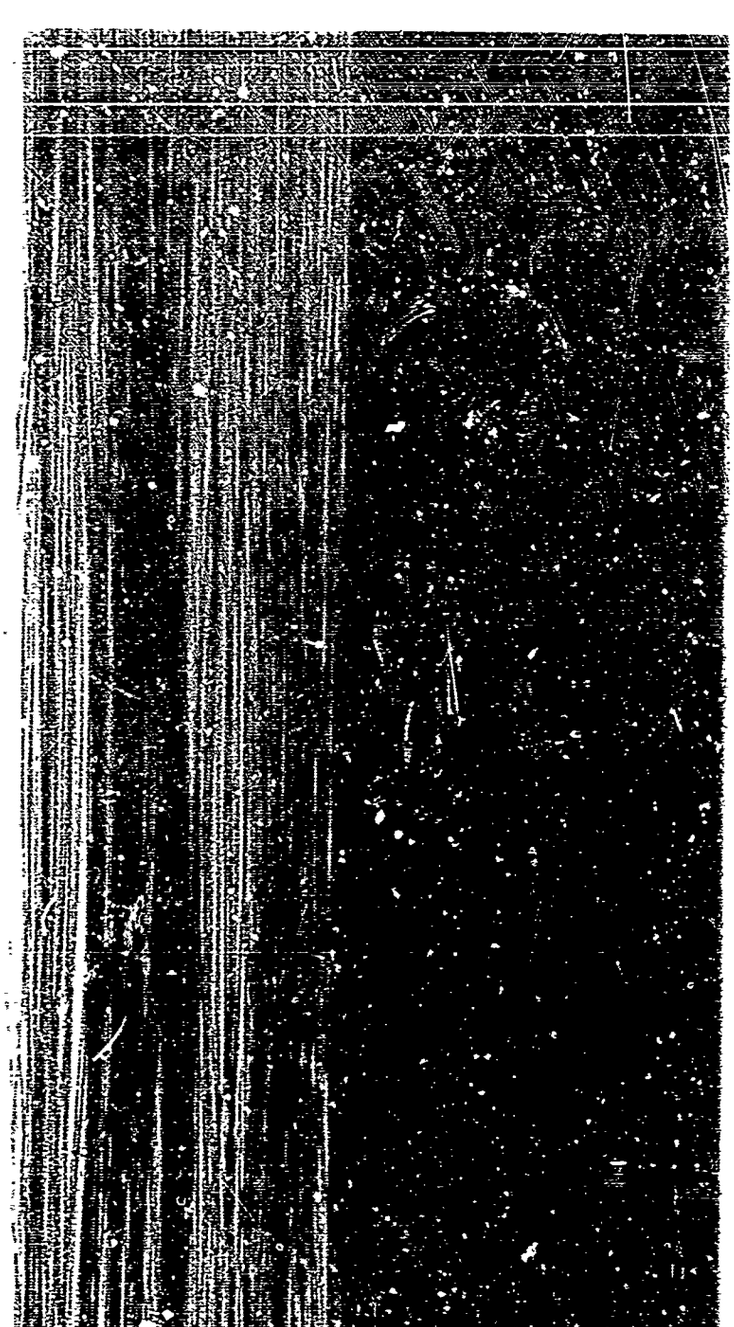


Figure 75. Tungsten-Copper 10-25 BF Evaluation Specimen at 90 KV, 3.75 MA, 2 MM Dia, 10 Min

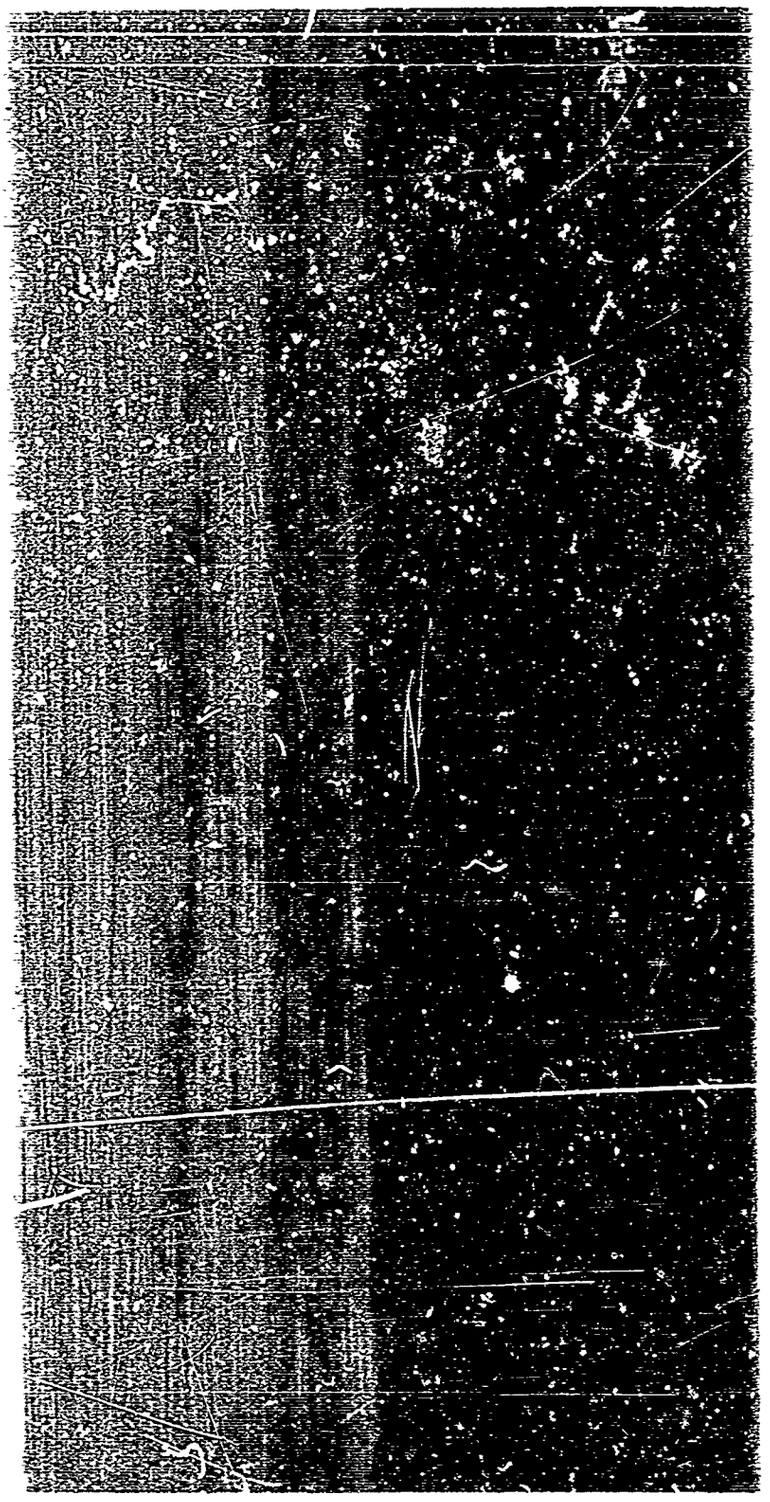


Figure 76. Tungsten-Copper 10-25 BF Evaluation Specimen at 90 KV, 3.75 MA, 2 MM Dia, 6 Min, With Lead Screen Both Sides

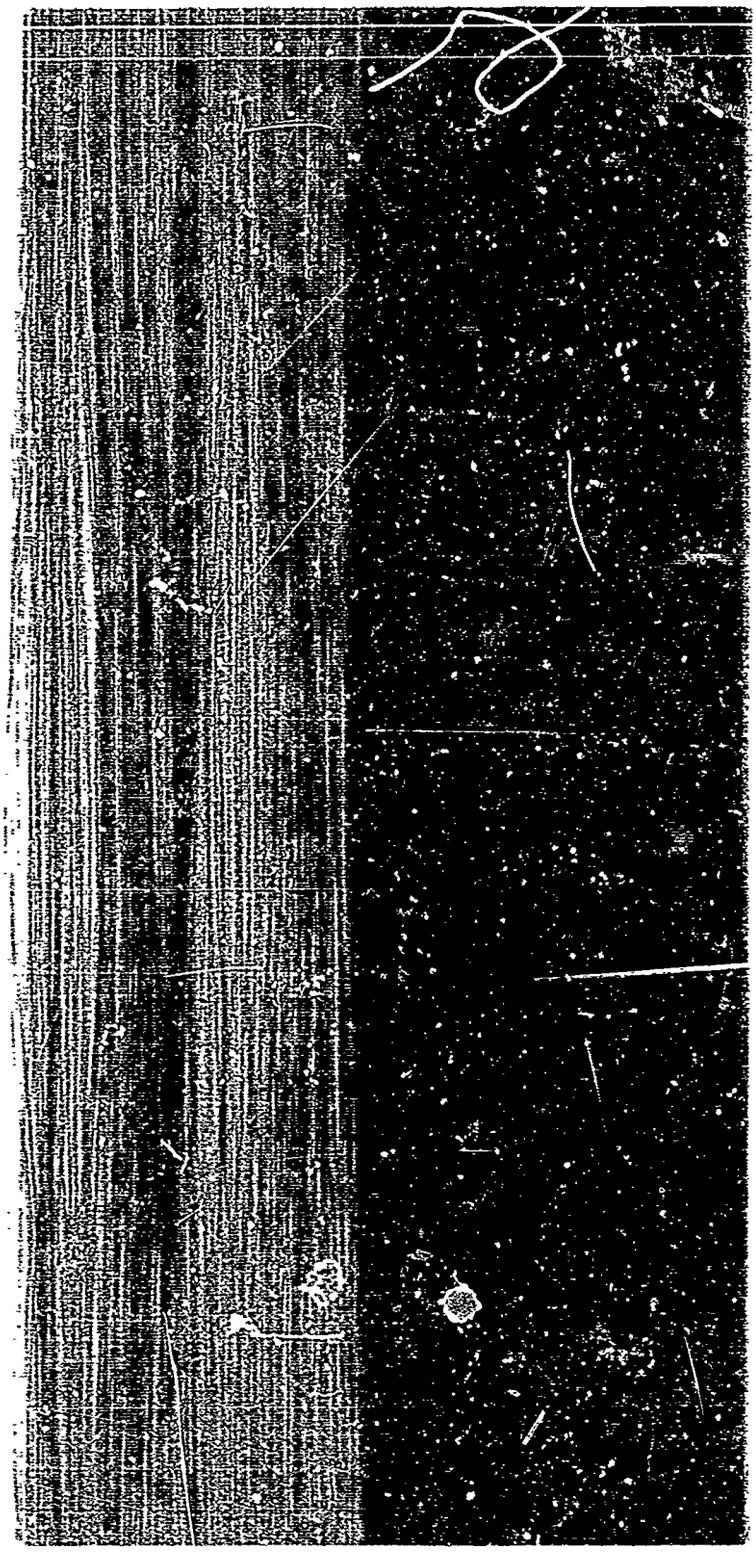


Figure 77. Tungsten-Copper 10-25 BF Evaluation Specimen at 90 KV, 3.75 MA, 2 MM Dia, 6 Min, With Lead Screen Below Film

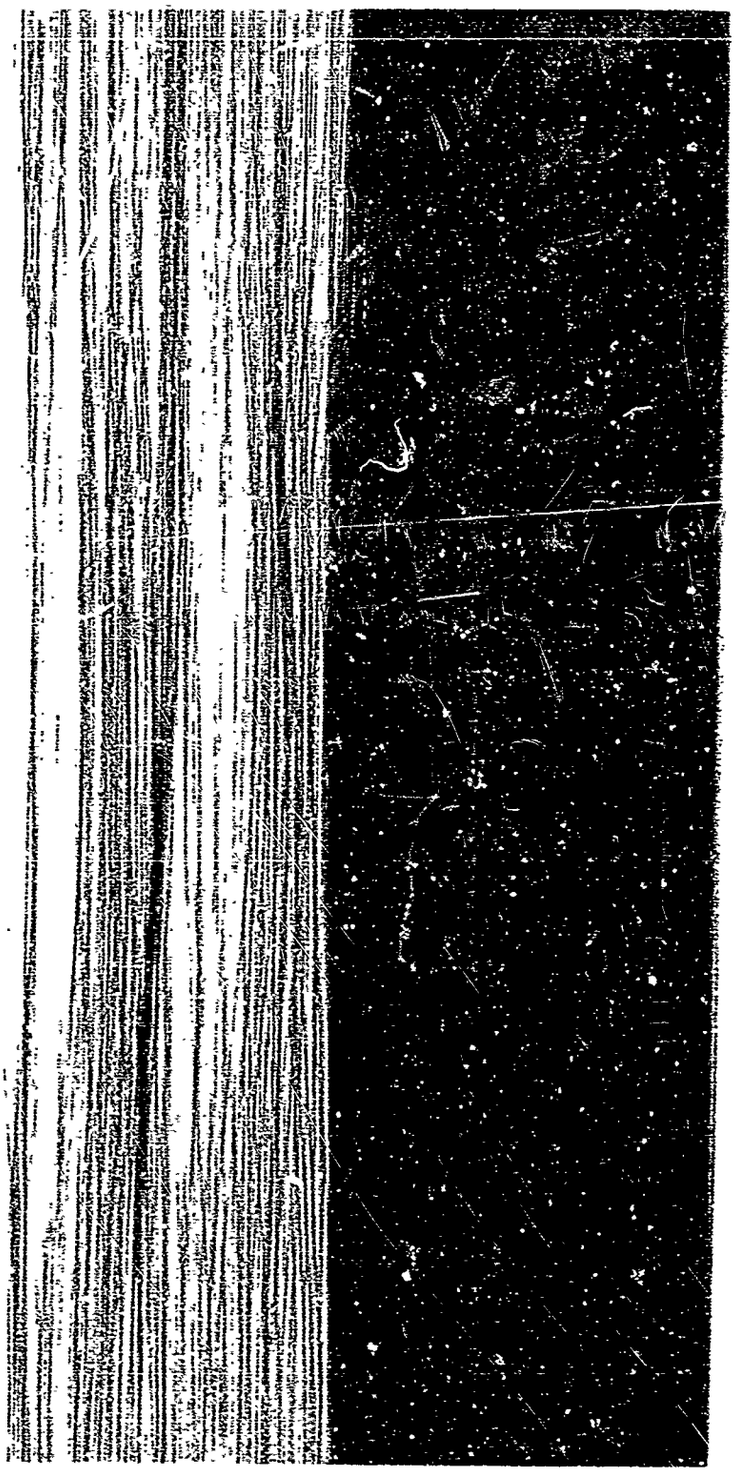


Figure 78. Tungsten-Copper 10-25 BF Evaluation Specimen at 150 KV, 3.75 MA, 2 MM Dia, 1.75 Min

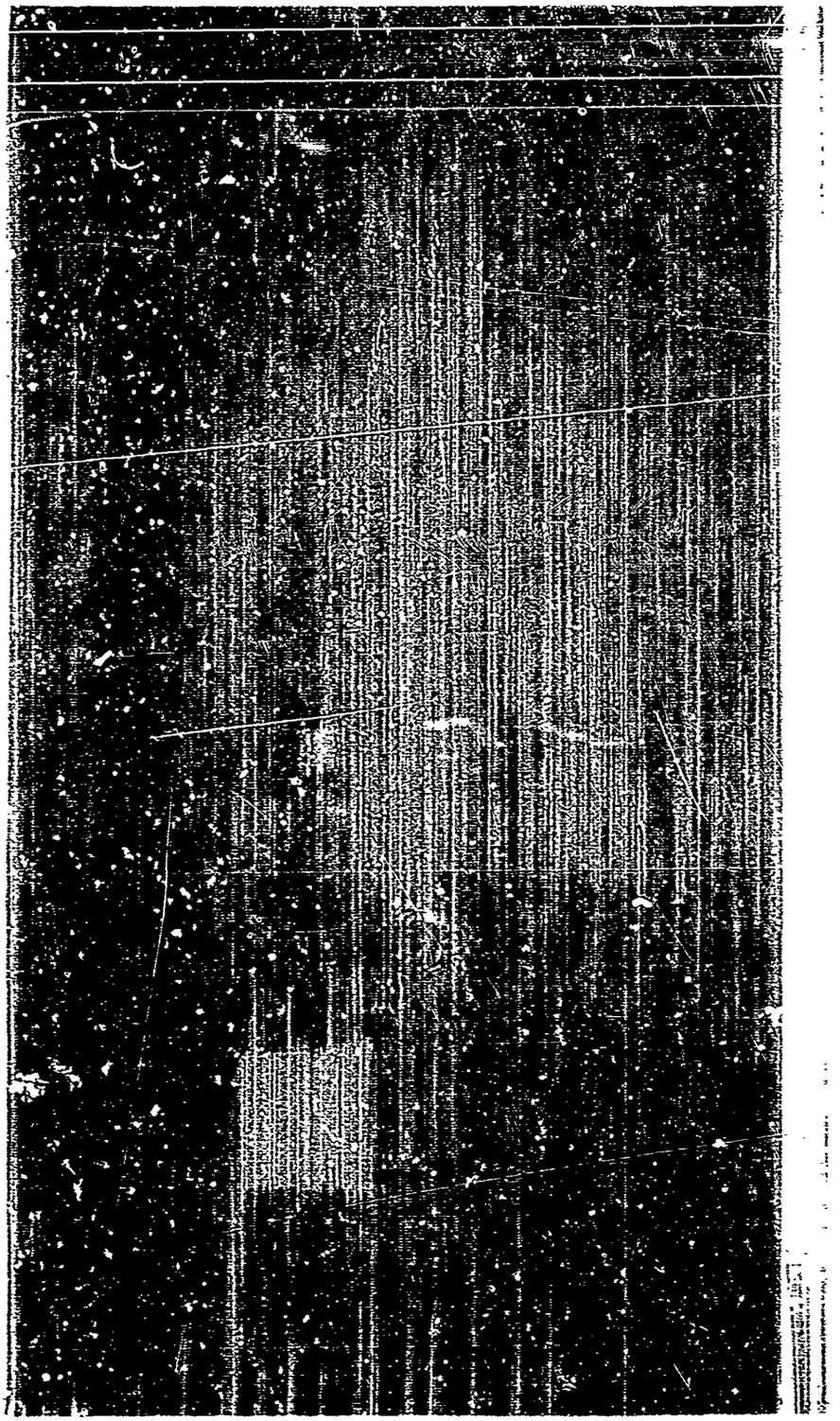


Figure 79. Tungsten-Copper 10 BF Specimen at 150 KV, 1.2 MM Dia, 1.25 Min

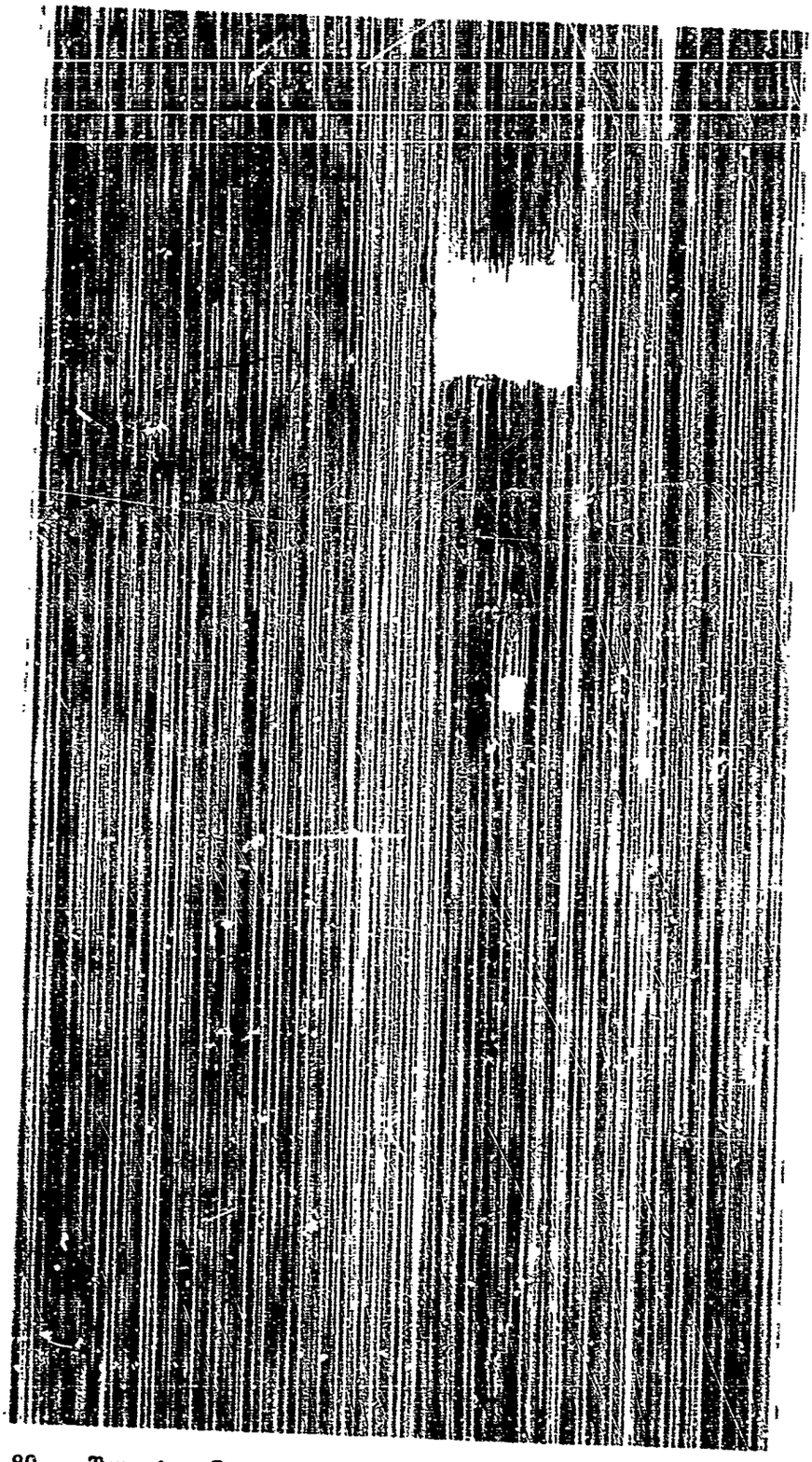


Figure 80 . Tungsten-Copper 15 BF Specimen at 150 KV, 1.2 MM Dia, 6 Min,

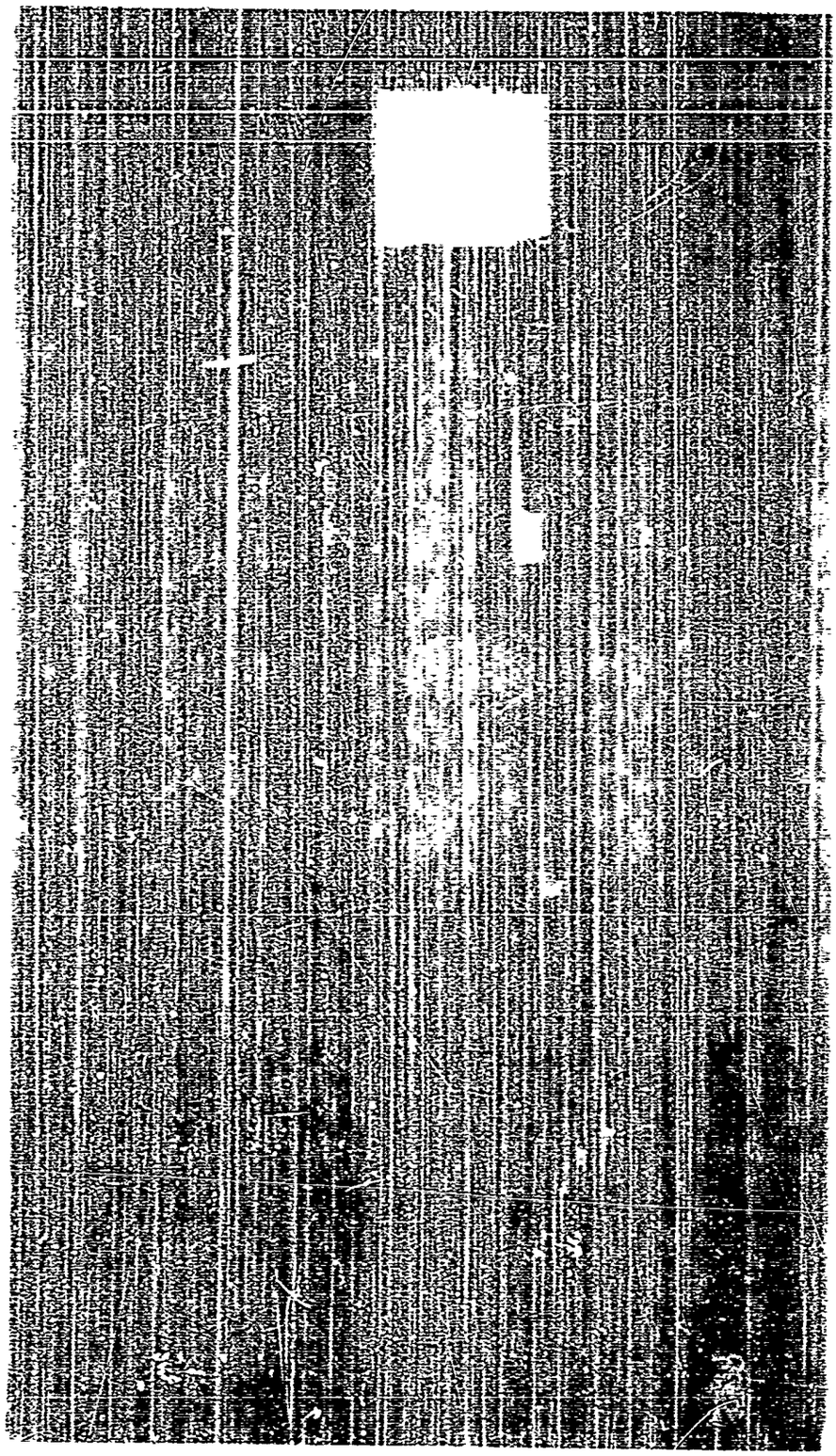


Figure 81. Tungsten-Copper 20 BF Specimen at 170 KV, 1.2 MM Dia, 2 Min

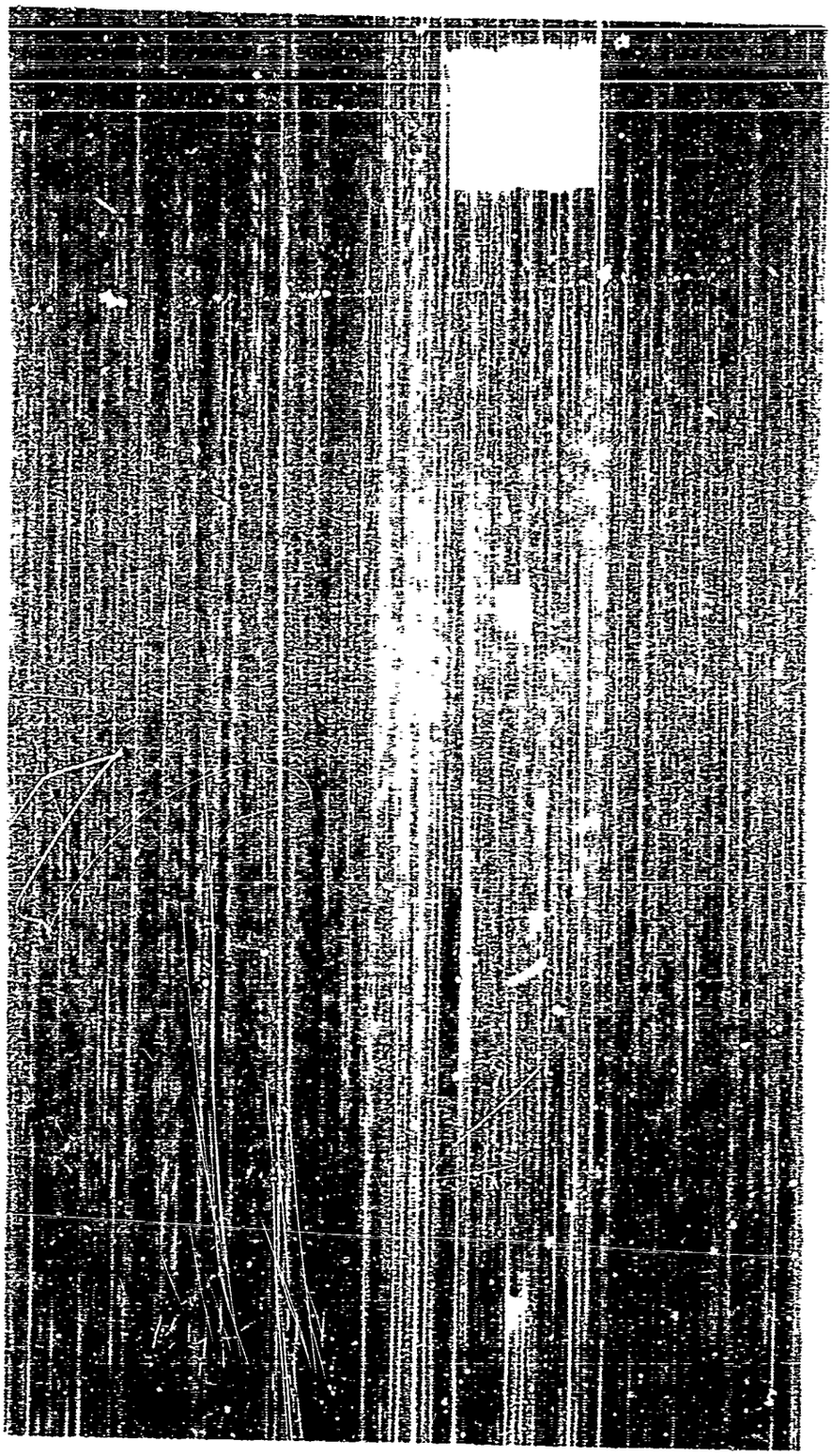


Figure 82. Tungsten-Copper 25 BF Specimen at 190 KV, 1.2 MM Dia, 2.25 Min



Figure 83 . Tungsten-Copper 15 PM Specimen at 170 KV, 1.2 MM Dia. 2.25 Min

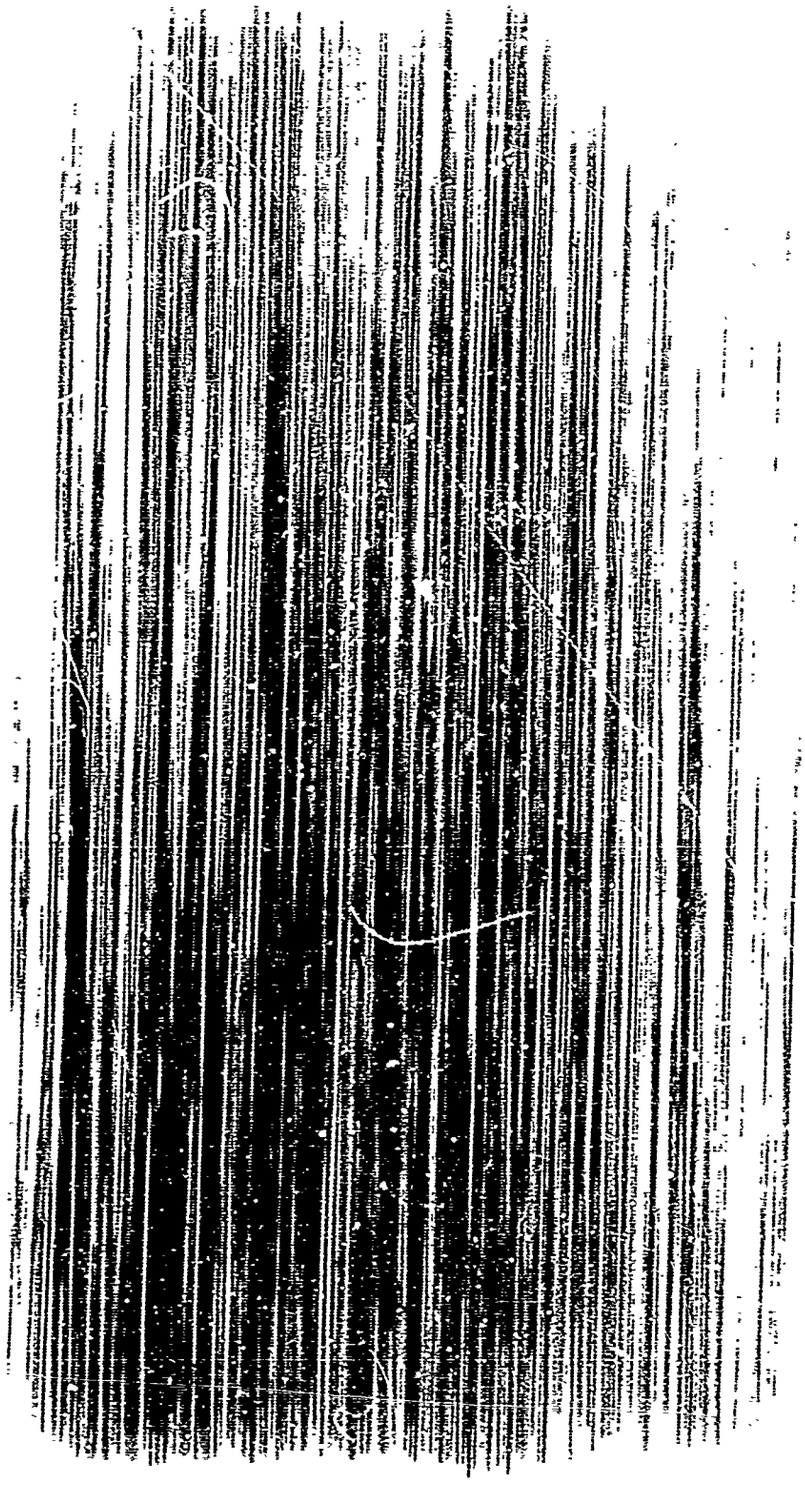


Figure 84. Tungsten-Copper 15 A Specimen at 190 KV, 1.2 MM Dia 4 Min



Figure 85. Tungsten-Copper 15 M Specimen at 250 KV, 1.2 MM Dia, 10 Min

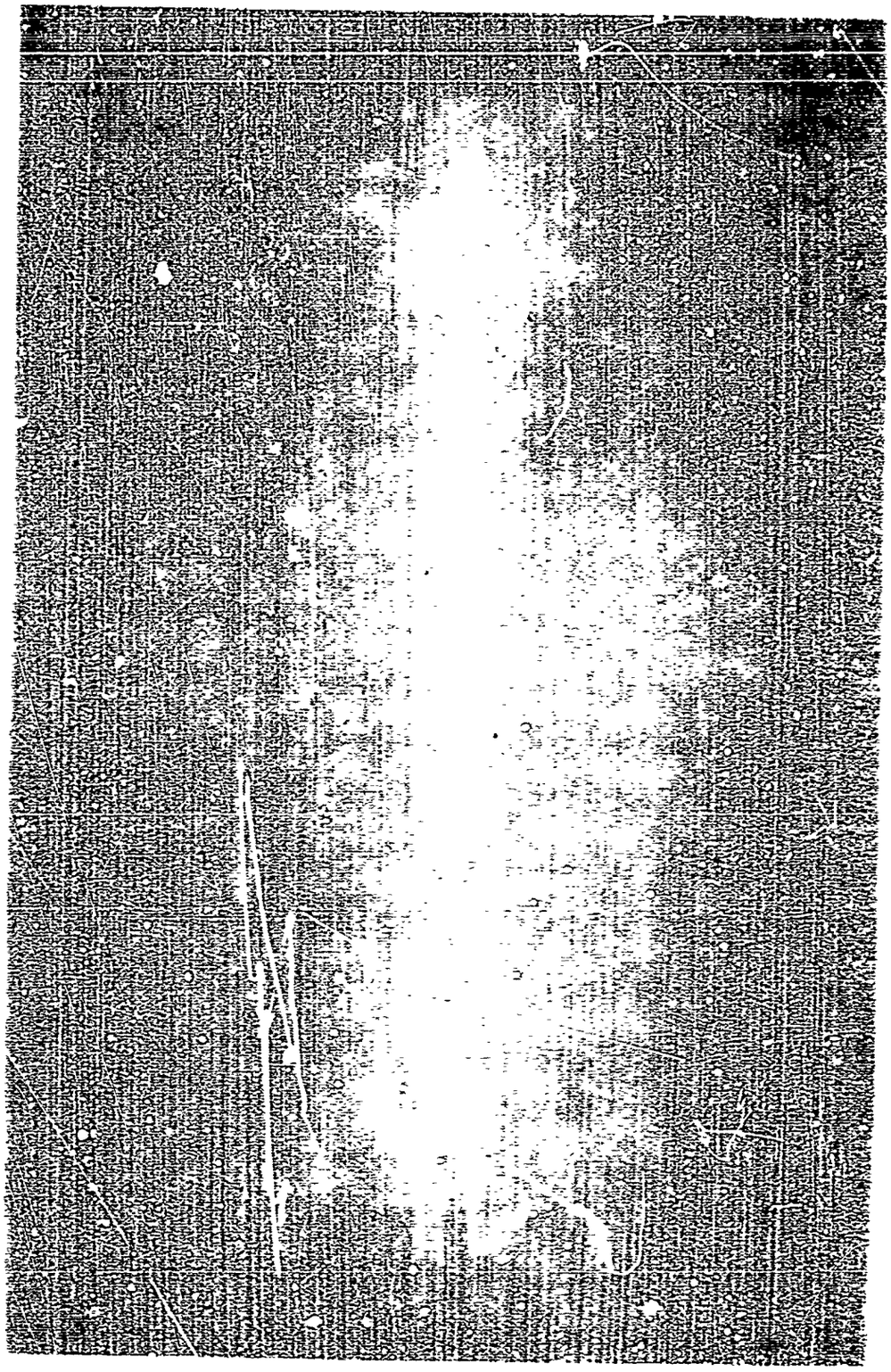


Figure 86. Boron-Titanium 10 BF Specimen (Front) at 90 KV, 3.5 MA, 1.2 MM Dia, 4.5 Min

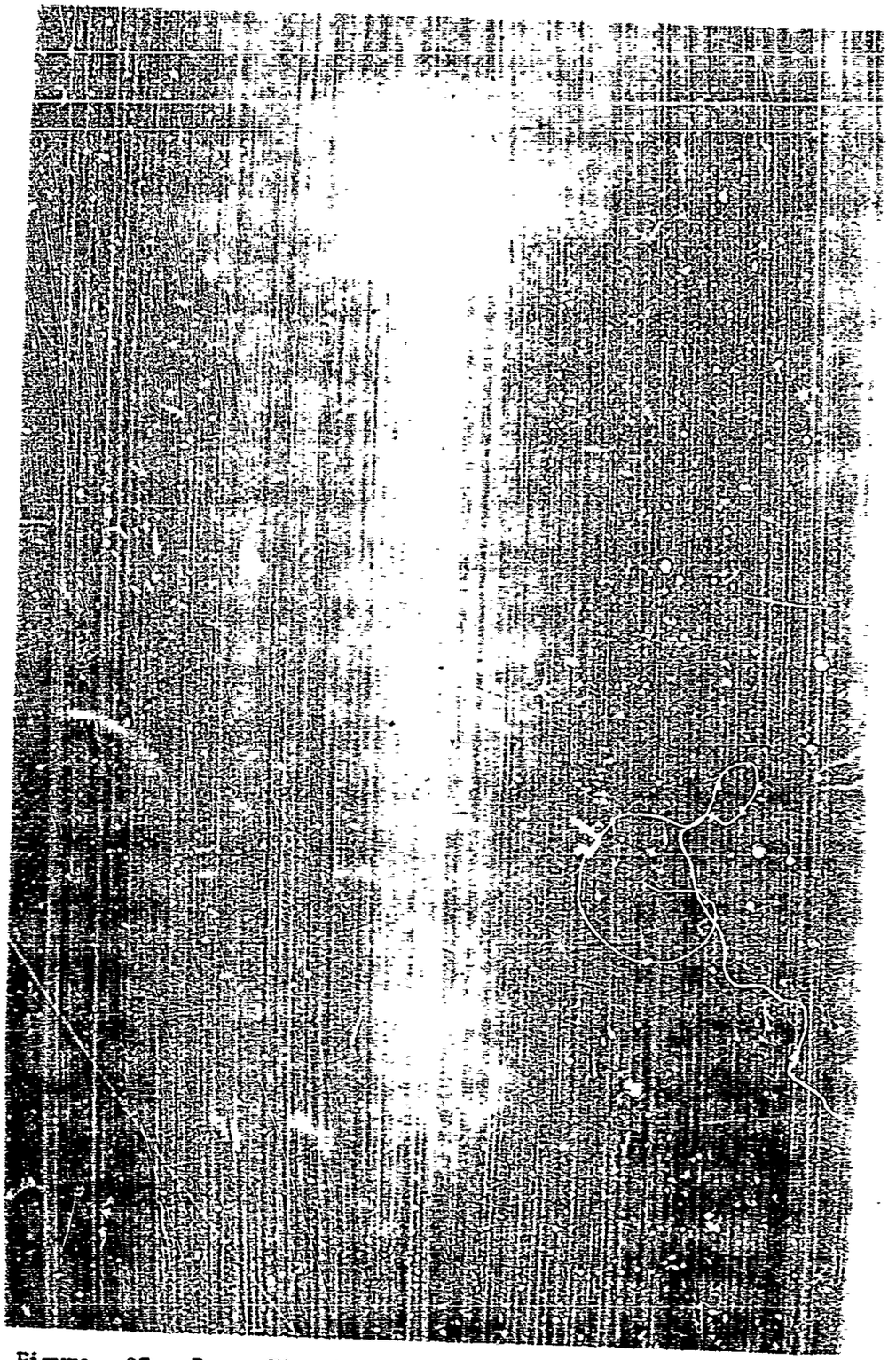


Figure 87. Boron-Titanium 10 BF Specimen (Back) at 90 KV, 3.5 MA, 1.2 MM Dia, 4.5 Min

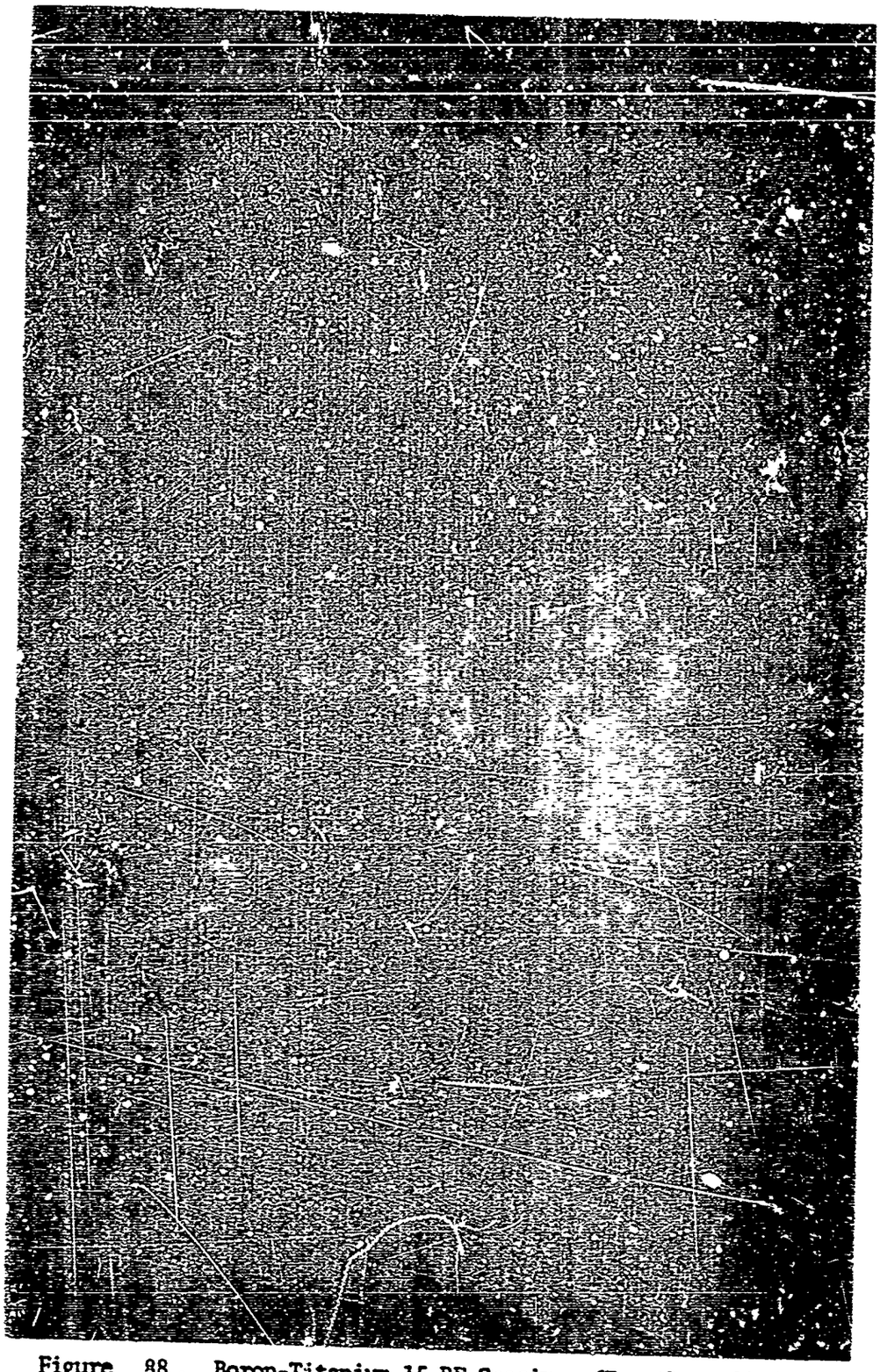


Figure 88. Boron-Titanium 15 BF Specimen (Front) at 90 KV, 3.5 MA., 1.2 MM Dia, 4.75 Min

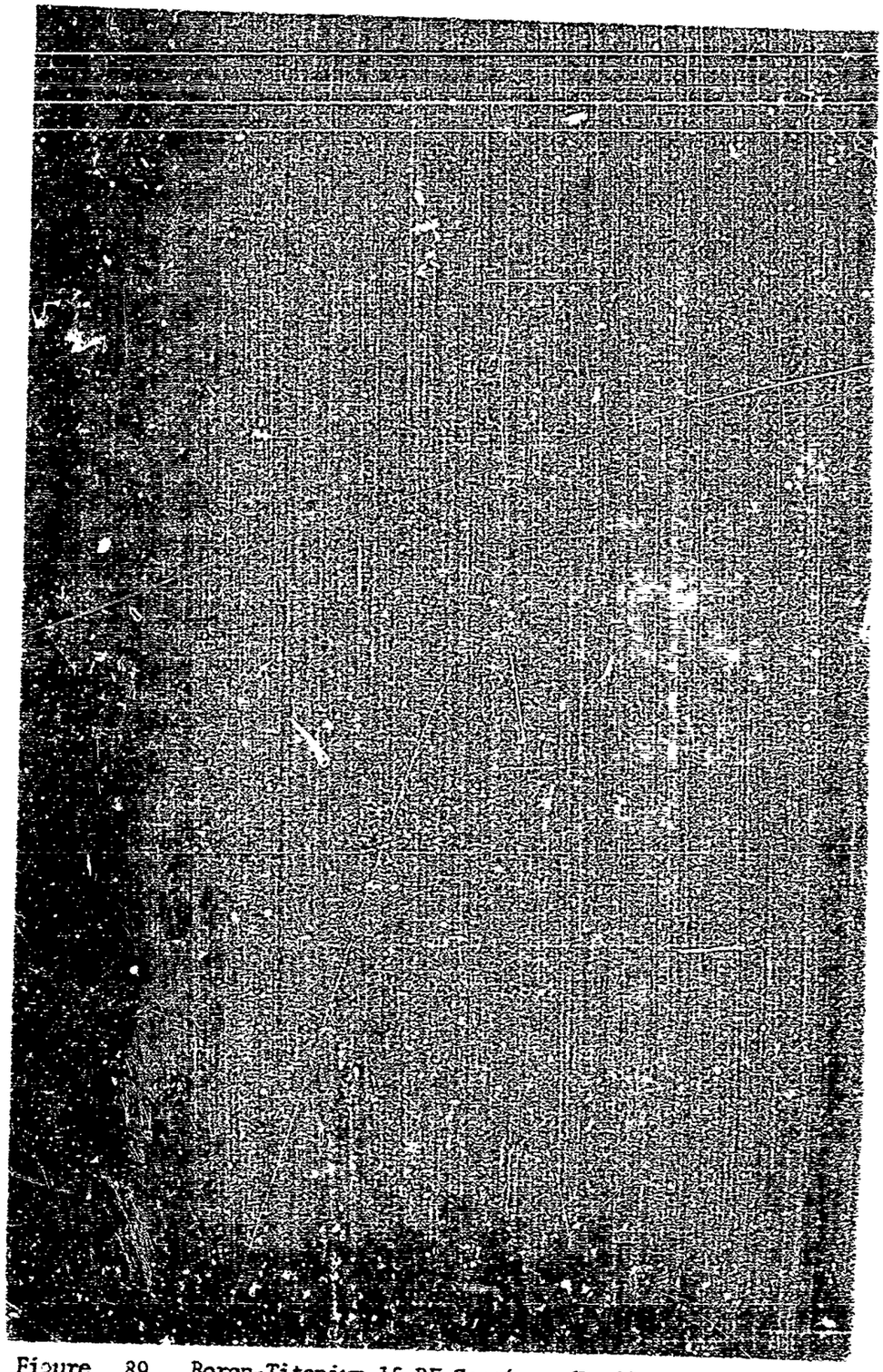


Figure 89. Boron-Titanium 15 BF Specimen (Back) at 90 KV, 3.5 MA, 1.2 Mil Dia, 4.75 Min

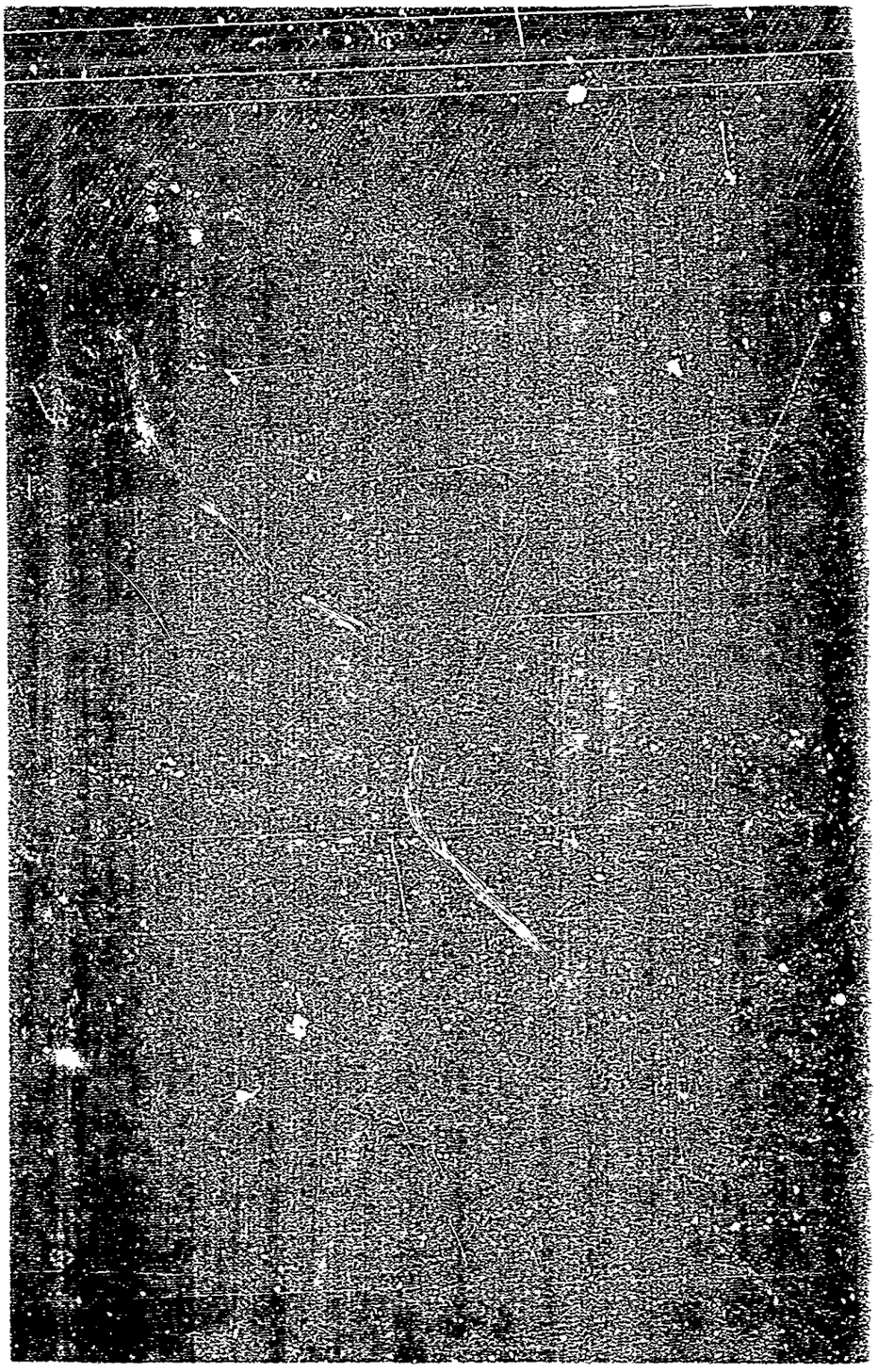


Figure 90. Boron-Titanium 20 BF Specimen (Front) at 90 KV, 4 MA, 1.2 MM Dia, 5 Min

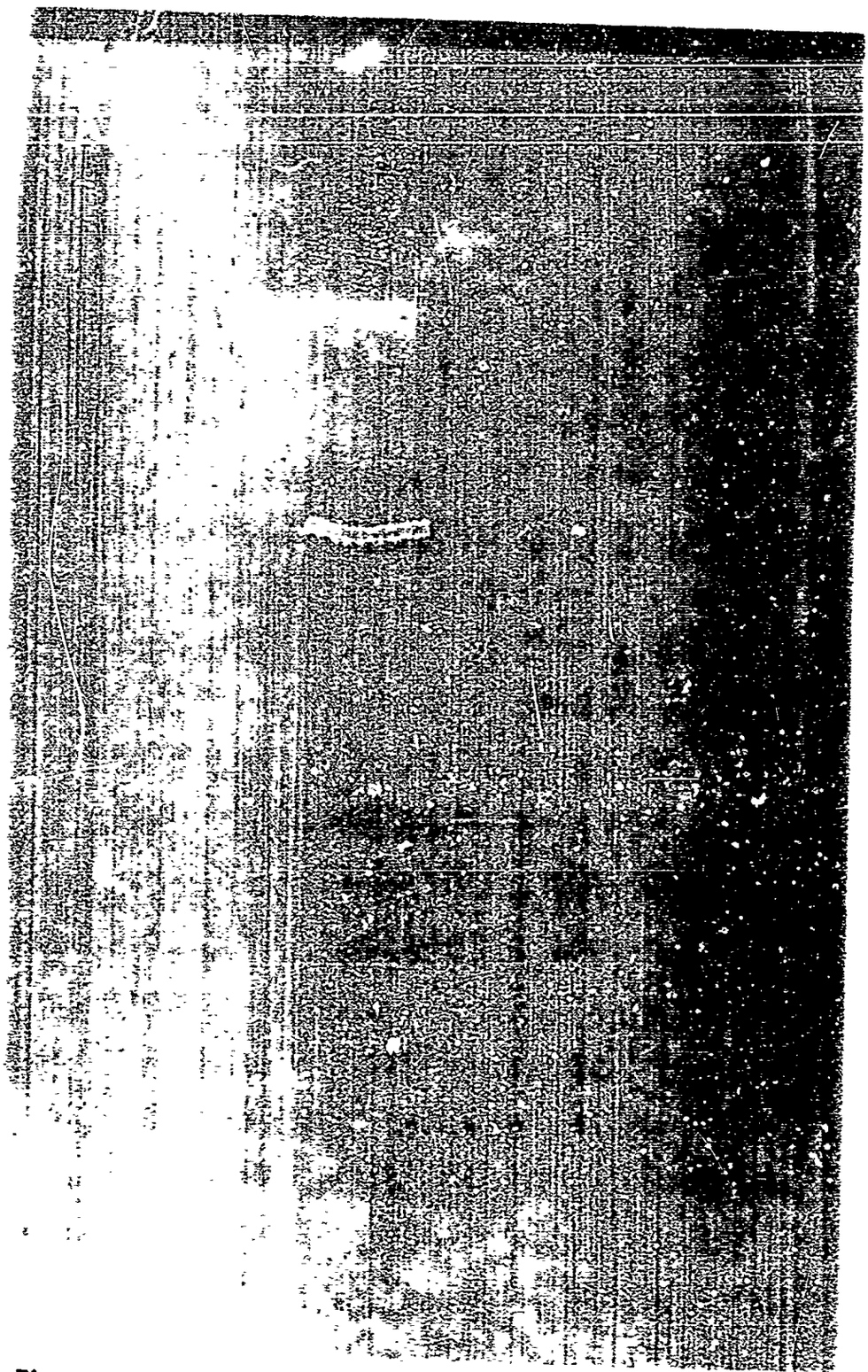


Figure 91. Boron-Titanium 20 BF Specimen (Back) at 90 KV, 4 MA, 1.2 MM Dia, 5 Min

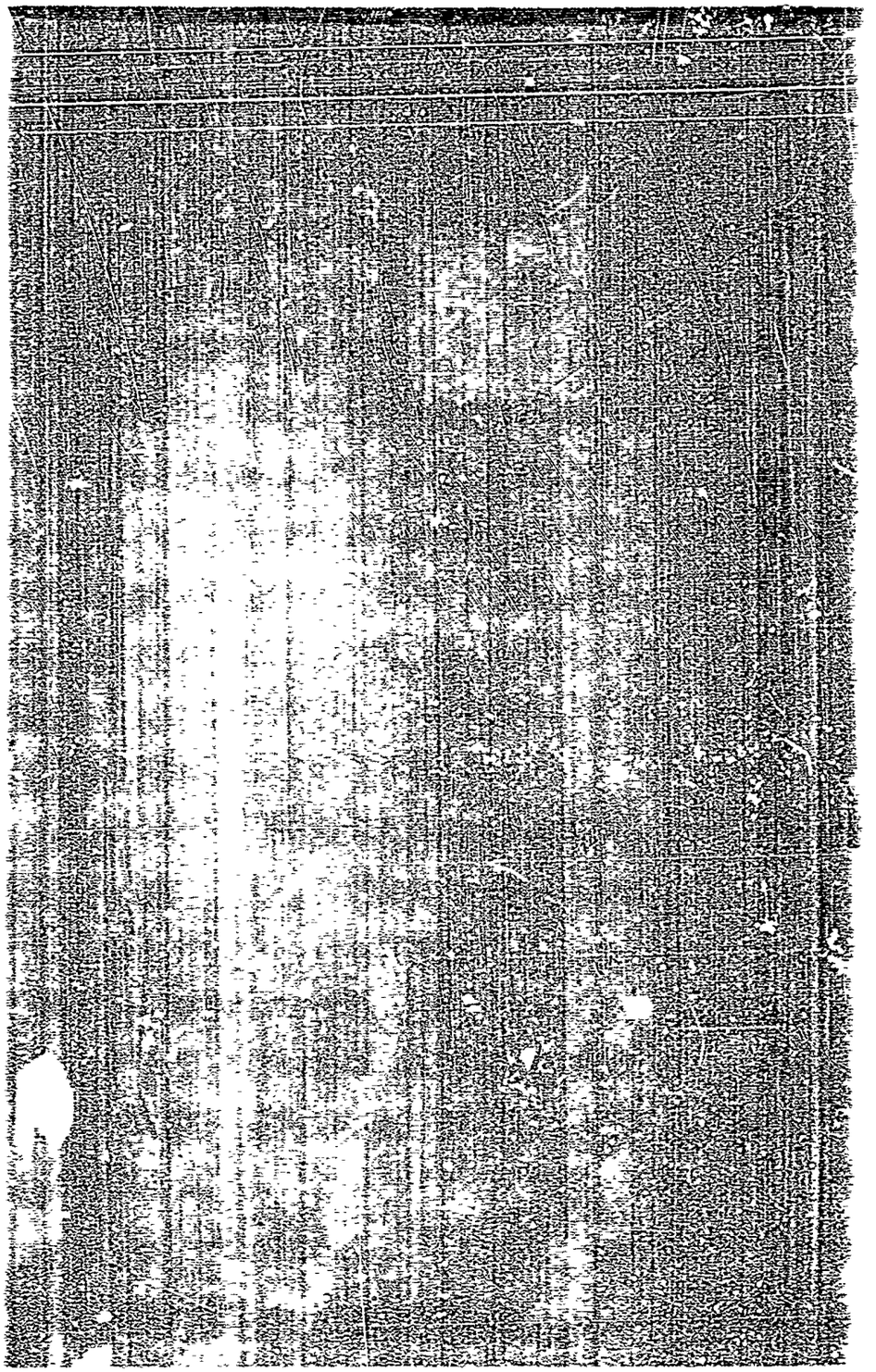


Figure 92. Boron-Titanium 25 BF Specimen (Front) at 90 KV, 4 MA, 1.2 Mil Dia, 5 Min

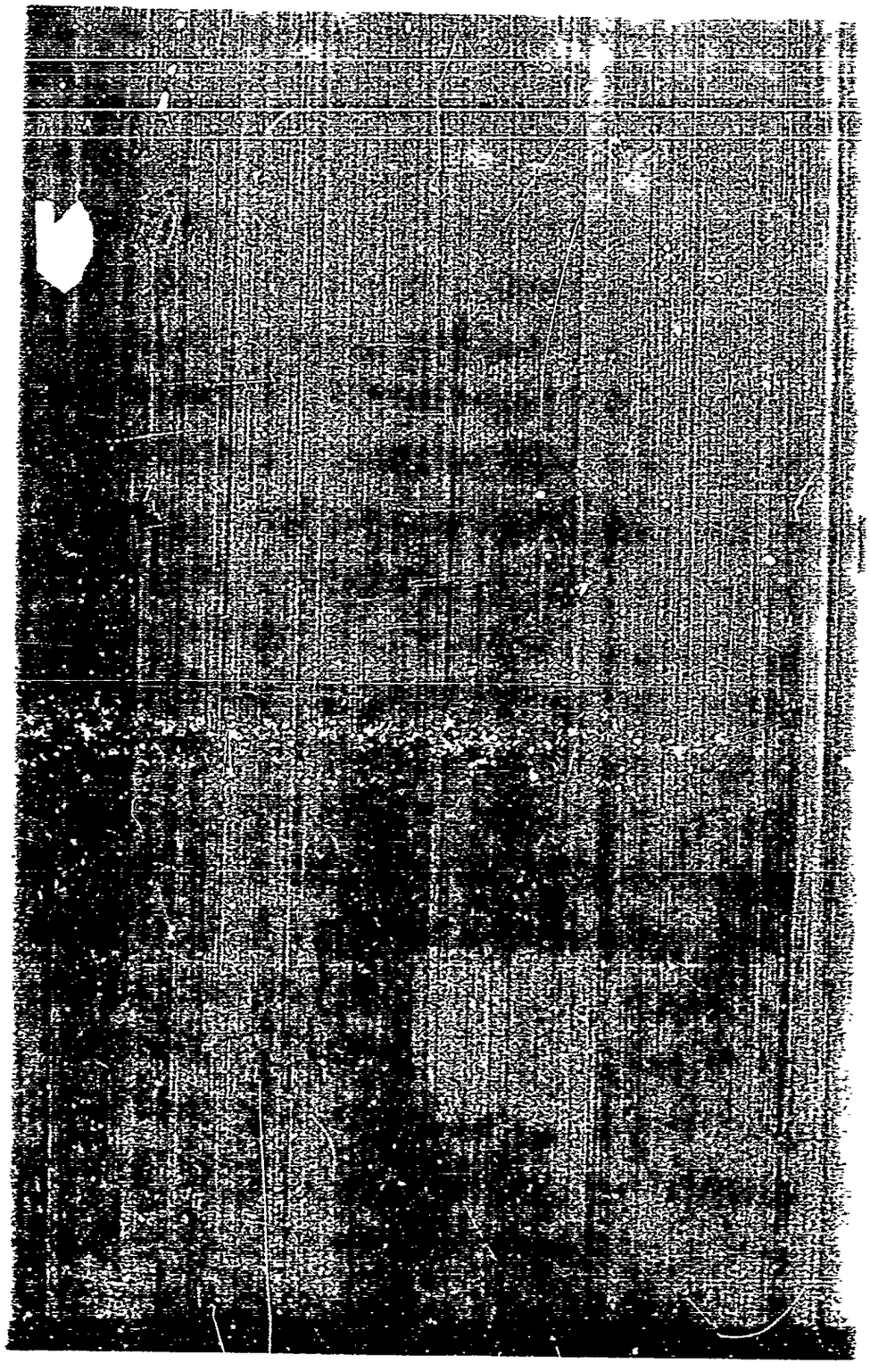


Figure 93. Boron-Titanium 25 BF Specimen (Back) at 90 KV, 4 MA, 1.2 MM Dia, 5 Min



Figure 94. Boron-Titanium 15 M Specimen (Front) at 130 KV, 4 MA, 1.2 MM Dia, 5 Min

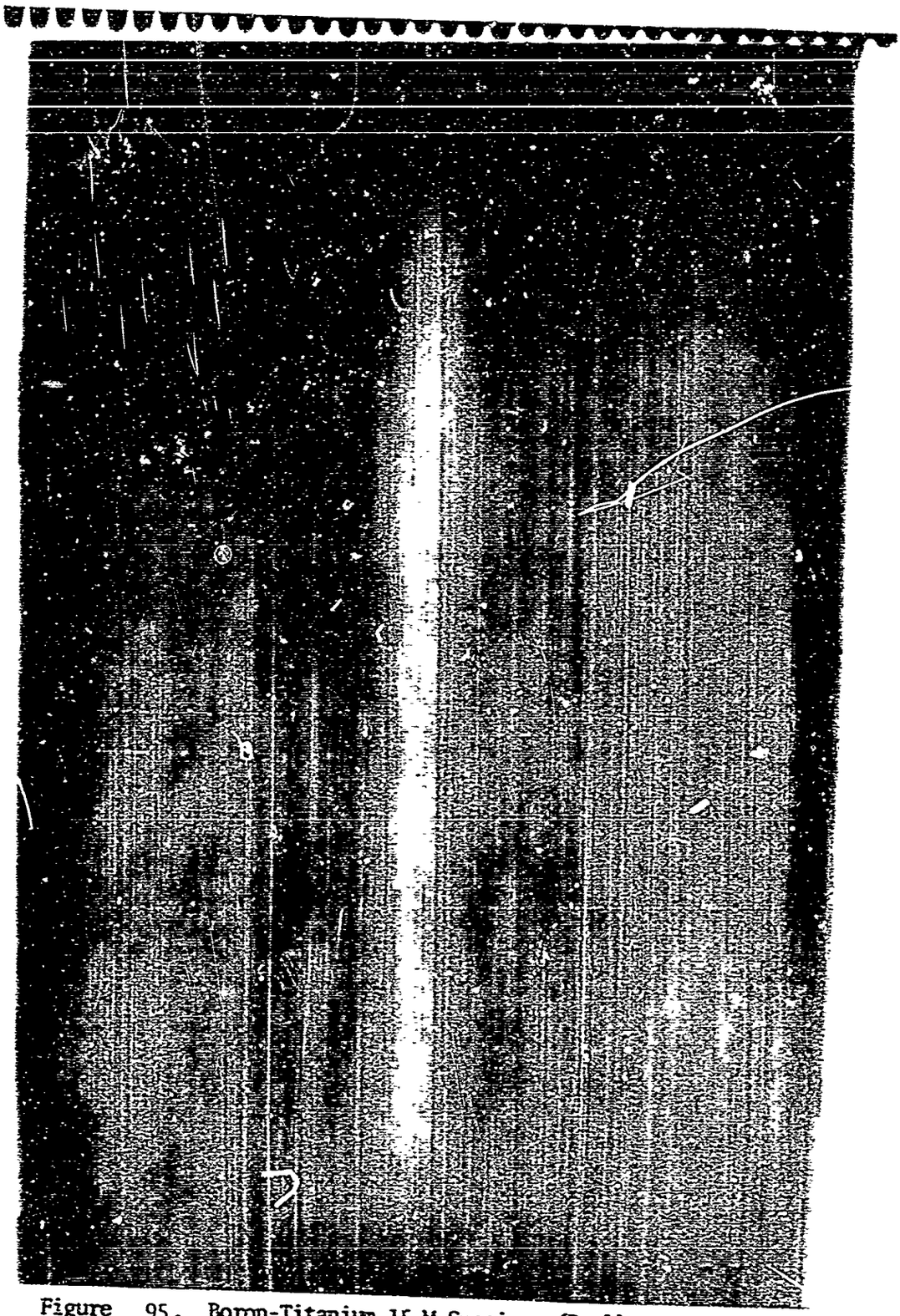


Figure 95. Boron-Titanium 15 M Specimen (Back) at 130 KV, 4 MA, 1.2 MM Dia, 5 Min

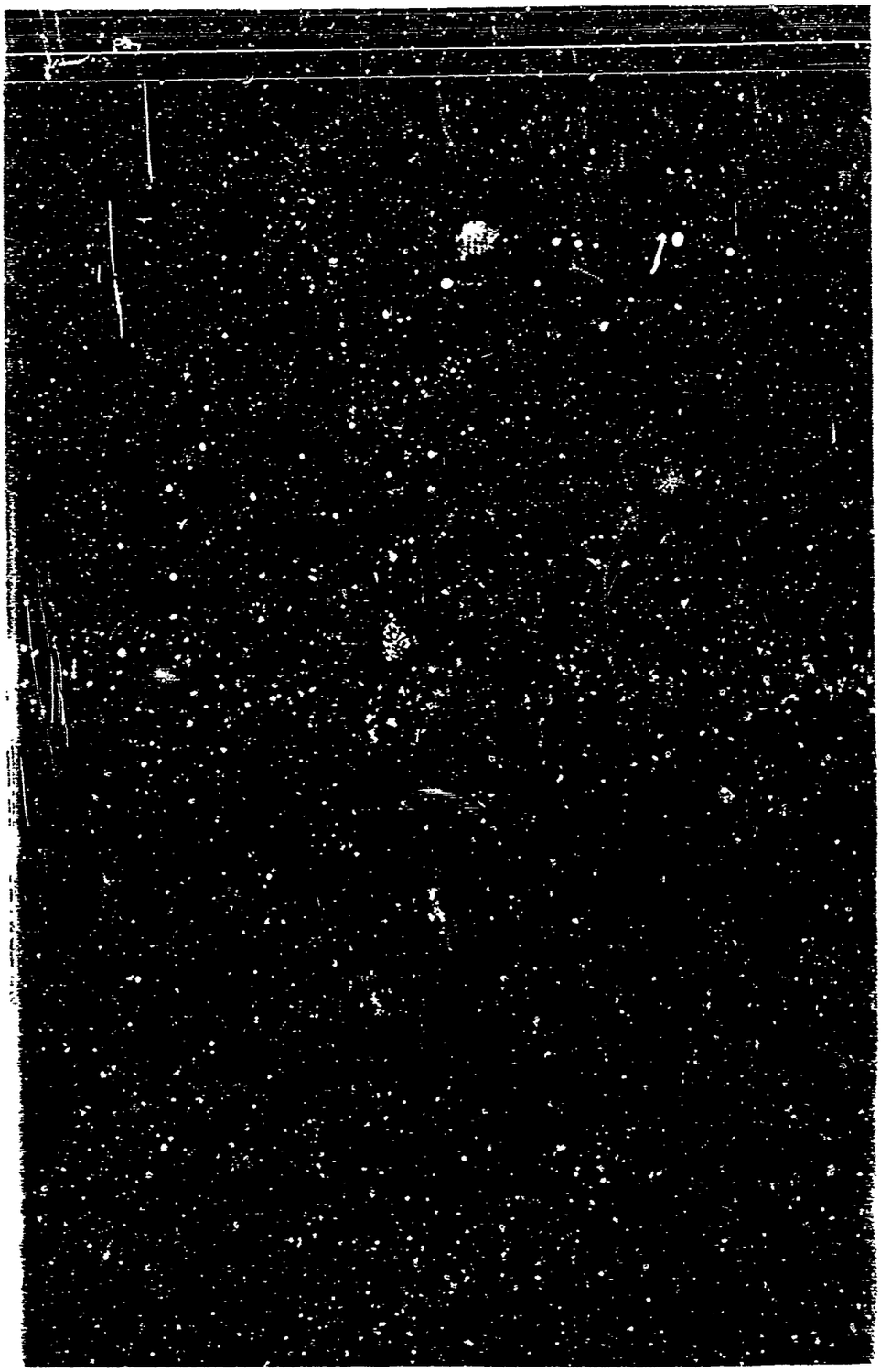


Figure 96. Boron-Titanium 15 F Specimen (Front) at 110 KV, 4 MA, 1.2 MM Dia, 5 Min

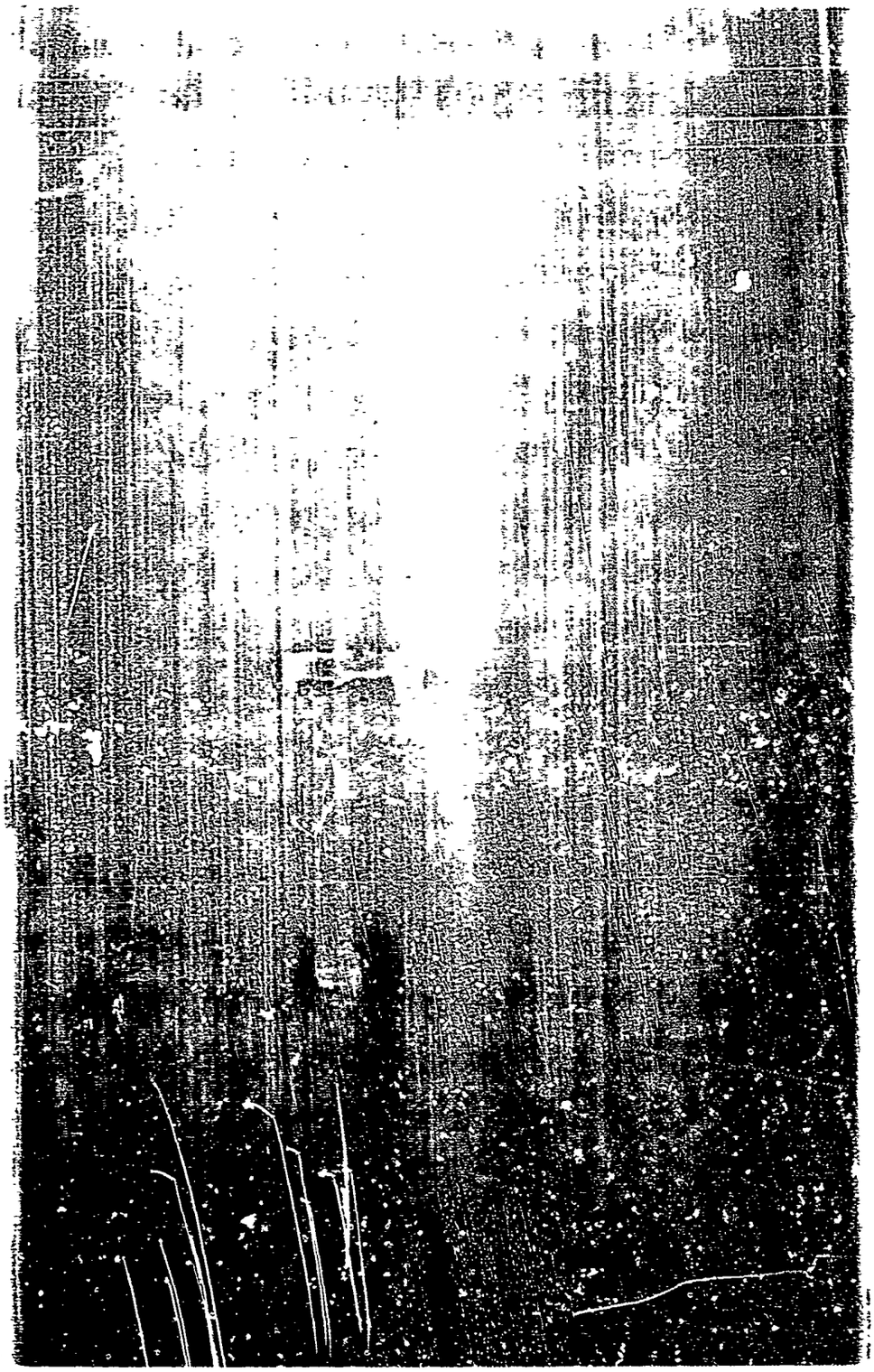


Figure 97. Boron-Titanium 15 F Specimen (Back) at 110 KV, 4 MA, 1.2 MM Dia, 5 Min

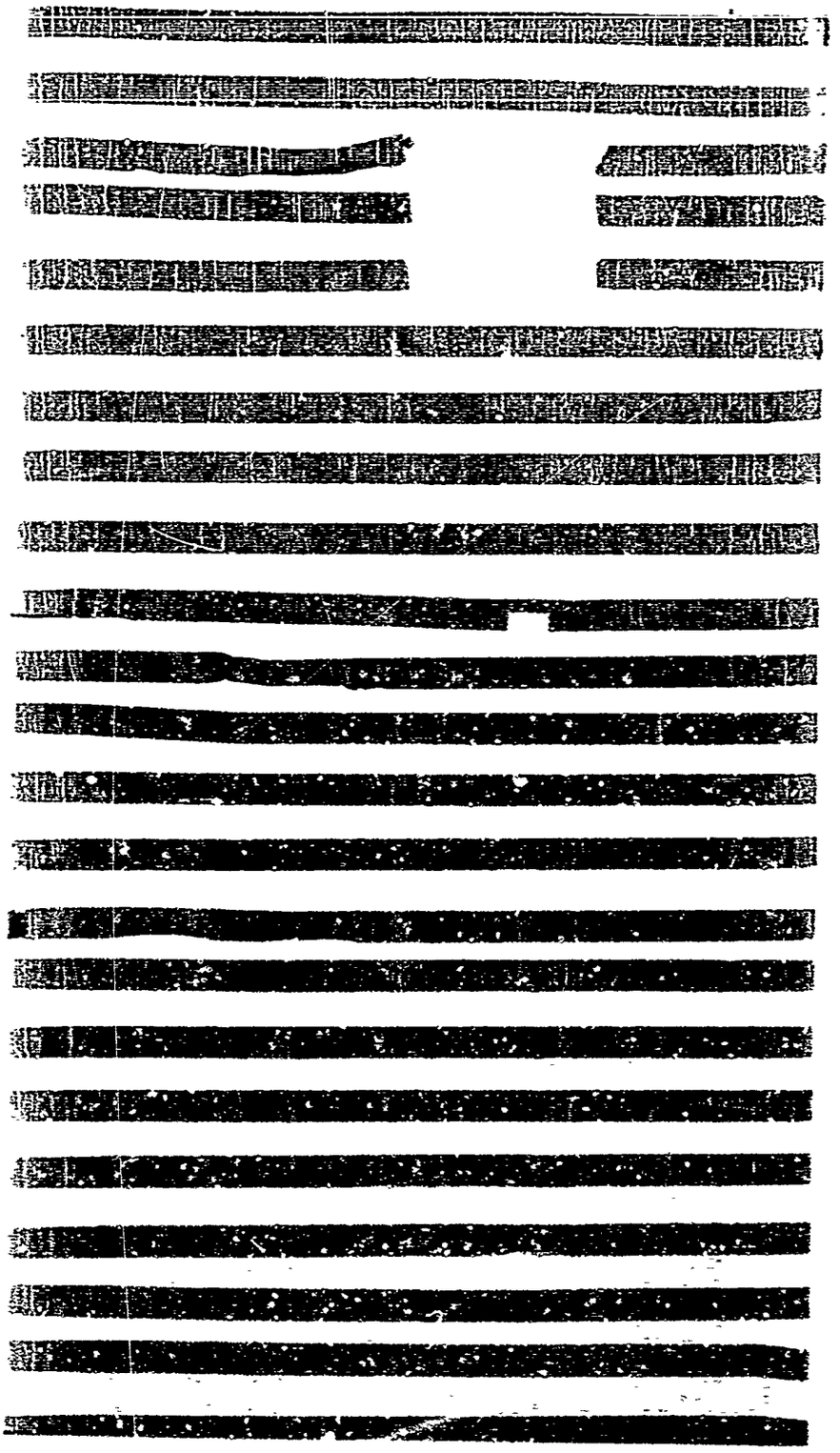


Figure 98 . Boron-Aluminum 10 BF Specimen at 90 KV, 4 MA, 1.2 MM Dia, 3.75 Min

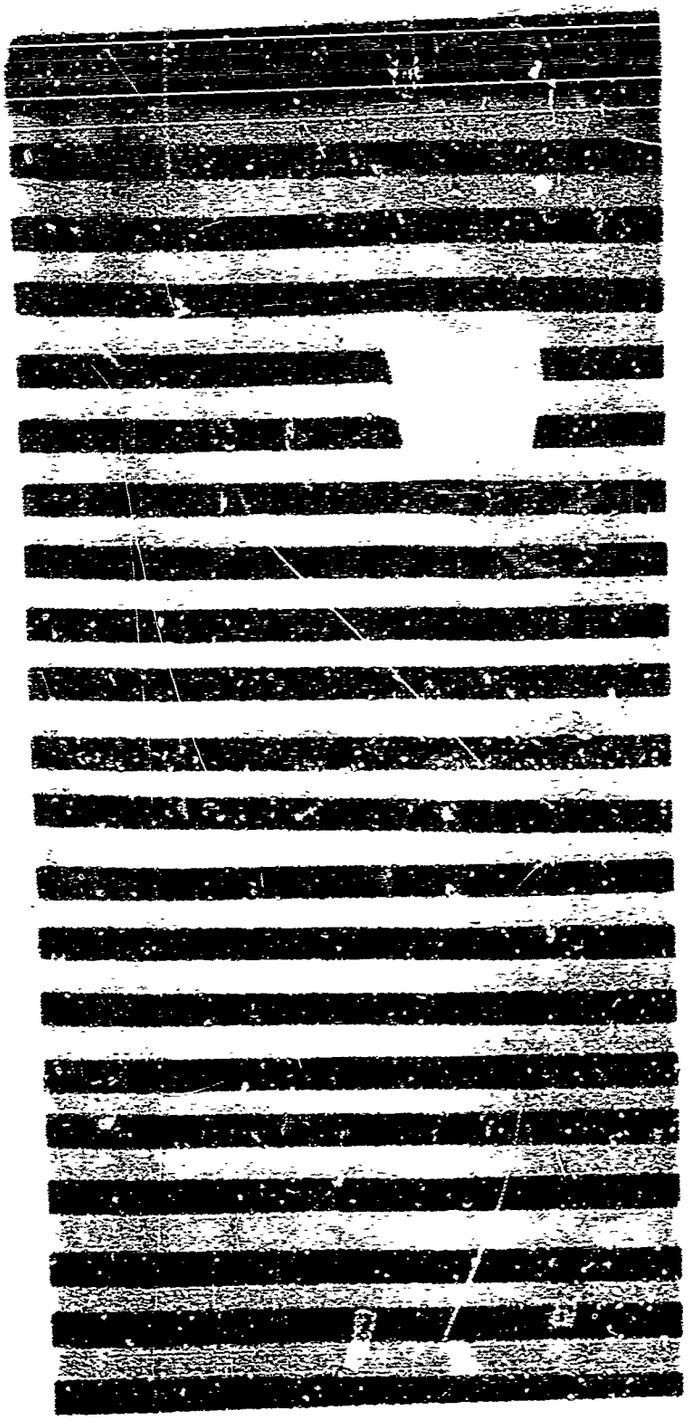


Figure 99. Boron-Aluminum 15 BF Specimen at 100 KV, 3 MA, 1.2 MM Dia, 4 Min

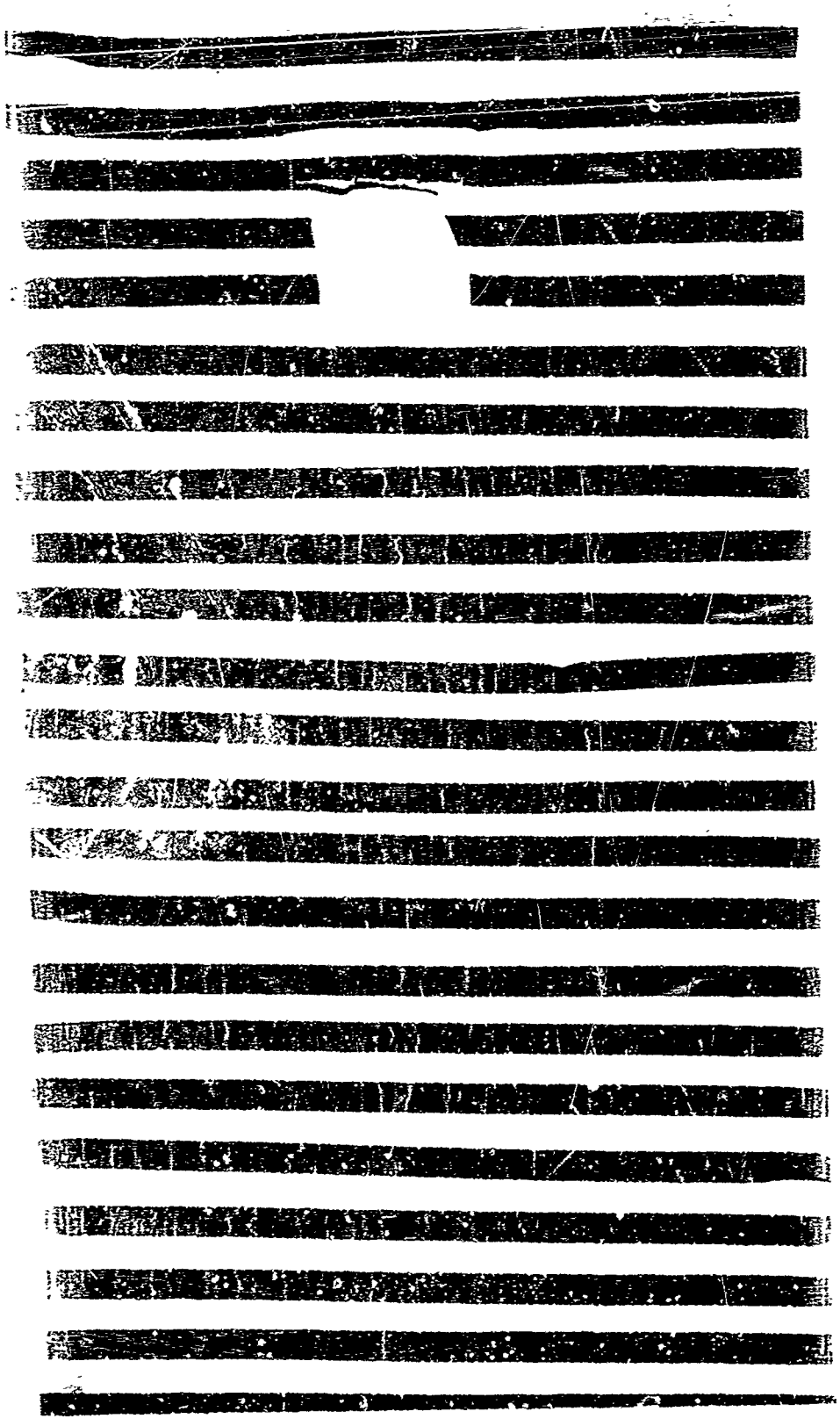


Figure 100. Boron-Aluminum 20 BF Specimen at 100 KV, 4 MA, 1.2 MM Dia, 3.5 Min

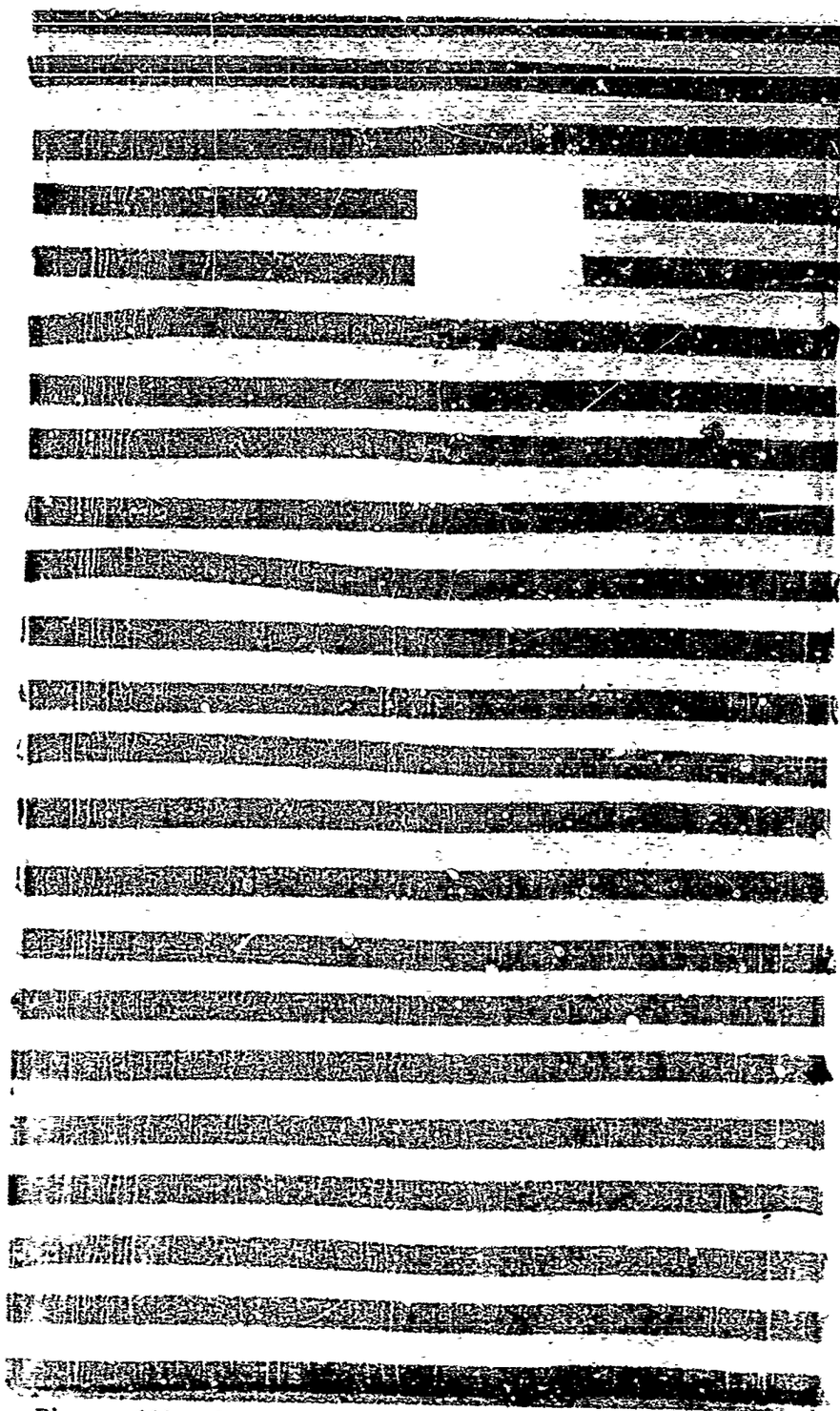


Figure 101. Boron-Aluminum 25 BF Specimen at 110 KV, 4 MA, 1.2 MM Dia, 3.5 Min

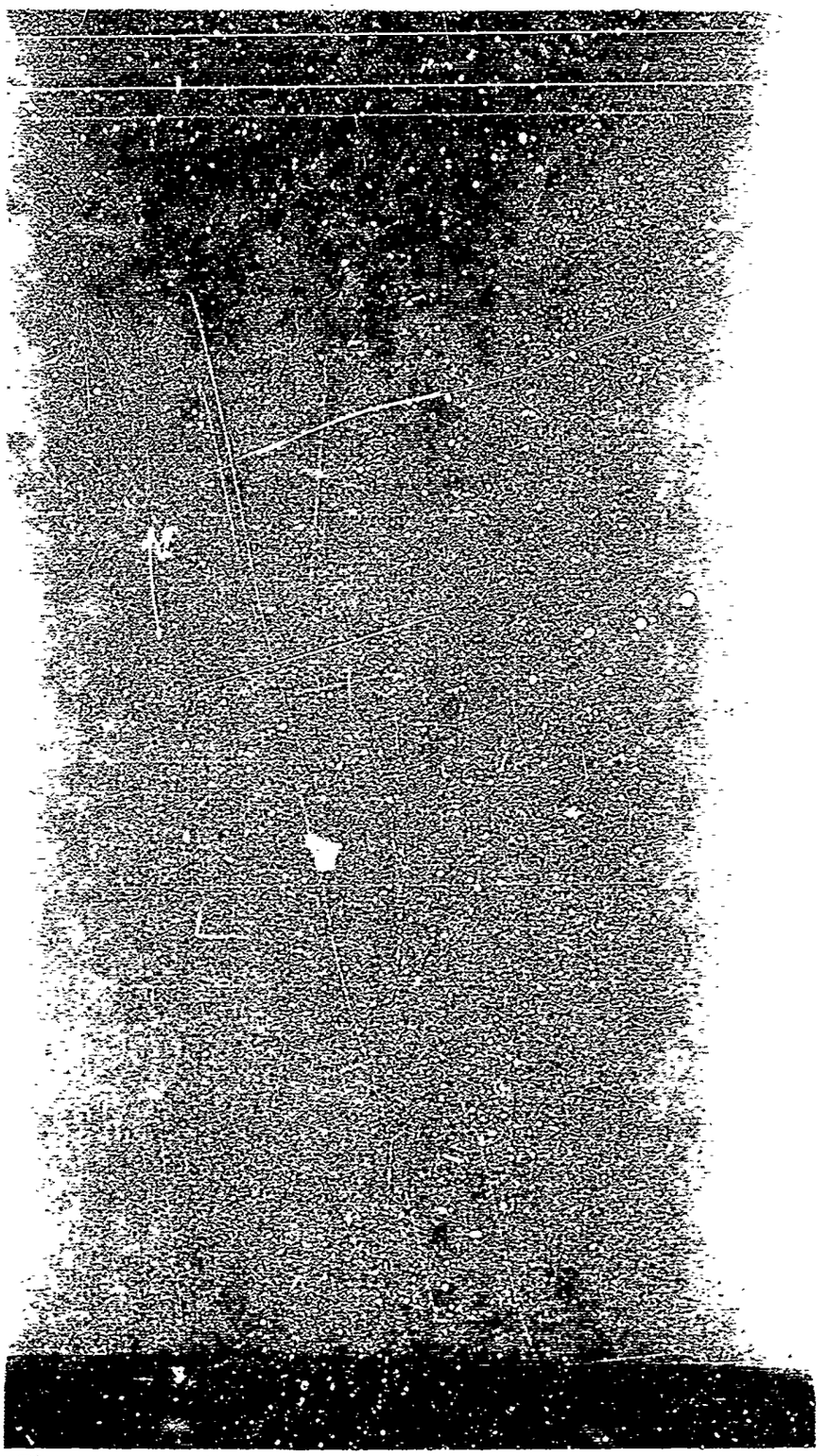


Figure 102 . Boron-Aluminum 15 M Specimen at 120 KV, 4 MA, 1.2 MM Dia, 4 Min

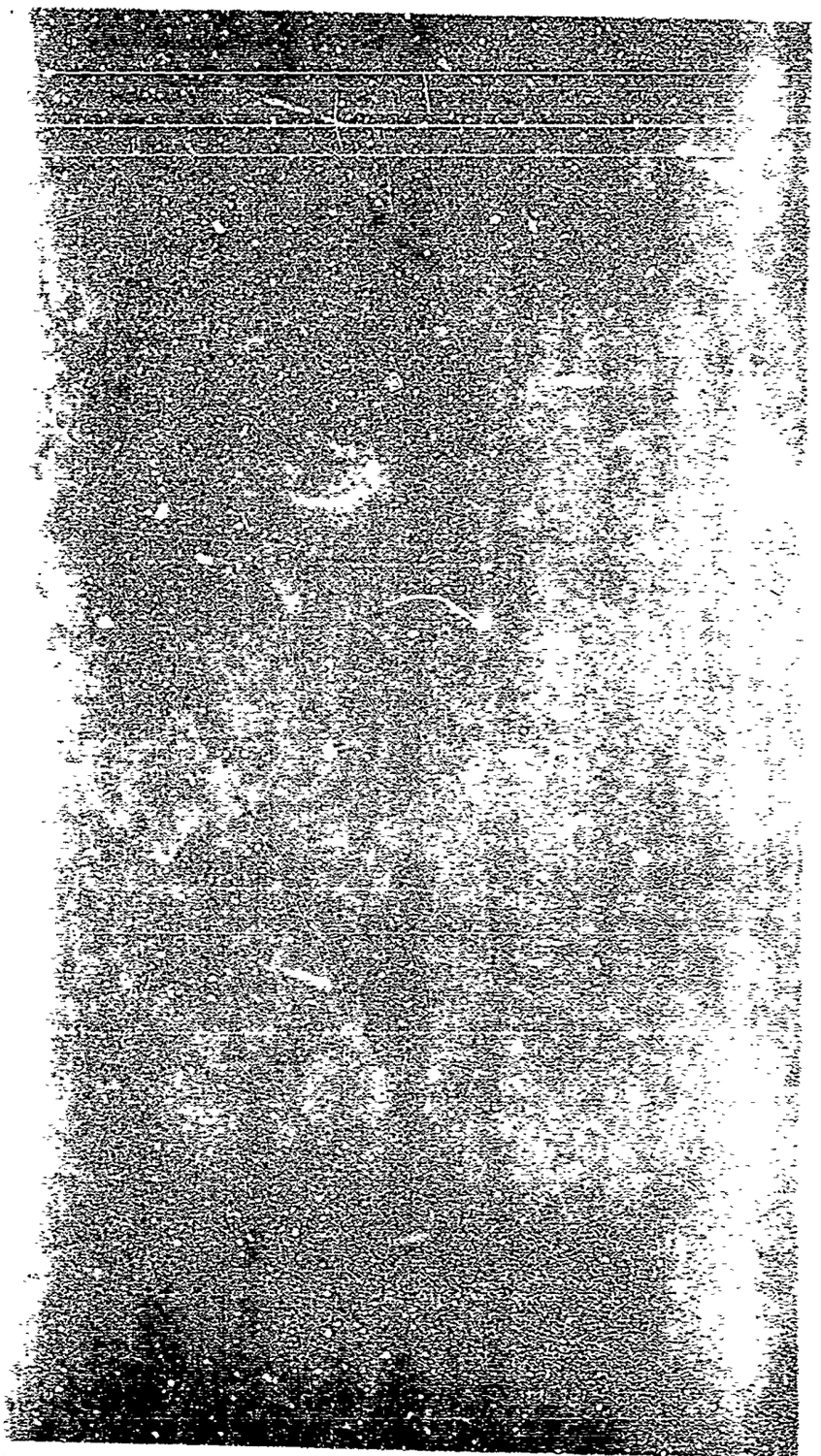


Figure 103. Boron-Aluminum 15 F Specimen at 110 KV, 4 MA, 1.2 MM Dia, 4 Min

Appendix III

ULTRASONIC C-SCAN RECORDS

Ultrasonic C-scan records were prepared for tungsten-copper, boron-aluminum, and boron-aluminum fiber-matrix composite specimens. This Appendix presents representative records for each specimen type. The sensitivity values were based on the ultrasonic response from appropriate Alcoa Series "D" Reference Blocks. Where the instrument response was lower than that of the largest reference standard, the sensitivity was expressed in terms of signal height from the back surface of the reference block. A detailed discussion of test conditions is presented in Section VI of this report. The following considerations should be kept in mind when interpreting the C-scan recordings:

1. The recorder was set to write on the first return signal from the reflector plate. Therefore, a loss of signal appears as a white area on the recordings.

2. The annular loss of a signal at the corners of the plate images were caused by the rubber grommets used to space the specimens over the reflector plate.

3. The record area is slightly larger than the specimens. This was done to prevent loss of information during testing. However, this technique makes exact location of specimen edges on the recordings somewhat difficult to determine.

4. The recording direction was normal to the fiber wrap direction.

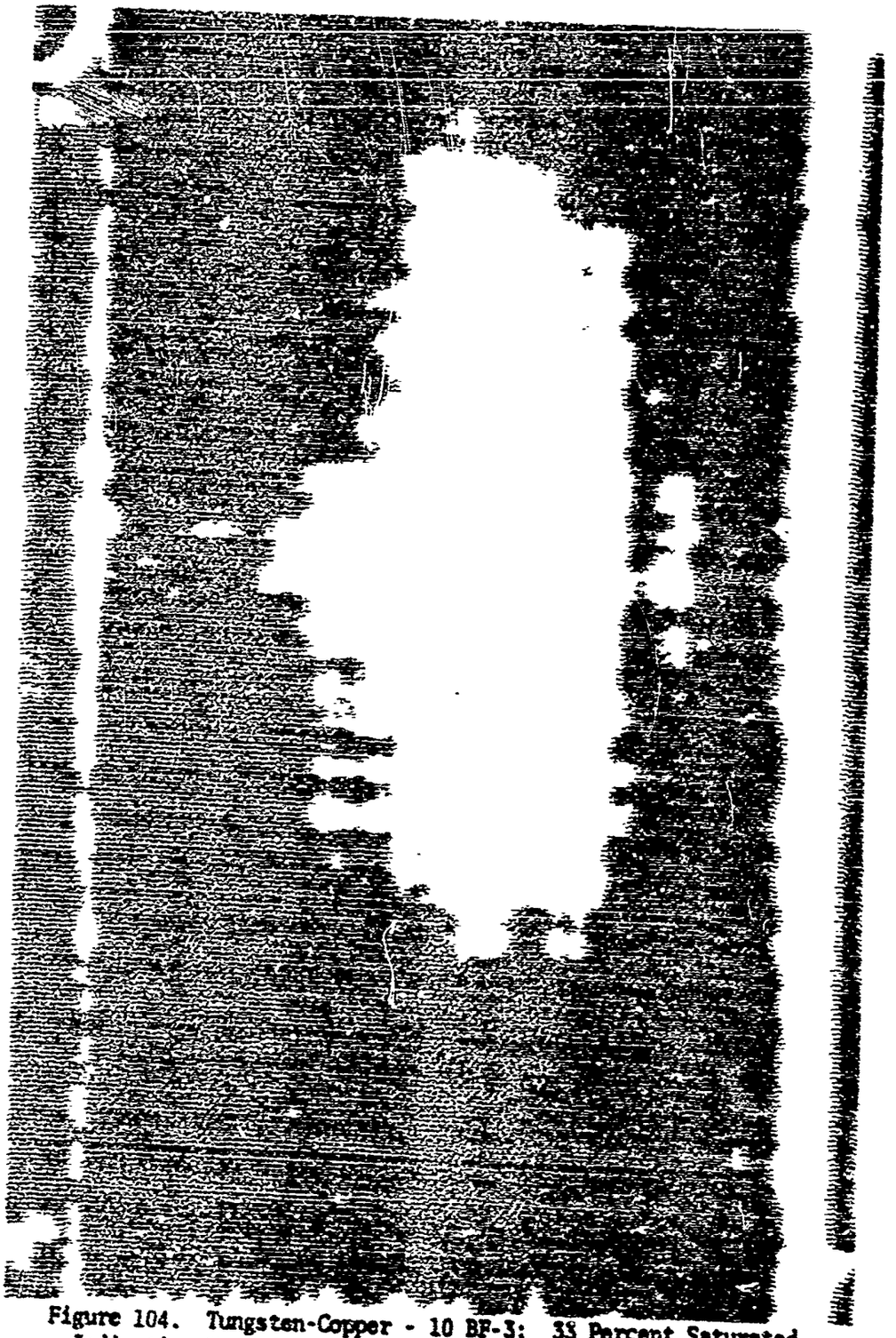


Figure 104. Tungsten-Copper - 10 BF-3: 33 Percent Saturated Indication From Flat Bottom Hole in a No. 8 Alcoa D Block

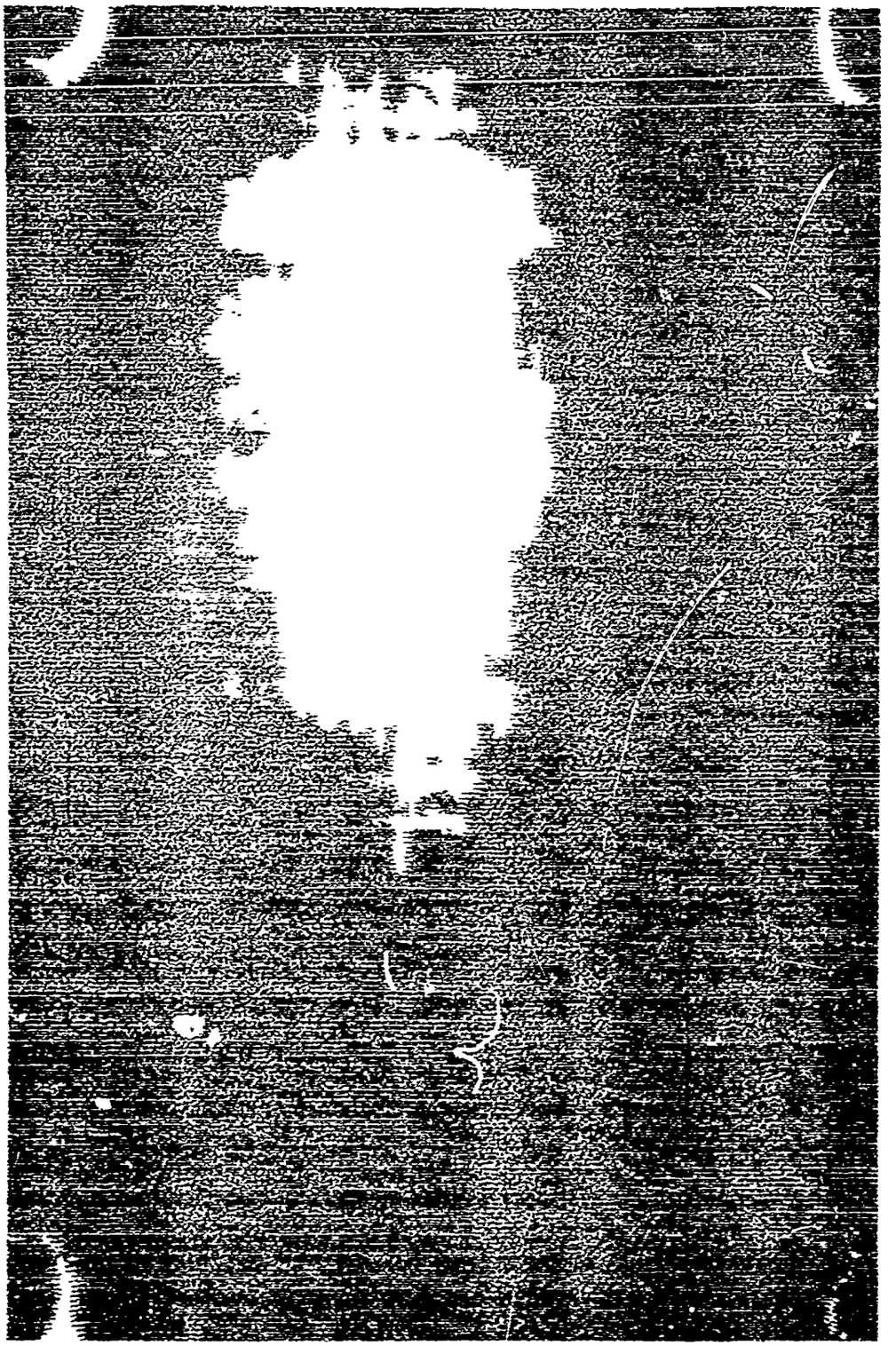


Figure 105. Tungsten-Copper - 15 BF-3: 95 Percent Saturated Indicating From Flat Bottom Hole in a No. 5 Alcoa D Block

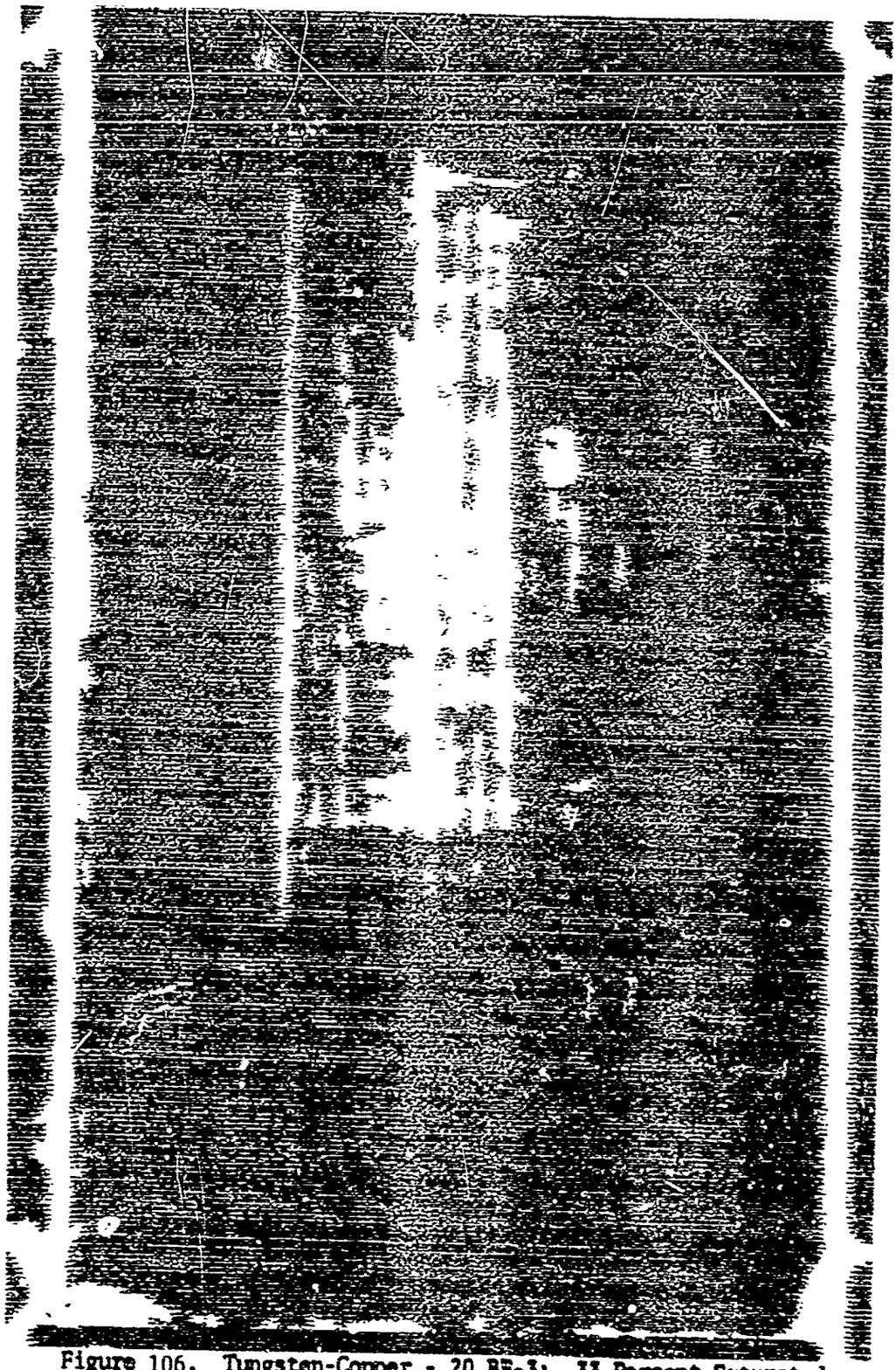


Figure 106. Tungsten-Copper - 20 BF-3: 33 Percent Saturated Indication From Flat Bottom Hole in a No. 8 Alcoa D Block



Figure 107. Tungsten-Copper - 25 RF-3: 70 Percent Saturated Indication From Flat Bottom Hole in a No. 8 Alcoa D Block

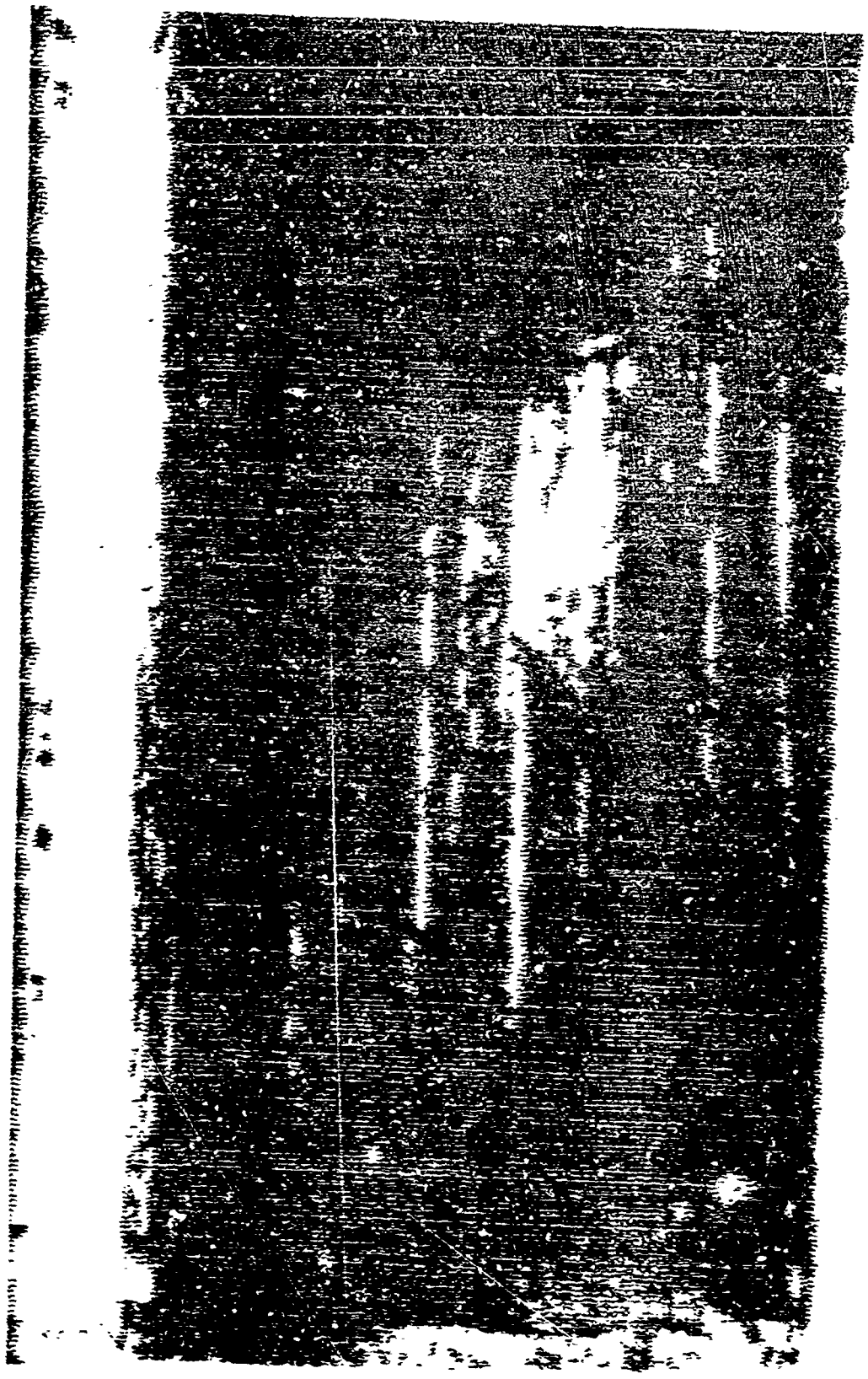


Figure 108. Tungsten-Copper - 15 A-S: 48 Percent Saturated Indication From Flat Bottom Hole in a No. 4 Alcoa D Block

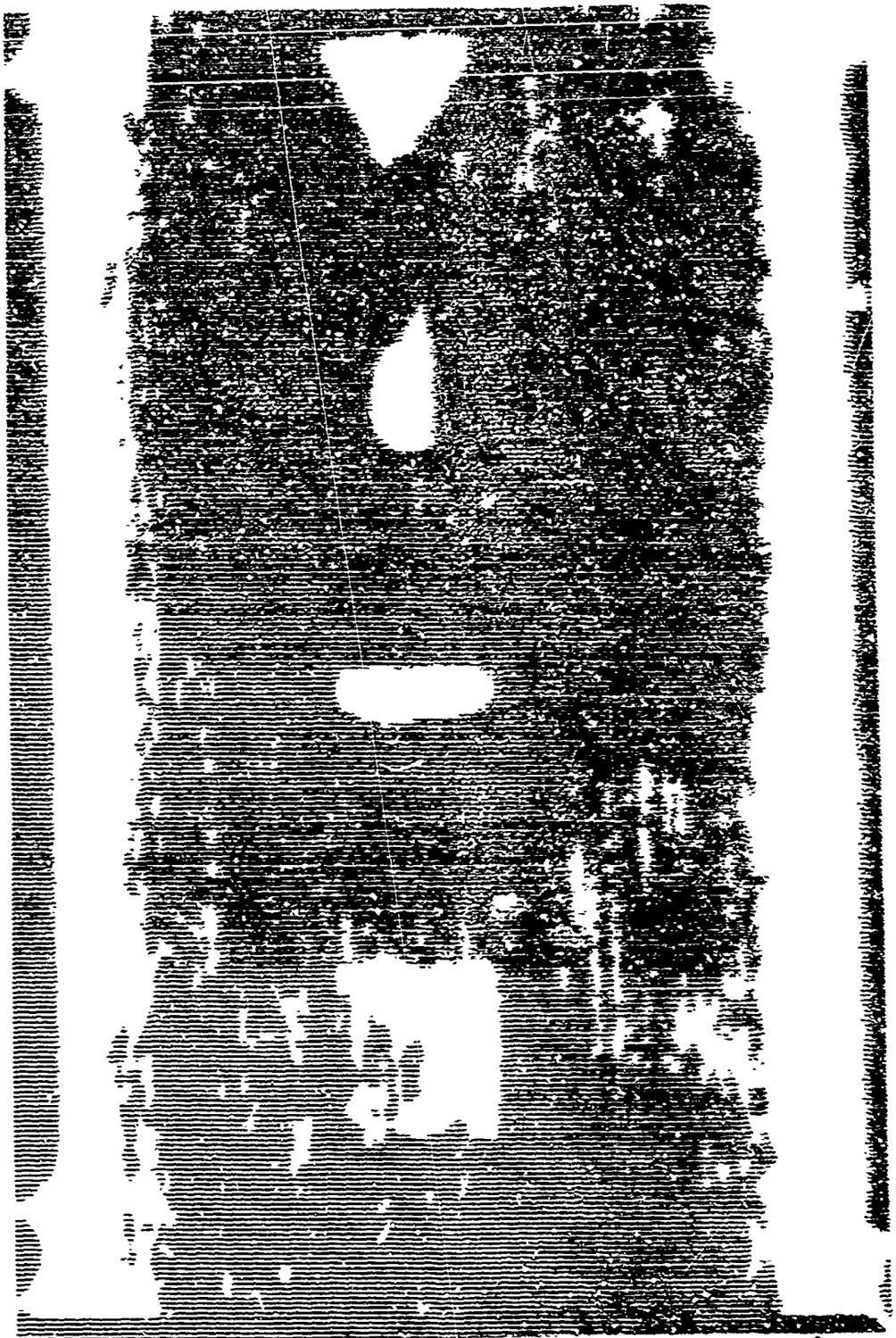


Figure 109. Tungsten-Copper - 15 FH-2: 82 Percent Saturated Indication From Flat Bottom Hole in a No. 8 Alcoa D Block

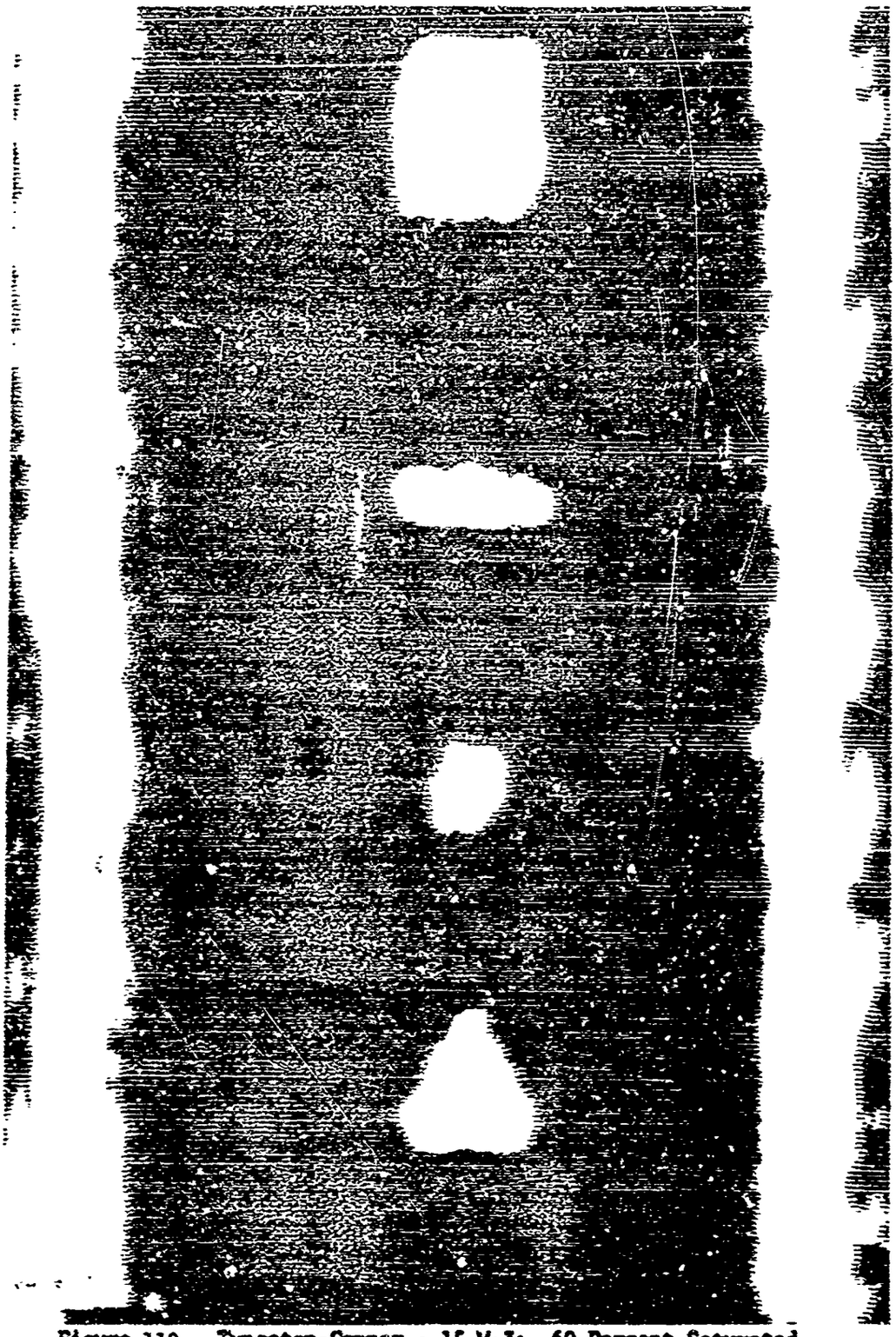


Figure 110. Tungsten-Copper - 15 M-3: 60 Percent Saturated Indication From Flat Bottom Hole in a No. 5 Alcoa D Block

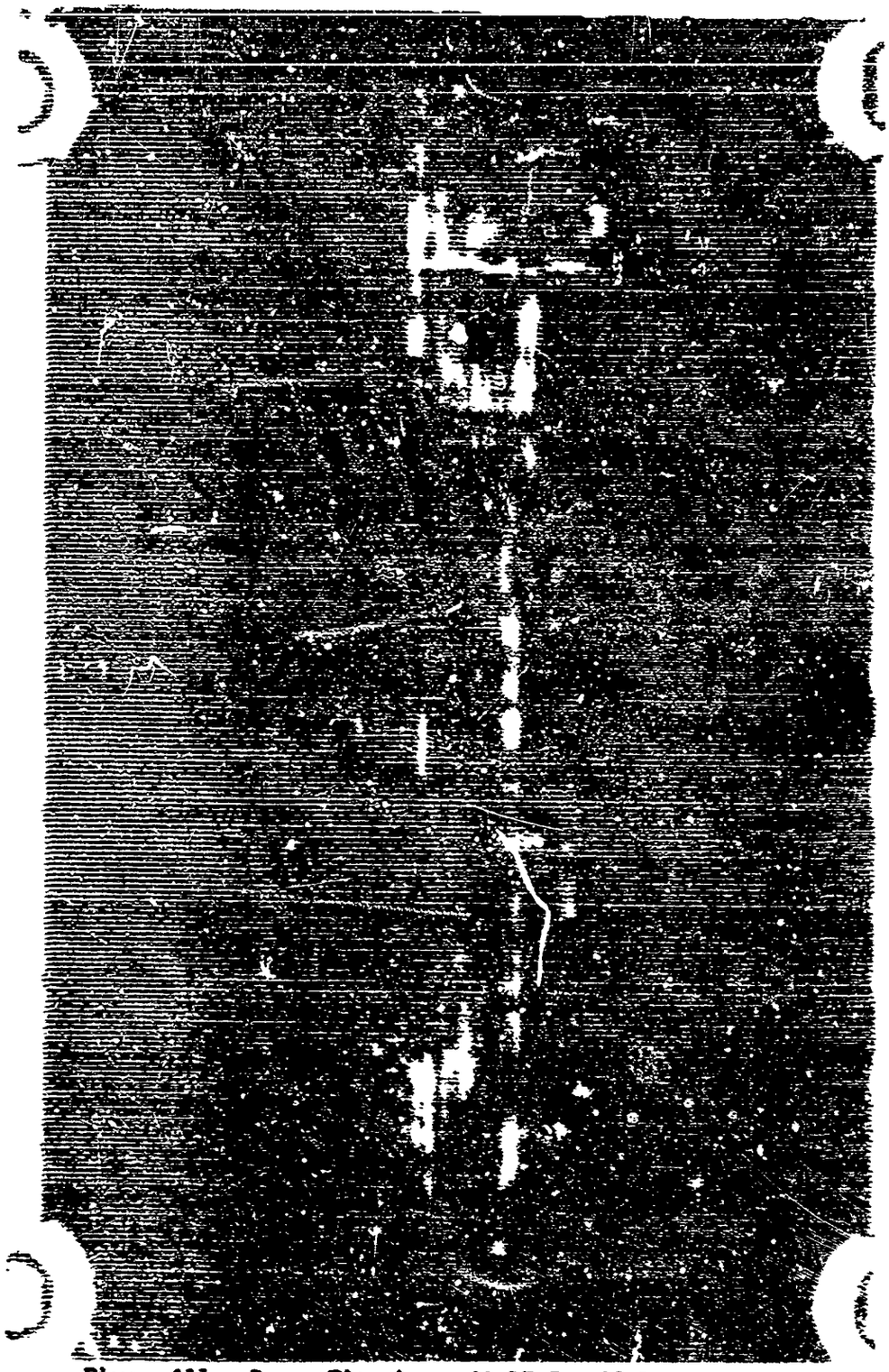


Figure 111. Boron-Titanium - 10 BF-3: 85 Percent Saturated Indication From Flat Bottom Hole in a No. 8 Alcoa D Block

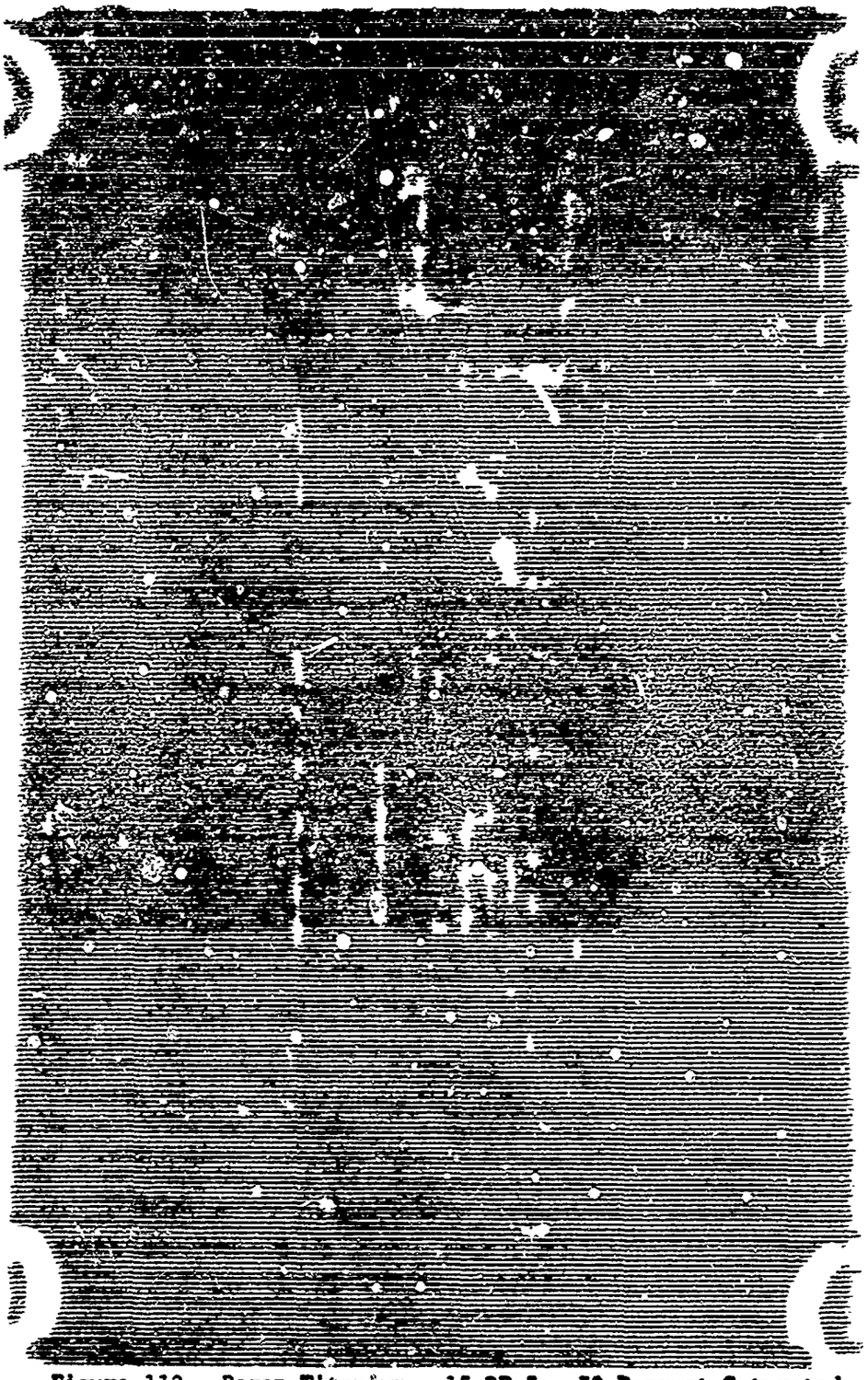


Figure 112. Boron-Titanium - 15 BF-3: 38 Percent Saturated Indication From Flat Bottom Hole in a No. 8 Alcoa D Block



Figure 113. Boron-Titanium - 20 BF-3: 68 Percent Saturated Indication From Flat Bottom Hole in a No. 8 Alcoa D Block

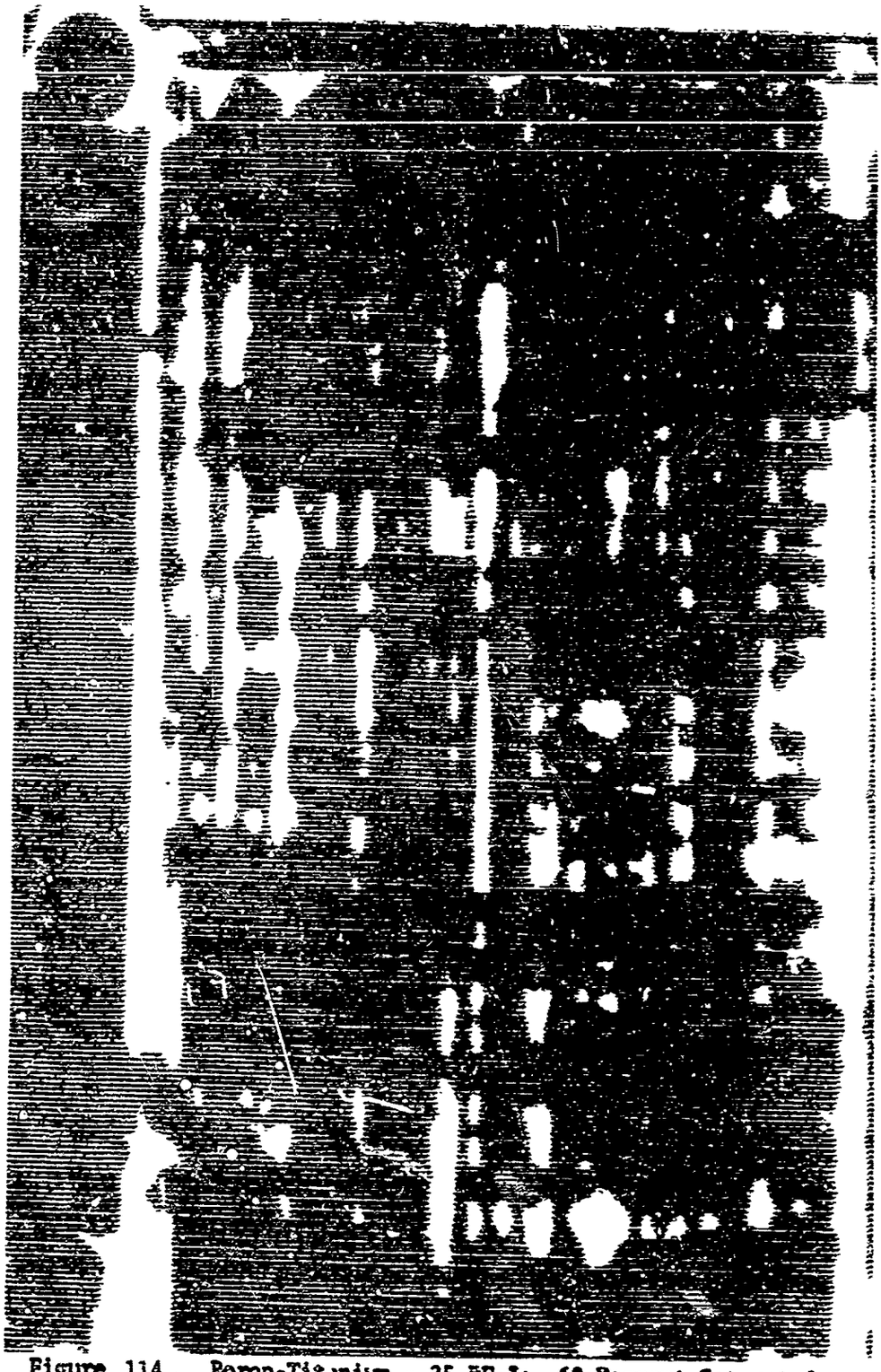


Figure 114.. Boron-Titanium - 25 BF-3: 68 Percent Saturated Indication From Flat Bottom Hole in a No. 8 Alcoa D Block

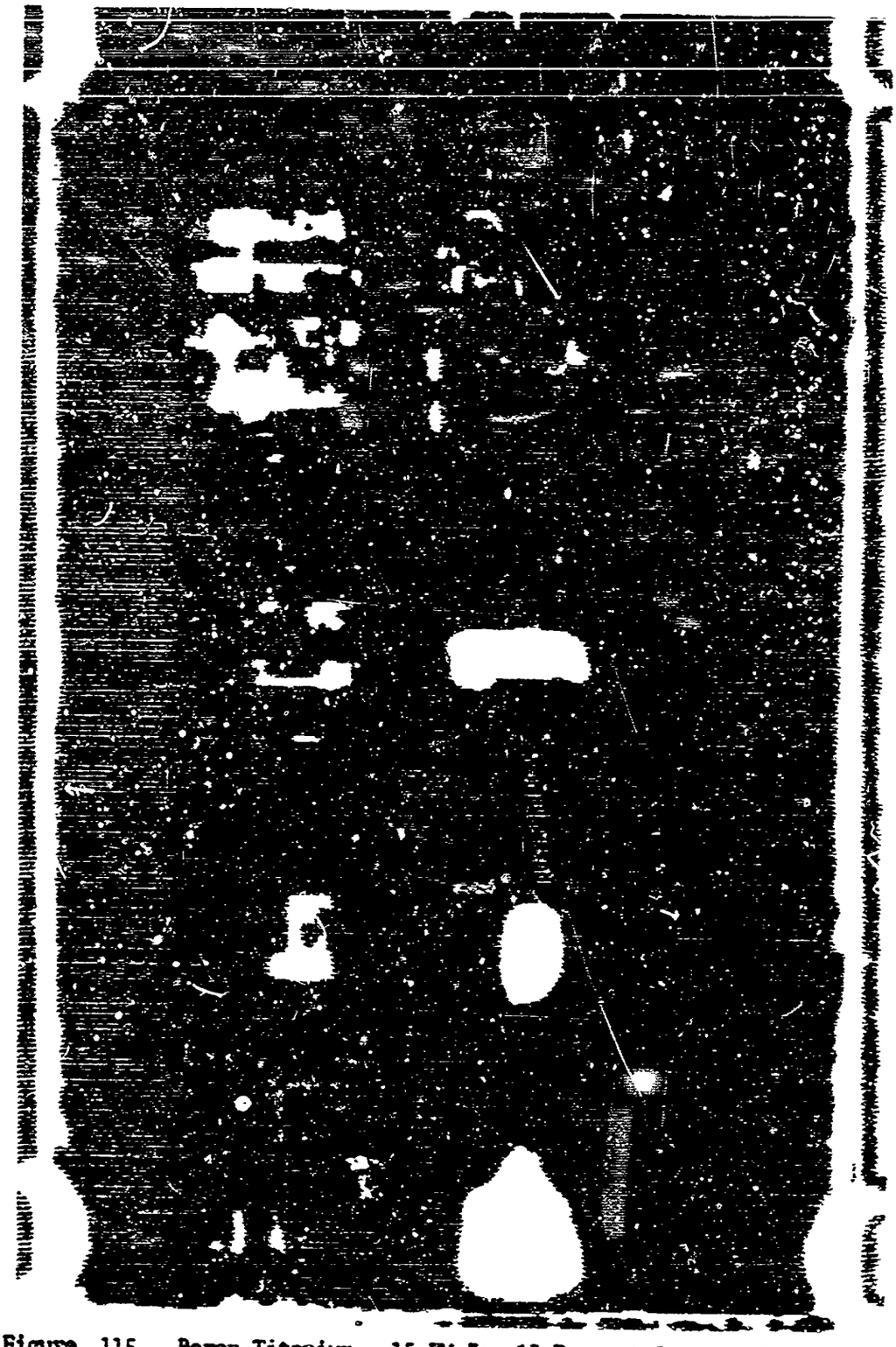


Figure 115. Boron-Titanium - 15 PM-3: 15 Percent Saturated Indication From Flat Bottom Hole in a No. 8 Alcoa D Block



Figure 116. Boron-Titanium - 15 M-2: 15 Percent Saturated Indication From Flat Bottom Hole in a No. 8 Alcoa D Block

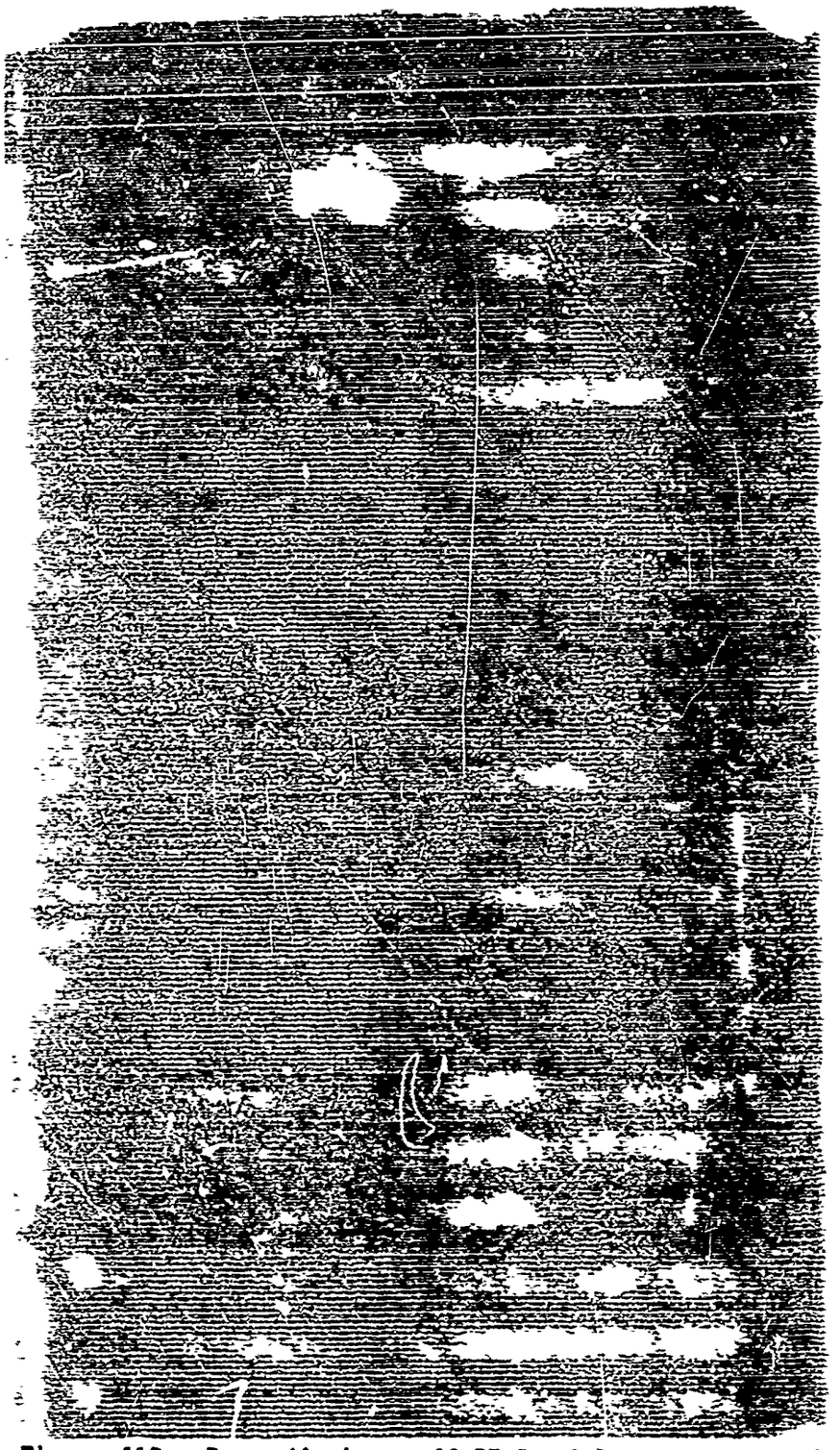


Figure 117. Boron-Aluminum - 10 BF-3: 8 Percent Saturated Indication From Flat Bottom Hole in a No. 8 Alcoa D Block

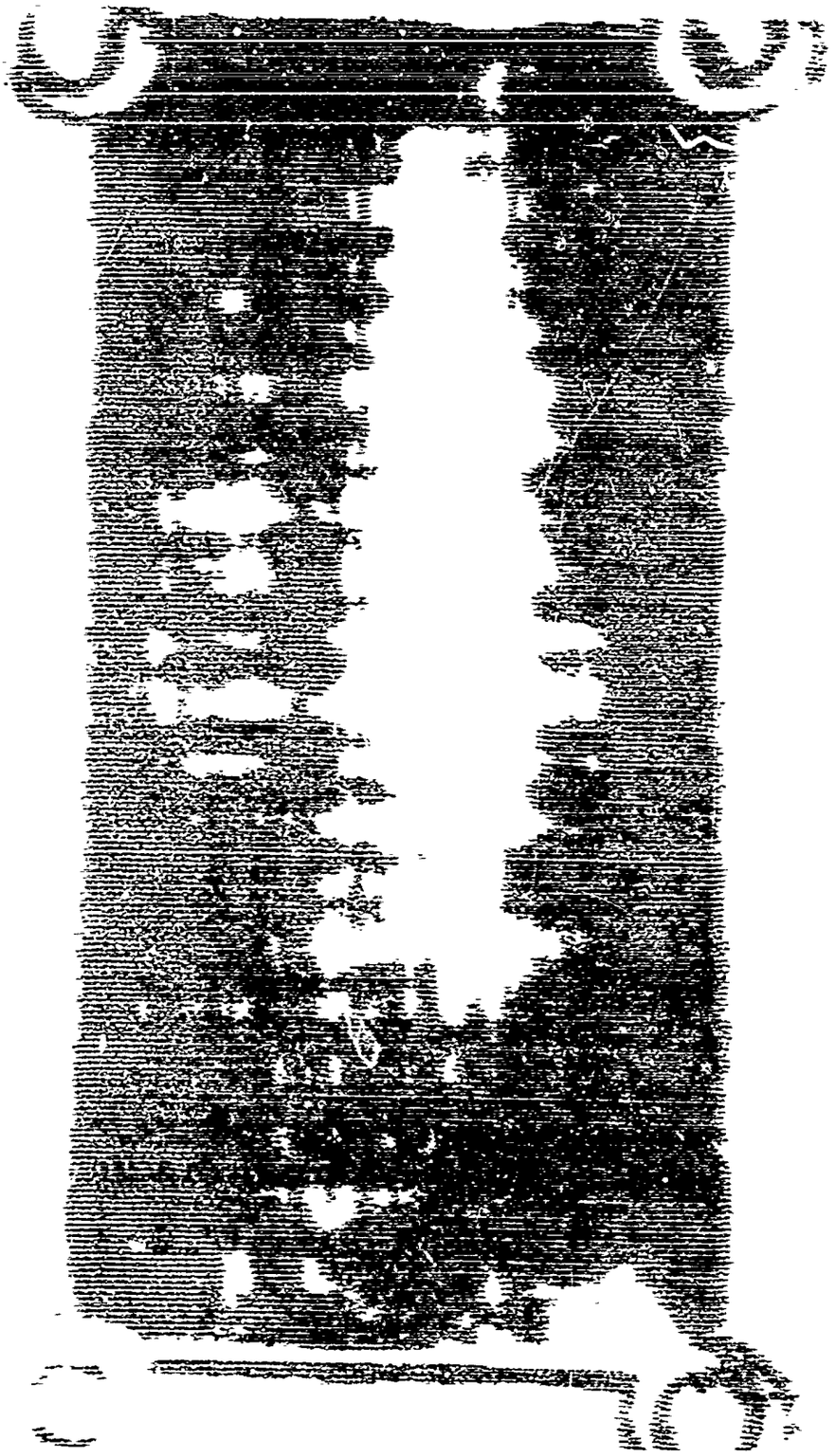


Figure 118. Boron-Aluminum - 15 BF-3: 15 Percent Saturated Indication From Flat Bottom Hole in a No. 6 Alcoa D Block

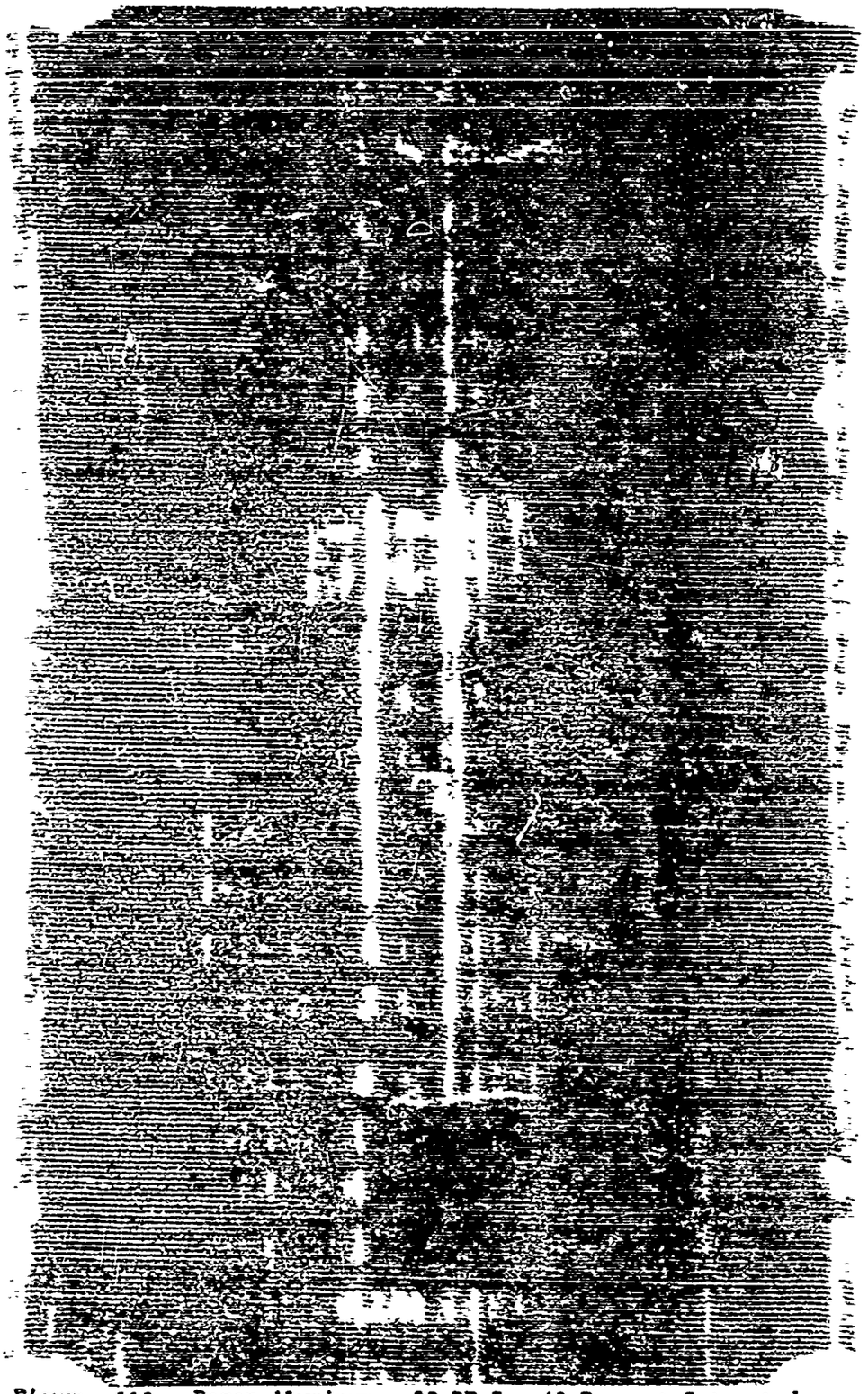


Figure 119. Boron-Aluminum - 20 BF-3: 40 Percent Saturated Indication From Flat Bottom Hole in a No. 8 Alcoa D Block

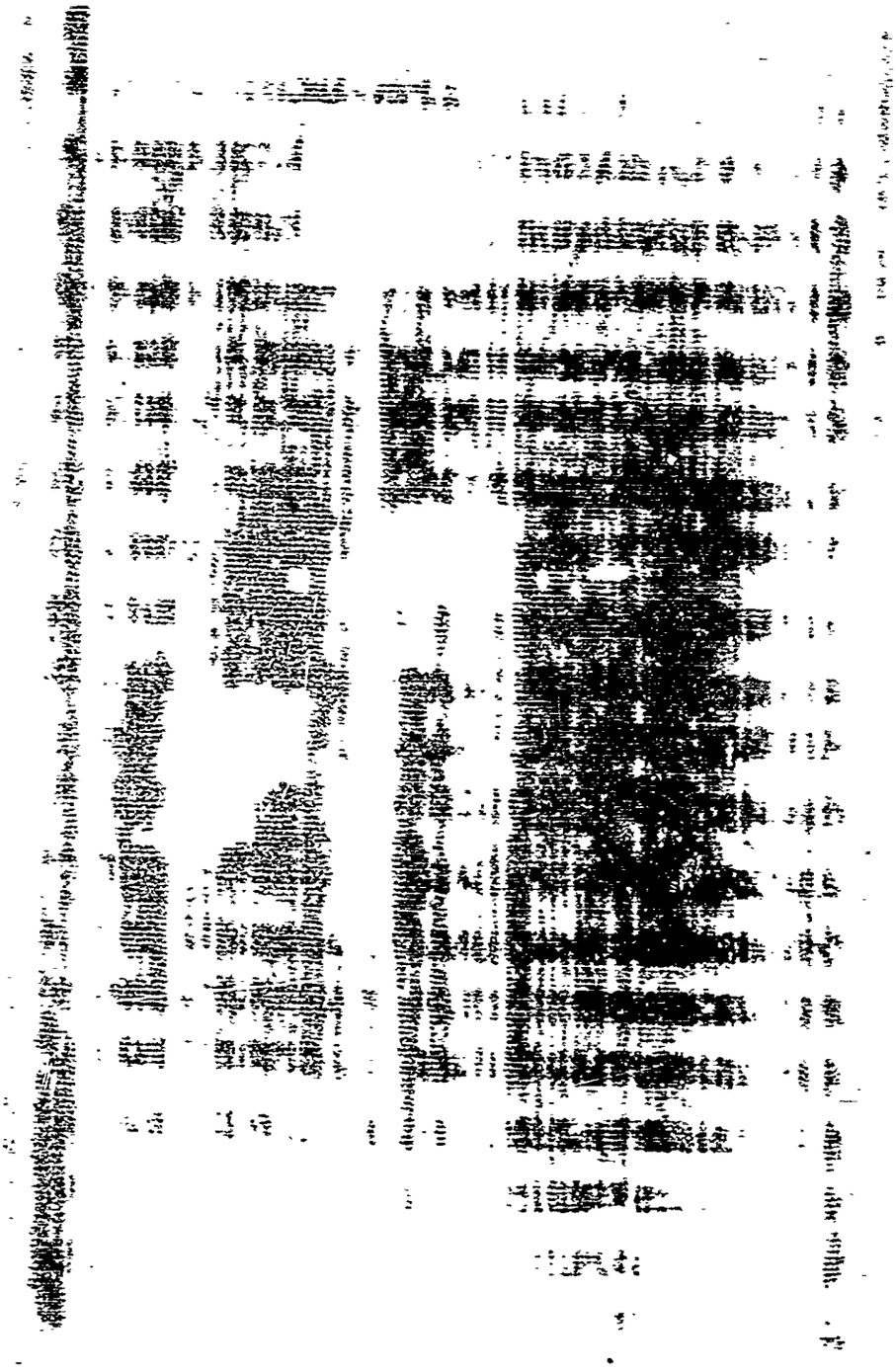


Figure 120. Boron-Aluminum - 25 BF-8-1: 5 Percent Saturated Indication From Flat Bottom Hole in a No. 8 Alcoa D Block; Sensitivity Control Set at 1 x 6

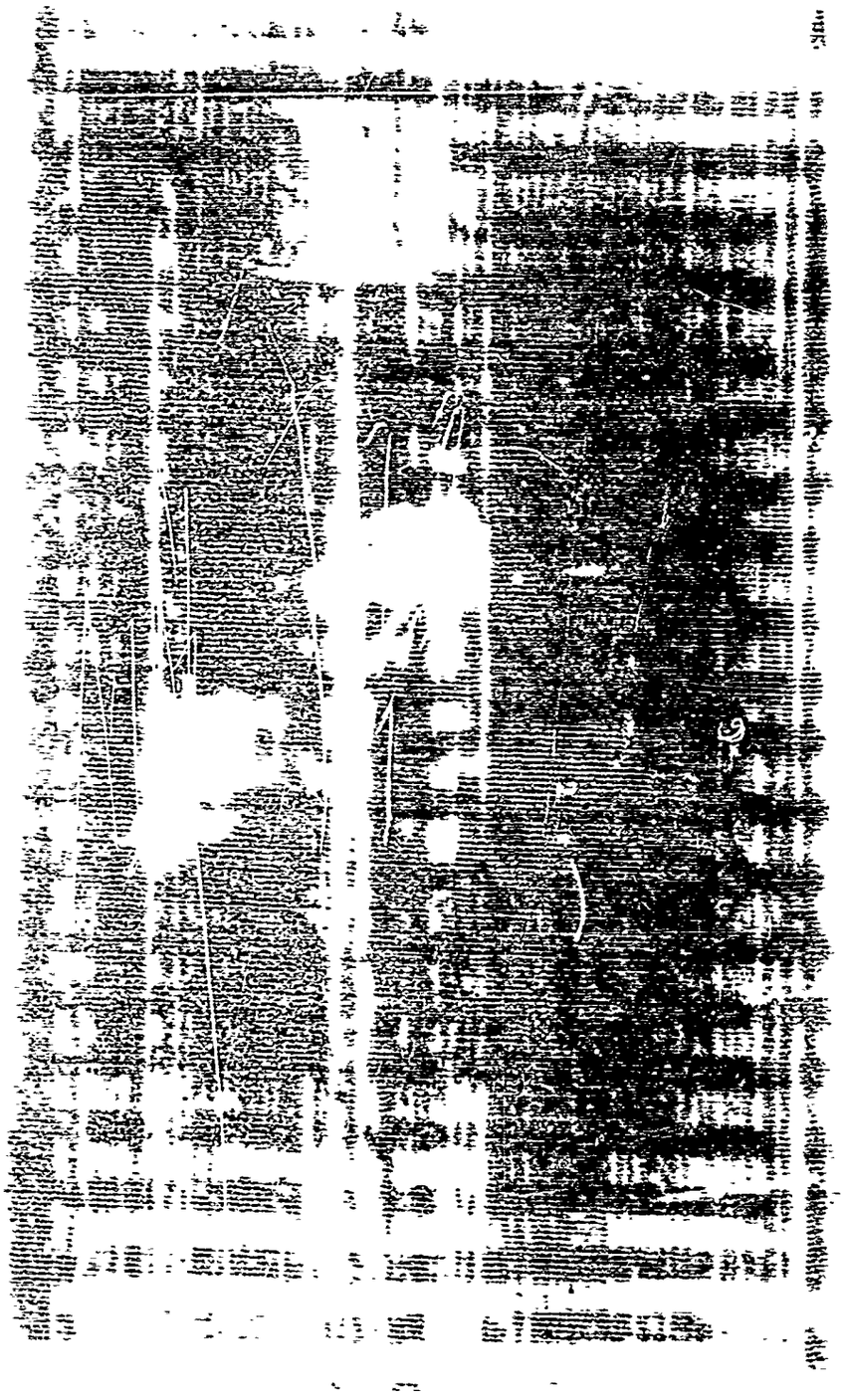


Figure 121. Boron-Aluminum - 25 BF-8-2: 5 Percent Saturated Indication From Flat Bottom Hole in a No. 8 Alcoa D Block; Sensitivity Control Set at 1 x 4

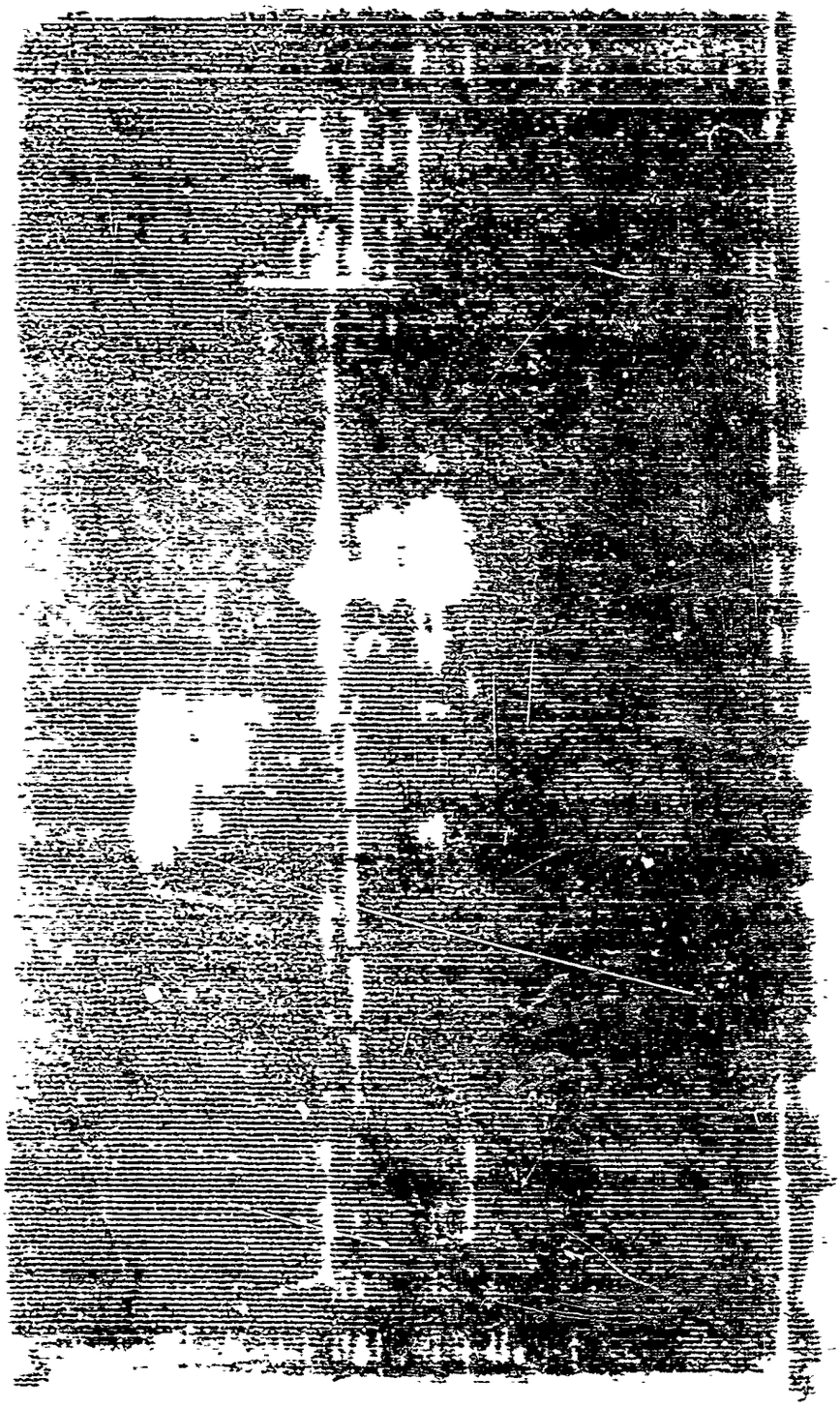


Figure 122. Boron-Aluminum - 25 BF-8-3: 5 Percent Saturated Indication From Flat Bottom Hole in a No. 8 Alcoa D Block; Sensitivity Control Set at 1 x 3

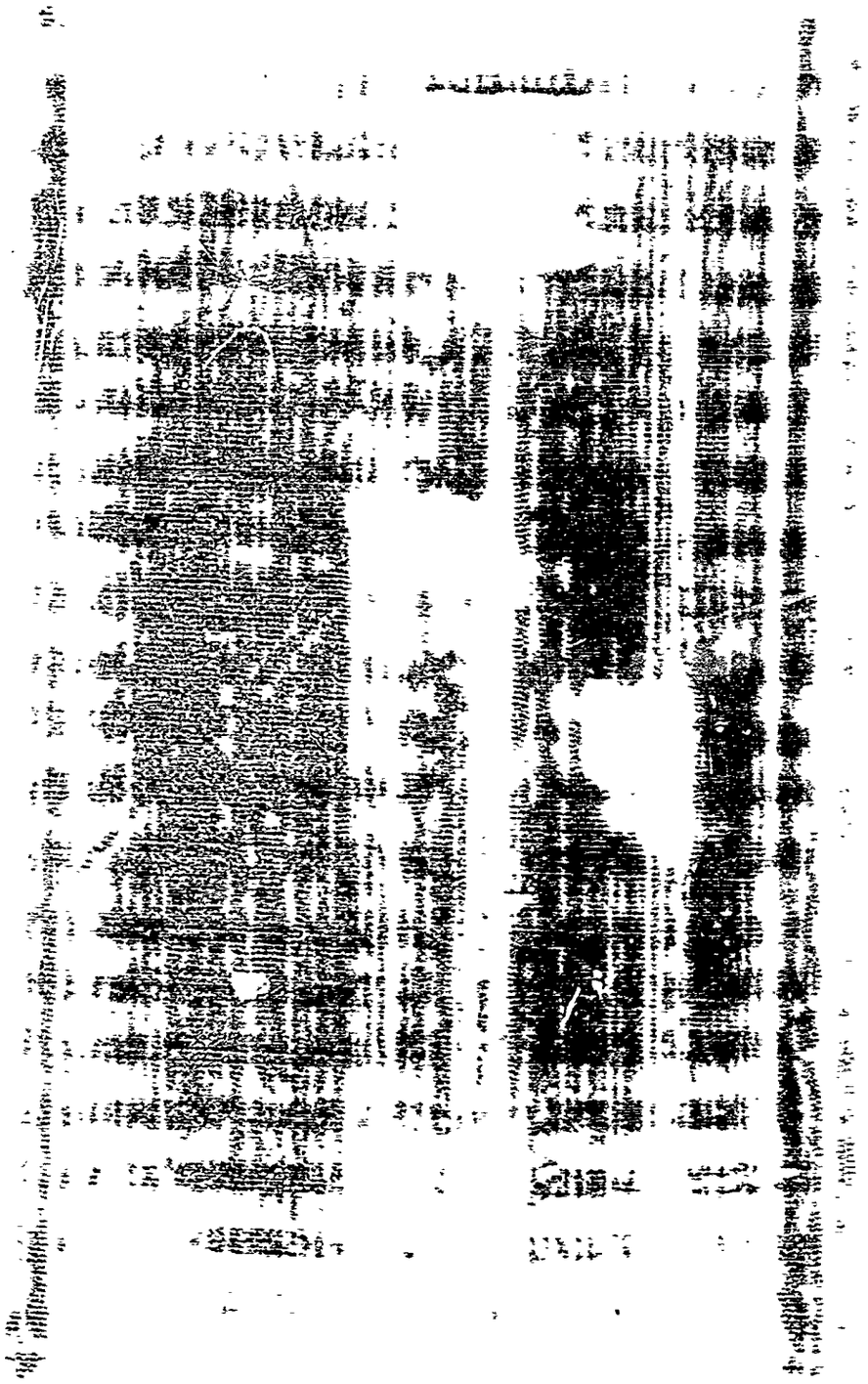


Figure 123. Boron-Aluminum - 25 BF-8-R-1: 5 Percent Saturated Indication From Flat Bottom Hole in a No. 8 Alcoa D Block; Sensitivity Control Set at 1 x 6

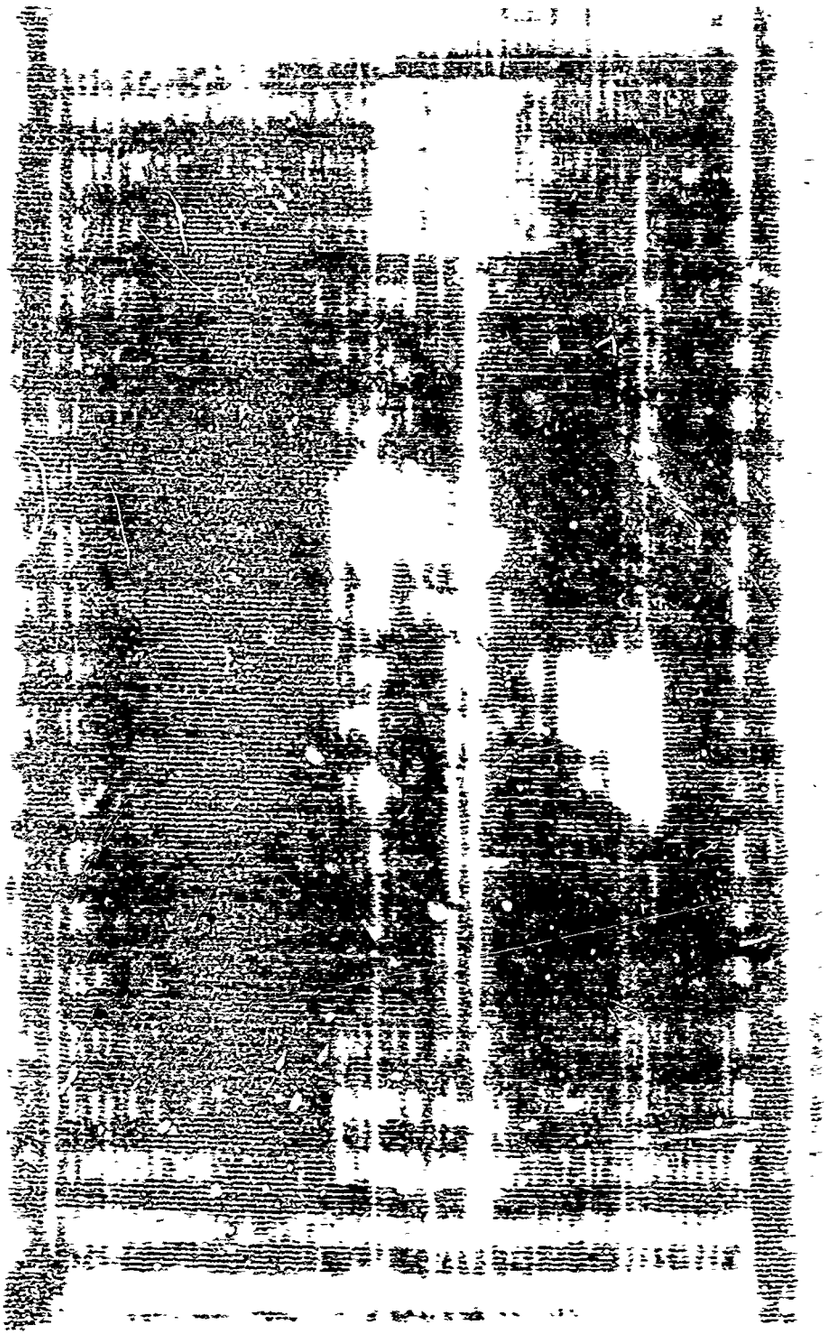


Figure 124. Boron-Aluminum - 25 BF-8-R-2: 5 Percent Saturated Indication From Flat Bottom Hole in a No. 8 Alcoa D Block; Sensitivity Control Set at 1 x 4

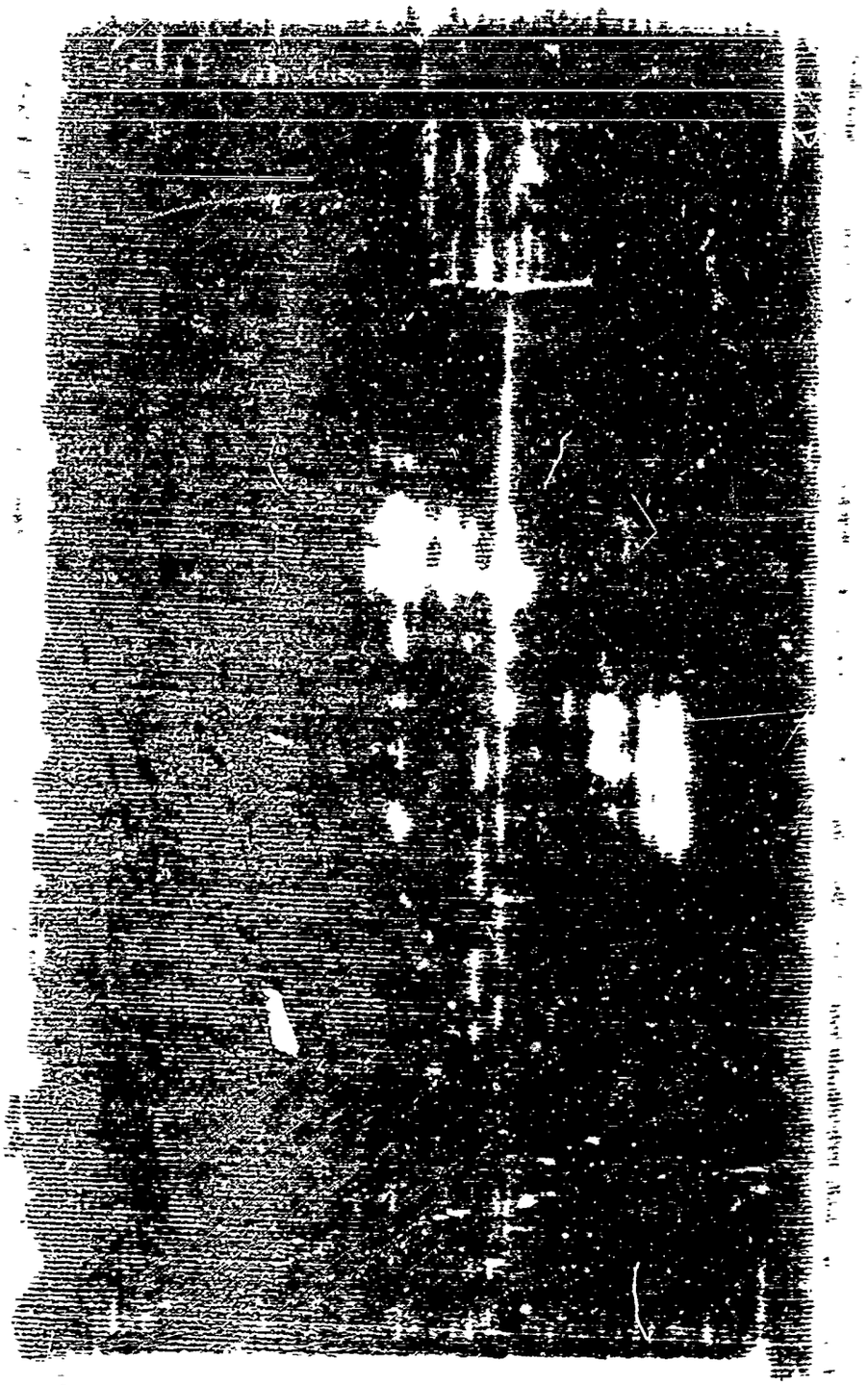


Figure 125. Boron-Aluminum - 25 B/-8-R-3: 5 Percent Saturated Indication From Flat Bottom Hole in a No. 8 Alcoa D Block; Sensitivity Control Set at 1 x 3



Figure 126. Boron-Aluminum - 15 F-3: 8 Percent Saturated Indication From Flat Bottom Hole in a No. 7 Alcoa D Block



Figure 127. Boron-Aluminum - 15 M-3: 40 Percent Saturated Indication From Flat Bottom Hole in a No. 7 Alcoa D Block

Appendix IV

LITERATURE SURVEY - NONDESTRUCTIVE TESTING OF METALLIC FIBER-MATRIX COMPOSITES

FOREWORD

The following literature survey was conducted by the Los Angeles Division of North American Aviation, Inc, under Contract AF33(615)-2865, "Development of Nondestructive Testing Techniques for Composites." Literature was surveyed during the initial phase of contract effort to establish theoretical and reported sensitivity levels of conventional nondestructive inspection equipment as applied to similar and/or allied materials. The survey was performed by the Metal Science Unit under the direction of Dr. George Martin, Program Manager, and J. Moore, Project Engineer. Survey results were reported in the Monthly Progress Report dated 10 August [illegible]5.

INTRODUCTION

This literature survey briefly summarizes the limits of defect detectability by nondestructive test methods, with special reference to metallic material-filament reinforced composites and candidate materials. Only standard methods are considered, but a quantitative assessment is made of radiographic and ultrasonic techniques to allow possible future extrapolation and optimization. In radiography, absorption coefficient data have been collected for the candidate materials and expanded into tables to allow estimates to be made of defect detectability for various radiation energies.

In the case of ultrasonics, a literature survey has been carried out on attenuation coefficients and sound velocity data abstracted from some 80 papers. Although most of these materials are not candidate materials in the present study, it is felt that this data collection can form a useful basis for a quantitative evaluation of possible shortcomings of existing systems and for selection of design parameters for future systems. In addition, this list indicates some of the factors that affect sound attenuation and velocity and thus assists in delineating the application of acoustic systems to specific defect detection.

ULTRASONIC INSPECTION

ULTRASONIC TECHNIQUES

Pulse echo techniques for thin sheet inspection are limited by the shortest echo time interval that can be resolved. This includes the recovery time of the

equipment and transducer and the velocity of sound in the test material. The resolving capability of commercial equipment is determined in industrial practice by the use of standards. These standards are normally made of the specific test material with defect simulated by drilled flat bottom holes. Standards for a number of materials are commercially available (ASTM E127-58T). The Immerscope 424A (L) is reported to have a resolving capability of a 3/64 Alcoa hole in 0.100-inch aluminum. Comparative figures for this instrument using titanium would be 3/64 Alcoa hole in 0.98-inch thickness, and 5/64 Alcoa hole in 0.775-inch thick copper.

Commercial Russian pulse echo equipment is reported by Merkulov (2) as having a defect detection capability of approximately 1/32 inch in metals. The device is described as an electronic depth gage and uses both vertical and prismatic barium titanate piezoelectric transducers. Automatic rolled sheet testers are also described; however, inspection is limited at sheet thickness of approximately 0.3 inch.

Albertson (3) conducted detection sensitivity tests on wire ranging from 10 to 100 microns. Conventional pulse echo equipment was used with specially developed transducer systems. Echo amplitudes varied approximately 1.5 times the ratio of wire diameters. The sonic beam was reported as approximately one mm diameter.

Ultrasonic pulse echo and through-transmission tests show remarkable detail sensitivity with large transducers. McMasters (4) has reported the detection of 1/64-inch diameter flat bottom holes in many materials when the effective transducer diameter is approximately one inch. Sensitivity in aluminum for a variety of commercial ultrasonic transducers and test frequencies is given in table XI (5).

Through-transmission tests conducted by Ross (6) detected disbond conditions on aluminum clad uranium slugs. The aluminum was approximately one inch thick and was bonded to 8-inch diameter uranium slugs. Disbonds 1/16-inch diameter were detected. The developed instrument drawings are available. In other tests, longitudinal waves are transmitted through thin sheets to a reflecting sheet (7); the presence of discontinuities are indicated by the lack of echo by the reflector.

Special focusing techniques can control the depth of penetration and improve defect resolution (Posakony8). This technique has successfully detected lack of bonding in brazed honeycomb sandwich material (9). Examples of transducer beam configurations are given in table XII.

McMasters (4) predicts improvement of defect resolution in thin-gage material by the use of acoustic lenses and higher frequencies. At the higher ultrasonic frequencies (10 to 50 MHz), sonic wavelengths in metals reduces to the range of thin-gage materials (25 to 5 mils). If ultrasonic systems were developed in the 100 to 500 MHz frequency range, the wavelength in metals would

Table XI

SENSITIVITY RESPONSES FOR CONVENTIONAL ULTRASONIC TRANSDUCERS - ALUMINUM

Element Dia. (In.)	Frequency (Mhz)	Sensitivity per Alcoa Flat Bottom Hole for Al-1/64 in.		
		Quartz	Lithium Sulfate	Ferroelectric
3/8	2.25	6	4	6
3/8	5.00	5	2	4
3/8	10.00	3	1	2
3/8	15.00	2	1	-
3/8	20.00	2	1	-
3/8	25.00	2	-	-
3/4	1.00	2	5	5
3/4	2.25	5	3	3
3/4	5.00	3	2	2
3/4	10.00	2	1	1
3/4	15.00	1	1	-
1	0.50	8	8	8
1	1.00	5	6	5
1	2.25	4	3	3
1	5.00	3	2	2
1	10.00	2	1	1
1.5	0.50	-	8	-
1.5	1.00	-	6	6
3	0.20	-	-	12
3	0.50	-	-	8

Ref: J. Posakony, Automation Industries, Boulder, Colorado

Table XII

BEAM CHARACTERISTICS FOR CONVENTIONAL FOCUSED LITHIUM SULFATE AND FERROELECTRIC TRANSDUCERS

Frequency (MHz)	Water Path (in.)	Metal Path (In.)	Focal Length	Beam Dia (In.)
2-1/4	3	1/2	Short	1/4
2-1/4	3	1-1/4	Medium	5/16
2-1/4	3-1/4	2-1/4	Long	3/8
2-1/4	3-1/2	6	Extra long	5/8
5	2	0.4	Short	1/8
5	2-1/4	1	Medium	3/16
5	3-1/2	2-1/4	Long	1/4
5	3-1/2	4	Extra long	3/8
10	2	0.4	Short	1/8
10	2-3/4	1	Medium	5/32
10	3-1/2	2-1/4	Long	1/4
10	3-1/2	4	Extra long	5/16
15	2	0.4	Short	1/8
15	2-3/4	3/4	Medium	5/32
15	3-1/4	1-1/2	Long	1/4
15	2-1/4	3	Extra long	5/16

Ref: Automation Industries, Boulder, Colorado

approach 2.5 to 0.5 mils. This technique would significantly improve defect detection and resolution, and could be useful in determining material properties.

It is concluded that conventional through-transmission testing appears applicable for testing all the subject matrix composites. Detectable defects include gross matrix disbonds, some groupings of fiber-matrix disbonds and the greater degrees of fiber misalignment. Broken fibers (still aligned) cannot be detected. Test sensitivity will be reduced due to the presence of the fibers, especially in the multilayer sample composites.

Pulse ringing or decrement testing has been indicated by several companies; however, published information is not available. Disbonds in thin laminants (0.60 inch) and honeycomb composites have been detected as small as 1/16-inch diameter. McClung (10) indicated that 3/32-inch diameter disbonds could readily be detected 0.65-inch deep (interface) in stainless steel. Disbonds areas, 1/32 x 1.16-inch rectangles, were detected through 0.020 inch of type 304 stainless steel. These tests were not conducted with a specific type of commercial equipment. However, the proper combination of standard electrical electronic components, with special transducers can be employed.

There is a considerable amount of literature relating to the use of impedance measuring equipment for detecting disbonds in thin laminar structures. Such instruments include the Vidigage (11), Sonizon (12), Fokker Bond Tester (13), Stub-Meter (14), and Coindascope (15). Experience and verbal reports indicate that the minimum diameter disbond detectable is between one-third to three-fourths the transducer diameter (or beam diameter) for thin laminants. Aveyard (16) used commercial resonance type equipment to determine unbond conditions in laminants. A specially developed collimated beam transducer was developed which proved superior to focused transducer in terms of disbond sensitivity. Aveyard concluded that commercial contact impedance methods are not satisfactory for disbond detection that are of the order of 0.039-inch diameter. Also, Bobbin and Harris (17) indicate that attenuative materials require that a low resonant frequency (less than 3 Mz) to be used if thickness or disbond measurements are to be made. Therefore, thin, highly attenuating materials cannot be satisfactorily tested if the lowest resonance frequency (fundamental) is above approximately 3 Mz.

It is concluded that thickness measuring impedance methods for void detection in the matrix composites will be monsiderably hindered by the combination of attenuation due to sonic scattering, etc, by the fibers, and high fundamental resonant frequency values. This will be particularly true for the multilayered composites. Impedance contact tests using lower frequencies, such as with the Fokker Bond Tester, and Coindascope, should be applicable for detecting sizable matrix voids and fiber misalignments. Shear wave testing is apparently not applicable to the matrix composites because they are too thin to permit pure shear wave generation with commercial equipment. A complex Lamb wave system will actually exist.

Worlton (18) and diNovi (19) describe the use of Lamb waves in thin sheets and tubing for the detection of discontinuities and changes of thickness. Successful tests at 10 Mz showed 0.0001-inch-diameter flaws in 0.005-inch-thick wall Inconel tubing. In 10-mil aluminum plate, a one-megacycle frequency shift is equivalent to one mil change in thickness.

ULTRASONIC ATTENUATION AND VELOCITY IN METALS

Table XIII is the result of a survey of the literature on various properties of metals whose relation with ultrasonic attenuation and velocity measurements has been determined. Attenuation coefficient and/or velocity data have been correlated to the nondestructive determination of the following material parameters:

1. Grain sizes
2. Properties of castings - gas porosity and microshrinkage - mechanical properties
3. Directional properties in single crystals - stress, strain, magnetic field
4. Integrity of structural components
5. General state of stress and strains
6. Tensile strength
7. Impact strength
8. Microstructure and condition - Martensite, bainite, austenite, ferrite, pearlite; annealed, cold-worked, cast, swaged, etc, also various heat-treat, quench, temper states
9. Alloy contest
10. Hardness
11. Magnetic field dependence of attenuation as a function of stress and strain
12. Elastic modulus and temperature dependence of
13. Shear modulus and temperature dependence of
14. Normal or superconducting state

Throughout the tabulation it is evident that a pulse technique was used exclusively for all measurements, with the pulse-echo method predominating. The frequencies used generally ranged from 1 to 100 mc/sec with pulse durations usually 1 to 10 sec. More attenuation measurements were made with longitudinal waves than shear waves. Attenuation values for transverse and longitudinal waves are fairly similar whereas longitudinal wave velocities are usually about double shear wave velocities for a given material.

It will be noted that comparison of attenuation measurements on a given material as determined by different investigators is virtually impossible because of widely varying test circumstances and necessary oversimplification of tabulated results. For example, one of the closest comparisons possible is the room temperature attenuation coefficient for longitudinal waves between 4150 steel (26) and a Russian 0.4 percent C steel (27) at about 15 mc/sec. Assuming a longitudinal velocity of 5.906×10^5 cm/sec for steel (an average of several very close results by different investigators), $\alpha_{4150} = 3.38$ dB/cm, and α 0.4 percent C = 3.47 dB/cm. This is a fairly close correlation, but is probably somewhat fortuitous since material compositions, grain size, etc, are different.

Velocity data for a given material are usually in good agreement among various authors since velocity is not particularly sensitive to material preparation or frequency under normal conditions.

Generally, ultrasonic attenuation increases with frequency, temperature, and stress, and decreases with hardness and impact strength. Velocity is fairly independent of frequency, decreases with temperature, and increases with tensile strength. However, these broad generalizations are sometimes reversible depending upon conditions.

Symbols and Abbreviations

The following abbreviations and symbols are used in Table XIII:

α OR δ	= Attenuation coefficient, $^{dB}/_{sec}$, $^{Nepers}/_{cm}$, $^{dB}/_{cm}$, $^{dB}/_{ft}$, $^{dB}/_{inch}$, $^{dB}/_{path}$, (1 Neper = 8.68 dB)
A	= Annealed
AC-HS	= Arc cast - hot swaged
AR	= As received
ARCR	= As received cold rolled
ASTM	= Standard grain size designation
Aus	= Austenite, austenitized
B	= Bainite
BHN	= Brinell hardness number
CRF	= Charpy breaking energy (ft-lb)
Comp.	= Compression waves

CR = Cold rolled
Δ = Change of
DIAQ = Dry ice - acetone quench
E = Elastic modulus
Eq = Equiaxed
ϵ = Strain
F = Ferrite
f = Frequency
FC = Furnace cooled
G = Shear Modulus
GS = Grain Size (mm)
H = Magnetic field, Oersteds where not specified
HR = Hot rolled
HTT = Heat treat temperature
IIS = Izod impact strength (ft-lb)
LNQ = Liquid nitrogen quench
LNQ-T = Liquid nitrogen quenched, and tempered
Long = Longitudinal waves
M = Martensite
Non-A = Nonannealed
Non-T = Nontempered
Orient = Orientation
P = Pearlite
PD = Plastically deformed
P-E = Pulse-echo
P-F = Pearlite-ferrite
Q = Quenched
RC = Rockwell "C" hardness
R.T. = Room temperature
Rx = Recrystallized
S = Stabilized
σ = Stress (psi unless otherwise specified)
Spec = Specimen
SR = Sperry reflectoscope
SUAC = Sperry ultrasonic attenuation comparator
T = Temper, tempered
TM = Tempered martensite
Trans = Transverse waves
TS = Tensile strength
TT = Tempering temperature
V = Velocity of sound
WQ = Water quenched

Table XIII

ULTRASONIC ATTENUATION AND VELOCITY IN METALS

Material	Test Conditions	Frequency	Test Temp	Data	Ref	Notes
Steel - 1020	Long, SUAC	3 mc/sec	R.T.	α = 0.055 - 0.133 dB/μsec for ϵ = 0 - 0.09% and H = 1100-0 for A and 1% PD specimens	21	
	Long, SUAC	1-7	R.T.	α = 0 -0.065 dB/μsec for H = 0 - 400	28	d.
	Long, SUAC,P-E	3	R.T.	α = 0 - 0.030 dB/μsec for ϵ = 0 - 40,000 for A, 1% PD, 10% PD specimens	21	a.
	Long, SUAC,P-E	3	R.T.	α = -0.040 -0.024 dB/μsec, H = 0 - 400 for A, AR, 1-25% PD specimens	21	a.
Steel - 4150	Long, P-E, 1-4 μsec	5-50	R.T.	α = 0-16 dB/inch for RC 61-14	22	
	Comp, P-E	10-75	R.T.	α = 0.001-2.40 dB/μsec for Ar,Q,T specimens and GS = 0.020 - 0.053	23	
	Trans, P-E	10-75	R.T.	α = 0.02-3.0 dB/μsec for T specimens, GS = 0.020	23	
	Long, P-E	100-1.5	R.T.	α = 5.0-0.015 dB/μsec for P-F, B, M, TM structures	24	
	Trans, P-E	80-3	R.T.	α = 2.0-0.017 dB/μsec for P-F, P, B, M, TM structures	24	
	Long, P-E	10	R.T.	V = 0.59446 -0.58796 cm/μsec, P-F, B, TM, M structures	24	
	Trans, P-E	10	R.T.	V = 0.32522 -0.31953 cm/μsec, P-F, B, TM, M structures	24	
	Long, P-E, 1 μsec	3-80	R.T.	α = 0.01 - 6.0 dB/μsec for T, Aus, AR specimens	25	
	Long, P-E, 1 μsec	30	R.T.	α = 1 dB/μsec for RC = 25-48	25	
	Long & Trans, P-E	5-100	R.T.	α = 0.0015-4.0 dB/μsec for T, Aus, HR specimens	26	

Table XIII, continued

ULTRASONIC ATTENUATION AND VELOCITY IN METALS (CONT)

Material	Test Conditions	Frequency	Test Temp	Data	Ref	Notes
Steel - 4150	Long, P-E	15-75	R.T.	α = 0-1.5 dB/μsec for RC = 15-50, WQ & FC specimens	26	
	Trans, P-E	18,35	R.T.	α = 0.20-1.2 dB/μsec for RC = 15-50, WQ & FC specimens	26	
	Long, P-E	15-70	R.T.	α = 0.002-1.7 dB/μsec for CBE = 125-5, WQ & FC specimens	26	
	Trans, P-E	18-63	R.T.	α = 0.02-2.0 dB/μsec for CBE = 120-5, WQ and FC specimens	26	
	Long, P-E	10-100	R.T.	α = 0.005-2.5 dB/μsec for ASTM 8-9 (0.02 mm)	26	
	Trans, P-E	5-100	R.T.	α = 0.008-2.0 dB/μsec for ASTM 8-9 (0.02 mm)	26	
	Long, P-E	5-15	R.T.	α = 0.2 - 2.0 dB/μsec	26	
	Long, P-E	18,54	R.T.	V = 0.2292-0.2354 $\frac{\text{inches}}{\mu\text{sec}}$ for TT 450-700°C, WQ, FC specimens	26	b.
	Trans, P-E	7-54	R.T.	V = 0.1256-0.1276 $\frac{\text{inches}}{\mu\text{sec}}$ for TT 450-700°C, WQ, FC specimens	26	b.
Steel - 3140	Long, P-E, 1μsec	3-30	R.T.	= 0.01-2.0 dB/μsec for T, Aus, AR specimens	25	
	Long, P-E, 1μsec	30	R.T.	α = 1-2.5 dB/μsec for RC = 40-10	25	
	Long, P-E, 1μsec	30	R.T.	α = 1.5-2.1 dB/μsec for CBE 5-30	25	
Steel - 4340	Long, P-E, SUAC	10	R.T.	V = 2.28 x 10^5 in/sec	54	1.
	Shear, P-E	2.25	R.T.-1500°F	G = 12 - 7 x 10^6 psi	56	

Table XIII, continued

ULTRASONIC ATTENUATION AND VELOCITY IN METALS (CONT)

Material	Test Conditions	Frequency	Test Temp	Data	Ref	Notes
Steel - 4340	Long, P-E, 1 μsec	2.25	R.T.-1600°F	E = 30 - 19 x 10^6 psi	57	m.
	Shear, P-E, 1 μsec	2.25	R.T.-1600°F	G = 12 - 8 x 10^6 psi	57	m.
	Long, P-E	5	R.T.-1500°F	E = 31 - 19 x 10^6 psi	56	
Steel - 4130	Long, P-E, SUAC	10	R.T.	V = 2.31 x 10^5 in/sec	54	1.
	Long, P-E,SUAC	5-35	R.T.	= 0.1 - 4.6 dB/μsec	54	1.
Steel - 4140	Long, P-E	5	R.T.-1500°F	E = 31 - 19 x 10^6 psi	56	
	Shear, P-E	2.25	R.T.-1500°F	G - 12 - 7 x 10^6 psi	56	
Steel - 9130 T*-16-25-6 347 A286	Contact tests with SR, Immersion tests with 424 Immerscope Long	2.25-10	R.T.	$\alpha x/\alpha 4130(\%)$ = 100-0 for alloys listed	30	
Steel - 403	Long, P-E,SUAC	10	R.T.	V = 2.31 x 10^5 in/sec	54	1.
Steel - V-1000	Long, P-E,SUAC	10	R.T.	V = 2.33 x 10^5 in/sec	54	1.
	Long, P-E, SUAC	5-35	R.T.	= 0.2 - 3.5 dB/μsec	54	1.
Steel - 17-4	Long, P-E,SUAC	10	R.T.	V = 2.32 x 10^5 in/μsec	54	1.
	Long, P-E,SUAC	5-35	R.T.	α = 0.2 - 3.5 dB/μsec	54	1.
Steel - 19-9 DL	Long, P-E	5	R.T.-1600°F	E = 29 - 20 x 10^6 psi	56	
Steel 35KhN3 (Russian Cr-Ni)	Long, pulse, 2-10 μsec	2-60	R.T.	α/f = 0.001 - 0.012 x 10^6 Nepers/cm, cps T & Non-T structure	27	

*Timkin 16-25-6

Table XIII, continued

ULTRASONIC ATTENUATION AND VELOCITY IN METALS (CONT)

Material	Test Conditions	Frequency	Test Temp	Data	Ref	Notes
Steel - 0.15% Carbon	Long, pulse, 2-10 μsec	2-19	R.T.	δ = 0 -0.5 Nepers/cm for GS = 0.025 - 0.5	27	
Steel - 0.17% Carbon	Long, P-E	1.25-5	R.T.	α = 0.3-2.2 dB/cm for HTT = 850-930°C	29	
	Trans, P-E	1.25-5	R.T.	α = 0.5-2.0 dB/cm for HTT = 850-930°C	29	
Steel 0.2% Carb.	Long	3	R.T.	α = 0.10-0.13 dB/usec for = 0 -16 x 10^{-4}, 10%PD	32	f,
Steel 0.3% Carb.	Long, P-E	1.25-10	R.T.	α = 0.2-4.5 dB/cm for HTT = 800-1240°C	29	
	Long, P-E	5	R.T.	α = 0.3-2.3 dB/cm for IIS = 40-10	29	
Steel 0.4% Carb.	Long, pulse, 2-10 μsec	2-16	R.T.	δ = 0-0.4 Nepers/cm for GS = 0.02-0.3	27	c.
Steel 1.2% Carbon	Long, pulse, 2-10 μsec	2-16	R.T.	δ = 0-0.6 Nepers/cm for GS = 0.03 -0.16	27	c.
Steel Alloy 50 (Russian)	Long, pulse	2.5	R.T.-1000°C	V = 5885-5200 m/sec, E = 21320-11950 Kg/mm^2	55	
	Trans, pulse	2.5	R.T.-1000°C	V = 3230-2370 m/sec, G = 8290-4425 Kg/mm^2	55	
Steel Alloy D-16 (Russian)	Long, pulse	2.5	R.T.-500°C	V = 6260-5185 m/sec, E = 7130-3900 Kg/mm^2	55	
	Trans, pulse	2.5	R.T.-500°C	V = 3115-2320 m/sec, G=2680-1420 Kg/mm^2	55	
Iron - Unalloyed	Not described	30	R.T.	V = 5.850 x 10^5 cm/sec	37	
	Long, pulse, 2-10 μsec	2-15	R.T.	δ = 0-3 Nepers/cm for GS = 0.04-0.25	50	
	Shear, pulse, 2-10 μsec	2-10	R.T.	δ = 0-1.4 Nepers/cm for GS = 0.04-0.05	50	

Table XIII, continued

ULTRASONIC ATTENUATION AND VELOCITY IN METALS (CONT)

Material	Test Conditions	Frequency	Test Temp	Data	Ref	Notes
Iron - Cast	Long, Type 1017 "Elastomat"	--	R.T.	TS = 0-57 vs ExBHN = 0-5.68 x 10^9 psi-BHN	33	
Iron - Cast (Flake graphite)	Not described, P-E	--	R.T.	V = 15-19 x 10^4 in/sec vs TS = 8-18 tons/in^2	29	e.
Iron - Cast (Flake & Nodular)	Not described, P-E	--	R.T.	V = 3800-5200 m/sec vs Solidif. temps 1300-800°C	29	
Iron 30% Nickel	Long, P-E	7	R.T.	V = 0.206-0.283 in./μsec, 9-100% Aus; LNQ, DIAQ, T, Rx struct.	20	
	Trans, P-E	7	R.T.	V = 0.099-0.104 in./μsec, 9-60% Aus; LNQ, T, DIAQ struct.	20	
	Long, P-E	4-23	R.T.	α = 0.1-4.0 dB/ sec, LNQ-T, Eq, DIAQ, ARCR struct.	20	
Aluminum - Single Crystal	Long, P-E	10-72	R.T.-400°C	α = 0.02-1.2 dB/cm	35	
	Long, pulse, 1 μsec	51	1.05-1.20°K	α = 4.5-6.6 dB/cm, superconducting state	38	
	Shear, pulse, 1 μsec	34.4	1.05-1.25°K	α = 6.3-10.7 dB/cm, superconducting state	38	
	Shear, pulse, 1 μsec	11-55	4.2°K	α = 0-19 dB/cm for H = 0-9000 gauss, normal state	38	
	Shear, P-E, 1 μsec	50	4.2°K	α = 0-5 dB/path for 1/H = 0-1.1 $kilogauss^{-1}$	40	
	Long, P-E	13	R.T.	$\Delta\alpha$ = 0-0.57 dB/μsec vs res shear σ = 0.300 gm/mm^2, 3 orientations	41	

Table XIII, continued

ULTRASONIC ATTENUATION AND VELOCITY IN METALS (CONT)

Material	Test Conditions	Frequency	Test Temp	Data	Ref.	Notes
Aluminum - Single Crystal	Shear, P-E	10	R.T.	$\Delta\alpha$ = 0-0.4 dB/μsec vs. res. shear = 0-300 gm/mm^2, 2 orientations	41	1.
	Long, P-E	13	R.T.	$\Delta V/V$ = 0-0.10 vs. shear = ϵ-1 x 10^{-2}, 3 orientations	41	
Aluminum - 99.95%	Long, P-E	0.540	60-1°K	α = 0.002-0.005 dB/cm	46	
	Long, P-E	1.07	4.2°K	α/f^2 = 7.8 x 10^{-15} dB-sec^2/cm	46	
Aluminum 99%	Pulse, .5-2 μsec	30	R.T.	Wave intensity = 0-minus 40 dB for Non-A, rolled, and A(420-600°C) plate vs distance, 0-10 inches, 3 orientations	37	
	Long, pulse	30	R.T.	V = 6.260 x 10^5 cm/sec	37	
	Long, P-E	7-64.8	R.T.-400°C	α = 0.027-0.7 dB/cm	35	
Aluminum	Long	1-36	R.T.	α = 0-48 dB/ft for GS = 0.23-0.13	49	
	Long	various	R.T.	V = 6.32 x 10^5 cm/sec	49	
	Shear	various	R.T.	V = 3.13 x 10^5 cm/sec	49	
	Not described	--	R.T.	$\Delta\alpha$ = 0-0.026 dB/μsec for tensile σ = 0-14 gm/mm^2	42	
	Shear (parallel and normal to stress), pulse	5	R.T.	ΔV = 0-0.26% vs. σ = 0-3.5 x 10^5	43	j.
	Long, pulse	5	R.T.	ΔV = 0-minus 0.12% vs = 0-3.5 x 10^5	53	
	Shear (parallel and normal to stress), pulse	5	R.T.	ΔV = 0-.27% vs long. = 0-2%	43	j.
	Long, pulse	5	R.T.	ΔV = 0-minus 0.1% vs long. ϵ = 0-2%	43	
Aluminum - Cast	P-E	0.5-5	R.T.	α arbitrary. Increased α in direction away from chill edge	36	g.

Table XIII, continued

ULTRASONIC ATTENUATION AND VELOCITY IN METALS (CONT)

Material	Test Conditions	Frequency	Test Temp	Data	Ref	Notes
Aluminum - 3 Cu-1.25 Mg	Long, P-E	4-25	R.T.-400°C	α = 0.025-2.3 dB/cm	37	
Aluminum 17ST	Long, pulse	5	R.T.	V = 6.32 x 10^5 cm/sec	39	
	Shear, pulse	5	R.T.	V = 3.13 x 10^5 cm/sec	39	
	Long, pulse	2.8-15	R.T.	α = 0.7-12 dB/ft for GS = 0.23-0.13	39	
	Shear, pulse	3.3-7	R.T.	α = 0.7-7 dB/ft for GS = 0.23-0.13	39	
Aluminum 24ST - duralumin-inum	pulse, .5-2 μ sec	30	R.T.	wave intensity = 0-minus 40 dB for Non-A, rolled, and A(350-560°C) plate vs. distance, 0-10 inches, 3 orientations	37	
Aluminum 7075-T6	Long, P-E,SUAC	5-64	R.T.	α = 0.2-3.9 dB/μ sec	54	1.
	Long, P-E,SUAC	10	R.T.	V = 2.45 x 10^5 inches/sec	54	1.
Aluminum 7079	Long, P-E,SUAC	10	R.T.	V = 2.38 x 10^5 inches/sec	54	1.
Aluminum 2014	Long, P-E,SUAC	10	R.T.	V = 2.42 x 10^5 in/sec	54	1.
Aluminum 2014-F	Long, pulse, 4 μ sec	SR 5	R.T.	ΔV = 0-minus 0.12% vs lateral = 0-.8%	34	
	Shear, pulse,	SR 5	R.T.	ΔV = 0-0.27% vs lateral = 0-.8%	34	
Aluminum 2024	Long, P-E, SUAC	10	R.T.	V = 2.42 x 10^5 in./sec	54	1.
Titanium 100	Long, P-E,SUAC	5-32	R.T.	α = 0.2-5.5 dB/ sec	54	1.
	Long, P-E,SUAC	10	R.T.	V = 2.36 x 10^5 in./sec	54	1.
Titanium 155	Long, P-E	5	R.T.-1200°F	E = 17-12 x 10^6 psi	56	
	Shear, P-E	2.25	R.T.-1200°F	G = 6.5-5 x 10^6 psi	56	
Titanium 6A1-4V	Long, P-E,SUAC	10	R.T.	V = 2.36 x 10^5 in./sec	54	1.

Table XIII, continued

ULTRASONIC ATTENUATION AND VELOCITY IN METALS (CONT)

Material	Test Conditions	Frequency	Test Temp	Data	Ref	Notes
Titanium 50 Ni	Long, pulse, .7 μsec	5	-20-130°C	V = 5100-5375 m/sec as function of: pressure (14.7, 40,000 psi), cooling or heating, alloy content (49.9-50.8% Ni), structure (AC-HS, S, A = 300-400°C)	52	
Copper Unalloyed	Not described	30	R.T.	$V = 4.7 \times 10^5$ cm/sec	37	
	Long and Shear	8.6	--	α(H)/ (0) = 1-0 for H = 0-6 Kilogauss, 2 field orientations	47	
	Shear	26	--	α = .6-minus 3.5 dB/cm for H = 0-12 Kilogauss, 2 field orientations	47	
	Long, pulse, 2-10 μsec	1-15	R.T.	α = 0-1.8 Nepers/cm for GS = 0.06-0.16	50	
	Shear, pulse, 2-10 μsec	2-8	R.T.	α = 0-2 Nepers/cm for GS = 0.06	50	
	Long, pulse, 2-10 μsec	1	R.T.	$V = 4.66 \times 10^5$ cm/sec, GS = 0.06 and 0.16	50	
	Shear, pulse, 2-10 μsec	1	R.T.	$V = 2.32 \times 10^5$ cm/sec, GS = 0.06	50	
Copper 35Zn (Brass)	Long, pulse	1-10	R.T.	α arbitrary, GS = 0.025-0.150	51	
Magnesium-Unalloyed	Long,	4-36	R.T.	α = 0-56 dB/ft	49	
	Shear	4-21	R.T.	α = 0-13 dB/ft	49	
	Long	various	R.T.	$V = 5.77 \times 10^5$ cm/sec	49	
	Shear	various	R.T.	$V = 3.05 \times 10^5$ cm/sec	49	
	Shear, pulse, 2-10 μsec	1	R.T.	$V = 3.06 \times 10^5$ cm/sec, GS = .028	50	
	Long, pulse, 2-10 μsec	1	R.T.	$V = 5.78 \times 10^5$ cm/sec, GS = .028	50	

Table XIII, continued

ULTRASONIC ATTENUATION AND VELOCITY IN METALS (CONT)

Material	Test Conditions	Frequency	Test Temp	Data	Ref	Notes
	Long, pulse, 2-10 μsec	2-110	R.T.	α = 0-0.8 Nepers/cm for GS = .028	50	
	Shear, pulse, 2-10 μsec	10-40	R.T.	α = 0-0.1 Nepers/cm for GS = .028	50	
	Not described	10-80	R.T.	α = 0.8-10 dB/inch for GS = 2-.21	37	
Magnesium	Long, P-E, SUAC	5-64	R.T.	α = 0.3-5 dB/μsec	54	1.
ZK-60	Long, P-E,SUAC	10	R.T.	V = 2.28 x 10^5 in./sec	54	1.
J-1	Long, P-E,SUAC	10	R.T.	V = 2.09 x 10^5 in./sec	54	1.
Zirconium-	Pulse, SR	1-5	R.T.	α = 0.82 dB/μsec	53	k.
Unalloyed	Long, SR, pulse	1-5	R.T.	V = 179,000 in./sec	53	k.
	Shear, SR,pulse	1-5	R.T.	V = 102,000 in./sec	53	k.
Zirconium-	pulse, 1-5 μsec,	5	R.T.	α = 0.8 dB/μsec	53	k.
Zircaloy 2	SR					
	pulse, 1-5 μsec, SR	25	R.T.	α = 2 dB/μsec, f^2 above 25 mc/sec	53	k.
Hafnium -	P-E, 1-5 μsec,SR	1-5	R.T.	α = 1.23 dB/μsec	53	k.
Unalloyed	Long, P-E, SR	1-5	R.T.	V = 152,000 in./sec	53	k.
	Shear, P-E, SR	1-5	R.T.	V = 82,000 in./sec	53	k.
	Long, P-E 1 μsec	2.25	R.T.-1600°F	E = 21-15 x 10^6 psi	57	m.
	Shear,P-E, 1 sec	2.25	R.T.-1600°F	G = 8-6 x 10^6 psi	57	m.
Inconel X	Long, P-E,SUAC	5-27	R.T.	α = 0.2-5.5 dB/μsec	54	l.
	Long, P-E, SUAC	10	R.T.	V = 2.35 x 10^5 in./sec	54	l.
Hastalloy	Long, P-E	5	R.T.-2000°F	E = 30-25 x 10^6 psi	56	
C	Shear, P-E	2.25	R.T.-2000°F	G = 11.5-8.5 x 10^6 psi	56	
	Shear, P-E, 1 μsec	2.25	R.T.-1600°F	G = 12 -9 x 10^6 psi	57	m.
	Long, P-E, 1 μsec	2.25	R.T.-1600°F	E = 30-22 x 10^6 psi	57	m.

Table XIII, continued

ULTRASONIC ATTENUATION AND VELOCITY IN METALS (CONT)

Material	Test Conditions	Frequency	Test Temp	Data	Ref	Notes
Molybdenum	Long, P-E, SUAC	9-45	R.T.	α = .3-4 dB/μsec	54	1.
C.P.	Long, P-E, SUAC	10	R.T.	V = 2.52 x 10^5 in./sec	54	1.
Lead - Single	Long, P-E, 1μsec	78	1.2°K	α = .4-4.4 Nepers/cm for H = 0-20 Kilogauss	44	
Crystal	Long, P-E, 1μsec	78	1.2°K	V = 2.20-2.56 Km/sec, 12 specimens	44	
Lead-Unalloyed	Long, pulse, 1-5 sec	26.6	2°K	α = 0.28 and 0.17 Nepers/cm, normal and superconducting	45,47	
Tin - Single	Long	54	1-3.7°K	α = 2-17 dB/cm, (001) direction	47	
Crystal	Long	33	--	α = 0-5 dB/cm for H = 0-1.5 Kilogauss	47	
Tin 99.999%	Long, P-E	.575	17-1°K	α = 0.0065-0.012 dB/cm	46	
	Long, P-E	.225-1.09	4.2°K	$/f^2$ = 18.9 - 16.0 dB-sec^2/cm	46	
Tin - Polycrystal	Shear	27.5	1-3.7°K	α= 0-6.8 dB/cm.	47	
Silver - Single Crystal	Shear, pulse, 1 μsec	4-18	R.T.	Modulus = 1.53 - 4.61 x 10^{11} dyn/cm^2	48	
Silver-Polycrystal	Transverse, pulse, 1 μsec	4-18	R.T.	V = 1,700 m/sec	48	
	Transverse, pulse, 1μsec	4-18	R.T.	Travel time/grain = 70-180 n sec for GS = .12 -.3	48	
	Long, pulse, 1 μsec	4-18	R.T.	Travel time/grain = 32-80 n sec for GS = .12-.3	48	
	Long, pulse, 1 μsec	4-18	R.T.	V = 3,700 m/sec	48	

Table XIII, concluded

ULTRASONIC ATTENUATION AND VELOCITY IN METALS (CONT)

NOTES

a. Attenuation curves show peaks with deformed specimens.

b. Velocity did not appear to vary with frequency but did increase with tempering temperature, independent of cooling method.

c. Longitudinal velocity for 0.4%C and 1.2%C steel = 5.82×10^5 cm/sec (2-16 ms/sec)

d. Also remanant state, $\alpha = 0\text{-}0.016 \frac{dB}{\mu sec}$ vs max appl field, H = 0-100 Oersteds.

e. Velocity measurements preferred for prediction of tensile strengths.

f. Measured dislocation damping effects.

g. Attenuation characteristics markedly affected by presence of gas and microshrinkage.

h. Attenuation measured in db/path where path was either twice or once the length of sample.

i. Measurements made during tensile deformation. Attenuation and velocity changes are greatest in [110], moderate in [111], and least in [100].

j. Initial shear velocity in aluminum = 1.22×10^5 in./sec at 5 mc/sec.

k. Author examined ingot integrity and integrity of structural components. Rayleigh (surface) waves, Hafnium, V = 76,000 in./sec (1-5 mc/sec)
Rayleigh waves, Zirconium, V = 96,000 in./sec (1 - 5 mc/sec)

l. Information presented here is summarized only. Reference 54 contains extensive attenuation and velocity data, the scope being beyond the space available in a tabulation of this type.

m. Describes a unique technique for getting both longitudinal and shear velocity data with one transducer, at high temperatures.

INFRARED TECHNIQUES

Considerable interest has been seen recently in the use of infrared techniques for thin-gage materials and structures. Recent work by Automation Industry and the Perkin-Elmer Corp have shown the feasibility of this approach. In most cases, however, the problems encountered in commercial equipment deal with thermal time constants of large structures and, therefore, have limited resolution. With thin-gage metallic structures, the thermal time constants are sufficiently short and should permit rapid testing.

Early thermal testing methods were limited in test sensitivity due to differences of emissivity. Specially prepared surfaces were found by Haley(58) and Sachs(60) to produce uniform emissivities. An alternate technique by Green (61) uses reflected infrared and is claimed to eliminate the influence of emissivity differences (62). Green also reports using the ratio of two IR radiometers signals to procude an emissivity independent of surface conditions. Aluminum clad uranium fuel elements used to evaluate this technique were 1-1/2-inch diameter cylinders with a 0.030-inch cladding. Artificial defects were made from 0.003-inch thick, 1/2- and 3/8-inch-diameter mica disks and inserted in the bond area, and were detected by this technique.

The commercial application of infrared techniques are commercially applied for electronic circuit boards (66) in this application, the part gives off infrared radiation and is scanned to give a "thermal signature." The infrared camera produces the equivalent of a 180 line TV picture, containing 60,000 data points per frame, produced in 12 minutes with a thermal sensitivity of 0.1°C. The part tested contains heat producing elements 1/16-inch-diameter by 3/4-inch length and up, such as diodes, rectifiers, etc. Commercial infrared inspection of parts at temperature in equilibrium with ambient are reported by McIntosh (63). Examples are given for brazed honeycomb inspection wherein heat is applied to the rear surface and the conducted heat pattern on the front surface indicated varying internal thermal anomalities. Radsliff (64) reports the use of Barnes Engineering equipment to detect deliberate disbonds (1/4 to one inch diameter) between the Polaris A-3 solid propellant motor case and lines. Fixed spot radiometric microscopes are used for inspecting semiconductors and integrated circuits. Here again, the parts are thermally active. However, resolution spot sizes are presently at 5 milli-inches.

In summary, the application of conventional IR techniques for the composite materials and structure does not seem practical at present because of the poor IR resolution and limited scanning capabilities. The application of techniques such as described by Haley (58) are promising, but require development.

EDDY CURRENT TECHNIQUES

Eddy current techniques are used to inspect electrically conducting materials for cracks, voids, inclusion, etc. McConnagle(67) has compiled an

extensive survey on commercial equipment and reported typical inspection capabilities. This survey apparently includes equipment in use through 1960 and is summarized in table XIV.

A second tabulation of commercial eddy current instruments is given by McMasters(74) which includes response characteristics and typical applications. Commercial equipment is reported extensively in the production of copper and aluminum foils, sheets and tungsten wire.

The eddy currents induced in a material are affected by changes in electrical conductivity. The gross differences in electrical restivity represented by the candidate composite materials would appear to give significant signal variations when scanned in composite structure. Further, the determination of fiber alignment is considered feasible. The localized induced eddy currents concentrate near the surface of a specimen. In the case of a plane conductor, the current falls off exponentially with the depth below the surface as an inverse function of frequency, magnetic permeability, and electrical conductivity. Jones(72) investigated the effect of increasing the frequency in the case of thin-gage nonferrous alloys to obtain accurate resistivity or conductivity measurements. Tests were conducted using a Magnatest FM-100 and aluminum alloys of about 1.35 to 2.30 microhm-inch resistivity. The critical limit at 60 KHz, resistivity measurements could be obtained on 0.01-inch-thick material of 0.674 microhm-inch, and on 0.06-inch-thick material 4.19 microhm-inches resistivity. Although some reduction in accuracy was reported at higher frequencies, it was concluded that the use of higher frequencies led to a still reasonable determination of thin material properties. Other materials tested included manganese bronze, copper beryllium, and copper, and confirmed this conclusion. It should be noted that, if this theory is extrapolated, increasing the frequency to 1000 times the limit frequency, a wire diameter variation of 0.1 percent would cause the same variation as a crack of 5 percent depth. Thus, a disadvantage of eddy current tests is the inability to separate measurement effects on required variables from less significant effects.

The application of eddy current tests for the distinction between various alloys, based on their varying conductivities, is widely practiced in industry. The widely varying conductivities of the specimen composites could thus be detected on gross comparative basis. Commercial instruments are available (Signiatest) with high and low conductivity sensing capability.

The use of high conductivity materials (copper, aluminum) in the metallic matrix composites suggest another eddy current approach. In conventional eddy current testing, the extremely high attenuation of high-frequency eddy current fields in good conductors requires the use of large coils, low frequencies and high power. Renken(73) has shown that higher surface resolution can be obtained by the use of a pulsed eddy current system employing a masked aperture probe. The masked probe restricts the application of a pulsed induction field to a small cross-sectional area, thereby permitting relatively thick sections to be

Table XIV

COMMERCIAL EDDY CURRENT EQUIPMENT

Equipment	Measurement	Materials	Defects
Cyclograph (J.W. Dice Co.)	Resistive impedance	Inconel tube 0.25 in. dia, 0.025 in. wall	0.001 in. deep intergranular crack
		1100 Aluminum 0.0003 to 0.0009 in. thick bonded to 1.0 in. dia. uranium rods	0.5 in. dia unbonded areas
Probology (Shell Development Company)	Phase, Impedance	Zircaloy tubing	0.005 in. deep x 0.5 in. long ID wall cracks
			Wall thickness changes of 1% in 0.5 in. length
Metal Comparator (General Electric)	Reference impedance vs test part	Magnetic and nonmagnetic	Material properties, thickness
Knolls Atomic Power Laboratory Tester	Induction, Impedance	Capillary tubes 0.050 to 0.226 in. dia	Cracks 0.0005 to 0.001 in. deep, 0.070 to 0.100 in. long
Forster Instruments Deflectometer Sigmaflux	Phase, Impedance	Nonferrous wire and rods, specifically for tungsten wire	Cracks in nonmagnetic material, alloy variations, gross cracks

tested with good resolution. Further, the inspection of thin materials is enhanced, since the pulse rate and length can be varied and reflected pulses are a function of the materials properties, structures, etc.

It can be concluded that inspection techniques using eddy currents is potentially feasible for the inspection of the matrix materials and the tungsten fiber. Boron fiber is not mentioned in the literature surveyed. No mention of fiber-matrix inspection was found. The detection of disbonds in clad materials and interlaminar corrosion was reported. The applicability of eddy current techniques for composites is considered beyond the level of conventional equipment. However, pulse techniques and carefully calculated high-frequency limit techniques are considered feasible on a laboratory basis.

RADIOGRAPHY

The detection of defects in metallic fiber-matrix composites by radiography depends on the relative absorption of X-rays by the composite materials and the material geometry. The materials are primarily the matrix and reinforcing fiber, but phases such as diffusion layers, gas entrapment, and others, which constitute defects, must also be considered. Radiation beams cover, generally, a spectrum of photon energies, whose integrated value is the effective X-ray energy. This value is less than the nominal input in the conventional X-ray tube and equipment which has a minimal value of about 20 kv. This value corresponds to an electron accelerating potential or operating voltage of about 45 kv. In the tables attached, only the effective energy is considered. Relative intensity changes over the area of the specimen will vary with attenuation of the photons as the specimens are scanned. In order to define the extent of defects in the plane dimension, intensities must be of a sufficient order to produce an observable change in the recording photographic film or plate. Plane resolution, therefore, also depends on the film characteristics including grain size and/or scatter effects. It is generally agreed that a resolution of 0.002 inch is a reasonable minimum for high-quality production. However, there are exceptions: small diameter cylindrical inclusions are most easily detectable if the cylinder is long and at right angles to the radiation direction. Likewise, very small, deep holes give sharp images.

In the case of flat sheet specimens as described in this report, radiographic conditions are more optimum than in the case of more complex shapes. For the present, only such flat sheet specimens are considered, although other shapes must be considered for future applications. In flat specimens, the minimum detectable defect, therefore, will depend principally on the radiographic conditions for which the following consideration apply:

$$0.00333 < \mu \Delta X < 0.0167$$

where

μ is the linear attenuation
ΔX is the minimum detectable defect depth.

The aforementioned inequality is based on the minimum detectable change in film density. Under nearly ideal conditions, most defects will not be detectable if $\mu\Delta X < 0.0033$, and most defects will be detected if $\mu\Delta X < 0.0167$. Production radiography rarely approaches such ideal conditions. The larger value is closer to the values obtained in radiographic practice.

Literature has been summarized in the following tables to assess the radiographic contrasts which can be obtained with various material and defect combinations. Table XV summarizes linear attenuation coefficients for the candidate materials for various effective voltages. It should be noted that these coefficients show discontinuities where the photon energy corresponds with the energy of characteristic spectrum lines of the materials involved. Table XVI summarizes the half value layers, i.e., the depth of layer through which one-half of the X-ray intensity is attenuated and also the maximum thicknesses which can be penetrated by photons of various energy. Table XVII gives the minimum size of material thickness change which can be determined radiographically under both ideal and practical production radiographic conditions. It should be noted that all energies given are the effective energies.

The discontinuities of absorption coefficients with varying energies deserve further attention. It is evident that maximum attenuation in a given material results if the radiation wave length is coherent with the effective radiation energy. This principle thus opens up a method of optimizing radiation to either filament or matrix material. For example, tungsten has an absorption line at 69.6 kv, with a corresponding absorption coefficient of 206 cm^{-1}. Thus, if for the examination of a tungsten fiber composite, a tungsten target emitting at an effective energy of 69.6 kv is used, maximum sensitivity to defects in the tungsten fiber will be attained. This principle can be applied to all other materials. However, it necessitates the use of X-ray tubes with various targets, which may not be readily available commercially. Lacking such special tubes, radiation energies must be chosen which provide the greatest difference in attenuation coefficient. For a boron-aluminum composite, for instance, maximum difference occurs at very soft voltages. Here again, the limitations in availability in commercial equipment must be considered. Normally, an effective energy of 20 kv is the lowest range of generally used equipment.

Other conclusions which can be drawn from the tables are that optimized conventional radiographic methods will locate fibers and complete breaks called out in the study program and have a good potential in locating broken fibers and some matrix and other bond defects. However, this method would not be satisfactory for the detection of changes in fiber diameter and defects in line with the direction of X-rays.

Table XV

NARROW BEAM LINEAR ATTENUATION COEFFICIENTS (CM^{-1})

Material	B	AL	Ti	CU	W
Density	2.45	2.7	4.5	8.9	18.7
Effective X-Ray Energy KV					
10	3.30	72.4	527	1750	2260
15	1.50	21.8	168	593	1020
20	.70	9.4	73.5	272	331
30	.50	3.1	22.9	87.7	151
40	.43	1.5	10.0	38.5	82
50	.39	.66	5.4	20.0	50
60	.37	.73	3.4	12.4	34
80	.34	.54	1.8	5.9	144
100	.32	.46	1.2	3.6	82
150	.30	.37	.75	1.7	28
200	.30	.33	.60	1.2	14

Table XVI

MAXIMUM MATERIAL THICKNESSES AND HALF VALUE LAYERS

(1) Half Value Layer ($X_{1/2}$) = $\left(\frac{.273}{\mu}\right)$ inches

(2) Maximum Thickness (X_{MAX}) = (3) $\left(\frac{.273}{\mu}\right)$ inches

Where μ = Linear Attenuation Coefficient in CM^{-1}

Effective X-Ray Energy - KV	B		AL		Ti		Cu		W	
	$X_{1/2}$	X_{MAX}	$X_{1/2}$	X_{MAX}	$X_{1/2}$	X_{MAX}	$X_{1/2}$	X_{MAX}	$X_{1/2}$	X_{MAX}
10	.083	..25	.0037	.01	.0005	.002	.0001	.0003	.0001	.0003
15	.182	.55	.013	.04	.0016	.005	.0004	.001	.0002	.0006
20	.390	1.17	.029	.08	.0037	.01	.001	.003	.0008	.002
30	.546	1.64	.088	.26	.012	.04	.003	.009	.002	.006
40	.635	1.91	.182	.55	.027	.08	.007	.02	.003	.009
50	.700	2.10	.284	.85	.051	.15	.014	.04	.005	.015
60	.738	2.21	.374	1.12	.080	.24	.022	.09	.008	.024
80	.803	2.41	.506	1.52	.152	.46	.046	.14	.002	.006
100	.853	2.56	.593	1.78	.228	.68	.076	.23	.002	.000
150	.910	2.73	.738	2.21	.364	1.09	.161	.48	.010	.040
200	.910	2.73	.827	2.48	.455	1.37	.228	.68	.020	.060

Table XVII

MINIMUM DETECTABLE DEPTH DIMENSIONS

Effective X-Ray Energy - KV	B		AL		Ti		Cu		W	
	MIN	MAX	MIN	MAX	MIN	MAX	MIN	MAX	MIN	MAX
10	.001	.005	.00005	.00025	-	-	-	-	-	-
15	.002	.010	.0002	.0010	-	-	-	-	-	-
20	.005	.025	.0004	.0020	.00005	.00025	-	-	-	-
30	.007	.035	.001	.005	.0001	.0005	.00004	.0002	-	-
40	.008	.040	.002	.010	.0003	.0015	.00009	.00045	.00004	.0002
50	.009	.045	.003	.015	.0006	.0030	.0002	.0010	.00007	.0003
60	.009	.045	.005	.025	.0010	.0050	.0003	.0012	.00010	.0005
80	.010	.050	.006	.030	.0020	.010	.0006	.0030	-	-
100	.010	.050	.007	.035	.003	.015	.0009	.0045	.00004	.0002
150	.011	.055	.009	.045	.004	.020	.002	.010	.0001	.0005
200	.011	.055	.010	.050	.006	.030	.003	.015	.0002	.001

INSPECTION ANALYSIS SYSTEMS

The nondestructive inspection of metallic fiber-matrix composites requires almost microscopic detail resolution. Automated scan/record systems for this type of inspection are a necessity when large areas and/or complex structures are considered. If the present inspection requirements of one to 2 percent sensitivity (measured in terms of material thickness) are extrapolated, resolution in the order of 10 to 1000 micro inches is required for the subject composites. This inspection level approaches the grain boundary sizes and complex signal to noise ratio problems occur. Further, the interpretation of test indications by a human operator becomes impractical and a form of automatic data processing becomes essential. For example, if discontinuities in the order of 100 microinches are significant, an inspection system must be capable of resolving 10^8 data points per square inch. Thus, the inspection of the 5 x 10-inch composite specimen would involve about 5×10^9 data points. Extrapolation from the specimen to production control of sheet or assembled vehicles requires automation as found in digital computer facilities. Lockheed and NAA/Columbus have, at present, incorporated digital computers for similar inspection problems. McMasters has proposed the development of high-resolution closed-circuit television systems for the display of on-line out-of-tolerance measurements. McMasters(65) has developed a high detail, enlarged X-ray imaging system, and recommends the readout of all nondestructive test systems through a common type of information transmission, analysis, and display system. Such a common system would certainly be sound economically, and would also permit simultaneous or subsequent viewing of several types of nondestructive test methods.

FIBER INSPECTION

The inspection of filaments as employed in fiber matrix composites is related directly to commercial wire inspection. The major difference is with respect to the size of material inspected. Commercial wire products and inspection are reported down to 0.0002-inch diameter and smaller. Inspection techniques applied to wire (fiber) cover practically all fields of current nondestructive testing.

G. Earnshaw (79) discusses the vastly expanding art of making wire and the immediate need for process inspection first at the material ingot form and as processed to the supplier. Three types of wire defects are traced to the wire rods: (a) steel-making defects such as axial segregation, pipe and inclusions; (b) surface defects arising from casting or rolling - laps, seams, fins, slivers, etc.; (c) structural defects as excessive decarburization, coarse grain size. A number of these defects, depending on nature and size, will be removed by the wire fabrication; however, others will be included in the final wire. Sulfur printing is recommended for detection of sulphur segregation. Deep etch tests are suggested for surface inspection after removal of mill

scale. H. Rainey (80) surveyed mechanical wire failures in wire production resulting in the following categories: inclusions, sliver, splits, mutilation, and stress. It was shown that inclusions could occur within or on the surface of the wire. M. J. Dashukewick (81) also stresses the need for rod or billet inspection prior to the wire drawing operation, not only to ensure good wire but also to keep continuity in the drawing operation. Systems are mentioned that combine eddy current (surface defects) and ultrasonic techniques (internal defects) for testing of the rod and the drawn wire. Segre (82) describes the problems of using stainless steel wire for producing wire mesh including the effects of wire spooling and annealing. The elastic properties of wire are not entirely a function of diameter and improper wire handling processes can easily degrade the tensile strength properties. Segre recommends a study of the field or wire plasticity and tensile strength as stress are developed in the entire wire cross section and/or on the wire surface. The importance of wires having an extra bright surface finish is emphasized because roughness or porosity on the surface represents preferential spots for corrosion. Wire yield strength, ultimate tensile strength, percent elongation and work hardening tendency are properties that depend primarily on the chemical composition. However, these properties are not independent from each other. Wire handling for a given application may be improved using a wire with a somewhat higher tendency to work-harden but at the same time having a plasticity range wide enough to reduce the risk of frequent breakages.

The manufacturing of approximately 0.00002 inch diameter tungsten wire is discussed by L. Walter (83). After the required wire diameter has been drawn and the wire annealed, the wire is dimensionally and mechanically tested.

Ultrasonic cleaning of ferrous and nonferrous wire is recommended by J. R. Logan (84). The application of ultrasonic energy to acid cleaning solutions is not recommended due to the reduction in wire diameter. However, ultrasonic cleaning using alkaline detergents does not attack most nonferrous materials. The use of high temperature cleaning with an alkaline solution further improves the process. Ultrasonic cleaning is recommended at various steps in the wire drawing process and for the final product. Ferrous materials such as stainless steel that require removal of the lead used in drawing could be accomplished by a continuous hot acid alkaline solution process by cleaning the wire directly after the annealing process. Cleaning is claimed down to the micron level.

A. K. Saltis (85) reports successful elimination of wire defects caused by mechanical discontinuities in the billot. The billots are approximately two inch square and thirty feet long and are automatically inspected in continuous magnetic particle inspection system. Defects found in the wire were generally attributed to the drawing process. An eddy current inspection is performed on the finished wire at speeds up to 700 feet per minuted. Inspection data was correlated to show the effect of discontinuities on the fatigue life

of the wire spring products. An additional article on the same program by H. G. Bogart (36) describes the eddy current inspection system in further detail. Depending on the material, the system is adjusted to indicate magnetic properties or conductivity changes. A differential eddy current coil system is described with two coils located close together. The coils are connected in series opposition so that general wire variations in diameter, hardness, temperature or chemical hardness occurring gradually along the wire will not cause false indications.

H. F. Ammarell and R. B. Moyer (87) utilize eddy current inspection equipment to define alloy composition, stress, metallurgical structure and various mechanical defects for evaluation of hot mill billets, etc. Particular emphasis is placed on the rotating search coil type inspection for all types of steel as well as nonferrous alloys. Standards are recommended using the actually defective wire products.

Callen (88) discusses a new tool designed to simulate defects in rod and wire products used in eddy current testing. The tool was developed based on the inadequacy of narrow-blade saws, millers, and arc erosion techniques for making accurate notches for eddy current standards. The tool, claimed to produce cool, shockless cutting with good controllability, uses a finely graded abrasive gas propelled through a tiny nozzle. Microphotographs are shown illustrating 0.002, 0.004 and 0.005 inch deep notches cut in 304 stainless steel. The cuts were made without work hardening or distortion of metal. The notch system is used for eddy current equipment.

The J. M. Ney Co. (89) describes eddy current inspection for wire as small as 0.005 inch diameter. The wire is used in printed circuits, slip rings, resistance windings, etc. Defects detected includes seams, cracks, and discontinuities.

Color reflectivity measurements for moving fine wire inspection is discussed by T. L. Weaver (90). The instrument consists of a system for pulsing and reflecting blue light alternately from a standard wire and the moving test wire. A photomultiplier tube detector measures the reflection intensities as a function wire surface condition. The system was applied to measure the amount of residual graphite remaining on 0.001 to 0.009 inch diameter wire following a cleaning process. A similar technique developed by F. S. Reed (91) employs two forms of radiation, emitted at different frequencies in a cyclical manner, and reflected by the material. The difference of absorbed radiation characteristics is a function the material properties. The author points out that the technique does not look at an absolute quantity of radiant energy and measure its absorption or shadow, but to scan rapidly through the area and use the ratio of the time the energy is observed versus the dark area caused by the wire.

L. C. Whitney (92) reports infrared inspection of aluminum clad wire ranging from 0.080 to 0.250 inch diameter. The inspection problem involved accurately determining the aluminum bond temperature and controlling the heater system. Destructive tests were made to establish the optimum bond temperature. This system concept has potential application at wire annealing or points where an infrared spectrum or frequency could indicate wire anomalies.

Ultrasonic wire inspection is reported by W. Lehfeldt (93) at speeds up to 200 feet per minute. The author states that pulse echo techniques using longitudinal or transverse waves are not usable for wire inspection. An ultrasonic pulse echo system was used to establish "wire waves" evidently similar to Lamb waves in thin sheet material. Pulses at 4 MHz were propagated through water to wire ranging from 0.004 to 0.2 inch diameter. A commercial test system was tested and detection of cracks was reported with a depth of 10 percent of the wire diameter. Tests were conducted on tungsten, silver solder, copper and steel wires. This system is reported to have found all defects as subsequently located by microscopic evaluation. This included both surface and internal wire defects.

Optical inspection of wires has been the subject of many papers, however, only three are reported here to show the general approaches. W. C. Hutchins (98) describes the development on optical diameter gage that operates on the light beam principle. A replaceable steel wire reference is compared with the test wire by projecting the wire images on two series-opposing photovoltaic cells. The instrument is sensitive to 0.0001 inch diameter variation on 0.003 wire. The wire may vibrate up to ± 1/16 inch from the normal path without significant error. The error limit is adjustable up to 0.005 inches. The response time of the wire diameter gage is less than two microseconds.

Iron Age (99) describes a noncontact optical micrometer that measures the diameter of red-hot wire. The instrument uses a narrow light beam scanned across a large lens with a photocell at the focal point. As the light beam is scanned across the lens, the wire is introduced and blocks the beam from reaching the photocell. The photocell under constant scanning conditions will trigger at the fiber edges; the time interval measurement is equivalent to the wire diameter. Since the time internal serves as the base for all diameter measurements, light-intensity fluctuations do not affect the data.

The optical inspection of 0.003 inch diameter glass filaments was described by C. A. Bouc (94) using a microscopic technique. A 200X transmission microscope was used to study the failure characteristics of a filament wound specimen under tensile loads. A percentage load was applied to the specimen and the fibers were inspected by manual scanning. A written and photographic record was made of five different microscopic modes of failure.

The presentation and analysis of data from wire inspection process is considered by several authors. M. H. Dashukewich (31) describes future wire inspection data may take the form of magnetic tape. The tape in turn could be programmed into wire processing equipment and the defective sections removed automatically.

J. J. Stefaniszyn (95) defines the present state-of-the-art in high speed motion picture photography as applied to wire inspection. Exposures up to 1500 frames per second or 1/10,000 second exposure time are considered for wire testing. The application of motion picture cameras is considered not only for viewing of the wire but also for studying the operation of wire feed and handling systems. Commercial photo optical recording systems are available from Photomechanisms (96) for processing large amounts of photographical data. These systems combine recording and data readout in a single operation.

E. F. Jubb (97) proposes the possibility of adopting statistical quality control techniques for wire inspection. He suggests that 50 percent of all testing can be eliminated by statistically analyzing the inspection data and keeping records of defect characteristics and occurrence for a given wire type.

CONCLUSIONS

From the survey of the limitations of commercial equipment for nondestructive testing, it can be concluded that the resolution limits of such equipment are at best at the border line of limits required for the inspection of defects in metallic matrix filamentary composite materials. Throughout the survey, only the simplest shape of metallic matrix filamentary composite material, i.e. sheets with parallel fibers, has been considered. However, it can be assumed that such materials will also find application in many more complex combinations and configurations such as turbine blades reinforced along principal stress directions. A number of methods and approaches are suggested which can improve the sensitivity of commercial test equipment, but these methods generally require nonstandard modifications to the test equipment. Considerable experimental work is, therefore, required to assess whether relatively minor modification of standard commercial test equipment will result in usable information as to composite material defects or whether major alterations or new equipment design and approaches will be required.

REFERENCES

1. "Operation and Maintenance Instruction For Immerscope, Model 424 A," Curtiss-Wright Corp, Industrial and Scientific Products Division, Caldwell, New Jersey, 1957

2. Merkulov, L. G., "Modern Ultrasonic Inspection," Material Research, July, 1962, p 98

3. Albertson, C., Van Valkenberg, H., "Ultrasonic Detection Sizing, and Counting of Sub Seive Particles," Proceedings of the Fourth International Conference on Nondestructive Testing, Butterworths, London, 1964

4. McMasters, R., Nondestructive Testing Handbook, Ronald Press, New York, 1959

5. Automation Industries, Inc, Research Division, "Ultrasonic Transducer Brochures" Nos. 401-2, 401-3, 401-4, 401-5, Industrial Park, Boulder, Colorado

6. Ross, J. D., "Ultrasonic Transmission Tester for Detection of Unbonded Areas," Symposium on Nondestructive Tests in the Field of Nuclear Energy, ASTM-STP 223, 1957

7. Redstreake, W. N., "Ultrasound Maps Flaws in Bonds," The Iron Age, 23 January 1964

8. Posakony, G. J., McMasters, R. C., "Analysis of Focused Ultrasonic Test Techniques," Proceedings of First National Symposium on Nondestructive Testing of Aircraft and Missile Components, 1960

9. "Instruction Manual for Type UT Ultrasonic Pulse-Echo Thickness Gage, Style 53B137 with Supplementary Circuit Diagrams for Modification 53D044," Sperry Products, Division of Automation Industries. (Modification by NAA/LAD - ref NAA Report CD-3792, 3803)

10. McClung, R., and Cook, K., "Ultrasonic Detection of Noulbond in Clud Structures," Proceedings of the Fourth International Conference on Nondestructive Testing, Butterworths, London, 1964

11. Vidigage, Branson Instruments, Inc, Stanford, Conn

12. Sonizon Model 50-300, Resonant Ultrasonic Tester, Magnaflux Corporation

13. R. J. Schliekelmann, Fokker Bond Tester, N. V. Kon. Nederlandse Vliegtuigenfabriek Fokker, Amsterdam, Departm. Manufacturing Research, Report Nr. R-296

14. Arnold, J.S., Vincent, C.T., "Development of Nondestructive Tests for Structural Adhesive Bonds," WADC Technical Report 54-231, Parts 1-7, 1959

15. Comindascope, Model 101-B, Pioneer Industries, Division of Almar - York Co. Ft Worth, Texas

16. Aveyard, S., and Sharpe, R., "Applications of Ultrasonic Pulse Interference," Proceedings of the Fourth International Conference on Nondestructive Testing, Butterworths, London, 1964

17. Bobbin, J., and Harris, R., "Frequency Dependent Effects in Ultrasonic Resonance Testing," Nondestructive Testing Journal, Sept - Oct 1960, Evanston, Ill

18. Worlton, D.L., "Applications of Lamb Waves in Ultrasonic Testing," Symposium on NDT in the Field of Nuclear Energy, April 1957, ASTM-STP No. 223

19. di Novi, "Lamb Waves; Their use in Nondestructive Testing," ANL-6630, March 1963

20. Papadakis, E.P., and Reed, E.L., "Ultrasonic Detection of Changes in the Elastic Properties of a 70-30 Iron-Nickel Alloy Upon Heat Treatment," J Appl Phys 32, 4, 682 (1961)

21. Bratina, W.J., and Mills, D., "Investigation of Residual Stress in Ferro Magnetics Using Ultrasonics," Nondestructive Testing, March-April 1960, Also Sperry Reprint 50-809

22. Roderick, R.L., and Truell, R., "The Measurement of Ultrasonic Attenuation in Solids by the Pulse Technique and Some Results in Steel," J Appl Phys, 23, 2, 267 (1952)

23. Papadakis, E.P., "Rayleigh and Stochestic Scattering of Ultrasonic Waves in Steel," J Appl Phys, 34, 2, 265 (1963)

24. Papadakis, E.P., "Ultrasonic Attenuation and Velocity in Three Transformation Products in Steel," J Appl Phys, 35, 5, 1474 (1964)

25. Papadakis, E.P., "Ultrasonic Attenuation in S.A.E. 3140 and 4150 Steel," J Am Acoust Soc 32, 12, 1628 (1960)

26. Papadakis, E.P., Sullivan, P.F., Waltman, D.J., "Ultrasonic Attenuation and Velocity in S.A.E. 4150 Steel," WAL TR 143/37 (December 1961)

27. Merkulov, L.G., "The Use of Ultrasonic Waves in Investigating the Structure of Steels," Soviet Physics, Tech Physics, V 2, p 282 (1957)

28. Martius, U.M., and Bratina, W.J., "Frequency Dependence of Ultrasonic Wave Attenuation in Armco Iron and Low-Carbon Steel," J Appl Phys 32, 3, 2805 (1961)

29. Lavender, J.D., Puller, A.G., "Ultrasonic Velocity and Attenuation Measurements for Determining the Properties and Structures of Cast Irons and Cast Steels," British Foundryman, p 54 (Feb 1965)

30. Adams, C.J., "Ultrasonic Attenuation Characteristics of Various Steel Alloys." Nondestructive Testing, Nov.-Dec. 1961, 393

31. Bratina, W.J., Martius, U.M., Mills, D., "Magnetic Contribution to the Ultrasonic Attenuation in Annealed and Deformed Steel (S.A.E. 1020)," J Appl Phys 31, 5, 241S (1960)

32. Bratina, W.J., and Mills, D., "Effect of Dislocations on the Ultrasonic Wave Attenuation in Deformed Carbon Steels," Acta Metallurgica, 10, 419, April 1962

33. Felix, W.A., "Nondestructive Tensile Testing of Cast Iron," Metal Progress, Feb 1963, 91

34. Bergman, R.H., and Shahbender, R.A., "Effect of Statically Applied Stresses on the Velocity of Propagation of Ultrasonic Waves," J Appl Phys 29, 12, 1736 (1958)

35. Tjaden, Von K., "Absorbtion Longitudinaler Ultraschallwellen in Aluminium bei Hohen Temperaturen," Acustica, 11 (1961), 127

36. Smolen, H., Rosenthal, H., "Ultrasonic Attenuation in Case Aluminum." Modern Castings, May 1959, 257

37. Roney, R.K., "The Influence of Metal Grain Structure on the Attenuation of an Ultrasonic Acoustic Wave." Thesis, Calif. Inst. of Technology, 1950, Pasadena, Calif.

38. Morse, R.W., Bohm, H.V., "Some Ultrasonic Measurements in Normal and Superconducting Aluminum," J Acoust Soc Am 31, 11 (1959), 1523

39. Mason, W.P., McSkimin, H.J., "Attenuation and Scattering of High Frequency Sound Waves in Metals and Glasses," J Acoust Soc Am 19, 3 (1947), 464

40. Jones, B.K., "The Attenuation of Ultrasound by Electrons in Aluminum," Philisophical Mag. 6, 98 (1964), 217

41. Hikata, A., Chick, B., Elbaum, C., Truell, R., "Ultrasonic Attenuation and Velocity Data on Aluminum Single Crystals as a Function of Deformation and Orientation," Acta Metallurgica 10, 423, April 1962

42. Brailsford, A.D., "Dislocation Contribution to Ultrasonic Harmonic Generation," Communications, Jan 1964, 2256

43. Shahbender, R.A., "Nondestructive Measurement of Tensile and Compressive Stresses," 1959 IRE Wescon Convention Record, Part 6A - 1959

44. Mackintosh, A.R., "Ultrasonic Attenuation in Lead," Proc Royal Soc 271, Jan. 1963, 88

45. Mackinnon, L., "Ultrasonic Attenuation." Contemporary Physics 4, 2, Dec. 1962, 123

46. Filson, D.H., "Low Temperature Ultrasonic Attenuation in Tin and Aluminum," Physical Review 115, 6, September 15, 1959, 1516

47. Morse, R.W., "Ultrasonic Attenuation in Metals at Low Temperatures," Progress in Cryogenics 1, 1959, 221.

48. Markham, M.F., "Scattering of Ultrasonic Stress Pulses in a Polycrystalline Solid," Appl Matrls. Research, April 1963, 109

49. Mason, W.P., McSkimin, H.J., "Energy Losses of Sound Waves in Metals Due to Scattering and Diffusion," J Appl Phys 19, Octo. 1948, 940

50. Merkulov, L.G., "Investigation of Ultrasonic Scattering in Metals," Soviet Physics, Technical Physics Vol. 1, 1957, p. 59-69

51. Worlton, D.L., "Nondestructive Grain Size Measurements with Ultrasonics," Nondestructive Testing, Nov - Dec, 1955, 24

52. Bradley, D., "Sound Propagation in Near-Stoichiometric Ti-Ni-Alloys," J Acoust Soc Am 37, 4, April 1965, 700.

53. Fink, F.W., "Ultrasonic Testing as a Method of Determining Variables in Processing Zircaloy and Hafnium," ASTM Special Pub. No. 223, From Nucl. Energy Symp. 4/57

54. Ramsey, J.B., Rowe, W.M., "Development of Ultrasonic Techniques for Defect Evaluation," ASD-TDR-62-8, Feb 1963

55. Kalugin, B.A., Mikhailov, I.G., "A New Ultrasonic Method for Measuring The Elastic Properties of Solids at High Temperature," Soviet Physics - Acoustics, Vol. 7, #2, Oct-Dec. 1961, p. 154

56. Levitt, A.P., Martin, A.G., "Ultrasonic Determination of Elastic Constants of Metals at Elevated Temperatures," Nondestructive Testing, Sept-Oct 1960, 333.

57. Dunegan, H.L., "High Temperature Dynamic Modulus Measurements by Use of Ultrasonics," Materials Evaluation, June 1964, 266

58. Maley, D.R., "Applied Research to Establish Infrared Detection Methods for Non-destructive Analysis of Metallic and Ceramic Structures," ASD-TR-62-385, March 1964

59. Anonymous, "Feasibility Study of a Non-destructive Testing Infrared Inspection System for Bonding Flaw Detection," Interim Reports for Watertown Arsenal.

60. Sachs, H.L., "A Thermal Infrared Inspection Procedure for Detection and Location of Flaws in Solid Propellant Rocket Cases," Proceedings of the Fourth Annual Symposium on Non-destructive Testing of Aircraft and Missile Components, 1963

Alzofan, F.E., Florant, L.E., Anderson, R.H., and Loomer, L.K., "Infrared Non-destructive Testing of Glass Filament Wound Rocket Motors," (same source as preceding)

61. Green, D.R., "Emissivity Independent Infrared Thermal Testing Technique," Materials Evaluation, February, 1965, p 79

62. Yoder, R., "Recent Developments in Infrared Thermography" Infrared Applications for Non-destructive Testing, Barnes Engineering.

63. McIntosh, Jr., R.B., "An Infrared Radiometric Microscope for Non-destructive Testing of Integrated Circuits, (same source as preceding)

64. Radsliff, J.L., "IR Image System Program, Second Progress Report, olaris A-3 NDT, November 1963

65. McMaster, R.C., "New Developments in X-ray Image Enlargment Systems," Norelco Reporter Vol. XI, No. 1 (Jan-Mar 1964)

66. Woodward, A., "Infrared Evaluation of Printed Circuit Boards," Fifth Annual Symposium on Nondestructive Evaluation of Aerospace and Weapons Systems Components and Materials, (San Antonio, Texas - Apr 1965)

67. McGonnagle, W.V., Nondestructive Testing, McGraw-Hill Book Co. p 346-390, 400-441 (1961)

68. Oliver, R.B., Allen, J.W., "Inspection of Small Diameter Tubing by Eddy Current Methods," ASTM STP 223 (1958)

69. Betz, R.A., "Two Applications of Eddy Current Instruments to Testing of Zircaloy Core Components," ASTM STP 223 (1958)

70. Robinson, R.C., "A Nondestructive Test for Intergranular Corrosion in Stainless Steel," ASTM STP 223 (1958)

71. Anon, "Eddy Current Unit Cuts Test Time on Precious Metal Products," Wire and Wire Products, Vol 39, No. 9, p 1322 (Sept 1964)

72. Jones, R.R., Hunter, D.B., "Effect of Frequency Variation Upon the Apparent Resistivity of Thin Gage Nonferrous Alloys"

73. Ronken, C.J., "Progress Report on Nondestructive Testing by Electromagnetic Methods," Argonne National Laboratory Report ANL-6414 (July 1962)

74. McMasters, R.C., Nondestructive Testing Handbook, The Ronald Press, N.Y. (1959)

75. Dodd, C.V., "Applications of a Phase Sensitive Eddy Current Instrument," Materials Evaluation, p 260 (June 1964)

76. Libby, H.L., "An Improved Eddy Current Tubing Test," Materials Evaluation, p 181, (May 1965)

77. Vandervort, P.S., Morris, J.W., Fitch, S.H., "Evaluation of Eddy Current Inspection for Hot Sodium Bonding in Stainless Steel Clad Uranium Carbide Reactor Fuel Elements," Materials Evaluation, p 196 (April 1965)

78. Green, D.K., "Ultra-Stable Eddy Current Method for Detecting Hydride in Zircaloy-2," Materials Evaluation, p 279 (June 1965)

79. Earnshaw, G. "A Brief Survey of Wire Rod Defects - Their Occurence and Detection," Wire and Wire Products, July 1961

80. Rainey, Jr., Horace, "Processes and Quality Control in the Production of 5056 Alclad Aluminum Redraw Rod and Aluminum Screen Cloth," Wire and Wire Products

81. Dashukewich, M. J., "Electronic Methods for Nondestructive Testing of Non-Ferrous Wire," Wire and Wire Products, September 1965

82. Segre, Enrico, Ing., "Stainless Steel Wire for the Production of Wire Mesh," Wire and Wire Products, November 1964

83. Walter, Leo, "The Manufacture of Fine Tungsten Wires," Wire and Wire Products

84. Logan, J. R., "Ultrasonics in Motion," Wire and Wire Products

85. Saltis, A. K., et al, "Finding Seams in Billets by Magnetic Particle Testing," Wire and Wire Products

86. Bogart, H. G., "Controlling Quality of the Surface of Wire by Non-destructive Test," Wire and Wire Products

87. Ammarell, H. F., and Moyer, R. B., "Surface Defect Detection," Wire and Wire Products, November 1961

88. Callan, J. M., "New Tool Induces Simulated Defects in Rod, Wire and Tubing to Establish Reference Levels for Eddy Current Testing Process," Wire and Wire Products, March 1963

89. J. M. Ney Co., "Eddy Current Unit Cuts Test Time on Precious Metal Products," Wire and Wire Products, September 1964, Vol. 39, No. 9.

90. Weaver, T. L., Michaels, A. I., and Nelson, R. C., "The Color Reflectometer; An Instrument for the Continuous Measurement of the Color and Reflectivity of Fine Wire," Wire and Wire Products

91. Reed, F. S., "New Techniques in Differnetial Measurement for the Wire and Cable Industry," Wire and Wire Products

92. Whitney, L. C., "Infrared Radiometer Improves Wire and Cable Production", Wire and Wire Products

93. Lehfeldt, W., "Wire Testing by Ultrasonics," Wire and Wire Products, September 1960

94. Bouc, C. A., "Microscopic Study of Mode of Fracture in Filament Wound Glass-Resin Composites," T & AM Report 234, Illinois University, November 1962

95. Stefaniszyn, J. J., "High Speed Motion Picture Photography in the Wire and Cable Industry," Wire and Wire Products, August 1963

96. Photomechanisms, Inc., "Design of Photographic Data Systems," New York, No. 4.

97. Jubb, E. F., "Quality Control in the Wire Industry," Wire and Wire Products

98. Hutchins, W. C., "An Improved Wire Diameter Gage with Automatic Control," Wire and Wire Products, Vol. 39, No. 6, June 1964

99. "Optical 'Mike' Gages Hot Wire," The Iron Age, 20 February 1964

GENERAL REFERENCES, RADIOGRAPHY

"Nondestructive Testing Handbook, Volume I," edited by Dr. R. C. McMaster 1959.

"Radiography in Modern Industry," published by Eastman Kodak Company, 1957.

"Encyclopedia of X-rays and Gamma Rays," edited by G.L. Clark, 1963.

"The Radiographic Examination of a Thin Object," by C. Casswell and E. Eisner; Nondestructive Testing, Volume XIX, No. 2; 1961

"Control of Radiographic Inspection Process," NAA Report CD-3673; 1959.

"Analysis of Radiographic Techniques,: by J. A. Holloway, D. Polansky, and E. L. Criscuolo, Nondestructive Testing, Volume XVIII, No. 5; 1960.

"Radiography and Visual Perception," by E. L. Criscuolo, Nondestructive Testing, Volume XX, No. 6; 1962.

"X-ray Image Contrast," by Dr. R. C. McMaster and F. J. Sattler, unpublished paper, Ohio State University, 1962.

"Gamma Characteristics of X-ray Image Systems," by Dr. R. C. McMaster and F. J. Sattler; unpublished paper, Ohio State University, 1962.

"Evaluation of Radiographic Systems for the Nondestructive Testing of Electronic Assemblies and Thin Materials," by J. M. Baker, Materials Evaluation, Volume XXII, No. 1; 1964.

"A Review of 100% X-ray Inspection of Semiconductors,: by S. Leonard, Materials Evaluation, Volume XXIII, No. 2, 1965.

"Automatic Particle Size Determination From Micro Radiographs," by O.M. Barlow, W. B. Distler and J. L. Hale; Nondestructive Testing, Volume XVIII, No. 5; 1960.

"Samarium 145, Samarium 153, Gadolium 153, and Thulium 170 Sources for Radiography," by F. L. Green, W. D. Cheek, R. E. Black and G. L. Graham; Nondestructive Testing, Volume XVIII, No. 6; 1960.

"Radiographic Sensitivity Data for the Isotopes Cobalt 60, Iridium 192, Cesium 137, Thulium 170 and Thorium 228," by M. B. Anderson, Nondestructive Testing, Volume XVII, No. 6; 1959.

"High Energy Radiography; 1-30 Mev," by J. H. Bly, Materials Evaluation, Volume XXII, No. 11; 1964.

"Neutron Radiographic Inspection of Heavy Metals and Hydrogenous Materials," by H. Berger and I.R. Kraska, Materials Evaluation, Volume XXII, No. 7; 1964.

"An Evaluation of the No. 3000 Polaroid Film for Industrial Radiography," by N. S. Beyer and K. Balarmamourthy, Materials Evaluation, Volume XXII, No. 2; 1964.

UNCLASSIFIED

Security Classification

DOCUMENT CONTROL DATA - R&D

(Security classification of title, body of abstract and indexing annotation must be entered when the overall report is classified)

1. ORIGINATING ACTIVITY (Corporate author)
North American Aviation, Inc.
Los Angeles Division
International Airport, Los Angeles, Calif. 90051

2a. REPORT SECURITY CLASSIFICATION
Unclassified

2b. GROUP
NA

3. REPORT TITLE
Research and Development of Nondestructive Testing Techniques for Composites

4. DESCRIPTIVE NOTES (Type of report and inclusive dates)
Summary Technical Report, 1 July 1965 to 30 April 1966

5. AUTHOR(S) (Last name, first name, initial)
Moore, John F. and Martin, George

6. REPORT DATE	7a. TOTAL NO. OF PAGES	7b. NO. OF REFS
February 1967	235 plus ii thru xiii	122

8a. CONTRACT OR GRANT NO.	9a. ORIGINATOR'S REPORT NUMBER(S)
AF 33(615)-2865	NA-66-466
b. PROJECT NO. 7360	
c. Task No. 736002	9b. OTHER REPORT NO(S) (Any other numbers that may be assigned this report) AFML-TR-66-270
d.	

10. AVAILABILITY/LIMITATION NOTICES This document is subject to special export controls and each transmittal to foreign governments or foreign nationals may be made only with prior approval of the Metals and Ceramics Division (MAM), Air Force Materials Laboratory, Wright-Patterson Air Force Base, Ohio 45433.

11. SUPPLEMENTARY NOTES
- - -

12. SPONSORING MILITARY ACTIVITY
Air Force Materials Laboratory,
Research and Technology Division

13. ABSTRACT

Results of a research and development program relating to evaluation of nondestructive testing techniques for fiber-reinforced metallic matrix composites are reported. A bibliography, based on an extensive literature search, was compiled. Methods for continuous cleaning and inspection of boron fibers were investigated and an experimental system developed. Boron-aluminum, boron-titanium, and tungsten-copper composite specimens were fabricated with fiber volume ratios ranging from 10 to 25 percent and containing specific anomalies. Nondestructive test methods used were radiography, ultrasonics, and magnetic testing. In addition, experiments proved the feasibility of an optical method for continuous fiber surface inspection. Radiographic methods were found to be adequate to determine single fiber breaks as well as major fiber gaps and general fiber alignment. The feasibility of microradiographic inspection was demonstrated for small single layer boron composites. Ultrasonic pulse echo methods are capable of determining matrix disbonds as small as 1/4 inch square. Ultrasonic velocity measurements show a relation between velocity and fiber ratio. In addition to the experimental work, a literature survey of the problem areas was carried out and recommendations for future extensions of the work are detailed.

DD FORM 1 JAN 64 1473 (Same distribution statement that is on the Abstract.) Unclassified

Security Classification

Unclassified

Security Classification

14. KEY WORDS	LINK A		LINK B		LINK C	
	ROLE	WT	ROLE	WT	ROLE	WT
Metallic Fiber-Matrix Composites						
Nondestructive Testing						
Ultrasonic Inspection						
Radiography						
Microradiography						
Electromagnetic Inspection						
Metallic Fibers						
Tungsten-Copper Composites						
Boron-Titanium Composites						
Boron-Aluminum Composites						
Composite Specimens						
Boron Fibers						

INSTRUCTIONS

1. ORIGINATING ACTIVITY: Enter the name and address of the contractor, subcontractor, grantee, Department of Defense activity or other organization *(corporate author)* issuing the report.

2a. REPORT SECURITY CLASSIFICATION: Enter the overall security classification of the report. Indicate whether "Restricted Data" is included. Marking is to be in accordance with appropriate security regulations.

2b. GROUP: Automatic downgrading is specified in DoD Directive 5200.10 and Armed Forces Industrial Manual. Enter the group number. Also, when applicable, show that optional markings have been used for Group 3 and Group 4 as authorized.

3. REPORT TITLE: Enter the complete report title in all capital letters. Titles in all cases should be unclassified. If a meaningful title cannot be selected without classification, show title classification in all capitals in parenthesis immediately following the title.

4. DESCRIPTIVE NOTES: If appropriate, enter the type of report, e.g., interim, progress, summary, annual, or final. Give the inclusive dates when a specific reporting period is covered.

5. AUTHOR(S): Enter the name(s) of author(s) as shown on or in the report. Enter last name, first name, middle initial. If military, show rank and branch of service. The name of the principal author is an absolute minimum requirement.

6. REPORT DATE: Enter the date of the report as day, month, year; or month, year. If more than one date appears on the report, use date of publication.

7a. TOTAL NUMBER OF PAGES: The total page count should follow normal pagination procedures, i.e., enter the number of pages containing information.

7b. NUMBER OF REFERENCES: Enter the total number of references cited in the report.

8a. CONTRACT OR GRANT NUMBER: If appropriate, enter the applicable number of the contract or grant under which the report was written.

8b, 8c, & 8d. PROJECT NUMBER: Enter the appropriate military department identification, such as project number, subproject number, system numbers, task number, etc.

9a. ORIGINATOR'S REPORT NUMBER(S): Enter the official report number by which the document will be identified and controlled by the originating activity. This number must be unique to this report.

9b. OTHER REPORT NUMBER(S): If the report has been assigned any other report numbers *(either by the originator or by the sponsor)*, also enter this number(s).

10. AVAILABILITY/LIMITATION NOTICES: Enter any limitations on further dissemination of the report, other than those imposed by security classification, using standard statements such as:

(1) "Qualified requesters may obtain copies of this report from DDC."

(2) "Foreign announcement and dissemination of this report by DDC is not authorized."

(3) "U. S. Government agencies may obtain copies of this report directly from DDC. Other qualified DDC users shall request through _____."

(4) "U. S. military agencies may obtain copies of this report directly from DDC. Other qualified users shall request through _____."

(5) "All distribution of this report is controlled. Qualified DDC users shall request through _____."

If the report has been furnished to the Office of Technical Services, Department of Commerce, for sale to the public, indicate this fact and enter the price, if known.

11. SUPPLEMENTARY NOTES: Use for additional explanatory notes.

12. SPONSORING MILITARY ACTIVITY: Enter the name of the departmental project office or laboratory sponsoring *(paying for)* the research and development. Include address.

13. ABSTRACT: Enter an abstract giving a brief and factual summary of the document indicative of the report, even though it may also appear elsewhere in the body of the technical report. If additional space is required, a continuation sheet shall be attached.

It is highly desirable that the abstract of classified reports be unclassified. Each paragraph of the abstract shall end with an indication of the military security classification of the information in the paragraph, represented as *(TS), (S), (C), or (U)*

There is no limitation on the length of the abstract. However, the suggested length is from 150 to 225 words.

14. KEY WORDS: Key words are technically meaningful terms or short phrases that characterize a report and may be used as index entries for cataloging the report. Key words must be selected so that no security classification is required. Identifiers, such as equipment model designation, trade name, military project code name, geographic location, may be used as key words but will be followed by an indication of technical context. The assignment of links, rules, and weights is optional.

Unclassified

Security Classification